THE UNIVERSITY
of EDINBURGH

In-vitro exposure of blue light on retinal pigment epithelium and its relevance to age-related macular degeneration

Ege Kaan Ozkaya

THE UNIVERSITY
of EDINBURGH

A thesis submitted for the degree of Doctor of Philosophy

The University of Edinburgh

2020

Declaration

I hereby declare that the research presented in this thesis and the thesis itself was composed by myself based on the work done at the School of Clinical Brain Sciences at The University of Edinburgh. The work done in collaboration has been stated.

This thesis has not entirely or in part been submitted for any other degree or professional qualification.

Ege Kaan Ozkaya

10th September 2020

Abstract

Age-related macular degeneration (AMD) is a complex disease arising from the interaction of multiple genes and environmental factors. AMD initially affects the pigmented monolayer in retina called retinal pigment epithelium (RPE) which is responsible for photoreceptor homeostasis. AMD causes the loss of the central vision and is the most common cause of registerable blindness in the developed world, and for patients with the atrophic or dry form of the disease there is no cure. Most of the electronic devices and ambient lighting today use light-emitting diode (LED) technology, emitting strong blue-light (470 nm) which is an exogenous risk factor for AMD. This study aimed to understand better the effect of blue-light (470 nm) on RPE cells and to leverage this understanding to develop a blue-light induced in-vitro disease model that recapitulates cellular features of AMD.

To this end, we designed an ad-hoc LED array to illuminate RPE cells cultured in multi-well plates. This allowed us to perform standard biochemical assays and immunostaining such as; detection of reactive oxygen species, Zonula occludens-1 (ZO-1) staining, Protein Kinase C-ζ (PKC-ζ) inhibition, senescence associated β-galactosidase staining and Mitotracker™. Then using specialists Electric Cell-substrate Impedance Sensing (ECIS) multi-well arrays, the time-course effect of blue-light on RPE cells was investigated and quantified in a label free manner.

We showed that blue-light exposure induced a dose-dependent decrease in the barrier function associated with tight junction formation before cell coverage declined. This damage induced by blue-light on tight junctions was mediated by oxidative stress through PKC-ζ activation. Then we demonstrated that ARPE-19 cells exposed to blue-light recapitulates cellular features associated with AMD; senescence, mitochondrial dysfunction and loss of barrier function, before cell coverage declined. Comparison of blue-light induced AMD model against TBHP- and H_2O_2- induced models showed statistically different response from APRE-19 cells. Blue-light induced AMD in-vitro model also demonstrated potential advantages such as easier

modulability and in-situ experiments for mimicking in-vivo AMD development process before RPE cell death. This research has given us insights for designing new high throughput screening assays to test efficiency of novel therapies such as PKC-ζ inhibition and has shown proof of principle for a new model for AMD based on blue-light damage.

Lay Summary

Age-related Macular Degeneration (AMD) is a chronic, progressive eye disease and the most common cause of registerable blindness in the developed world. The ‘dry’ form of the disease affects most patients with AMD and there is no treatment. The target cell for AMD is retinal pigment epithelium (RPE) which is responsible for maintaining health of the overlying photoreceptors. Most of the electronic devices and ambient lighting currently uses light-emitting diode (LED) technology, emitting blue-light (470 nm). Little is known about the long-term impact of intermittent and sustained ambient exposure on RPE. This study aimed to understand better the effect of blue-light (470 nm) on RPE cells and leverage this understanding to develop a blue-light induced disease model that recapitulates cellular features of AMD in-a-dish.

To this end, we designed a blue LED array to illuminate RPE cells cultured in multi-well tissue-culture plates. This allowed standard tissue culture techniques to be applied; biochemical assays and immunostaining. Then we cultured RPE cells on microelectrode arrays to quantitatively characterize changes in their morphology/behaviour in real time, in order to study the effect of blue light on RPE cells.

We showed that blue light exposure induced a dose dependent decrease in the integrity of cell-cell junctions before cell death occurred. This damage induced by blue-light on cell-cell junctions was mediated by oxygen-damage through dislocation of junction protein; PKC—ζ. Then we demonstrated that RPE cells exposed to blue-light recapitulates cellular features of AMD. Comparison of blue-light induced changes against current widely used oxygen-damage inducers; TBHP and H_2O_2, showed difference in their response on RPE cells. The LED-RPE model allowed manipulation without interfering with experimental conditions providing novel insights into mechanisms of RPE cell dysfunction and death. This research has paved the way for designing new high throughput screening assays to test efficiency of

novel therapies such as drugs against PKC-ζ translocation and has shown proof of principle for a new model of blue light damage in RPE relevant to AMD.

Acknowledgements

First of all, I would like to express my deepest gratitude to my PhD supervisors; Dr. Pierre Bagnaninchi and Prof. Baljean Dhillon for giving me the opportunity to work on such an exciting project, their help, support, constant encouragement, motivation and guidance, and formally declare that they are the best supervisors in the universe and in the possible multiverse!

I give thanks to my examiners Dr. Roly Megaw and Prof. Tariq Aslam for their time evaluating the manuscript and their useful feedback, which has allowed me to significantly improve the quality of this thesis. I would like to thank Dr. Leonard Nelson and Dr. Veronique Vitart, for their valuable advice and support! My sincere thanks to Dr. Tom MacGillivray and everyone at Edinburgh Eye Lab meetings for sharing their science! I also deeply thank Dr. Vlastimil Srsen for all his help around the culture lab, for his passion and enthusiasm to teach me new techniques and broadening my knowledge! I would like to thank Dr. Wesam Gamal for teaching me, very patiently, all about cell culture when I first joined the lab and Dr. Dimitrios Tsikritsis for passing on his knowledge and experience! I thank Dr. Fiona Rossi and the whole flow cytometry facility, as well as Dr. Matthieu Vermeren and the whole imaging facility at the Centre for Regenerative Medicine for their help! I also would like to acknowledge and thank the great members of the Bagnaninchi Lab! Special thanks to Graham Anderson, for all the discussions, support and ideas, and Dr. Jonathan Mason for lunches and coffees we shared!

I would like to sincerely thank some of my lovely and kind friends: Dr. Bianca Vezzani for all the wonderful pep talks and introducing me to apperativo; Telma Ventura, Catarina Galego for all the road trips and picnics; Simone and Ludo for fun times and their gladiator spirits; Dr. Diana Sa da Bandeira for hosting great brunch and parties; Dr. Zaniah Gonzalez for sharing lunch time salads; Ryoma Ogawa, David Craig, Dr. Mario Gomez and Dr. Isaac Shaw for humour and karaoke! I would also like to thank Dr. Drake Ramoray for keeping me sane during these times!

I would like to send kisses to my grandmas & grandpas and say “sizi çok seviyorum”. I am eternally grateful to my parents for everything! And Zofia’cım, from the bottom of my heart eternal thanks to you for being my family, my inspiration and making me feel special!

Contents

List of Figures

List of Tables

Glossary

1q32	Chromosome 1, Locus 32
10q26	Chromosome 10, Locus 26
3AB	3-aminobenzamide
3D	3-Dimensional
8W1E	8 wells, 1 electrode/well
96W1E	96 wells, 1 electrode/well
A2E	N-retinylidene-N-retinylethanolamine
A69S	Alanine to Serine change at nucleotide position 69
AC	Alternating Current
ADP	Adenosine Diphosphate
AGEs	Advanced Glycation End Products
AMD	Age-related Macular Degeneration
APOE	Apolipoprotein E
ARMS2	Age-related Maculopathy Susceptibility 2
ATP	Adenosine Triphosphate
BRB	Blood Retina Barrier
C2	Complement Component 2
CFB	Complement Factor B
CFH	Complement Factor H
CoQ	Coenzyme Q

CRALBP	Cellular Retinaldehyde Binding Protein
C-Terminal	Carboxyl Domain
Cu^{2+}	Copper (II) ion
CytCox	Cytochrome C Oxidase
CytCred	Cytochrome C Reductase
DAPI	4',6-diamidino-2-phenylindole
DDR	DNA Damage Response
DMEM	Dulbecco’s Modified Eagle Medium
DMEM/F12	Dulbecco’s Modified Eagle Medium/ Ham's F-12 Medium
DMSO	Dimethylsulfoxide
DNA	Deoxyribonucleic Acid
ECIS	Electric Cell-substrate Impedance Sensing
ER	Endoplasmic Reticulum
EU	European Union
FAD	Flavin Adenine Dinucleotide
FCS	Fetal Calf Serum
FDA	United States Food and Drug Administration
Fe^{2+}	Iron (II) Ion
Fe^{3+}	Iron (III) Ion
FGF	Fibroblast Growth Factor
FMN	Flavin Mononucleotide

G1	Gap 1 Cell Cycle Phase
G2	Gap 2 Cell Cycle Phase
H^+	Hydrogen Ion
H_2O_2	Hydrogen Peroxide
HBSS	Hank's Balanced Salt Solution
hESCs	Human Embryonic Stem Cells
hfRPE	Human Fetal Retinal Pigment Epithelium
hiPSCs	Human Induced Pluripotent Stem Cells
hTERT	Human Telomerase Reverse Transcriptase
HTRA1	High Temperature Requirement Factor 1
HUVEC	Human Umbilical Vein Endothelial Cells
ISC	Inter-System Crossing
iso-A2E	N-retinylidene-N-retinylethanolamine Isomer
JAM	Junctional Adhesion Molecule
L^-	Unsaturated Lipid Free Radical
LED	Light Emitting Diode
LEI	Leukocyte Elastase Inhibitor
LH	Unsaturated Lipid
LOO^-	Lipid Peroxyl Radical
LOOH	Lipid Hydroperoxide
mtDNA	Mitochondrial Deoxyribonucleic Acid

MerTK	Mer Tyrosine Kinase
NAD	Nicotinamide Adenine Dinucleotide
NADH	Nicotinamide Adenine Dinucleotide (NAD) + hydrogen (H)
ND	Neutral Density
nDNA	Nuclear Deoxyribonucleic Acid
NF-κB	Nuclear Factor κ-light-chain enhancer of activated B cells
N-terminal	Amino Domain
O_2	Ground State Oxygen
$^1O_2$	Singlet Oxygen
O_2^-	Superoxide Anion
OGG1	8-oxoguanine-DNA glycosylase 1
•OH	Hydroxyl Radical
OH^-	Hydroxide Anion
•OOH	Hydroperoxyl Radical
ON	Nitric Oxide
$ONOO^-$	Peroxynitrite
P	Ground State Photosensitizer
^1P	Excited Singlet State
^3P	Excited Triplet State
P^-	Free Radical

$p16^{INK4a}$	Cyclin-Dependent Kinase Inhibitor Protein 2A
p21	Cyclin-Dependent Kinase Inhibitor Protein 1
p53	Tumor Protein 53
Par3	Protease-activated Receptor 3
PAR4	Prostate Apoptosis Response 4
Par6	Protease-activated Receptor 6
PARP	Poly ADP-Ribose Polymerase
PBS	Phosphate Buffer Serine
PKC-ζ	Protein Kinase C-ζ
RBP	Retinal Binding Protein
RDH	Retinal Dehydrogenase
RIP	Receptor Interacting Protein
RPE	Retinal Pigment Epithelium
Rpe65	Retinal Pigment Epithelium Specific 65 kilodalton Protein
ROS	Reactive Oxygen Species
S-phase	Synthesis Cell Cycle Phase
SASP	Senescence Associated Secretory Profile
SNP	Single Nucleotide Polymorphism
SOD	Superoxide Dismutase
TBHP	Tert-Butyl Hydroperoxide
TEER	Trans-Epithelial or Trans-Endothelial Electrical Resistance

TGF-β	Transforming Growth Factor-β
TNF-α	Tumor Necrosis Factor-α
UPR	Unfolded Protein Response
UV	Ultra Violet
VEGF	Vascular Endothelial Growth Factor
Y402H	Tyrosine to Histidine change at nucleotide position 402
ZO-1	Zonulae Occludens-1

List of Symbols

α	ECIS cell-substrate adhesion parameter
A	Surface area
C_C	Cellular capacitance
C_E	Capacitance of the electrode
C_m	Cell membrane capacitance
d	Separation of electrodes
D	Optical density
ε	Dielectric constant
E	Energy of a single photon
E_e	Irradiance
E_e^i	Initial irradiance
E_e^t	Transmitted irradiance
f	Frequency
f_0	Threshold frequency
h	Plank's constant (6.62607004 × 10-34 J·s)
H_e	Radiant exposure
I	Current
K	Kinetic energy gained by a single electron
R	Resistance

R_b	Cell-cell junctional resistance (barrier function)
R_C	Cellular resistance
R_m	Cell membrane resistance
R_{Med}	Resistance of the culture media
t	Time
τ	Transmittance
V	Voltage
Φ_e	Radiant flux (Radiant energy per second)
ϕ_q	Photon flux (The number of photons per second)
X_C	Cellular reactance
X_E	Reactance of the electrode
Z	Impedance
Z_C	Cellular impedance

List of Publications

Ozkaya, E. K., Anderson, G., Srsen, V., Dhillon, B., & Bagnaninchi, P., 2020. ARPE-19 exposed to blue light recapitulates cellular features associated with Age-related Macular Degeneration. [under review]

Ozkaya, E. K., Anderson, G., Dhillon, B., & Bagnaninchi, P., 2019. Blue-light induced breakdown of barrier function on human retinal epithelial cells is mediated by PKC-ζ over-activation and oxidative stress. Experimental Eye Research, 189, 107817. https://doi.org/10.1016/j.exer.2019.107817

Ozkaya, E. K., Anderson, G., Dhillon, B., & Bagnaninchi, P., 2019. Real-time monitoring of blue-light induced decline of the Retina pigmented epithelium barrier function with Electrical Cell-substrate Impedance Sensing. BioMedEng19 Conference, London. 5-6/9/2019.

Ozkaya, E. K., Anderson, G., Dhillon, B., & Bagnaninchi, P., 2018. Investigating the effect of blue-light on Retinal Pigment Epithelial cell lines and its potential to model Age Related Macular Degeneration in-vitro. 2018 Impedance Based Cellular Assays Conference, Edinburgh. 6-8/6/2018.

Ozkaya, E. K., Dhillon, B., & Bagnaninchi, P., 2017. Investigating blue light illumination on human retinal pigment epithelial cell lines and its potential to model Age Related Macular Degeneration in vitro. 17th Congress of the European Society for Photobiology, Pisa. 4-8/9/2017.

1 Introduction

1.1 Rationale behind the research

Age-related macular degeneration (AMD) is a complex disease arising from the interaction of multiple genes and environmental factors. AMD causes loss of central vision and is the most common cause of registerable blindness in the developed world, and for patients with atrophic or dry form of the disease there is no cure or efficient prevention method (Green and Enger, 1993; Evans and Wormald, 1996; Seddon, 2001; Johnson et al., 2005). AMD initially affects pigmented monolayer in retina called retinal pigment epithelial (RPE) which is responsible for photoreceptor homeostasis. While the exact cause of AMD is not known, the presence of extracellular deposits, called drusen between RPE and underlying Bruch's membrane is a primary feature for AMD leading to RPE dysfunction, followed by photoreceptor death and severe vision loss (Sarks et al., 1988; Killingsworth et al., 1990; Sarks et al., 1994). Main cellular features associated with RPE dysfunction in AMD are RPE barrier function breakdown (Sarks et al., 1988; Killingsworth et al., 1990; Johnson et al., 2005; Curcio and Johnson, 2013), premature senescence (Glotin et al., 2008; Davalli et al., 2016) and mitochondrial damage (Liang and Godley, 2003; Jarrett et al., 2008).

AMD is a late- or slow-onset disease with damage accumulating over time, similar to the aging process (King et al., 2004; Klein et al., 2010), consequently the major risk factor for AMD is the old age (Smith et al., 2001). Oxidative stress damage is an underlying factor in aging and many age-related neuro-degenerative diseases including AMD (Beatty et al., 2000; Jarrett et al., 2010; Jomova et al., 2010; Romano et al., 2010). Oxidative stress damage causes cellular damage mediated by reactive oxygen species (ROS). ROS are chemically reactive species that contain oxygen and occur as natural byproduct of oxygen metabolism. Intracellularly, ROS can be generated by mitochondrial activity, enzymatic processes or through photosensitizers. Throughout life, ROS can also be acquired through exogeneous activities such

as solar exposure, smoking or diet that are rich in oxidant sources (Jarrett and Boulton, 2012). Mitochondria has been identified as the main initiator of intercellular ROS damage (Liang and Godley, 2003; Jarrett et al., 2008; Brantley and Sternberg, 2012).

The retina is one of the highest oxygen consuming tissues in the human body due to its high energy demand. It contains high levels of photo-sensitizers while frequently being exposed to visible light. This micro-environment of human retina make it susceptible for ROS damage (Jarrett and Boulton, 2012). Due to its high energy and ability to induce oxidative stress in the retina, blue-light has been identified as the most dangerous part of the spectra for the retina (Young, 1988; Rozanowska et al., 1995; King et al., 2004). Previous studies on RPE showed that blue-light induced ROS generation (Rozanowska et al., 1995) originating from the mitochondria (King et al., 2004; Godley et al., 2005; Jarrett et al., 2008; Alaimo et al., 2019; Tao et al., 2019).

Most of the electronic devices today from ophthalmoscopes and ophthalmic operating microscopes to the smartphones, tablets, computers and TVs use blue light-emitting diode (LED) technology with an emission peak of 470 nm, to improve brightness and clarity (Yam and Hassan, 2005; Rozanowska et al., 2009). Moreover, in the EU, following the advice of The European Directive for the eco-design of Energy Using Products, a decision was made to progressively suppress least energy-efficient light sources and replace them with LEDs for domestic lighting, hence there is an increase in the use of low energy white LEDs, as a source of general lighting, which have a strong emission peak at 470 nm, in the blue region of the spectra (Behar-Cohen et al., 2011).

The impact of blue-light on the susceptible macula has clinically significant implications in age-related macular degeneration (AMD) pathogenesis and progression. However, the shortcomings and inconsistencies inherent in epidemiological studies to date have not allowed clinical researchers to make evidence-based recommendations on how best to prevent or reduce

progression in AMD with respect to blue-light protection (Hyman et al., 1983; West et al., 1989; Taylor et al., 1992; Cruickshanks et al., 1993; Darzins et al., 1997; Downie et al., 2019; Modenese and Gobba, 2019). Nevertheless, in clinical practice patients are advised to wear blue/UV blocking glasses and blue-blocking intraocular lenses are used in cataract surgery. Little is known about the long-term photobiological impact of intermittent and sustained ambient exposure on the target tissue relevant to AMD, the retinal pigment epithelium (RPE). In order to better understand the mechanisms and derive evidence to inform clinical practice, relevant in-vitro studies are required to define the risk and mitigate long term consequences especially with increased use in blue-emitting devices. In addition blue-light exposure levels in terms of power and duration needs better defined to allow a logical approach to the risk/benefit both for individuals at risk of AMD and those already affected, stratified by genotype-phenotype (Popoola, 2016; Downie et al., 2019; Modenese and Gobba, 2019).

1.2 Aims and Objectives

The main aims of this research was **1)** to understand better the effect of blue-light (470 nm) on RPE cells and **2)** to leverage this understanding to develop a blue-light induced in-vitro disease model that recapitulates cellular features of AMD. To this end, we designed an ad-hoc LED array to illuminate RPE cells cultured in multi-well plates. This allowed us to perform standard biochemical assays and immunostaining such as; detection of reactive oxygen species, Zonulae occludens-1 (ZO-1) staining, Protein Kinase C-ζ (PKC-ζ) inhibition, senescence associated β-galactosidase staining and Mitotracker™. Then using specialists Electric Cell-substrate Impedance Sensing (ECIS) multi-well arrays, the time-course effect of blue-light on RPE cells was investigated and quantified in a label free manner.

The first part of the research aimed to study the effect of blue-light (470 nm) on the tight junction associated barrier function of human RPE cells, for the first time and evaluate the potential recovery/protective effect of PKC- ζ

inhibition against blue-light induced barrier function breakdown. In addition, the effect of shorter wavelength blue-light (420nm & 400 nm) as well as green light (525 nm) on the barrier function has also been investigated.

The second part of the research leveraged the knowledge acquired previously to recapitulate in-vitro the cellular features associated with AMD with blue-light (470 nm). Premature senescence, barrier function breakdown and mitochondrial damage, before cell death occurred were modelled simultaneously for the first time in an in-vitro model induced by only blue-light (470 nm). We compared our blue-light induced in-vitro model against TBHP- and H_2O_2- induced models for their ability to allow studying/recapitulating the cellular features of AMD before cell coverage declined. Moreover, the potential of designing an in-vitro AMD model induced by daily/intermittent blue-light exposure that takes into account the emergent effect of post exposure oxidative stress was investigated. Finally, the possibility of enhancing the blue-light induced AMD model with pigment granules, has also been explored.

2 Theoretical Background

2.1 Age Related Macular Degeneration

Age-related macular degeneration (AMD) is a genetically complex chronic progressive neurodegenerative disease interacting with environmental factors. AMD is a leading cause of vision loss worldwide, with currently no cure or efficient prevention method (Green and Enger, 1993; Evans and Wormald, 1996; Seddon, 2001; Johnson et al., 2005; Lim et al., 2012). AMD primarily affects pigmented monolayer in the central retina called retinal pigment epithelium (RPE), which is responsible for homeostasis of overlaying photoreceptor cells. While the exact cause of AMD is still unknown, primary feature for AMD is the presence of extracellular deposits called drusen between the RPE and underlying Bruch's membrane (Sarks et al., 1988; Killingsworth et al., 1990; Sarks et al., 1994).

The disease occurs in two stages; Early-AMD and Late-AMD. Most of the vision loss occurs in the late stages of the AMD where the damage to RPE substantially and progressively increase with age (Lim et al., 2012) eventually leading to RPE dysfunction, followed by photoreceptor death (Sarks et al., 1988; Killingsworth et al., 1990; Sarks et al., 1994). Symptoms for Early-AMD are soft indistinct or reticular drusen, any soft drusen type with RPE depigmentation or with increased retinal pigment (Killingsworth et al., 1990; Green and Enger, 1993; Sarks et al., 1994; Seddon, 2001; Holz et al., 2012). Late-AMD has two forms; dry and wet (Sarks et al., 1988; Holz et al., 2012). Atrophic AMD or geographic atrophy is the dry form of Late-AMD and the symptoms are membranous debris, dot-like soft drusen and characteristic lesions with atrophied (degenerated) RPE. This eventually leads to RPE loss in affected areas in which choroidal vessels are more visible than in surrounding areas in fundus examination (Sarks et al., 1988; Holz et al., 2012). Neovascular-AMD or exudative-AMD is the wet form and symptoms include soft drusen, leaky choroidal vessels breaking through Bruch's membrane and RPE, leading to RPE detachment and disciform scarring where retinal tissue

is replaced by vascular scar tissue (Killingsworth et al., 1990; Green and Enger, 1993; Holz et al., 2012). In both forms of the disease the outer blood-retina barrier (outer BRB) formed by the tight junctions between RPE cells are altered or lost (Sarks et al., 1988; Killingsworth et al., 1990; Johnson et al., 2005; Curcio and Johnson, 2013). In addition other cellular features associated with RPE dysfunction seen in AMD are premature senescence (Glotin et al., 2008; Davalli et al., 2016) and mitochondrial damage (Liang and Godley, 2003; Jarrett et al., 2008).

2.1.1 AMD Risk factors

The major risk factor for AMD is ageing. Late stages of AMD are observed with more than 10 % of people who are older than 80 years. In addition female sex is also reported as a risk factor for AMD (Smith et al., 2001).

Systemic risk factors are cigarette smoking (Seddon et al., 1996; Chakravarthy et al., 2010), obesity (Seddon et al., 2003), excessive sun-light exposure (Mitchell et al., 1998) and cardiovascular risk factors such as hypertension (Snow and Seddon, 1999; Chakravarthy et al., 2010; Reynolds et al., 2010). People with AMD possess higher risk for cardiovascular diseases and stroke (Snow and Seddon, 1999).

Ocular risk factors are darker iris pigmentation (Snow and Seddon, 1999), history of cataract surgery (Cugati et al., 2006) and farsightedness (hyperopia) (Sandberg et al., 1993). Statistical analysis combining data from multiple studies suggested that history of cataract surgery to be a strong risk factor for AMD (Snow and Seddon, 1999; Modenese and Gobba, 2019). Operating microscopes used during cataract surgery utilize blue LED technology that can reach up to 9700 W/m^2 and the operation can last up to 2 hours (Kirkness, 1986; Rozanowska et al., 2009). In the studies by Cruickshanks et al., (1993) and Klein et al. (1998) increased risk of AMD progression has been directly correlated with increased exposure to blue-light. The phototoxic effect of light from ophthalmic instruments are well documented (Jaffe et al., 1988; Michels and Sternberg, 1990; Michels et al., 1992; Davidson and Sternberg, 1993).

Even though blue-light from ophthalmic instruments apply acute exposure to the retina, the oxygen dependent nature of the damage indicates an oxidative mechanism (Margrain et al., 2004). In a study by Age-Related Eye Disease Study Research Group (2001) dietary anti-oxidant supplements (vitamins C and E, β-carotene and zinc) have been shown to slow the progression of AMD from early to late stages, and both animal studies and in-vitro experiments have demonstrated generation of reactive oxygen species (ROS) in RPE, which strengthen the hypothesis of blue-light phototoxicity has important implications in AMD pathogenesis (Margrain et al., 2004; Lim et al., 2012).

2.1.2 Genetic factors in AMD

Genome wide analyses revealed that Complement Factor H (CFH) gene (1q32) and the ARMS2 (10q26) locus are the major susceptibility factors for AMD pathogenesis, being responsible for more than 60% of severely affected cases, while Complement Component 2 (C2), Complement Factor B (CFB) and Apolipoprotein E (APOE) genes confer a smaller effect (Holz et al., 2012).

Complement cascade is a part of our innate immune system and is formed by over 30 proteins, which regulate immune response against microbes through the release of pro-inflammatory cytokines. Histological studies have shown the presence of complement factors in drusens (Patel et al., 2008; Holz et al., 2012). A single nucleotide polymorphism (SNP) on Complement Factor H (CFH) gene, is identified as a major susceptibility factor for AMD being responsible for approximately 43 % of the cases (Haines et al., 2005). CFH is the key regulatory protein of an alternative pathway that initiates a proteolytic cascade that releases pro-inflammatory anaphylatoxins leading to formation of membrane attack complexes that lyse the cell. CFH limits the amplification phase of the alternative complement cascade. Y402H allele of the CFH gene on chromosome 1q32 impairs this regulatory function of CFH and complement over-reacts to cellular damage and retinal debris (Patel et al., 2008; Holz et al., 2012).

Two other factors in complement cascade, which are also identified to contribute to AMD pathogenesis are Complement Component 2 (C2) and Complement Factor B (CFB). C2 and CFB are the activators of the classical and alternative pathways respectively. 4 variants of the CFB and C2 genes resulting from polymorphisms are identified to show protective effect against AMD pathogenesis. The genome wide analysis showed that 74 % of the individuals with AMD lacked the protective variants of either CFH, CFB or C2 genes. On the other hand, 56 % of the individuals without AMD had a protective variant of either of these genes (Patel et al., 2008; Gold et al., 2010; Holz et al., 2012).

AMRS2/HTRA1 locus at 10q26 is another strong susceptibility factor associated with AMD. A single nucleotide polymorphism (SNP) called rs10490924 at this locus resulting in alanine to serine change (A69S change), found to increase the risk of AMD up to 15 times (Holz et al., 2012). However two nearby genes age-related maculopathy susceptibility 2 (AMRS2) and high-temperature requirement factor 1 (HTRA1) show strong linkage disequilibrium at this locus, therefore it has not been possible to identify the genetic association of this locus between these two genes (Fritsche et al., 2008). While Oka et al. (2004) suggests that a change in HTRA1 gene may inhibit Transforming Growth Factor – β (TGF - β) which is a negative growth regulator in RPE. Fritsche et al. (2008) suggests a change in ARMS2 gene may cause mitochondrial dysfunction in RPE.

Apolipoprotein E (APOE) gene which regulates lipid and cholesterol transport in the central nervous system has also been associated with AMD pathogenesis. In the eye APOE is expressed in Bruch membrane, RPE, photoreceptor cells, retinal ganglian cells and Muller cells. There are 3 common variants of APOE gene; E2, E3, E4; E3 being the most prevalent. Allele and genotypic studies showed that E4 had a protective effect against AMD while E2 has a causative effect. As a result of cellular damage and inflammation, APOE gene gets upregulated and dimerized. APOE E4 prevents

dimerization, thus allows faster transportation of lipids, cholesterol and RPE degeneration products away from RPE across Bruch membrane, preventing accumulation that would lead to drusen and AMD. Furthermore, while E2 variant enhances the expression of angiogenic cytokines; vascular endothelial growth factor (VEGF) and fibroblast growth factor (FGF), E4 variant supresses expression of these cytokines to limit neovascularization (Patel et al., 2008; Holz et al., 2012).

2.1.3 Blood-Retina Barrier in AMD

The blood-retinal barrier (BRB) plays a fundamental role in the retinal microenvironment by regulating the selective nutrient-waste exchange between the blood and the retina. It prevents leakage into the retina and contribute to the homeostasis of the retinal tissue (Cunha-Vaz, 2009; Ambati et al., 2013). The integrity of BRB is important in order to maintain normal visual function. The BRB consists of two components: inner BRB and outer BRB. The tight junctions (zonulae occludentes) between the retinal endothelial capillary cells establish the barrier function at the inner BRB, while the barrier function at the outer BRB is established by the tight junctions between retinal pigment epithelium (RPE) cells (Figure 1) (Cunha-Vaz et al., 2011).

The retinal endothelial capillary cells are directly associated with the differentiation and polarisation of the inner-BRB function. These endothelial cells sit on the retinal capillary basal lamina formed by pericytes and Muller cells. The endothelial cells together with Muller cells regulate the diffusional barrier. Any changes in the retinal neural circuitry are transmitted by pericytes and Muller cells to the retinal endothelial cells to influence the activity of the inner-BRB. On the other hand, a single layer of RPE cells forming the outer-BRB, maintains retinal adhesion, separates the neural retina from the choriocapillaries and regulates nutrient-waste exchange between blood and the photoreceptors, contributing to the photoreceptor homeostasis. This metabolic relationship between the RPE and photoreceptor cells at the outer-BRB is very critical to establish normal visual function. Clinical studies, showed

that alterations in the outer-BRB is related to pathologies of RPE in AMD (Cunha-Vaz, 2009).

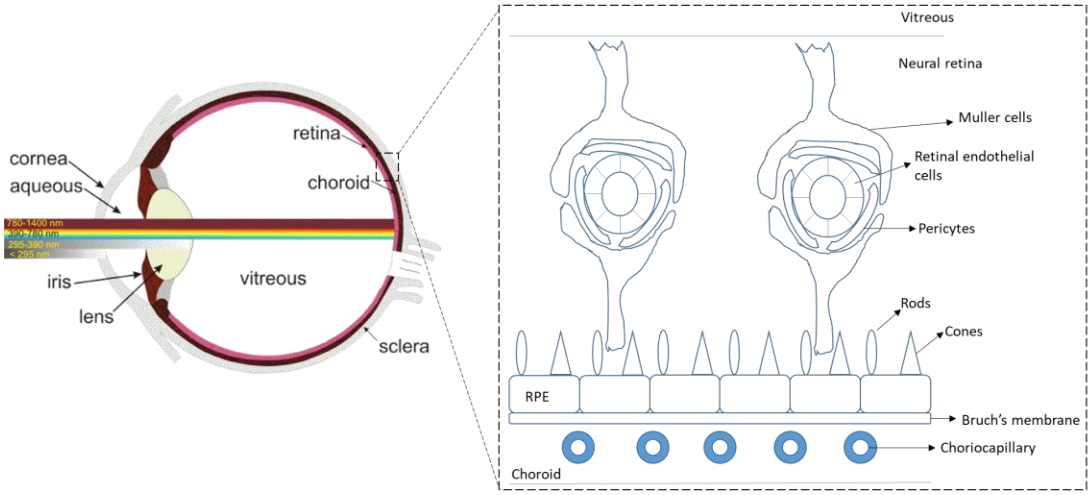

Figure 1 The inner and outer blood-retina barriers and their relative locations. The tight junctions (zonulae occludentes) between the retinal endothelial capillary cells establish the barrier function at the inner BRB, while the barrier function at the outer BRB is established by the tight junctions between retinal pigment epithelium (RPE) cells. [Modified from Tomi and Hososya (2008) and Rozanowska et al. (2009)]

Multiple protein complexes play an important role in the integrity of the outer-BRB tight junctions. The trans-membrane protein complex at the tight junctions is formed by occludin, claudin, junctional adhesion molecule and tricellulin. The scaffold protein Zonulae occludentes-1 (ZO-1) is responsible for cross-linking and adhering these proteins together by interacting with their intra-cellular C-terminal domain (Jain et al., 2011). The protein scaffold complex Par6/Par3/PKC-ζ has a critical role regulating the polarity of the tight junctions (Henrique and Schweisguth, 2003). Protein Kinase C zeta (PKC-ζ) from this protein complex also phosphorylates occludin on specific threonine residues to promote tight junction assembly (Figure 2) (Jain et al., 2011).

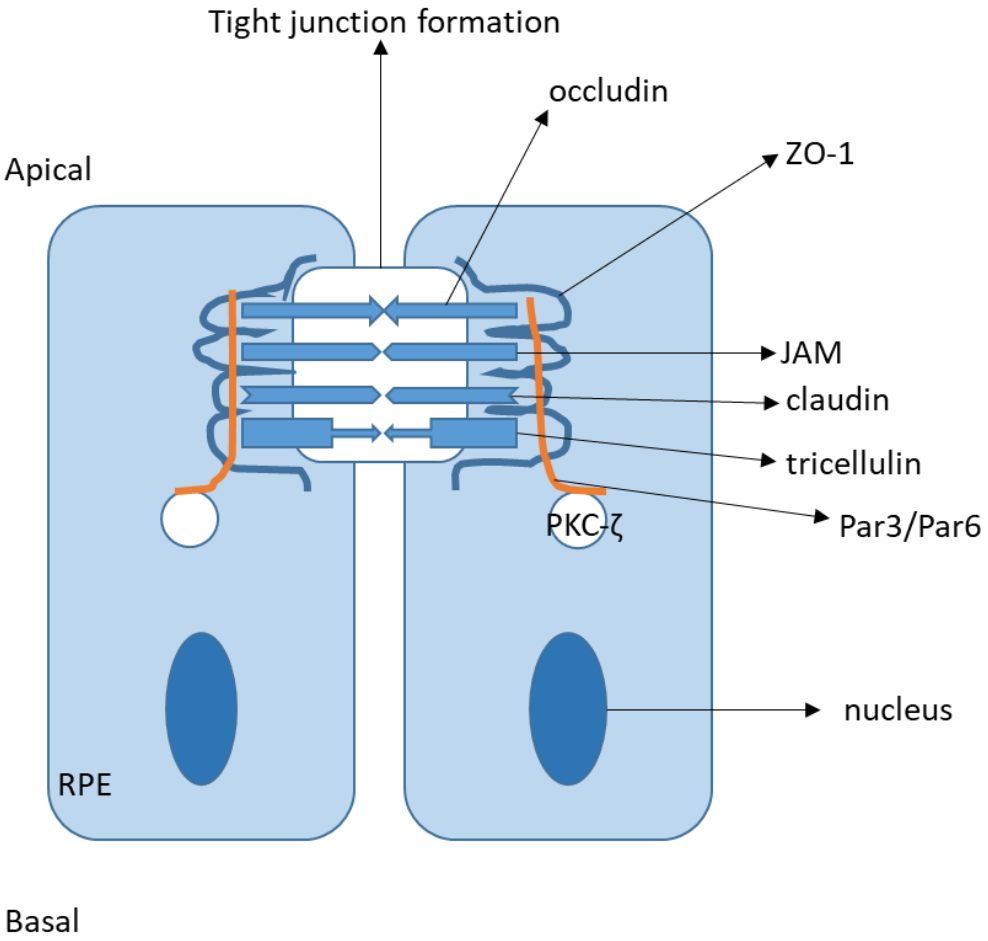

Figure 2 Tight junction protein complex at the outer blood-retina barrier. Occludin, claudin, junctional adhesion molecule (JAM) and tricellulin form the trans-membrane protein complex at the tight junctions. ZO-1 interacts with C-terminal domains of these proteins and cross-links and adheres these proteins together. Par6/Par3/PKC-ζ scaffold complex is responsible for regulating the polarity of the tight junctions. To promote the tight junction assembly PKC-ζ also phosphorylates occluding on specific threonine residues. [Modified from Omri et al., (2010)]

Normally PKC-ζ localizes in the tight-junction protein complexes of RPE and in photoreceptor inner segments (Omri et al., 2013). As a result of pro-inflammatory cytokine response initiated in AMD, pro-inflammatory cytokines activate PKC-ζ. Upon induced activation (phosohorylation at threonine 410), PKC-ζ delocalizes from the plasma membrane leading to outer-BRB breakdown (Crisanti et al., 2006; Omri et al., 2013; Jaadane et al., 2015b; Jaadane et al., 2017).

VEGF and TNF-α, key regulators of vascular permeability in the pathogenesis of the AMD, are also activated as a result of pro-inflammatory cytokine response (Mirshahi et al., 2012; Lin et al., 2018). VEGF and TNF–α induce vascular permeability through different mechanisms (Lin et al., 2018). While VEGF induces vascular permeability through phosphorylation, ubiquitination and degradation of occludin (Murakami et al., 2009; Murakami et al., 2012). TNF – α induces vascular permeability through NF-κB activation and downregulation of claudin-5 and ZO-1 (Aveleira et al., 2010). In mouse models Lin et al. (2018) demonstrated the activation of PKC–ζ in response to both VEGF and TNF-α activation. Furthermore, they have demonstrated that the early inhibition of PKC–ζ prevented both VEGF- and TNF– α- induced vascular permeability, showing that the activation of PKC–ζ is required for both VEGF- and TNF–α- induced vascular permeability response. Therefore, PKC-ζ is a potential target for drugs against AMD pathogenesis.

Recent blue-light studies on rats by Jadaane et al. (2015a; 2017) placed PKC-ζ at the interface of apoptosis, oxidative stress response and necrosis. These studies showed that upon blue light exposure PKC-ζ gets activated (by phosphorylation at threonine 410) and initially delocalizes to the cytoplasm. Following stress, activated PKC-ζ initiate the phosphorylation cascade that leads to the activation of NF-κB (by phosphorylation on serine 311), which is a cell survival pathway in stress response, modulating apoptosis through the synthesis of anti-apoptotic factors (Jaadane et al., 2017). Previous studies on rats also showed that blue-light induced retinal degeneration activates a caspase-independent pathway; LEI/L-DNase-2 which induces apoptosis (Chahory et al., 2004; Chahory et al., 2010). Cytoplasmic leukocyte elastase inhibitor (LEI) gets activated through cleavage by proteases and is transformed into the nuclear protein L-DNase-2 to induce apoptosis (Chahory et al., 2004; Chahory et al., 2010). However, Jaadane et al.,(2015b) showed that PKC-ζ activation by blue-light inhibited L-DNase-2 translocation to nucleus consequently inhibiting induction of apoptosis by this pathway. Prolonged stress conditions such as blue-light exposure increases the expression of

PKC-ζ leading to over-activation of PKC-ζ (Omri et al., 2013; Jaadane et al., 2017). Over-activation of PKC- ζ has also been shown to activate receptor-interacting protein kinases (RIP kinases) 1 and 3, which mediate necrosis (Jaadane et al., 2015a; Jaadane et al., 2017; Jorgensen et al., 2017). On the other hand, it has also been shown that while expression of prostate apoptosis response 4 (PAR4), a tumor suppressor protein that induce apoptosis, is low in early blue-light response, prolonged exposure increases PAR4 expression. Consequently, PAR4 associates to activated PKC-ζ resulting in inhibition of NF-κB survival pathway and can induce apoptosis (Wang et al., 2005; Jaadane et al., 2015b). While the conditions that lead to these different cell fates still need investigation, translocation of PKC- ζ to the nucleus was observed in both apoptosis and necrosis mediated cell death (Crisanti et al., 2006; Jaadane et al., 2015a; Jaadane et al., 2017).

2.1.4 Drusen in AMD

Extracellular deposits accumulating between RPE and Bruch's membrane or sometimes between RPE and photoreceptor cells are called drusen (Curcio et al., 2013). Presence of soft drusen in the macular is a major risk factor in AMD with increased numbers and sizes of drusen correlating with the increased risk of advanced AMD (Sarks et al., 1994; Crabb et al., 2002).

The major source of drusen components is RPE (Hageman et al., 2001). Proteomic, histologic and biochemical analyses of drusen revealed that its main components are albumin, apolipoprotein E (APOE), complement factors immunogloblulins and amyloid-β (Crabb et al., 2002). Crabb et al. (2002) showed that 65 % of the identified proteins were common in drusen from both normal and AMD donors. However, they have identified that oxidative protein modifications associated with drusen proteins were more abundant in AMD compared to normal donors, indicating the contribution of oxidative stress to AMD pathogenesis.

Wang et al., (2009) showed that drusen contains autophagy and exosome markers. Furthermore, they have demonstrated that increased mitochondrial

DNA damage due to oxidative stress resulted in increased autophagy markers and exocytosis activity and decreased the lysosomal activity. In their experiments, Wang et al. (2009) also demonstrated that exosomes released by mitochondrially damaged RPE were coated with complement factors and can bind to CFH. Therefore, it is hypothesized that drusen biogenesis may occur as a result of increased autophagy and the release of intracellular proteins via exosomes by the aged RPE.

2.1.5 Lipofuscin in AMD

Photoreceptor outer segments and RPE cellular components are continually being phagocytosed and renewed by RPE in a process called autophagy. During this process lysosome fuses with phagosome and the content undergoes lysosomal degeneration. However with age, cumulative oxidative stress, causes acidification of lysosome/phagosome, as well as oxidation of their lipid and protein content (Boulton and Dayhaw-barker, 2001). This results in incomplete lysosomal degeneration and formation of residual bodies. The general name given to these intracellular residual bodies is age pigment or lipofuscin (Rozanowska et al., 2009; Rozanowska, 2012).

RPE lipofuscin granules are different from lipofuscin in other tissues in buoyant density, composition and extractability (Eldred, 1987). They are highly unsaturated lipids that test negative for cholesterol and glycolipid, sulfhydryl compounds (Brizzee and Ordy, 1981). Lipofuscin accumulation starts as early as 16 months in the basal and peripheral portions of healthy RPE (Streeten, 1961). Mature lipofuscin granules appear homogenously and they show resistance against extraction with fat solvents (Brizzee and Ordy, 1981). By the age of 50, lipofuscin granules begin to appear among apically located melanin granules forming melanolipofuscin granules. So as the number of lipofuscin granules increases, the number of true RPE melanin decreases, which corresponds to the increase in melanolipofuscin granules (Free-Burns and Katz, 1992).

Lipofuscin granules are auto-fluorescent when illuminated with light between 340-640 nm (Boulton et al., 1990; Marmorstein et al., 2002). Therefore, lipofuscin accumulation can be detected by laser scanning ophthalmoscopy (Schmitz-Valckenberg et al., 2002) or in histological section with fluorescence microscopy (Sohal, 1984; Seehafer and Pearce, 2006; Jung et al. 2010). Lipofuscin granules contain different fluorophores (Docchio et al, 1991) with an excitation maximum around 340–395 nm, which shows two emission maxima (430–460 nm and 540–640 nm). When excited at 364 nm, RPE lipofuscin exhibits a main emission peak at 600-610 nm (golden-yellow) as well as lesser peaks at 470 nm (blue) and 550nm (green), and in the case of individuals over 50 years old, another peak at 680 nm (red). The red component of lipofuscin emission was consistently found to increase with age. Similar emission peaks were observed as the excitation wavelength was set at 488 nm (Boulton et al., 1990; Marmorstein et al., 2002; Borrelli et al., 2019). Importantly, Bruch's membrane under RPE, also exhibit strong autofluorescence at 485±5 nm, when excited with 364 nm light. On the other hand, at 488 nm excitation, Bruch's membrane and sub-retinal deposits in healthy eyes show minimal autofluorescence (Marmorstein et al., 2002). Therefore, in clinical practice short-wavelength autofluorescence at 488 nm is commonly used to evaluate RPE health and presence of geographic atrophy, as areas affected by geographic atrophy show very low to extinguished autofluorescence as RPE cell death is accompanied by loss of lipofuscin (Teussink et al., 2017; Borrelli et al., 2019). Lipofuscin shows broad structureless absorption spectra between 300 - 550 nm with the absorption declining with increasing wavelength (Figure 3a) (Avalle et al., 2005). When irradiated with narrow-band light (290 - 578 nm) in aerobic conditions, lipofuscin granules uptake oxygen. This oxygen uptake is both wavelength- and age- dependent. The rate of oxygen uptake exponentially increases with decreasing wavelength of light in the range of 578nm to 290nm, and is at minimal levels in the green spectral range (Rózanowska et al., 1995). In addition, the photoreactivity of lipofuscin granules increase with age

(Rózanowska et al., 2004). As lipofuscin granules contains an abundance of polyunsaturated lipids, photo-excitation of lipofuscin granules with blue-light leads to generation of singlet oxygen, superoxide, hydrogen peroxide, lipid hydro-peroxides and melondialdehyde (Boulton et al., 1993). The action spectrum for singlet oxygen production by lipofuscin is between 300 – 450 nm with a peak at 380 nm (Figure 3b) (Avalle et al., 2005).

Lipofuscin granules have both chloroform-soluble and chloroform-insoluble part, both capable of undergoing photo-oxidation. However it is not known whether the primary photo-oxidizing chromophores are in the chloroform-soluble or insoluble fraction. To date, only one type of lipofuscin granule is identified; N-retinylidene-N-retinylethanolamine (A2E), which is chloroform soluble. A2E has been shown to be phototoxic to RPE in vitro however it only has a minor role in lipofuscin photoreactivity and phototoxicity (Rózanowska et al., 2004). Photochemical studies on A2E further revealed that A2E and its isomer; iso-A2E exist in a photo-equilibrium of 4:1 (A2E: iso-A2E) ratio (Parish et al., 1998). The action spectra for ROS production by A2E is associated to be between 415-455 nm with a peak at 430 nm (Figure 3d) (Avalle et al., 2005; Arnault et al., 2013; Marie et al., 2018). As this action spectra is different from ground state action spectra of lipofuscin it indicates that more reactive species than A2E are present in lipofuscin (Avalle et al., 2005). The absorbance spectra of A2E is between 300 – 550 nm and displays a major peak at 435 nm and a lesser peak at 335 nm (Figure 3c) (Parish et al., 1998). On the other hand, emission spectra of A2E varies depending on the hydrophobic nature of the solvent (Sparrow et al., 1999). A2E in methanol shows an emission peak at 600 nm generated by an excitation spectrum between 320 – 550 nm with a peak at 418 nm (Figure 3e) (Sparrow et al., 2000). The internalized A2E in paraformaldehyde fixed RPE showed an emission peak between 565-570 nm, when excited with 488 nm light (Figure 3f) (Sparrow et al., 1999).

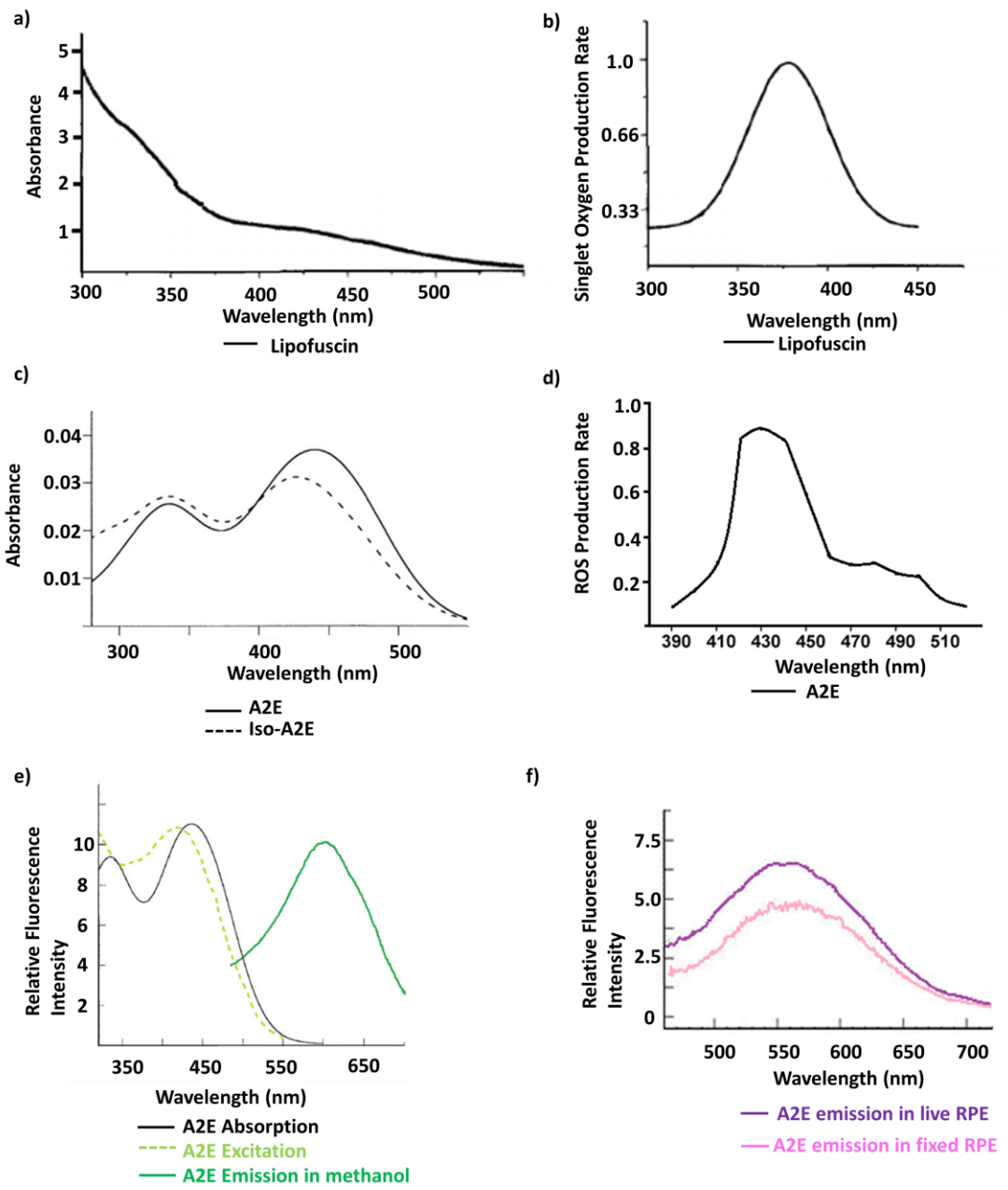

Figure 3 Lipofuscin & A2E Absorption, Action, Excitation & Emission Spectra. **a)** Absorption Spectrum of lipofuscin in chloroform **b)** Action Spectrum for singlet oxygen production by lipofuscin in chloroform **c)** Absorption spectra of A2E and iso-A2E in chloroform **d)** The action spectra associated with A2E as characterized by increase in ROS production in A2E-fed porcine RPE cells under solar irradiance levels **e)** Absorption, excitation and emission spectra of A2E in methanol **f)** Emission spectra of A2E in live- and fixed-RPE cells. [Modified from Parish et al., (1998); Sparrow et al., (1999); Sparrow et al., (2000); Avalle et al., (2005); Rozanowska et al., (2009); Arnault et al., (2013)]

A2E occurs as a byproduct of the visual cycle and is a derivative of all-trans retinal (Firestone et al., 1979). Photoreceptor cells, namely rods and cones are

responsible for visual photo-transduction. Rhodopsin is a visual pigment and a chromophore found in rods. Rhodopsin is a G-protein coupled receptor with 11-cis retinal. Rhodopsin photo-bleaches as a results of interacting with blue-light. Photo-bleaching and regeneration of rhodopsin is an essential cycle for vision (Palczewski, 2006). During photo-bleaching, 11-cis retinal as part of rhodopsin is converted into all-trans retinal upon interaction with blue-light, forming meta rhodopsin 2 (Rozanowska and Sarna, 2005). As a result of this interaction A2E, a deuterated Vitamin A, occurs as a byproduct. While A2E is headed to RPE cells for lysosomal degradation, Meta rhodopsin 2 is transferred into cones and converted into all-trans retinol (Vitamin A) by retinal dehydrogenase enzyme (RDH). All trans retinol then is carried to RPE cells for regeneration of 11-cis retinal and returned to the photoreceptor cells (Figure 4) (Bavik et al., 2015).

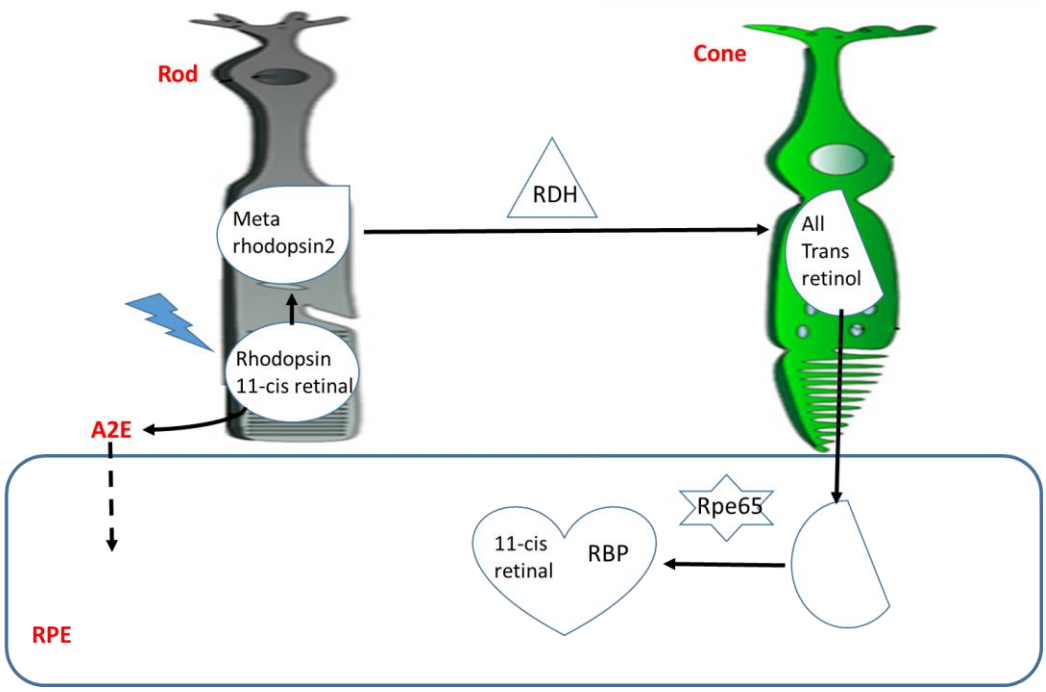

Figure 4 Rhodopsin cycle. 11-cis retinal as part of rhodopsin cycle is converted into all-trans retinal upon interaction with blue-light, forming meta rhodopsin 2. Meta rhodopsin 2 is transferred into cones and converted into all-trans retinol by retinal dehydrogenase (RDH) enzyme. All-trans retinol is then carried to RPE cells for regeneration of 11-cis retinal. First all-trans retinol is acquired to retinal binding protein (RBP) by Rpe65 protein then all-trans retinol is converted into 11-cis retinal by RBP and is returned to photoreceptors (Bavik et al., 2015). [Modified from Kazilek and Cooper (2010)]

2.1.6 Melanosomes in AMD

Retinal pigment epithelium (RPE) is heavily pigmented with melanosomes, which are cytoplasmic organelles of lysosomal origin. Melanosomes in RPE synthesize melanin during fetal development and the first year of life. Due to limited melanin turnover in postmitotic cells once formed melanin is present in RPE throughout life (Rózanowski et al., 2008). Melanin serves as a natural UV and blue-light protection, it absorbs light in 300-700 nm range, where absorption coefficient increases with decreasing wavelength (Boulton et al., 1990). Melanin converts absorbed photon energy into heat preventing excited triplet state formation (Rózanowski et al., 2008). Moreover, melanin contain centres that scavenge free radicals and ROS. However as we age melanosomes undergo significant age-related changes through a combination of photochemical modification and lysosomal degradation which alter their spectral characteristics (Boulton et al., 1990; Rózanowski et al., 2008; Boulton, 2014). The total number of pure melanin granules in RPE is observed to decline after 40 years of age. This loss of pure melanin granules correlate with association of melanin to lysosome and/or lipofuscin granules. Association of melanin to the lysosome leads to typical loss of its cigar-shaped structure and this is believed to indicate melanin under repair, modification or degradation. On the other hand, origins of melanolipofuscin granules is unclear. While it has been suggested that melanolipofuscin forms from a fusion of lipofuscin granules with melanin. Due to heterogeneity of melanolipofuscin granules it is also suggested that a process where lipofuscin is actively deposited on melanin is also suggested (Boulton and Dayhaw-barker, 2001).

2.1.7 Senescence in AMD

Senescence is a phenomenon characterized by cellular arrest in G1 or G2 phase of the cell cycle, increased cell size and increased β-galactosidase activity (Sikora et al., 2011). Senescent cells show elevated DNA damage, especially double strand breaks and corresponding DNA damage response. Senescence induce limit in cell division and resistance to apoptosis (Blasiak et al., 2017). Senescent cells are still metabolically active and stay alive for a long

time. They secrete lots of inflammatory cytokines and chemokines, matrix remodelling proteases and growth factors. This secretory phenotype known as senescence associated secretory profile (SARP) can initiate abnormal immune system response, induce cancer development and low grade inflammation which promote aging and age-related diseases (Franceschi et al., 2006; Freund et al., 2010; Hoare and Narita, 2013; Van Deursen, 2014).

Senescence can be induced under certain stress conditions due to environmental and lifestyle factors. In aging retina, majority of RPE cells become senescent due to stressors such reactive oxygen species, incomplete lysosomal degradation which affects homeostasis and DNA damage response. Senescent RPE cells can no longer repair the damaged RPE, which may lead to AMD (Blasiak et al., 2017).

2.1.8 Mitochondrial damage in AMD

Significant decrease in mitochondrial number and area have been observed in RPE of AMD donors with increased age (Feher et al., 2006). Nordgaard et al., (2008) reported increased deficiency in cytochrome c oxidase complex with the progression of AMD. Cytochrome c oxidase is the last enzyme in the electron transport chain and it is responsible for catalysing electron transfer from reduced cytochrome c to oxygen (Abdulhag et al., 2015). It has been demonstrated that impaired cytochrome c oxidase activity increases mitochondrial reactive oxygen species (ROS) production in the mitochondria (Srinivasan and Avadhani, 2012).

Wang et al., (2008) showed that in the aged RPE cells the primary DNA damage occurred in mitochondrial DNA rather than nuclear DNA. In their study, mitochondrial DNA damage were found to be due to the decreased expression of DNA repair enzymes; 8-oxoguanine-DNA glycosylase 1 (OGG1), DNA glycosylase in an age-dependent manner. Furthermore, Godley et al. (2008) showed that in AMD, RPE mitochondrial respiration is decreased and mitochondrial DNA damage increases and repair capacity is impaired. The cause of decreased mitochondrial DNA repair is reported to be due to the

decreased expression of DNA repair enzymes; OGG1, DNA polymerase γ and DNA ligase III in mitochondria. All in all these findings suggest that susceptibility of RPE mitochondria to oxidative damage, increased mitochondrial DNA damage and decreased mitochondrial DNA-repair mechanisms in AMD play a major role in RPE dysfunction observed in AMD pathogenesis (Jarrett et al., 2008).

2.1.9 Treatment Methods for AMD

Currently no cure is available for dry AMD or wet AMD. In the latter case palliative treatments are available such as; Anti-VEGF treatment, photodynamic treatment and laser treatment.

2.1.9.1 Laser photocoagulation

In the 1980s, laser photocoagulation was used in selected cases of patients with AMD, showing small extrafoveal and juxtafoveal choroidal neovascularization. Treatment with laser was successful in preventing further vision loss. However these treatment presented 41 % risk of immediate moderate vision loss and 50 % recurrence risk. Laser photocoagulation is now much less used (Green and Enger, 1993; Lim et al., 2012).

2.1.9.2 Photodynamic Treatment

In photodynamic treatment, first the drug verteporfin is administered intravenously and is then activated by shining infra-red light on the abnormal blood vessels. This treatment was only effective in stabilizing the condition in 53 % of the patients. Now photodynamic therapy is rarely used (Earnshaw et al., 2007; Lim et al., 2012).

2.1.9.3 Anti-VEGF treatment

VEGF is a key regulator of angiogenesis, showing four isoforms in humans. Withdrawal or interference with VEGF function disrupts vascular growth and leads to neo-vascular regression. It has been shown in animal studies that VEGF expression induces choroidal neovascularization. Therefore in recent years, new drugs based on suppression of VEGF were introduced against

choroidal neovascularization. Fist drug to be approved by FDA for wet-AMD, was pegaptanib (Macugen, Pfizer), which is a small oligonucleic acid that binds specifically against one isoform of VEGF (Lim et al., 2012). In clinical studies by Gragoudas et al. (2004) intravitreous injections into one eye per patient of pegaptanib, at a dose of 0.3, 1.0 or 3.0 mg, or “sham injections” (placebo) were delivered every 6 weeks over a 48-week period. The study found that compared to patients receiving “sham injections”, pegaptanib treatment resulted better mean visual acuity in patients, as early as six weeks after beginning the treatment and at all subsequent points. Later, more successful drugs; ranibizumab (Lucentis, Genentech/Novartis) and bevacizumab (Avastin, Genentech), that target all isoforms of VEGF have been developed.

Second drug approved by FDA for wet-AMD; ranibizumab is a recombinant humanized, monoclonal antibody Fab that neutralizes all active forms of VEGF by binding to VEGF and interrupting the binding of VEGF with its receptors (Lim et al., 2012). Clinical studies by Brown et al. (2006), compared monthly intravitreal injections of ranibizumab (0.3 or 0.5 mg) against photodynamic treatment with verteporfin, which was done every 3-months when indicated on 423 patients. The mean visual acuity increased by 8.5 letters and 11.3 letters respectively for 0.3 mg and 0.5 mg ranibizumab treatment groups, while the mean visual acuity decreased by 9.5 letters in the photodynamic treatment group. In 2 years long clinical studies with 716 patients, Rosenfeld et al. (2006) compared 24 monthly intravitreal injections of ranibizumab (0.3 or 0.5 mg) against “sham injections” control. Patients were evaluated for the same criteria as in the study by Brown et al. (2006). After 12 months, 94.5 % of patients given 0.3 mg ranibizumab and 94.6 % of patients given 0.5 mg ranibizumab lost fewer than 15 letters at visual acuity test, as opposed to 62.2 % of those receiving “sham injections”. The benefit in visual acuity due to ranibizumab was maintained at 24 months.

The third anti-VEGF drug used against wet-AMD is bevacizumab which is a full-length antibody related to parent ranibizumab molecule and is commonly

used as an off-label alternative to ranibizumab due to its cheaper cost as opposed to ranibizumab (Lim et al., 2012). Clinical trials by Martin et al. (2012) showed that ranibizumab and bevacizumab has equivalent efficiencies and found that monthly injections of bevacizumab was not inferior to monthly injections of ranibizumab. Finally a fourth anti-VEGF drug for wet-AMD, aflibercept (VEGF Trap-Eye, Regeneron/Bayer) was developed. Aflibercept is an engineered protein that binds to all VEGF isomers and is an FDA approved drug for wet-AMD (Lim et al., 2012). After an initial loading phase (which can last up to 3-months) where aflibercept was administered monthly, 2 mg of aflibercept given every 2-months showed similar efficiency to monthly ranibizumab injections in terms of stabilising vision over a 1-year period (Dixon et al., 2009; Lim et al., 2012). Importantly, recent population based date showed that registered blindness cases attributed to AMD was reduced by 50 % over a period of 10-years since the introduction of anti-VEGF treatments (Bloch et al., 2012; Lim et al., 2012). In 2-year treatment with ranibizumab, the risk of endophtalmis (inflamation of the interior of the eye) and uveitis (inflammation of the middle of the eye) was reported to be less than respectively 1.0 % and 1.3 % (Rosenfeld et al., 2006). However, these treatments may cause prolonged suppression of VEGF levels in the plasma, which may cause higher risk of vascular events, such as stroke or haemorrhage (Lim et al., 2012).

2.2 Oxidative Stress & Aging

Oxidative stress damage is an underlying factor in many neuro-degenerative diseases including AMD (Beatty et al., 2000; Jarrett et al., 2010; Jomova et al., 2010; Romano et al., 2010). Oxidative stress damage is cellular damage that is caused by reactive oxygen species (ROS). ROS are chemically reactive species that contain oxygen and occur as natural byproduct of oxygen metabolism. ROS are free radicals with one or more unpaired electrons, species with a higher energy level or powerful oxidizing agents such as superoxide anion, hydroxyl free radical, hydroperoxyl radicals and lipid peroxyl radicals. ROS acts as signalling molecules in regulatory pathways such as

apoptosis, gene expression and cell proliferation. Intracellularly, ROS can be generated by mitochondrial activity, enzymatic processes or through photosensitizers. ROS can also be acquired through exogenous activities such as irradiation, smoking or diet that are rich in oxidant sources (Jarrett and Boulton, 2012).

The body is protected from the negative effects of ROS by means of anti-oxidants that capture ROS and efficient repair mechanisms. Antioxidants in RPE are divided into two groups; enzymatic and non-enzymatic antioxidants. Enzymatic antioxidants are superoxide dismutase (SOD), catalase and glutathione peroxidase that breakdown ROS to their non-reactive components. On the other hand non-enzymatic antioxidants are glutathione, ascorbate, tocopherol and carotenoids that inactivate ROS by donating their hydrogen atoms to them (Boulton and Dayhaw-barker, 2001). Even though non-enzymatic antioxidants enter radical form, due to their ring structure they are stabilized. While glutathione can be synthesized by amino acids in RPE, other non-enzymatic antioxidants need to be supplied in diet (Davidson et al., 1994; Birben et al., 2012). As ROS are captured by antioxidants, the damaged compartments of the RPE are repaired or replaced by lipid and protein synthesis from endoplasmic reticulum complex (Fagone and Jackowski, 2009). However with age, the repair mechanisms and the antioxidant capacity of the body become weakened creating an imbalance between ROS and the protective mechanisms. This imbalance favoring ROS is defined as oxidative stress (Jarrett and Boulton, 2012). “The Free radical Theory of Aging” states that aging occurs due to cumulative damage from reactions involved by ROS (Wickens, 2001). According to “The Evolutionary Theory of Aging” as the age increases, activation of beneficial traits in the genome for reproduction and survival declines and the genes that promote senescence that may be present in the genome become promoted (Beatty et al., 2000; Gavrilov and Gavrilova, 2002).

The main source of ROS generation is mitochondria (Figure 5) (Liang and Godley, 2003; Jarrett et al., 2008; Brantley and Sternberg, 2012). Superoxide anion (O_2^-) is formed by mitochondrial electron transport chain complexes 1 and 3, as a byproduct of aerobic respiratory chain. As first part of the biochemical defence response, highly reactive O_2^- is converted by superoxide dismutase (SOD) enzyme to form dioxygen and hydrogen peroxide (H_2O_2) in the mitochondria. H_2O_2 is reduced to water and oxygen by two different enzymes; catalase and glutathione peroxidase as the second part of biochemical defence response (Farber, 1994; Jarrett et al., 2008).

On the other hand, by receiving an electron, the oxygen-oxygen bond in H_2O_2 can be broken down into hydroxide anion (OH^-) and hydroxyl radical ($\bullet OH$). In the mitochondria, the best electron source to reduce H_2O_2 are transition metal cations such as Fe^{2+} and Cu^{2+}. Reduction of H_2O_2 in the presence of these redox active metal ions occurs via Fenton chemistry to generate highly reactive hydroxyl radical ($\bullet OH$) and hydroxide anion (OH^-). Hydroxyl radical ($\bullet OH$) is responsible for the majority of the mitochondrial DNA damage (Farber, 1994; Jarrett et al., 2008).

Furthermore, superoxide anion (O_2^-) generated in the mitochondria can induce damage to Fe-S centres of mitochondrial proteins. These Fe-S centres are found in subunits of electron transport chain complexes 1, 2 and 3 as well as aconitase enzyme which regulate iron-sulphur transport. Aconitase has an active $[Fe_4\text{-}S_4]^{2+}$ cluster and interaction between O_2^- and $[Fe_4\text{-}S_4]^{2+}$ coverts this cluster to its inactive form; $[Fe_3\text{-}S_4]^{2+}$ while releasing both Fe^{2+} and H_2O_2 which contribute to Fenton chemistry. In Fenton chemistry, Fe^{2+} is oxidized by H_2O_2 to form Fe^{3+}, hydroxyl radical ($\bullet OH$) and hydroxide anion (OH^-). Then, Fe^{3+} can be reduced by reacting with another H_2O_2 to form Fe^{2+}, hydroperoxyl radical ($\bullet OOH$) and H^+ (Jarrett et al., 2008).

In addition superoxide anion (O_2^-) may react with nitric oxide (NO) which is an intracellular signalling molecule produced by mitochondrial nitric oxidase enzyme, to form peroxynitrites ($ONOO^-$) which can lead to lipid peroxidation (Rubbo et al., 2000; Jarrett et al., 2008). Lipid peroxidation (LOO^-) leads to the formation of lipid hydroperoxides (LOOH) which initiate a lipid peroxidation chain reaction (Esterbauer, 1996; Nair et al., 2007; Jarrett et al., 2008).

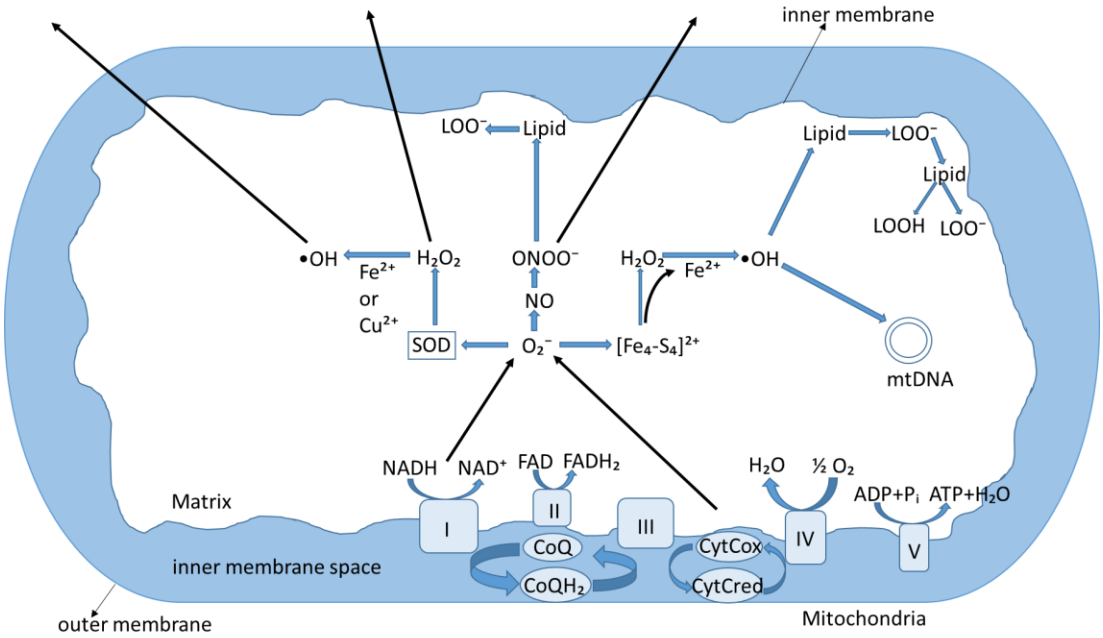

Figure 5 Major ROS generation sites in the mitochondria. Superoxide anion (O_2^-) is formed by mitochondrial electron transport chain complexes 1 and 3, as a byproduct of aerobic respiratory chain. As first part of the biochemical defence response, highly reactive O_2^- is converted by superoxide dismutase (SOD) enzyme to form dioxygen and hydrogen peroxide (H_2O_2) in the mitochondria. By receiving an electron from transition metal cations such as Fe^{2+} and Cu^{2+}, the oxygen-oxygen bond in H_2O_2 can be broken down into hydroxide anion (OH^-) and hydroxyl radical (•OH). In addition superoxide anion (O_2^-) generated in the mitochondria can induce damage to Fe-S centres of mitochondrial proteins to release both Fe^{2+} and H_2O_2. Fe^{2+} can be oxidized by H_2O_2 to form Fe^{3+}, hydroxyl radical (•OH) and hydroxide anion (HO^-). Then, Fe^{3+} can be reduced by reacting with another H_2O_2 to form Fe^{2+}, hydroperoxyl radical (•OOH) and H^+. Moreover, superoxide anion (O_2^-) may react with nitric oxide (NO) which is an intracellular signalling molecule produced by mitochondrial nitric oxidase enzyme, to form peroxynitrites ($ONOO^-$) which can lead to lipid peroxidation. Lipid peroxidation (LOO^-) leads to the formation of lipid hydroperoxides (LOOH) which initiate a lipid peroxidation chain reaction. [Modified from Jarrett et al., (2008)]

2.2.1 Oxidative damage to mitochondria

Phospholipids at the outer and inner mitochondrial membranes are subject to lipid peroxidation due to their interaction with mitochondrial ROS (Farber, 1994).

Furthermore, ROS can interact with NADH dehydrogenase, cytochrome c oxidase and ATP synthase found in mitochondrial inner membrane. NADH dehydrogenase, cytochrome c oxidase and ATP synthase are part of mitochondrial respiratory chain complex which catalyse phosphorylation of ADP to ATP. Therefore oxidative damage to the mitochondrial respiratory chain complex impairs mitochondrial energy production (Guo et al., 2013).

Compared to nuclear DNA (nDNA), mitochondrial DNA (mtDNA) is more prone to oxidative damage as it is located in mitochondrial matrix near the electron transport chain where ROS are generated. In addition mtDNA are not covered by histone proteins therefore they are directly exposed to ROS. Also mtDNA lacks introns; non-coding sequences, therefore any ROS damage is on the mtDNA is coded, furthermore it has a less efficient DNA repair mechanism than nDNA. Unlike nDNA, mtDNA is continuously replicated therefore mtDNA damage is amplified with mitochondrial and cellular division (Liang and Godley, 2003). Interaction of reactive hydroxyl radical (•OH) with deoxyribose in the mtDNA can induce loss of DNA base similar to single strand breaks. Hydroxyl radical (•OH) can also react with thymine in the mtDNA and this reaction sites are removed from the mtDNA by repair enzymes to give rise to single strand breaks (Imlay and Stuart Linn, 1988; Farber, 1994).

2.2.2 Oxidative damage to outer Blood Retina Barrier

Normally PKCs have two cysteine rich zinc finger regions at the N-terminal domain which can be oxidized by ROS. Upon oxidation, regulatory domain compromises its auto-inhibitory function and PKC gets activated (Gopalakrishna and Jaken, 2000). PKC-ζ at the tight junctions is an atypical PKC that lack one of the two cysteine-rich zinc finger regions in its regulatory

N-terminal domain (Martelli et al., 2006). This feature makes PKC-ζ more susceptible to oxidative stress (Cosentino-Gomes et al., 2012). PKC-ζ is a serine/threonine kinase which phosphorylates target proteins (Jain et al., 2011). At the tight junctions, PKC-ζ phosphorylates occludin on specific threonine residues, and co-localizes with ZO-1, to link ZO-1 with occludin (Stuart and Nigam, 1995; González-Mariscal et al., 2008; Jain et al., 2011). Rao et al., (2002) demonstrated that oxidative stress induced tyrosine-phosphorylation of both occludin and ZO-1. As a result, Rao et al., (2002) showed that oxidative stress disrupted PKC-ζ induced binding of ZO-1 to occludin and caused redistribution of ZO-1 from the apical part to the lateral and basal parts.

2.2.3 Oxidative stress induced senescence

Excessive ROS production can induce senescence through disrupting protein folding, gene transcription, DNA replication and shortening telomeres (Colavitti and Finkel, 2005; Passos et al., 2007; Lu and Finkel, 2008; Moiseeva et al., 2009; Imai et al., 2014; Van Deursen, 2014; Ziegler et al., 2015). Disruption of protein folding, gene transcription, DNA replication as well as telomeres shortening activate unfolded protein response and DNA damage response. As part of unfolded protein response (UPR) and DNA damage response (DDR) cellular signalling cascades p53 and $p16^{Ink4a}$ gets activated. Activation of p53 activates p21 to induce a temporal cell-cycle arrest through repression of target genes required to progress into S-phase. Activation of $p16^{Ink4a}$ also represses target genes required for S-phase progression and induce cell-cycle arrest. Upon continuation of stress conditions temporal cell-cycle arrest transitions into senescence (Passos et al., 2010; Van Deursen, 2014; Ziegler et al., 2015). Regardless of the stressor, senescent cells induce pro-inflammatory transcriptome (Van Deursen, 2014). UPR and DDR activate NF-κB family of transcriptional factors (Mohammed-Ali et al., 2015; Wang et al., 2017), which have been shown to regulate pro-inflammatory response (Liu et al., 2017). It has been shown by Adler et al. (2007) that NF-κB activity to be continually required to enforce many features of aging. Moreover many studies

documented NF-κB to be constitutively activated upon aging (Kriete et al., 2008; Salminen et al., 2008; Kriete and Mayo, 2009). It has been suggested by Kuilman and Peeper, (2009) and Rovillain et al. (2011) that activation of NF-κB signalling reinforced cellular senescence, implicating a possible direct or indirect cross-talk between NF-κB and signalling cascades p53 and/or $p16^{Ink4a}$.

2.3 Blue-Light and retina

Photobiological effects upon human retina highly depends on spectral characteristics of exposure and optical exposure geometry (Sliney, 2005). The light passes through cornea, lens and vitreous respectively in order to reach retina. Light with a shorter wavelength than 295 nm is absorbed in cornea and the lens absorbs the wavelengths UVB (295 – 315 nm) and UVA (315 – 390 nm). Both cornea and lens absorb some parts of infra-red especially at 980, 1200 and 1430 nm. The vitreous absorbs between 1400 nm and 10 μm. Hence, the non-ionizing radiation reaching the retina is between 390 and 760 nm which is called the visible spectrum and some infra-red between 760 and 1400 nm. The transmittance of the young eye starts from 390 nm and reaches ~80% (its maximum) at 450 nm. Due to age related changes in cornea and lens by the age of 22 only 0.1 % UV reaches the retina, and at the age 60, the transmittance begins at 400nm but only reaches ~80% at 540 nm (Figure 6) (Boettner, 1967; Rozanowska et al., 2009; Arnault et al., 2013).

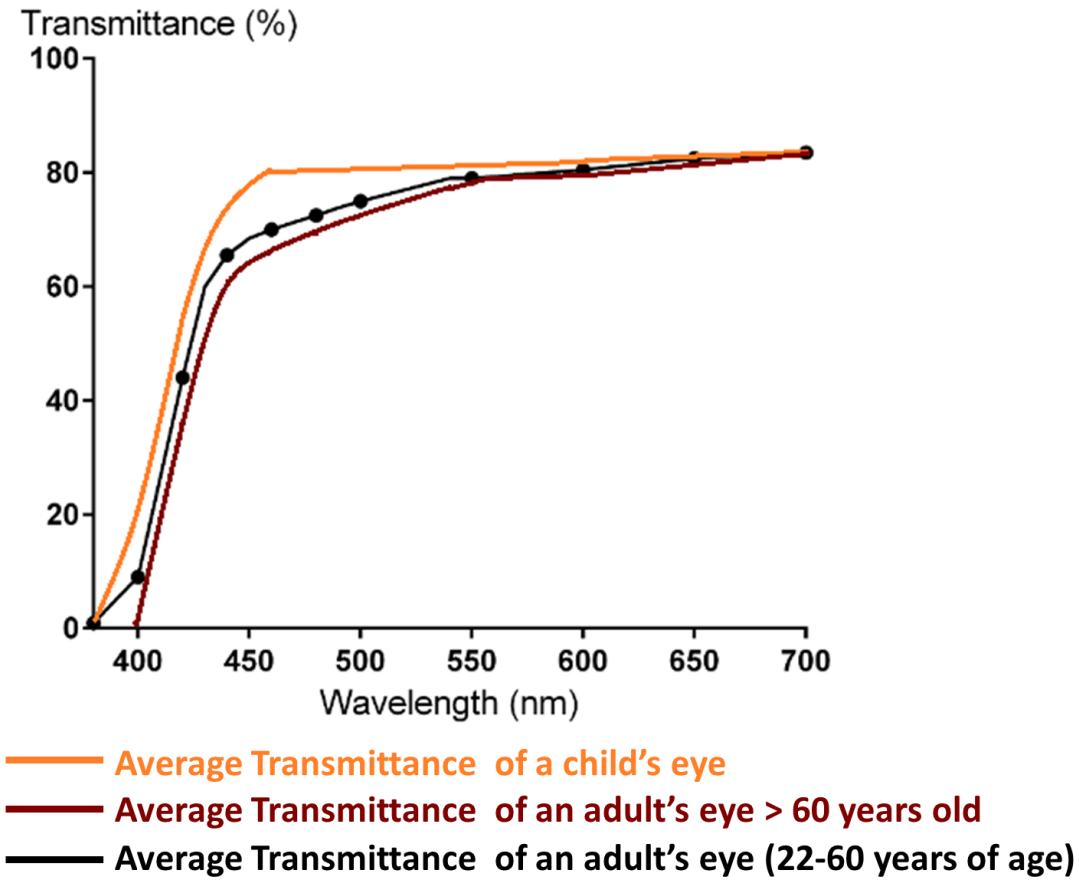

Figure 6 Age-related changes in the transmittance of the eye. The transmittance of the young eye starts from 390 nm and reaches ~80% (its maximum) at 450 nm. Due to age related changes in cornea and lens by the age of 22 only 0.1 % UV reaches the retina, and at the age 60, the transmittance begins at 400nm but only reaches ~80% at 540 nm. [Modified from Boettner, (1967); Arnault et al., (2013)]

Most of the electronic devices today from ophthalmoscopes and ophthalmic operating microscopes to the smartphones, tablets, computers and TVs use blue light-emitting diode (LED) technology with an emission peak of 470 nm, to improve brightness and clarity (Yam and Hassan, 2005; Rozanowska et al., 2009). Moreover, in the EU, no traditional incandescent light source is available since 2016 and there is an increase in the use of low energy white LEDs, as a source of general lighting, which have a strong emission peak at 470 nm, in the blue region of the spectra (Behar-Cohen et al., 2011). Blue-light is able to penetrate through the lens to the retina and can lead to irreversible photochemical retinal damage (Rózanowska,1995; Bi and Sun, 2014) through production of reactive oxygen species (ROS) (Crockett and Lawwill, 1984;

Rózanowska,1995). Due to its high energy and ability to induce oxidative stress in the retina, blue-light has been identified as the most dangerous part of the spectra for the retina (Young, 1988) and an important risk factor for AMD (Cruickshanks et al., 1993; Klein et al., 1998).

The retina is susceptible to photochemical injuries as it is one of the highest oxygen consuming tissues in the body. It is abundant in polyunsaturated fatty acids and contains high levels of photo-sensitizers while frequently being exposed to visible light. This micro-environment of retina along with its high energy demand promote generation of reactive oxygen species (ROS). The retina is protected from the negative effects of ROS by antioxidants that capture ROS and efficient repair mechanisms. However with age, the repair mechanisms and the antioxidant capacity of the retina become weakened creating an imbalance between ROS and the protective mechanisms of retina. This imbalance favouring ROS results in oxidative stress to the retina (Jarrett and Boulton, 2012).

Godley et al., (2005) demonstrated that blue-light can induce chromatin breaks in the mtDNA and ROS production in the mitochondria in primary human RPE. Furthermore King et al., (2004) showed in ARPE-19 cells that the main source of the blue-light induced ROS is the mitochondrial electron transport chain. Major mitochondrial chromophores which have an absorption peak in the blue light range are porphyrins and flavins. Porphyrin-containing proteins in the mitochondria are mainly cytochromes. On the other hand, main mitochondrial flavin-containing proteins (flavoproteins) are flavin adenine dinucleotide (FAD) and flavin mononucleotide (FMN) found in respiratory complex I and II. Mitochondrial cytochromes and flavoproteins absorb throughout the blue-light spectrum with absorption peaks between 420-440 nm and 450-520 nm respectively (Hockberger et al., 1999; Tao et al., 2019) (Figure 7).

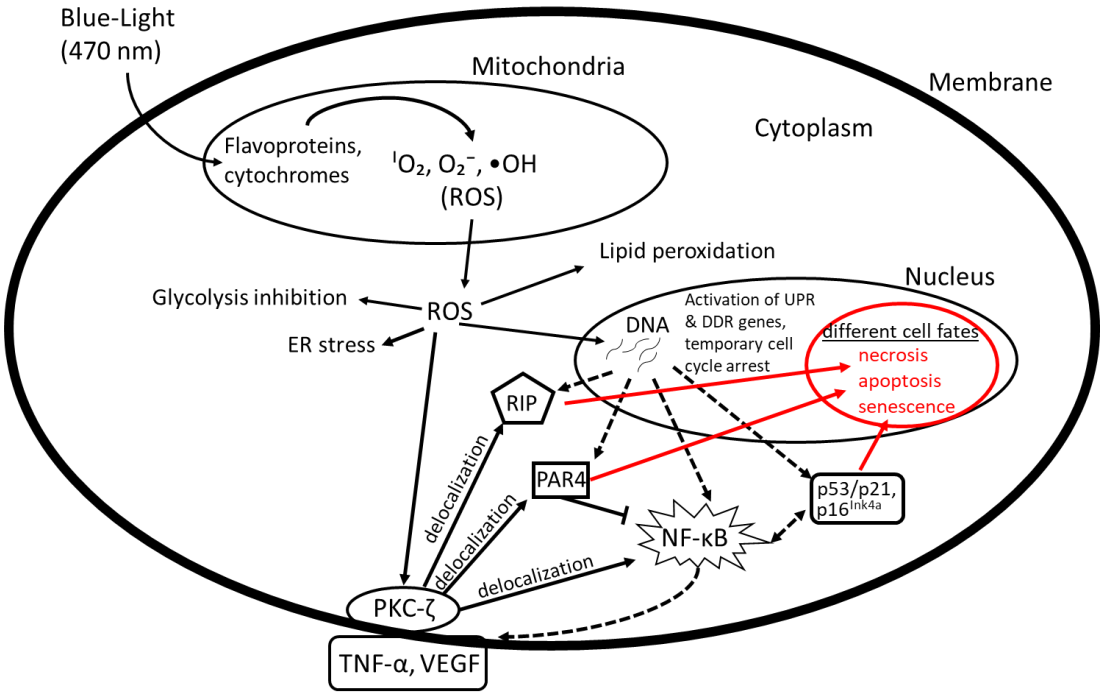

Figure 7 Likely consequences of blue-light (470 nm) induced ROS production in RPE cells. Blue-light (470 nm) may interact with flavoproteins and cytochromes in the mitochondria to induce production of ROS such as superoxide anion (O_2^-), hydroxyl radical (•OH) and singlet oxygen ($^1O_2$). When ROS exceed critical levels in the mitochondria, they can diffuse into the cytoplasm where they can react with surrounding lipids&proteins, induce endoplasmic reticulum stress (ER stress) and inhibit glycolysis (Hockberger et al., 1999). ROS such as hydroxyl radical can also cause telomere shoretening and also act as signalling molecule and activate unfolded protein response and DNA damage response genes and senescence factors. Upregulation of these genes induce pro-inflammatory cytokine response to cause PKC-ζ activation. Activated PKC-ζ delocalizes from the plasma membrane inducing barrier function break-down (Jaadane et al., 2015b). Alternatively, ROS can stimulate PKC-ζ activation by binding to PKC-ζ regulatory domain, which again results in PKC-ζ delocalization from the plasma membrane (Gopalakrishna and Jaken, 2000). Delocalized PKC-ζ can also initiate the phosphorylation cascade that leads to the activation of NF-κB, which may be simultaneously to DNA signals that activate NF-κB or it can present an alternative pathway for NF-κB activation. NF-κB is a cell survival pathway in stress response, modulating apoptosis through the synthesis of anti-apoptotic factors (Jaadane et al., 2017). In the cell, NF-κB activity is continually required to enforce many features of aging (Adler et al., 2007). Prolonged blue-light exposure has been shown to increase the expression of PKC-ζ leading to over-activation of PKC-ζ (Omri et al., 2013; Jaadane et al., 2017). Over-activation of PKC- ζ has also been shown to activate receptor-interacting protein kinases (RIP kinases) 1 and 3, which mediate necrosis (Jaadane et al., 2015a; Jaadane et al., 2017; Jorgensen et al., 2017). On the other hand, it has also been shown that while expression of prostate apoptosis response 4 (PAR4), a tumor suppressor protein that induce apoptosis, is low in early blue-light response, prolonged exposure increases PAR4 expression. Consequently, PAR4 associates to activated PKC-ζ resulting in inhibition of NF-κB survival pathway and can induce apoptosis (Wang et al., 2005; Jaadane et al., 2015b). Therefore depending on different blue-light parameters various stress response pathways can be activated in the cell resulting in various cell fates. [Modified from Hockberger et al., (1999)]

2.3.1 Blue-Light Induced Photo-oxidative stress

Most biological molecules are in a singlet state in their ground state meaning that they have no unpaired electrons. After photoexcitation of the molecule, an electron jumps from the highest occupied molecular orbit to the lowest unoccupied molecular orbit, resulting in an electronically excited singlet state. Intersystem Crossing (ISC) is one of the deactivation pathways against the electronically excited singlet state. ISC changes the orientation of the spin of the photoexcited electron resulting in an excited triplet state before transitioning into the ground state. The lifespan of an excited triplet state is at least 3 orders of magnitude longer than the lifespan of an excited singlet state. Therefore an electron at the excited triplet state is more likely to interact with its surrounding molecules, leading to photosensitized damage (Rozanowska et al., 2009).

There are 3 types of photosensitized damage (Figure 8). When a molecule at the excited triplet state (^3P) transfers an electron (or a hydrogen atom) to or form another molecule, causing the formation of a free radical (eg. P^-), it is classified Type 1 damage. Type 2 damage occurs when a molecule in the excited triplet state (^3P) transfers its energy to an oxygen molecule which is in triplet state in its ground state. As result of this energy transfer, oxygen is activated into an excited singlet state, forming singlet oxygen ($^1O_2$) molecule, while the photo-excited molecule (^3P) returns to its ground state (P). Singlet oxygen ($^1O_2$) is very unstable and it can react with surrounding unsaturated lipids (LH) to give rise to lipid hydroperoxides (LOOH). Type 3 photosensitized damage starts when a molecule at the excited triplet state (^3P) subtract an electron (or a hydrogen atom) from an unsaturated lipid (LH). This results in the formation of one free radical from the photosensitizer (P^-) and one free radical from the unsaturated lipid (L^-). The free radical from the photosensitizer (P^-) may donate its electron to an oxygen molecule (O_2) to give rise to superoxide anion (O_2^-). On the other hand, the free radical formed from the unsaturated lipid (L^-) can give rise to peroxidation chain reaction by interacting

with an oxygen molecule (O_2) to form lipid peroxyl radical (LOO^-). The lipid peroxyl radical (LOO^-) may subtract one electron (or a hydrogen atom) from another unsaturated lipid (LH). As a result of this interaction a lipid hydroperoxide (LOOH) and a new lipid free radical (L^-) is formed. It is important to note that a single molecule of photosensitizer can give rise to numerous free radicals and singlet oxygen ($^1O_2$) molecules by continuously being recycled to the ground state (Rozanowska et al., 2009).

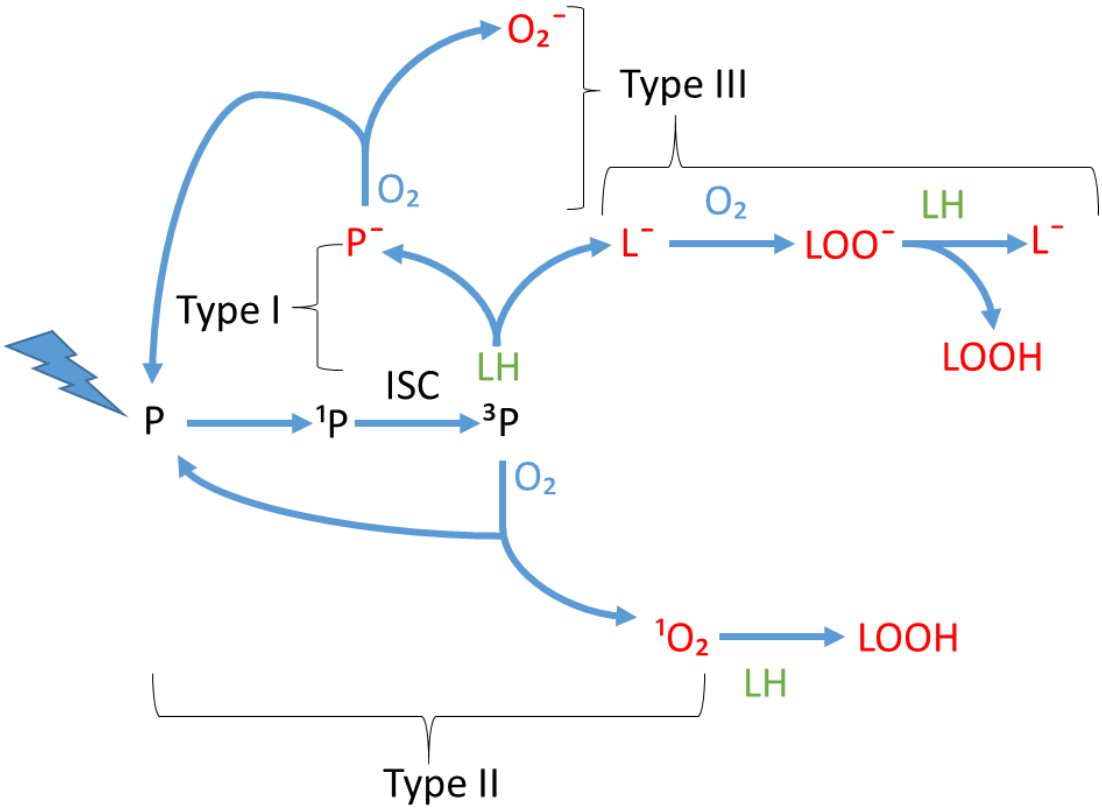

Figure 8 Diagram showing three types of photosensitized damage. Type 1 damage occurs when a molecule at the excited triplet state (^3P) transfers an electron (or a hydrogen atom) to or form another molecule, causing the formation of a free radical (eg. P^-). Type 2 damage occurs when a molecule in the excited triplet state (^3P) transfers its energy to an oxygen molecule. As result of this energy transfer singlet oxygen ($^1O_2$) molecule is formed. Type 3 photosensitized damage starts when a molecule at the excited triplet state (^3P) subtract an electron (or a hydrogen atom) from an unsaturated lipid (LH), resulting in the formation of one free radical from the photosensitizer (P^-) and one free radical from the unsaturated lipid (L^-). As a result of the interaction between the free radical from the photosensitizer (P^-) and an oxygen molecule (O_2), superoxide anion (O_2^-) is formed. On the other hand, interaction between the free radical formed from the unsaturated lipid (L^-) and an oxygen molecule (O_2)

can give rise to lipid peroxidation chain reaction. See the main text above for full description. [Modified from Rozanowska et al. (2009)]

2.4 Age-related Macular Degeneration Disease Modelling in-vitro

In-vitro models of AMD would be much preferred to animal models due to easier control of experimental conditions (Hornof et al., 2005). Also amongst animals; mice, rats, rabbits, pigs and non-human primates which have been used to model AMD, only few live long enough to develop AMD (Pennesi et al, 2012). The challenge of in-vitro disease models is that cells with desired phenotypes do not usually behave the same way as in-vivo case hence do not guarantee to model the disease (Cristofalo and Pignolo, 1995). To date, scientists have not been able to produce an accurate in-vitro model for AMD.

2.4.1 RPE Cell-lines

Primary cultures of human fetal RPE (hfRPE) represents the gold standard for in-vitro AMD models in terms of their function and resemblance to in-vivo RPE metabolism (Ablonczy et al., 2011). However hfRPE are expensive and have a limited life-time (Adijanto and Philp, 2014). Moreover, the use of fetal RPE has raised ethical concerns as they are associated with abortion (Lo and Parham, 2009). Throughout the literature various RPE cell lines such as ARPE-19, hTERT-RPE1, and RPE derived from human embryonic stem cells (hESC) and human induced pluripotent stem cells (hiPSC) have been used to model AMD in vitro. RPE cells derived from hESC and hiPSC exhibit a RPE phonotype including pigment granules. However, complex procedures and the time taken to culture (3 – 4 months) decreases the efficiency of this model for studying AMD (Boulton, 2014). Both, ARPE-19 and hTERT-RPE1 cell lines are immortal cell lines that lack melanin, lipofuscin and rhodopsin. hTERT-RPE1 cells are immortalized using human telomerase reverse transcriptase (hTERT) and they exhibit high telomerase activity preventing them from senescence (Leão et al., 2018). On the other hand, ARPE-19 cells are spontaneously arising immortal RPE cells (Dunn et al., 1996). Dunn et al. (1998) showed that monolayers of ARPE-19 exhibit polarized structural and functional properties

similar to those of RPE cells in vivo indicating that the ARPE-19 cell line is a valid model for studies of RPE cell polarity. Furthermore, as opposed to hTERT-RPE1 cell line, ARPE-19 express RPE specific markers; retinal pigment epithelium-specific 65 kDa protein (RPE-65) and cellular retinaldehyde-binding protein (CRALBP) that are involved in 11-cis retinal regeneration in visual cycle (Dunn et al., 1996). ARPE-19 cells are normally grown in DMEM/F12 medium as standard (Dunn et al. 1996), but its phenotype is dependent on culture conditions (Ahmado et al., 2011). Ahmado et al. (2011) documented that ARPE-19 cells cultured with DMEM media with 1% FCS modified with high glucose and pyruvate promoted differentiation markers such as CRALBP and Mer tyrosine kinase (MerTK) (which is an apical RPE receptor playing a role in phagocytosis of shed RPE), enhanced RPE65, VEGF secretion and showed photoreceptor outer segment phagocytosis.

2.4.2 RPE Pigmentation

Pigmented primary RPE cells, rapidly depigment in primary culture due to the sharing of pigment granules between the daughter cells (Flood et al., 1980; Boulton et al., 1984). Even though calcium switch protocol (Rak et al., 2006) and extracellular matrices; corneal endothelial matrix (Campochiaro and Hackett, 1993) and laminin & fibroblast growth factor (Smith-Thomas et al., 1996) have been reported to promote repigmentation, unequivocal melanogenesis in adult and fetal primary cultures has not been demonstrated yet (Boulton, 2014). However, it has been demonstrated in both primary and immortalised RPE cells (ARPE-19) (Boulton, 2014), that RPE can be loaded with mature melanosomes (Rózanowski et al., 2008) and lipofuscin (Davies et al., 2001; Godley et al., 2005). Alternatively, both primary and immortalised RPE cells (ARPE-19), can be fed with synthesized A2E, a bisretinoid component of lipofuscin (Sparrow et al., 2000; Vives-Bauza et al., 2008). Furthermore, many reports documented accumulation of auto-fluorescent granules as a result of phagocytosis of photoreceptor outer segments (POS) into primary or immortalised RPE (Boulton et al., 1989; Erik et al., 2003; Kaemmerer et al., 2007; Thampi et al., 2012; Guha et al., 2013; Lei et al.,

2013). However, these auto-fluorescent granules did not exhibit identical spectral and compositional characteristics of RPE lipofuscin (Boulton, 2014).

2.4.3 Oxidative stress inducers

Current in-vitro studies of AMD mostly use tetr-butyl hydroperoxide (TBHP) and hydrogen peroxide (H_2O_2) to induce oxidative stress. Disadvantage of H_2O_2 is that it is thermodynamically unstable and can easily break down to give out water and oxygen. Therefore TBHP, is used as a more stable organic peroxide alternative to H_2O_2 (Zhao et al., 2017). However, Spector et al., (2002) demonstrated that treatment with TBHP and H_2O_2 induced significantly different impact on epithelial cells. While H_2O_2 reacts directly on DNA causing single strand breaks, TBHP primarily reacts through membrane disruption (Spector et al., 2002). Under comparable conditions, Ma et al., (2002) showed that DNA damage examined by single strand breaks was significantly increased by H_2O_2 while DNA damage induced by TBHP was much less. Interestingly, even though H_2O_2 had a greater effect on DNA damage, the rate of cell death with H_2O_2 was lower compared with TBHP. This was due to high polyADP-ribosyl polymerase (PARP) activation induced by H_2O_2, causing a decline in nicotinamide adenine dinucleotide (NAD) and adenosine tri-phosphate (ATP) levels. While H_2O_2 stimulated PARP activity by 6-fold, TBHP caused only a 30 % increase. Subsequently, while H_2O_2 decreased NAD by 9-fold, no decrease was observed with TBHP. A rapid decline in ATP levels was observed with H_2O_2, while ATP decline was much slower with TBHP. Furthermore, while H_2O_2-induced ATP decline was prevented by 3-aminobenzamide (3AB), an inhibitor of PARP, 3AB treatment did not affect TBHP-induced ATP decline. All in all, compared to TBHP, H_2O_2 was shown to have much greater impact on energy generating systems, through rapid loss of ATP. The loss of ATP has a major effect on ATP utilization for oxidative stress repair mechanisms, therefore recovery against H_2O_2-induced oxidative stress is much slower compared to recovery against TBHP induced oxidative stress (Ma et al., 2002).

Ma and Kleiman (2004) documented that DNA damage due to ROS involves formation of hydroxyl radicals (•OH). They also showed that the cytotoxic mechanism of TBHP involves formation of superoxide anions (O_2^-) but may not involve hydroxyl radicals (•OH). On the other hand, H_2O_2 is thermodynamically unstable (Zhao et al., 2017) and known to generate hydroxyl radicals (•OH) via Fenton chemistry (Farber, 1994; Jarrett et al., 2008). Therefore while H_2O_2 treatment generates hydroxyl radicals (•OH) to induce DNA damage, TBHP treatment primarily damage cellular and mitochondrial membranes via generation of superoxide anions (O_2^-).

2.5 Light as Electromagnetic Radiation

Light is an electromagnetic radiation conveyed by photons. When an atom is energized (eg. heated), its electron jumps to a higher energy state (orbital). The electron falls from this higher energy state to its original energy state, by emitting a photon, an energy particle, with a specific frequency that matches the distance the electron falls. Subsequently, photons oscillate in electric and magnetic fields through space or media, carrying electromagnetic radiant (radiation) energy (Einstein, 1905). The Planck-Einstein relation states that the energy of a single photon (E) [J] is proportional to its frequency (f) [s^{-1}]:

$$E = h \cdot f \qquad \textbf{Eq.1}$$

where *h* refers to Planck's constant (6.62607004 × 10^{-34} J·s) (Pais, 1979).

The science that measures the electromagnetic radiation (eg. light), which is formed by beam of photons, is called radiometry. Radiometry utilizes spectroradiometers to measure the number of photons per second (photon flux) (ϕ_q) [s^{-1}] for each wavelength of the spectrum, falling on the spectroradiometer detector. First, through the spectroradiometer software the measured photon flux (ϕ_q) is converted into the radiant energy per second (radiant flux) (Φ_e):

$$\Phi_e = E\phi_q \qquad \textit{Eq.2}$$

where Φ_e is the radiant flux [W], E is the energy of single photon [J] and ϕ_q is the photon flux [s^{-1}]. Then the spectroradiometer software further calculates the irradiance (flux density) (E_e) [W/m^2] which is defined as the radiant flux (Φ_e) [W] per unit area:

$$E_e = \frac{\partial \Phi_e}{\partial A} \qquad \textit{Eq.3}$$

where *A* is the surface area of spectroradiometer detector [m^2]. Therefore the total radiant energy received by a unit area (radiant exposure, fluence) (H_e) [J/m^2] during an exposure can be calculated as:

$$H_e = \int_0^T E_e(t)\, dt \qquad \textit{Eq.4}$$

where t is the exposure time [s] (Sliney, 2005).

As light interacts with a chromophore in the cell, each absorbed photon transfers its energy to individual electrons of the chromophore. This energy transfer from a photon to an electron is called the photoelectric effect. As a result of the photoelectric effect electrons may gain kinetic energy and dislodge from ground state to excited state. However, electron displacement only occurs when a photon exceeds a threshold frequency, indicating that there is a threshold energy for electron binding that must be exceeded in order to remove an electron from its ground state (Einstein, 1905). Therefore, Einstein (1905) proposed that some of the energy from a single photon is consumed to exceed the threshold energy required to overcome electron binding, and the rest is converted to kinetic energy to the electron. Hence, the kinetic energy gained by a single electron can be calculated as:

$$K = E - h \cdot f_0 \qquad \textit{Eq.5}$$

where E is the energy of a single photon, h is the Planck's constant and f_0 is the threshold frequency which varies according to electronegativity of the chromophore (Pais, 1979).

All in all, the effect of light on biological organisms and chemical compounds depend upon both its frequency and irradiance. Keeping the irradiance fixed, when the frequency of the light increases, the kinetic energy gained by each electron increases. This increases the energy level (excited state) reached by each electron. Hence the probability of an electron to reach an excited triplet state increases. Similarly, keeping the frequency fixed, when the irradiance increases, the number of electrons with the same kinetic energy increase. Hence, more electrons reach the singlet excited state. Presence of increased number of electrons at the singlet excited state also increases the probability of electrons reaching the excited triplet state (Einstein, 1905).

According to Bunsen and Roscoe (1855), the effect of a photochemical or photobiological reaction is directly proportional to the radiant exposure dose, irrespective of the administration regime. As radiant exposure is the product of irradiance and time of exposure, this effect suggested by Bunsen and Roscoe (1855) is also defined as reciprocity. However to date, photochemical and photobiological studies have suggested that reciprocity may be valid only for certain irradiance and exposure time combinations which need to be individually defined for each reaction (Schindl et al., 2001; Morgan et al., 2009). Furthermore, for photo-carcinogenesis resulting from UV-induced DNA damage on melanocytes (Gilchrest et al., 1999), UV induced psoralen (a light sensitive drug to treat certain skin conditions) photochemical activity on human erythrocytes leading to haemolysis (Potapenko et al., 1991), the effect of blue-light irradiation on DNA synthesis of HeLa cells (Karu, 1989) and the effect of red light on proliferation and collagen synthesis of fibroblast cultures (Van Breughel and Bar, 1992) it has been shown that for a constant total dose, the irradiance of the light is a major factor contributing to the effect of the photochemical and photobiological response. For photobiological and

photochemical research more studies investigating reciprocity of irradiance and exposure time are needed, in order for comprehensive understanding the way living matter such as cells and tissues, respond to electromagnetic radiation (Schindl et al., 2001).

The photo-biological or photo-chemical effectiveness of an organism or a compound, is determined by its action spectrum. An action spectrum indicates the overall efficiency of biological or chemical activity at each wavelength of light absorbed. It is calculated by plotting a biological response (eg. photosynthesis, cell viability) against wavelength of light. It is typically written as unit-less response with the peak response corresponding to one (Caldwell et al., 1986; Gorton, 2010).

2.5.1 Transmission of Light

As light travels through various media (eg. air, DMEM, glass, plastic) to reach the RPE, some of the photons are absorbed by each medium, decreasing the total radiant energy carried by light. The total radiant energy reaching the RPE depends upon each medium's effectiveness in transmitting the radiant energy carried by light. This effectiveness in transmitting radiant energy of a medium is called transmittance and it can be calculated as:

$$\tau = \frac{E_e^t}{E_e^i} \qquad \textbf{Eq.6}$$

where τ is the transmittance, E_e^i is the initial irradiance and E_e^t is the transmitted irradiance (Progelhof and Throne, 1974).

2.5.1.1 Neutral Density Filters

In optical studies, neutral density (ND) filters are commonly used to reduce the irradiance of light. The absorption properties of an ND filter is determined by its optical density, which depend on its thickness and the concentration of atoms inside. Therefore, the transmittance of an ND filter can be calculated as:

$$\tau = 10^{-D} \quad \textit{Eq.7}$$

where τ is the transmittance of the ND filter and D is its optical density (Rickers et al., 2008).

2.6 Light emitting diode (LED) arrays

2.6.1 Light Emitting Diodes

Light emitting diodes (LEDs) are based on semi-conductors with a conductance (p) and a valance band (n), linked by a p-n junction. By providing a current to the LED (forward bias) the free electron in the conductance band can go through the p-n junction and fall into the hole containing valence band releasing energy by emitting a photon. Therefore, LEDs are commonly used in electrical circuits to convert the current into light in an energy efficient manner (Black et al., 1963; Zhang et al., 2009).

LEDs allow electron flow only in one direction (forward direction), from anode to cathode. To start emitting light, all LEDs require a minimum voltage across them in the forward direction (minimum forward voltage). The minimum LED forward voltage and the colour of emitted light depend upon the material used to construct the LED. When the applied forward voltage exceeds the threshold of minimum forward voltage, the forward current passing through increases exponentially. As too much current can damage an LED, forward current passing through the LED should be limited in an electrical circuit by the use of resistors (Black et al., 1963; Zhang et al., 2009).

2.6.1.1 Light emitting diode arrays in electrical circuits

Combination of series and parallel electrical circuits can be used to construct ad hoc LED arrays to illuminate 8- and 96-well cell culture plates. These electrical circuits should follow Ohm's and Kirchhoff's laws. According to Ohm (1827) the voltage (V) [V] across a resistor is defined as:

$$V = I \cdot R \quad \textit{Eq.8}$$

where I is the current [A] passing through the resistor and R is the resistance [Ω] of the resistor. Furthermore, according to Kirchhoff (1847) while all components connected in series carry the same current, the same voltage is applied to all branches connected in parallel and the total current in the circuit is the sum of the currents passing through each branch (Figure 9).

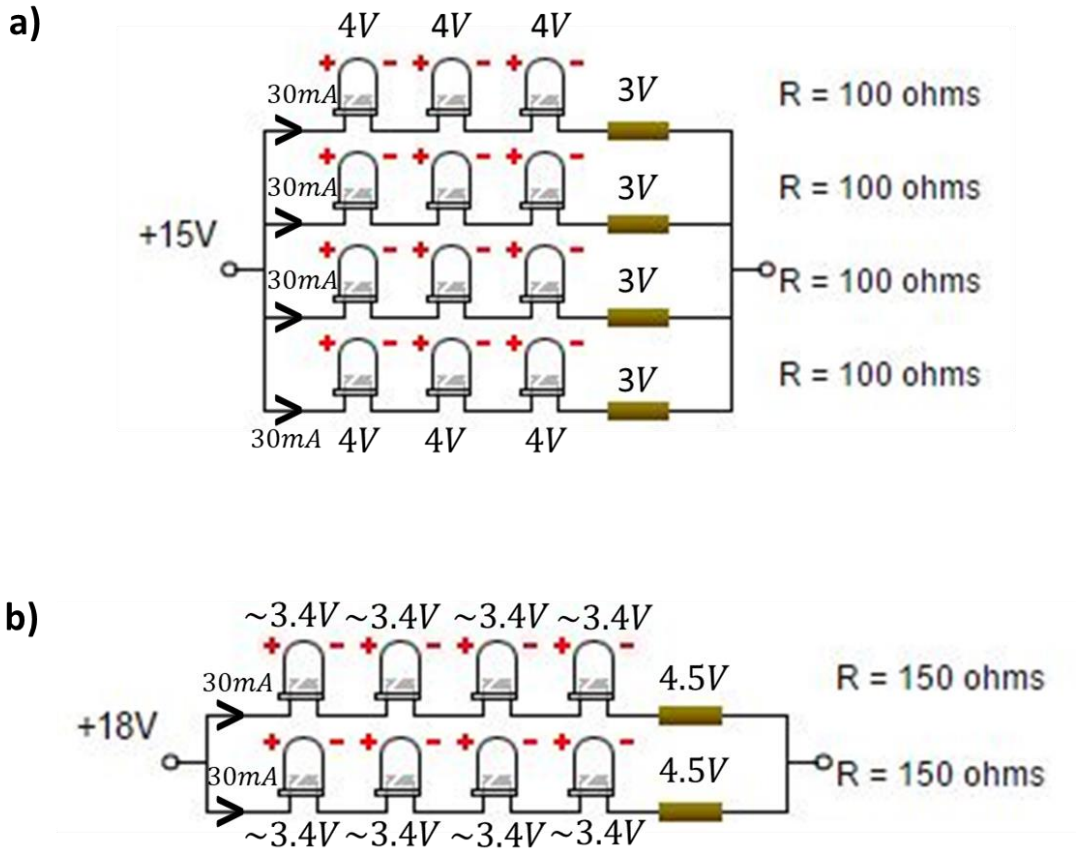

Figure 9 Ad-hoc LED array circuit design. **a)** Ad-hoc LED array designed to illuminate 96-well ECIS plate. Each LED was used to illuminate an area covered by 4-wells. The unilluminated wells were used as dark controls. **b)** Ad-hoc LED array designed to illuminate 8-well ECIS plate. Each LED was used to illuminate 1 well. Dark controls were designed by wrapping black aluminium foil around selected ECIS wells.

It is important to consider that different LEDs may spread the light at different angles from the source. This angle is called the LED angle. Therefore, depending on the LED angle and desired illumination area, the ad hoc LED array should be placed at a certain height from the bottom of cell culture plate (Figure 10) (Greenham et al., 1994).

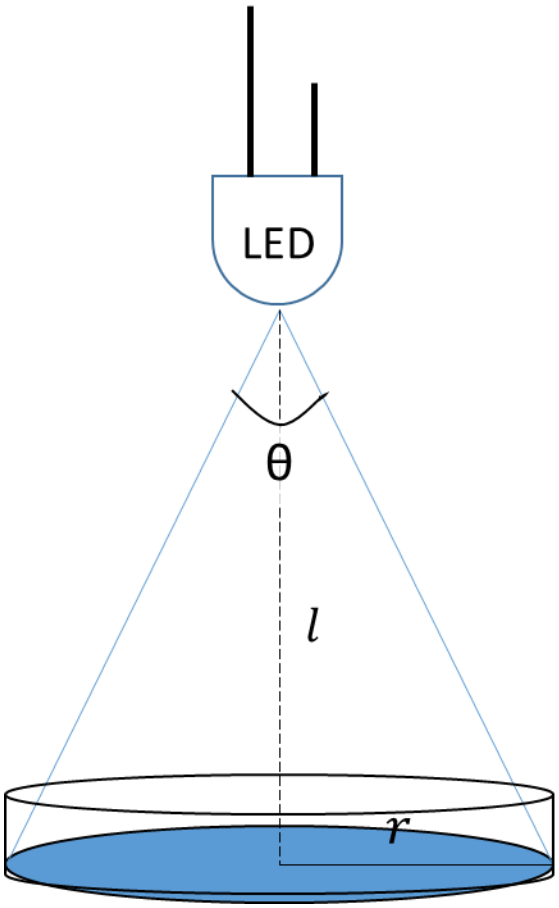

$$\tan\left(\frac{\theta}{2}\right) = r/l$$

Figure 10 Placement of LED array relative to ECIS cell culture plate. LED angle can be used to calculate how far the ad hoc LED array should be placed from the bottom of the ECIS cell culture plate to illuminate cultured cells.

2.7 Impedance Sensing

The common feature of all animal cells is their plasma membrane formed by phospholipid bilayer. This phospholipid bilayer is an electrical insulator which functions both as a resistor and a capacitor. While due to its lipid and protein content, plasma membrane acts as an insulator and exerts a resistance to the movement of charges across it, its small thickness (5 nm) allows accumulation and interaction of opposite charges from the cytoplasm and the extracellular matrix, acting as a capacitor. Hence, plasma membrane is a bio-dielectric. In other words, as opposed to transmitting electricity with conduction, where electrical charges flow through the material, the charges in the plasma membrane only slightly shift from their standard equilibrium positions causing dielectric polarization with an applied electric field. This ability of the cell

membrane to transmit electric current by dielectric polarization is referred as its permittivity (Weaver and Schoenbach, 2003).

Due to its dielectric properties, under alternating current (AC) plasma membrane exerts an impedance, which is a two-dimensional vectoral opposition against the passing of current. Impedance is described by the ratio between the voltage and the AC and is determined by Ohm's law:

$$Z = \frac{V}{I} \qquad \textit{Eq.9}$$

where V is the changing potential and I is the applied AC. Impedance is formed by two vectoral components; resistance and reactance (capacitative resistance). While cellular resistance (R_C) is caused by cell membrane components acting as a resistor against the current, cellular reactance $(X_C(f))$ is caused by the opposition that the charges around the membrane show against the current. Therefore cellular impedance $(Z_C(f))$ can be expressed as:

$$|Z_C(f)| = \sqrt{{R_C}^2 + \left(X_C(f)\right)^2} \qquad \textit{Eq.10}$$

where R_C is the cellular resistance, $X_C(f)$ is the cellular reactance which is:

$$X_C(f) = \frac{1}{2\pi f C_C} \qquad \textit{Eq.11}$$

where f is the frequency of the AC and C_C is the cellular capacitance which describes the separation of charged particles at the insulating bi-layers (Szulcek et al., 2014).

As the cell membrane acts as a capacitor, dielectric properties of the cell are frequency dependent. As the frequency of the current increase, dielectric polarization can no longer compensate with the frequency oscillations, hence the charges start to move away from their equilibrium positions and flow with

the current. The passing of higher frequency AC results in charge redistribution in the membrane, declining the natural dielectric polarization ability of the membrane. Therefore, while its electrical permittivity and reactance decline, its electric conductivity increases. Due to this, a high frequency AC can penetrate the cell better than a low frequency AC. Subsequently, different frequencies of AC follow different paths on the cellular surface due to its changing electric permittivity (Schwan, 1957).

The variations in relative electrical permittivity of the cell in response to frequency occur through a series of steps. Each step change occurs under a specific frequency range which is called frequency dispersion. The frequency dispersions occur due to loss of certain polarization modes in the cell. There are four dispersion regions described in the cell; α-, β-, δ-, and γ- dispersion (Figure 11a). The α-dispersion region occurs between 10 Hz – 10 kHz, near the cell membrane (where the movement of charged particles are limited) due to ionic diffusion, and is correlated with tangential flow of current across charged surface. The β-dispersion region occurs between 10 kHz - 10 MHz, as cytoplasmic charges, with opposite polarities, start to accumulate respectively inside basal and apical membranes in response to increased frequency. Therefore, at the β-dispersion region the current can capacitively couple through the membrane, and pass through the cell (Figure 11b). The changes in dielectric properties of the cell at frequencies above 0.1 GHz is attributed to dipolar moments of the intracellular molecules. The δ-dispersion region occurs between 0.1 GHz – 5 GHz, due to changes in electrical dipole moments of large molecules such as proteins. On the other hand, the γ-dispersion region occurs at frequencies above 10 GHz, due to changes in dipolar moments of intracellular electrolytes such as water (Schwan, 1957; Nasir and Al Ahmad, 2020).

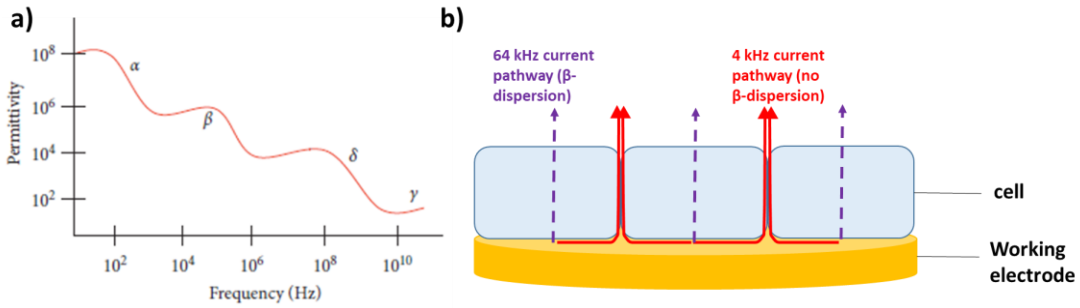

Figure 11 Frequency dispersions and different current pathways. **a)** The variations in relative electrical permittivity of the cell in response to frequency occur through a series of steps known as the α-, β-, δ- and γ- dispersions. Each frequency dispersion occurs due to certain polarization modes in the cell. Figure modified from Nasir and Al Ahmad (2020) **b)** Due to the changes in cellular permittivity with frequency, different frequencies of AC follow different paths on cellular surface. While at 4 kHz, the lack of β-dispersion region forces AC under and between the cells, around the membrane surface, 64 kHz AC travels via β-dispersion region, through the cell membrane, coupling with cytoplasmic charges.

2.7.1 Electric Cell-Substrate Impedance Sensing

Electrical Cell Substrate Impedance Sensing (ECIS) is a non-invasive, label-free quantitative technique pioneered by Giaever and Keese (1991), in which monolayer of adherent cells is cultured directly on gold micro-electrodes and the changes in impedance at different AC frequencies is recorded in real-time. Multiple frequency measurements (f = 62.5, 125, 250, 500, 1000, 2000, 4000, 8000, 16000, 32000 and 64000 Hz) utilize α- and β-dispersions to reveal information on different cellular compartments and behaviour. ECIS uses a two-electrode set-up in which a small working (sensing) electrode (0.05 mm^2) is coupled with a larger counter electrode (18 mm^2) on planar surface at the bottom of each well. A small non-invasive 1 μA current with a given frequency is applied through the electrodes via an AC source connected through a 1MΩ resistor. When these electrodes come in contact with an electrolyte such as cell culture medium, due to unequal distribution of charges at each electrode/electrolyte interface an electric potential arises between the electrodes. By maintaining the total current (I) constant, the voltage (V) changes across the electrodes are measured via lock-in amplifier by the ECIS instrument. Then, the impedance across the electrodes is determined by the Ohm's law (Giaever and Keese, 1991) (Figure 12).

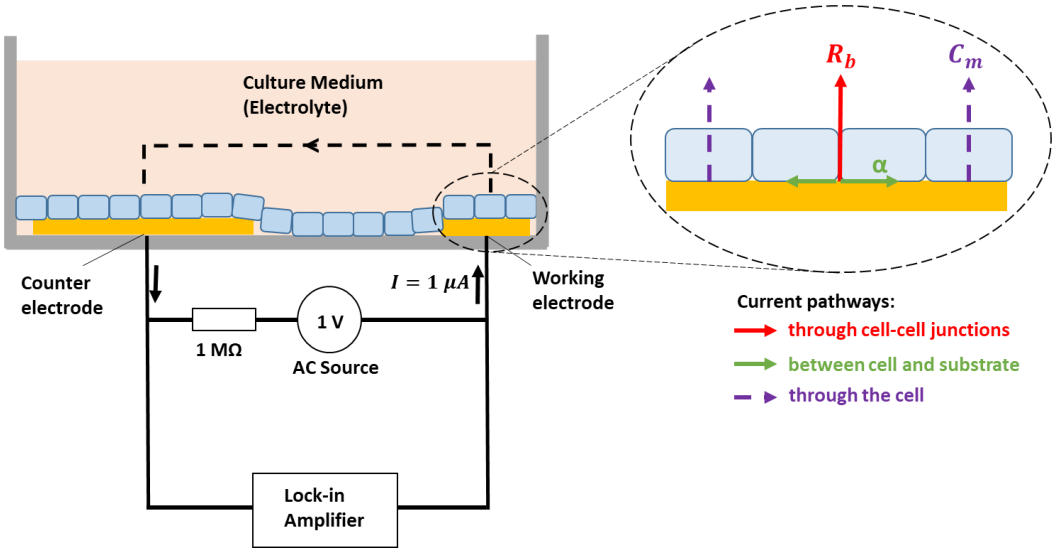

Figure 12 ECIS Setup. ECIS uses a two-electrode setup in which a small (working) and a large (counter) electrode are coupled on the planar surface of each well. A small non-invasive 1 µA current is applied through the electrodes via an AC source connected through a 1 MΩ resistor. The impedance is measured using a lock-in amplifier. Scanning of the impedance at different frequencies gives information on different current pathways which is translated through ECIS mathematical model into data on cell-cell junctions (barrier function) ($\boldsymbol{R_b}$), cell-electrode adhesion ($\boldsymbol{\alpha}$) and cell membrane capacitance ($\boldsymbol{C_m}$). Modified from Szulcek et al. (2014).

When the cells are cultured on top of the electrodes, due to their insulating properties they increase the impedance. As the cells grow and cover the electrodes, the current is impeded in relation to the number of cells covering the electrodes, their morphology and the adherent nature of the cells. The measured impedance increases until it reaches a plateau as the cells form a confluent monolayer. When the cells are stimulated with a stressor that forces a functional change, these changes in cell morphology alter the impedance. Therefore data on impedance is recorded over time to record any changes in cell morphology induced by a stressor (eg. blue-light) (Giaever and Keese, 1991).

2.7.1.1 ECIS Model

In ECIS circuit, the cells are grown in culture media which has a resistance, on top of working and counter electrodes, which act as a capacitor (Figure 13).

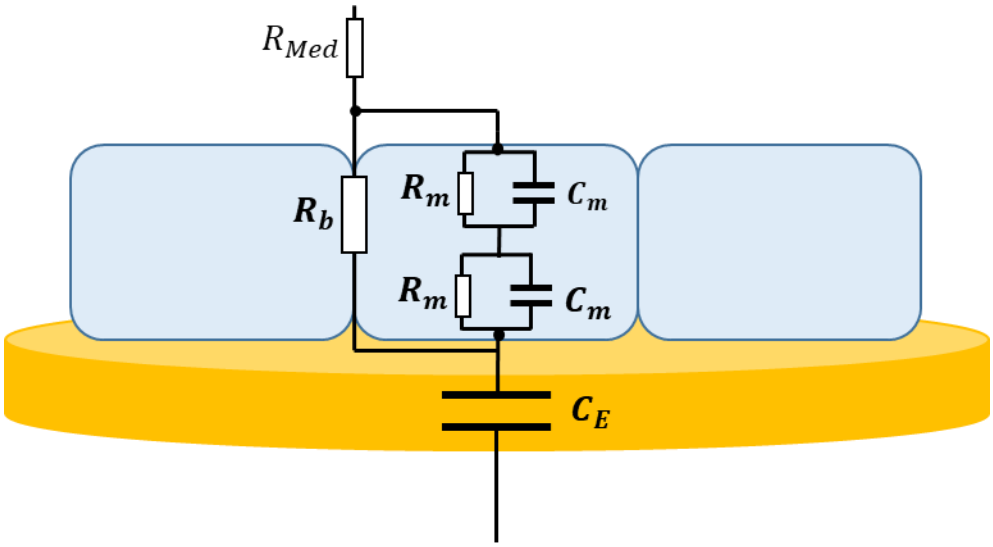

Figure 13 ECIS Model. ECIS measures the sum of all individual contributions of impedance. The resistance of culture media ($\boldsymbol{R_{Med}}$), the capacitance of the electrode ($\boldsymbol{C_E}$) as well as cellular resistance ($\boldsymbol{R_C}$) and cell membrane capacitances ($\boldsymbol{C_m}$) are all need to be considered. Cellular resistance against the current varies depending on the different current pathways. At low frequencies (<10 kHz) as the current flows in between the neighbouring cells, the cellular resistance is related to cell-cell junction resistance ($\boldsymbol{R_b}$), while at high frequencies (>40 kHz), as the current can couple through the plasma membranes, the cellular resistance is related to membrane resistances ($\boldsymbol{R_m}$). Modified from Szulcek et al. (2014).

Therefore, the sum of all individual contributors of impedance: resistance of the culture medium (R_{Med}), reactance of the electrode ($X_E(f)$) and cellular impedance ($Z_C(f)$) are calculated. Hence, the total impedance can be described as:

$$|Z_{Total}(f)| = \sqrt{(R_{Med} + R_C)^2 + (X_E(f) + X_C(f))^2} \qquad \textit{Eq.12}$$

where $X_E(f) = \frac{1}{2\pi f C_E}$ in which C_E is the capacitance of the electrode, and $X_C(f) = \frac{1}{2\pi f C_C}$ in which C_C is the capacitance of the cell which results from combination of apical and basal membrane capacitances (Szulcek et al., 2014). The capacitance of the single cell membrane (C_m) is given by $C_m = 2C_C$ [µF/cm^2] and in all their calculations C_m was originally set as 1 µF/cm^2 by Giaever and Keese (1991).

Once the total impedance has been determined, scanning of the impedance at different frequencies creates different current pathways which is translated

through ECIS mathematical model into biologically significant data on: **a)** cell attachment, spreading and proliferation; **b)** resistance as a measure of barrier quality; **c)** micromotion; **d)** wound-healing. Determining the most sensitive measurement frequency for different current pathways is very important for accurate interpretation of ECIS data. The most sensitive frequency measurement for a specific cell type can be observed by comparing frequency scans for cell-free and cell-covered electrode on a resistance vs frequency log - log graph. The frequency where the difference between cell-free and cell-covered electrode is biggest for each dispersion region indicates the frequency where cellular components block the current most effectively in that dispersion region (Szulcek et al., 2014). While 4 kHz is used for cell motility (Lo et al., 1993), morphology (Keese and Giaever, 1994) and tight junction studies (Giaever and Keese, 1991; Szulcek et al., 2014), frequencies over 40 kHz is used for studying cell coverage and plasma membrane capacitance with high sensitivity (Giaever and Keese, 1991; Wegener et al., 2000; Szulcek et al., 2014).

2.7.1.1.1 Cell attachment, spreading and proliferation

As cells attach and spread over the electrode, they restrict the current flow, subsequently capacitance of the electrode decrease linearly in relation to the percentage of open area on the electrode. This relation can be described as:

$$C_E = \varepsilon \frac{A}{d} \qquad \textit{Eq.13}$$

where C_E is the capacitance of the electrode, ε is the dielectric constant, A is the open area on the electrode and d is the separation of electrodes. As current at 64 kHz directly couples through the cell, the decrease in electrode capacitance (C_E) at this frequency is proportional to the electrode coverage. Therefore, cell attachment, spreading and proliferation can best be quantified by recording electrode capacitance (C_E) at 64 kHz. Furthermore, resistance at 64 kHz, shows a direct measure for the differentiation and maturation of the cells into a confluent layer. Therefore using a combination of electrode

capacitance and resistance at 64 kHz allows to distinguish between different stages of the growth phase. It is important to note that every cell type presents specific attachment and growth curve that can be affected by differences in seeding density, coating with extracellular medium and various stimuli (Giaever and Keese, 1991; Wegener et al., 2000; Szulcek et al., 2014).

2.7.1.1.2 Resistance as a measure of barrier quality

In vivo, monolayers of epithelial and/or endothelial cells form barriers formed by cell-cell junctions and regulate the passage of molecules between tissues and/or different cellular compartments. Similarly when most epithelial and endothelial cells are cultured in vitro to form confluent monolayers, they form barriers between cells by various junctional proteins (Giaever and Keese, 1991). To estimate cell monolayer integrity, impedance sensing technology measures trans-epithelial or trans-endothelial electrical resistance (TEER). The TEER across an epithelial or endothelial layer correlates with the tight-junction formation between neighbouring cells. Passive electrical behaviour of cells, on the contrary to active electrophysiological potential, is largely due to the presence of bi-layer membrane which separates cell culture media rich in ions (Gamal et al., 2018). Hence, resistance component of the impedance measures biological barrier quality, as it omits capacitive component from membrane and electrode. Due to insulating properties of the plasma membrane, the electrical current can flow;

i) between basal surface of the cells and the electrode;
ii) between the cells that can form a barrier with tight cell-cell junctions;
iii) directly through the cells (at high frequency).

ECIS software possess a built-in feature to model two-parameters to distinguish between cell-cell junctions and cell-electrode adhesion. In their mathematical model Giaever and Keese (1991) defined these two-parameters as; R_b resistance between cell-cell junctions per unit area [Ω·cm^2] which is the inverse measure of cell-cell junction permeability, and α the cell-substrate

adhesion parameter [$\Omega \cdot cm^{0.5}$] which is correlated with the electrolyte resistivity towards the current.

In addition to the model, we can often directly compare the time-course resistance at 4 kHz (para-cellular resistance) and at 64kHz as the low frequency part is highly sensitive to the presence of cell-cell junctions, and is a measure of the barrier function quality while the higher frequency part will only reflect partially the presence of a barrier function as the current flow directly through the cells. On the other hand, as current at 64 kHz flows through the cells, resistance at this frequency is correlated with cell electrode coverage and can be used to monitor changes in the cellular confluency. Furthermore, at this frequency the cell membrane capacitance (C_m) can also be calculated to determine any changes on the plasma membrane properties and morphology (Giaever and Keese, 1991; Wegener et al., 2000; Szulcek et al., 2014).

2.7.1.1.3 Cellular Micromotion

Nanometers changes in the cell diameter and even sub-nanometer changes in cell-substrate distance, result in fluctuations in resistance measurements at 4 kHz (Giaever and Keese, 1991; Lo et al., 1993). These fluctuations are mainly caused by vertical motion of the cells resulting from metabolic activity, and are characteristic of the cell type. This subtle aspect of cell motility is called cellular micromotion (Lo et al., 1993; Opp et al., 2009; Lovelady et al., 2009; Láng et al., 2017).

Micromotion is usually calculated with high sensitivity as the moving variance of resistance data at 4 kHz (Lo et al., 1993; Szulcek et al., 2014; Chiu et al. 2019). In a recent study, Chiu et al. (2019) demonstrated that the changes in cellular micromotion is correlated with the mitochondrial activity, and showed that reducing mitochondrial respiration and ATP production resulted in a decline of cellular micromotion variance.

2.7.1.1.4 Wound Healing

Wound healing assays can be combined with ECIS by applying a mechanical, chemical or electrical stress. Wounding manifests itself as a transient drop in resistance. When cells migrate on the electrode from all sides, migration rate correlates with the rate of resistance increase. Furthermore, by adding drugs and antioxidants to the culture media the healing effect of various compounds on cells can be quantitatively investigated in real-time.

2.7.1.2 AMD disease model on ECIS

To model and quantitatively study RPE loss in AMD, a tissue-on-a-chip approach combining ECIS with reproducible electrical wound healing assays of hiPSC were developed by Gamal et al., (2015). First, RPE cells were seeded on ECIS microelectrode arrays, and the establishment and maturation of RPE layers were monitored. After RPE cells reached confluency, a spatially controlled RPE layer damage was created through electrical wounding to mimic cell loss in AMD. The developed disease model on a chip enabled real-time, quantitative and reproducible patient-specific RPE cell repair studies and all in all demonstrated that the tissue-on-a-chip approach is a powerful tool for RPE and AMD studies.

3 Materials and Methods

Unless otherwise stated all experiments were carried out within a sterile laminar flow hood after the establishment of a barrier function, which was evaluated by Electrical Cell-Substrate Impedance Sensing (ECIS). All cell cultures were incubated at 37ºC and 5% CO_2. As measured by an infrared thermometer (RS-1327, RS PRO), no temperature increase was detected during light experiments.

3.1 Immortalised Cell-line based ECIS model for AMD studies

3.1.1 Immortalised Cell-line cultures in-vitro

hTERT-RPE1 cells (ATCC CRL-4000) and ARPE-19 cells (ATCC CRL-2302) were initially seeded on T75 flasks (5.2 x 10^4 cell/cm^2) in 15 mL of Dulbecco's Modified Eagle Medium (DMEM) (1X) 4.5g/L D-Glucose, L-Glutamine (41965-039, Life Tech.) supplemented with 10% Fetal Calf Serum (FCS) (10270106, Life Tech.), 1% penicillin streptomycin (pen-strep) (15140-122, Invitrogen) and 1mM sodium pyruvate (S8636, Sigma). The media was renewed every other day, 3 times a week. When the cells were 100 % confluent (after 5 days) on T75 flask, the cells were passaged. During passaging, first the media in the flask was removed and the cells were washed using 3 mL modified Phosphate Buffer Saline (PBS) without magnesium chloride and calcium chloride (D8537, Sigma). Then 3.0 mL of Trypsin-EDTA, 0.25% (25200-072, Life Tech.) was added to the flask for 1 minute and then removed. Trypsin-EDTA treated cells in T75 flask was incubated at 37ºC and 5% CO_2 for 10 minutes. After the incubation the cells were collected by adding 15 mL complete culture media to the flask using a pipette. Then the cells were seeded as a monolayer (5.2 x 10^4 cell/cm^2) into cell culture plates where the experiments were conducted. Before the experiments were conducted in cell culture plates, the cells were kept in Dulbecco's Modified Eagle Medium (DMEM) (1X) 4.5g/L D-Glucose, L-Glutamine (41965-039, Life Tech.) supplemented with 10% Fetal Calf Serum (FCS) (10270106, Life Tech.), 1% penicillin streptomycin (pen-strep) (15140-

122, Invitrogen) and 1mM sodium pyruvate (S8636, Sigma). Media was changed 3 times a week until confluence. When cells in culture plates were 100 % confluent, the media was changed to DMEM (1X) 4.5g/L D-Glucose, L-Glutamine supplemented with 1% FCS, 1% pen-strep and 1 mM sodium pyruvate. The cells were kept in DMEM (1X) 4.5g/L D-Glucose, L-Glutamine supplemented with 1% FCS, 1% pen-strep and 1 mM sodium pyruvate for 3 weeks, during which the media was renewed 3 times a week, and just before the experiments were conducted. This cell culture protocol we have followed was established by Ahmado et al. (2011) as a cell culture protocol that promote RPE differentiation markers.

3.1.2 ECIS arrays

8WE1 and 96W1E ECIS arrays from Applied BioPhysics™ were used for immortalised cell-line based assays in our study. ECIS 8WE1 array consists of 8 wells of 0.8 cm^2 surface area with a single 250 µm diameter sensing micro-electrode in each well. ECIS 96W1E has 96 wells of 0.32 cm^2 surface area and has a single 250 µm diameter sensing micro-electrode in each well. Microelectrodes under each well are manufactured by Applied BioPhysics™ on a transparent Lexan polycarbonate substrate onto which 50 nm thick gold electrodes are coated and passivated with 2 µm polymer resin (Gamal et al., 2015). All ECIS arrays were incubated at 37^oC and 5% CO_2 with Dulbecco's Modified Eagle Medium (DMEM) (1X) 4.5g/L D-Glucose, L-Glutamine (41965-039, Life Tech.) supplemented with 10% Fetal Calf Serum (FCS) (10270106, Life Tech.), 1% penicillin streptomycin (pen-strep) (15140-122, Invitrogen) and 1mM sodium pyruvate (S8636, Sigma) for 30 minutes before cell seeding.

ECIS arrays were seeded with hTERT-RPE1 or ARPE-19 cell lines with a seeding density of 5.2 x 10^4 cell/cm^2. These cultures were maintained in Dulbecco's Modified Eagle Medium (DMEM) (1X) 4.5g/L D-Glucose, L-Glutamine (41965-039, Life Tech.) supplemented with 10% Fetal Calf Serum (FCS) (10270106, Life Tech.), 1% penicillin streptomycin (pen-strep) (15140-122, Invitrogen) and 1mM sodium pyruvate (S8636, Sigma) until they reached

confluence. When the cells were 100% confluent, the media were changed to DMEM (1X) 4.5g/L D-Glucose, L-Glutamine supplemented with 1% FCS, 1% pen-strep and 1 mM sodium pyruvate. The resistance was measured in a time-course manner every 180 seconds for 8W1E and every 15 minutes for 96W1E at 11 frequencies. For the sake of clarity, only the resistances at 4 kHz and 64 kHz were plotted, however the full spectroscopic information was used to model the barrier function. For each well, a model was used to quantify the changes in the barrier function associated with tight junction formation using ECIS software.

As the cells attach and grow over the electrode, they restrict the current flow, subsequently capacitance of the electrode (C_E) decreases linearly in relation to the percentage of open area on the electrode. Until the cells reach confluence, the capacitance of the electrode (C_E) declines. Previous work has shown that as current at 64 kHz directly couples through the cell via cytoplasmic charges, after the cell reached confluence on the electrode, an increase in C_E at 64 kHz is due to a decrease in cell coverage that is likely due to cell death and detachment (Giaever and Keese, 1991; Wegener et al., 2000; Szulcek et al., 2014; Pennington and Van de Walle, 2017; Robilliard et al., 2018; Chiu et al., 2019).

3.1.3 Resistance data analysis

Generally, normalized data was used to provide a more accurate way of comparing resistances of different culture wells. First, no cell media control was subtracted from the resistance. Unless otherwise stated, normalization of the data was performed by dividing the resistance (or its corresponding modelling parameters) by its value at the starting point (t = 0) to have 1 for all lines at the start of the experiment.

3.2 LED Circuit Design

3.2.1 470 nm LED array circuit design

Blue-light at 470 nm was chosen for investigation, with the rationale that most of the electronic devices today use blue light-emitting diode (LED) technology with an emission peak of 470 nm, to improve brightness and clarity (Yam and Hassan, 2005; Rozanowska et al., 2009). Also there is an increase in the use of low energy white LEDs as a source of general lighting, which have a strong peak at 470 nm in the blue region (Behar-Cohen et al., 2011). In addition, due to the transmittance of the human eye, most of the blue-light at 470 nm reaches the human retina (Figure 6) (Boettner, 1967; Arnault et al., 2013).

Cells cultured on 96-well ECIS plates, were exposed using an ad hoc LED array circuit with 12 LEDs (Cree 5 mm Blue, 470 nm) and four 100 Ω resistances connected on a breadboard. The forward current and LED angle of each LED were respectively 30 mA and 15º. The resulting irradiance as characterized by using a spectroradiometer (SR9910, Irradian Limited, UK), was 127 W/m^2 (Figure 14).

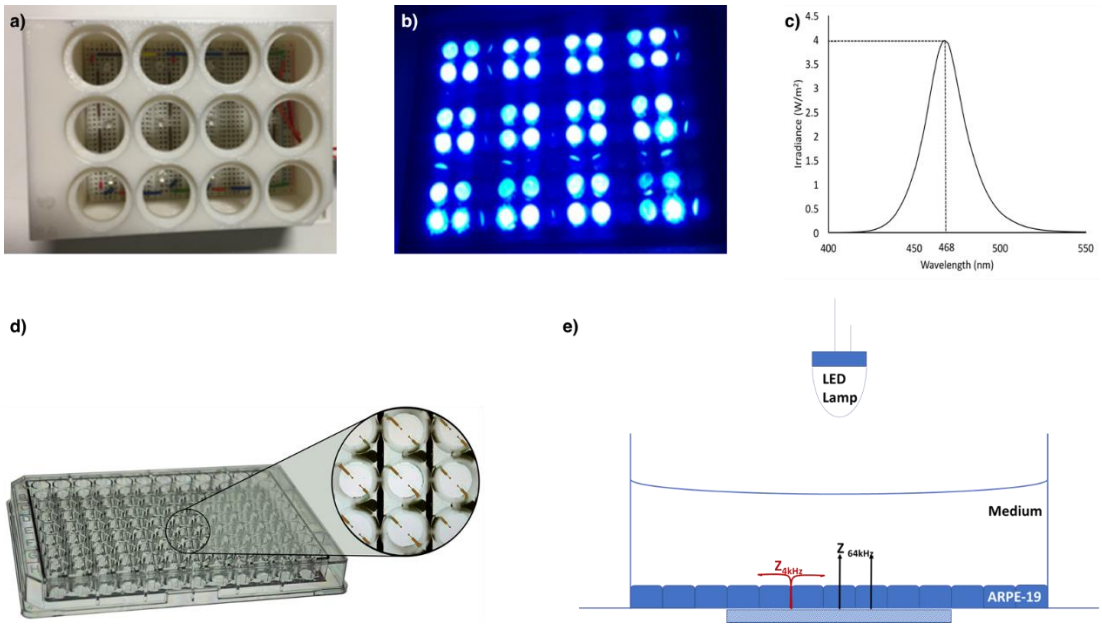

Figure 14 96W1E ECIS plate blue-light (470 nm) illumination setup. An ad hoc LED array circuit with 12 LEDs (Cree 5 mm Blue, 470 nm) and four 100 Ω resistances were connected on a breadboard. By using this ad hoc LED array illumination system together with a set of

neutral density filters and a 3D printed filter holder, ECIS multi-well arrays with a single 250 µm diameter micro-electrode in each well, were exposed to a gradient of irradiances (118.1 W/m², 74.65 W/m², 47.05 W/m² and 29.67 W/m²) of blue-light with a peak at 468 nm. The resistances at 4 kHz and 64 kHz, and capacitance at 64 kHz were plotted during the exposure. **a)** Ad hoc LED array illumination system with 3D printed filter holder. **b)** Blue light exposure on 96 well ECIS plate. **c)** Irradiance peak of 470 nm blue LED as measured by using a spectroradiometer (SR9910, Irradian Limited, UK). **d)** 96W1E, an example of an ECIS multi-well array with single 250 µm diameter micro-electrodes which allowed resistance and capacitance to be measured in a time-course manner every 15 minutes at 11 frequencies **e)** Diagram of our experimental set-up designed by combining an ad hoc LED array illumination system with ECIS multi-well arrays. Z in the figure stands for impedance.

Cells cultured on 8-well ECIS plates, were exposed using an ad hoc LED array circuit with 8 LEDs (Cree 5 mm Blue, 470 nm) and two 150 Ω resistances connected on a breadboard. The resulting irradiance as characterized by using a spectroradiometer, was 151 W/m^2 (Figure 15).

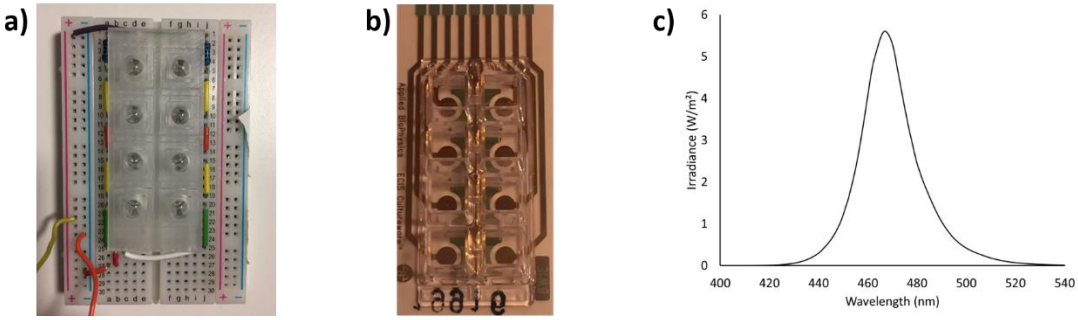

Figure 15 8W1E ECIS plate blue-light (470 nm) illumination setup. An ad hoc LED array circuit with 8 LEDs (C503B-BAN-CZ0A0451, Cree 5 mm Blue, 470 nm) and two 150 Ω resistances connected on a breadboard. By using this ad hoc LED array illumination system together with ECIS multi-well arrays with a single 250 µm diameter micro-electrode in each well, were exposed to 140.4 W/ m² total irradiance (area under the curve) of blue-light with a peak at 468 nm. The resistances at 4 kHz and 64 kHz were recorded during the exposure. **a)** Ad hoc LED array illumination system used. **b)** 8W1E, an ECIS multi-well array with single 250 µm diameter micro-electrodes which allowed resistance to be measured in a time-course manner every 180 s at 11 frequencies. **c)** Irradiance peak of 470 nm blue LED as measured by using a spectroradiometer (SR9910, Irradian Limited, UK).

3.2.2 420 nm Blue-Light Setup

Previous blue-light studies showed that photochemical effect of the light in the retina increased as wavelength of light was decreased (Ham et al., 1976; Wu et al., 2006; Behar-Cohen et al., 2011). In our study, blue-light at 420 nm was chosen to test what effect the shorter wavelength blue-light have on the cells and if the severity of the damage on cells was increased with shorter wavelength, compared to 470 nm blue-light. Cells cultured on 8-well ECIS

plates, were exposed using a 120 Watt metal halide epifluorecence lamp (BS039085, X-Cite 120, Excelitas Technologies, USA) with a 420nm band pass filter (FB420-10, Thorlabs, 420 ±10). The resulting irradiance as characterized by using a spectroradiometer, was 17 W/m^2 (Figure 16).

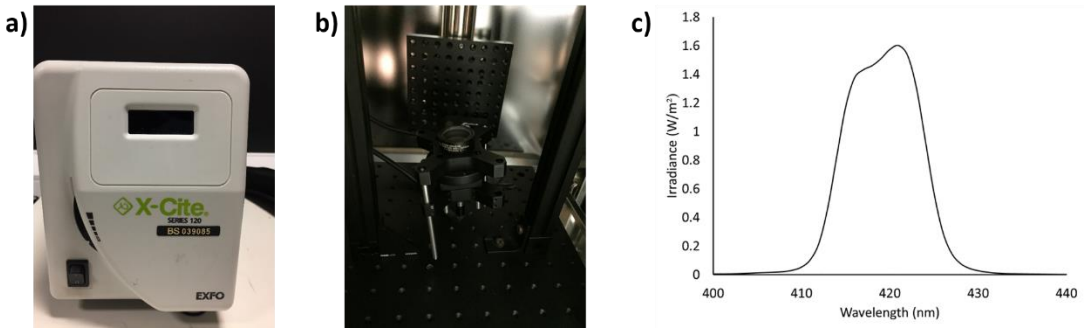

Figure 16 8W1E ECIS plate blue-light (420 nm) illumination setup. **a)** 120 Watt metal halide epifluorecence lamp (BS039085, X-Cite 120, Excelitas Technologies, USA) was used in combination with a **b)** 420nm band pass filter (FB420-10, Thorlabs, 420 ±10) to illuminate cells cultured on 8-well ECIS plates. **c)** Irradiance peak of 420 nm blue-light as measured by using a spectroradiometer (SR9910, Irradian Limited, UK).

3.2.3 400 nm LED array circuit design

Light at 400 nm was chosen to further confirm the effect of shorter wavelength light on the cells. Cells cultured on 8-well ECIS plates, were exposed using an ad hoc LED circuit with 8 LEDs (SLLP-F586-1520-UV, Semileds, 400 nm) and two 100 Ω resistances connected on a breadboard. The forward current and LED angle of each LED were respectively 20 mA and 30^o. The resulting irradiance as characterized by using a spectroradiometer, was 19 W/m^2 (Figure 17).

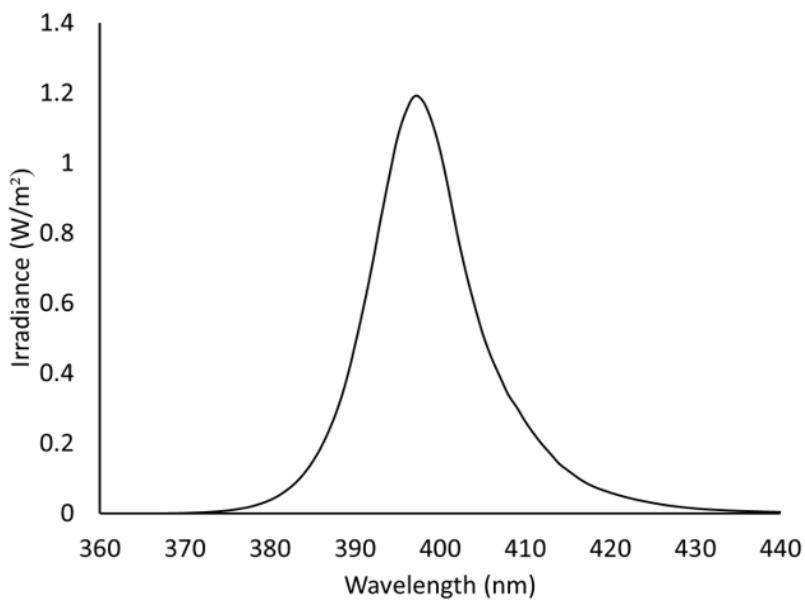

Figure 17 8W1E ECIS plate blue-light (400 nm) spectra. Irradiance peak of 400 nm blue LED coming from an ad hoc LED array illumination system modified from **Figure 15** by using 8 LEDs (SLLP-F586-1520-UV, Semileds, 400 nm) and two 100 Ω resistances.

3.2.4 Green (525 nm) LED array circuit design

Previous studies by Jaadane et al. (2015a) on albino rats demonstrated that the blue component of white LED is the cause of retinal injury. Hence in our study we wanted to include a green-light control different from shorter wavelength blue-light. Cells cultured on 8-well ECIS plates, were exposed using an ad hoc LED circuit with 16 blue LEDs (Kingbright L-17114VBC/DS-D, 5 mm, 470 nm), 4 green LEDs (Kingbright L-7113VGC-H, 5mm, 525 nm) and five 10 Ω resistances connected on a breadboard. However, this ad hoc LED circuit was only used as a source of green-light and blue LEDs were covered with black foil during exposures. The forward current and LED angle of each green LED were respectively 20 mA and 20^{o}. The resulting green-light irradiance as characterized by using a spectroradiometer, was 20.1 W/m² (Figure 18).

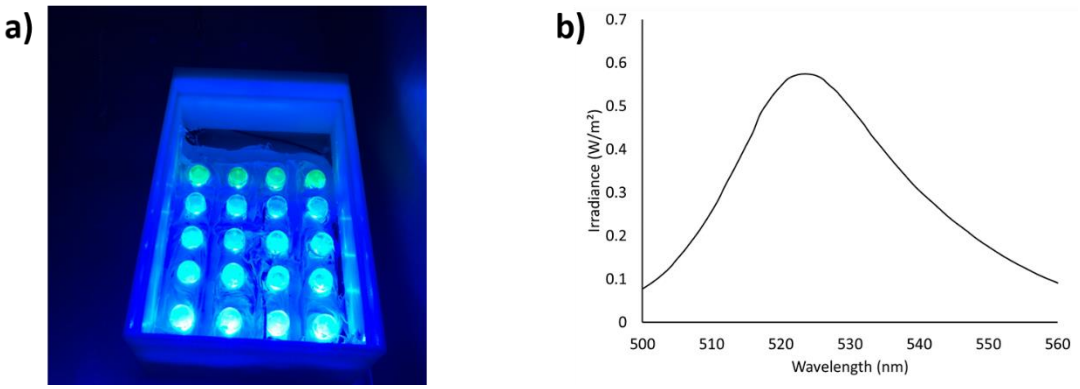

Figure 18 8W1E ECIS plate green-light (525 nm) illumination setup. **a)** Ad hoc LED circuit with 16 blue LEDs (Kingbright L-17114VBC/DS-D, 5 mm, 470 nm), 4 green LEDs (Kingbright L-7113VGC-H, 5mm, 525 nm) and five 10 Ω resistances connected on a breadboard was only used as a source of green-light by covering blue LEDs with black aluminium foil during exposures. **b)** Irradiance peak of 525 nm green-light LED as measured by using a spectroradiometer (SR9910, Irradian Limited, UK).

3.3 Light Exposure

All the light exposures were performed in the dark, in an incubator set at 37°C and 5% CO_2 to control the background lighting. A spectroradiometer (SR9910, Irradian Limited, UK) was used every-time when an experiment was set up to confirm the light irradiances and wavelength applied to cells in culture.

3.3.1 Continuous Blue-Light (470 nm) exposure on ARPE-19 cultured on 96W1E ECIS arrays

ARPE-19 cells cultured on 96 well ECIS arrays were exposed to continuous blue-light using the ad hoc LED array circuit with 12 LEDs (Cree 5 mm Blue, 470 nm) and four 100 Ω resistances. Using a spectroradiometer (SR9910, Irradian Limited, UK) the blue-light irradiance reaching the cells through the media was measured to be 118.1 W/m^2. Using neutral density filters, the ARPE-19 cells cultured in 96-well ECIS plate were exposed to 118.1 W/m^2, 74.65 W/m^2, 47.05 W/m^2 and 29.67 W/m^2 of blue-light.

3.3.2 Continuous and Daily Blue-Light (470 nm) exposure on ARPE-19 cultured on 8W1E ECIS arrays

ARPE-19 cells cultured on 8 well ECIS arrays were exposed to blue-light using the ad hoc LED array circuit with 8 LEDs (Cree 5 mm Blue, 470 nm) and two

150 Ω resistances. Using a spectroradiometer (SR9910, Irradian Limited, UK) the blue-light irradiance reaching the cells through the media was measured to be 140.4 W/m^2. Experiments were carried out where ARPE-19 were exposed to continuous blue-light, 4 h of exposure for one day (daily i), 4 h of exposure each day for 2 days (daily ii), and 4 h of exposure each day for 3 days (daily iii).

3.3.3 Continuous Blue-Light (420 nm) exposure on ARPE-19 cultured on 8WE1 ECIS arrays

ARPE-19 cells cultured on 8 well ECIS arrays were exposed to continuous blue-light using the 120 Watt metal halide epifluorescence lamp (BS039085, X-Cite 120, Excelitas Technologies, USA) with a 420nm band pass filter (FB420-10, Thorlabs, 420 ±10). Using a spectroradiometer (SR9910, Irradian Limited, UK) the blue-light irradiance reaching the cells through the media was measured to be 15.8 W/m^2. Using neutral density filters, the ARPE-19 cells cultured in 8 well ECIS arrays were exposed to 15.8 W/m^2 and 9.97 W/m^2 of blue-light.

3.3.4 Continuous Blue-Light (400 nm) exposure on ARPE-19 cultured on 8WE1 ECIS arrays

ARPE-19 cells cultured on 8 well ECIS arrays were exposed to continuous blue-light using the ad hoc LED circuit with 8 LEDs (SLLP-F586-1520-UV, Semileds, 400 nm) and two 100 Ω resistances. Using a spectroradiometer (SR9910, Irradian Limited, UK) the blue-light irradiance reaching the cells through the media was measured to be 17.66 W/m^2.

3.3.5 Continuous Green-Light (525 nm) exposure on ARPE-19 cultured on 8WE1 ECIS arrays

ARPE-19 cells cultured on 8 well ECIS arrays were exposed to continuous green-light using the ad hoc LED circuit with 16 blue LEDs (Kingbright L-17114VBC/DS-D, 5 mm, 470 nm), 4 green LEDs (Kingbright L-7113VGC-H, 5mm, 525 nm) and five 10 Ω resistances. Using a spectroradiometer (SR9910,

Irradian Limited, UK) the green-light irradiance reaching the cells through the media was measured to be 18.7 W/m^2.

3.4 Zonula Occludens-1 (ZO-1) Staining

ARPE-19 cells cultured in glass-bottom 12 well plates (Cellvis, P12-1.5H-N) (5.2 x 10^4 cell/cm^2) were exposed to 118.1 W/m^2 and 74.65 W/m^2 blue-light with a peak at 468nm for 4 hours with an ad hoc LED illumination system. Immediately after the exposure, media were discarded and cells were washed with modified PBS twice. Cells were fixed in 4% formaldehyde (9713.9010, VWR Chemicals) for 15 minutes at room temperature. Formaldehyde was washed off with modified PBS twice. The plates were blocked using Super-Block® solution (37515, Thermo Fisher Scientific) for 15 minutes at room temperature. The cells were then incubated over-night at 4°C within an antibody solution consisting of rabbit anti-ZO-1 (1 mg/ml; ab216880, Abcam) diluted in Super-Block® at 1:1000 ratio. The ZO-1 antibody was washed off with modified PBS five times. The cells were then incubated, in the dark, for 1 hour at room temperature with AlexaFluor 488-conjugated anti-rabbit immuno-globulin G (IgG) (2 mg/ml; A11034, Invitrogen) diluted in Super-Block® solution at 1:100 ratio. Finally, cells were counterstained using 4',6-diamidino-2-phenylindole (DAPI) (1 mg/ml; 62248, Thermo Fisher Scientific) diluted in modified PBS at 1:1000 ratio, for 1 minute before being imaged using an inverted fluorescent microscope (Widefield Zeiss Observer). ImageJ software was used to analyse and quantify the images of staining experiments.

3.5 Reactive Oxygen Species (ROS) Detection

ROS was detected/quantified using the Image-iT LIVE Green Reactive Oxygen Species Detection Kit (I36007, Invitrogen, Thermo Fisher Scientific) containing 275 µg carboxy-H2DCFDA to detect general reactive oxygen species. A stock solution of 10 mM was prepared by adding 50 µL of dimethylsulfoxide (DMSO) (20688, Thermo Fisher Scientific) to a vial containing 275 µg carboxy-H2DCFDA. Then an intermediate dilution of 2 µM of carboxy-H2DCFDA was made by dissolving 10 µL of this stock solution in 50mL of cell

culture media. Equal volume of 2 µM of carboxy-H2DCFDA solution and cell culture media were mixed to give the final concentration of 1 µM carboxy-H2DCFDA working solution. As the positive control, 50 µL 7.78 M 70% tert-butyl hydroperoxide (TBHP) in water was provided as a part of the Image-iT LIVE Green Reactive Oxygen Species Detection Kit. First, an intermediate dilution of 50 mM was prepared and then it was diluted in the cell culture media to prepare 200 µM TBHP working solution. After the ARPE-19 cells were exposed to 118.1 W/m^2 blue-light for 4 h or incubated with 200 µM TBHP working solution for 30 min, the cell culture media were discarded and the cells were incubated with 1 µM carboxy-H2DCFDA working solution for 30 min at 37^{o}C. The Flow Cytometry analysis was performed with a NovoCyte flow cytometer (ACEA Biosciences, San Diego, USA samples). Cell viability was assessed via Deep Red Anthraquinone 7 (DRAQ7) (ab109202, Abcam) exclusion. The R780/60 channel was set for DRAQ7 and the B530/30 channel was set for carboxy-H2DCFDA.

3.6 Protein Kinase C Zeta (PKC- ζ) Inhibition

3.6.1 Preparation of PKC- ζ Inhibitor

To inhibit selectively PKC-ζ, myristoylated PKC-ζ pseudo substrate inhibitor (539624-500UG, Calbiochem) was used. To prepare a 500 µM stock solution, 500 µg of the inhibitor was dissolved in 500 µL of water. Then, to prepare 100 nM PKC-ζ inhibitor working solution, 10 µL of the stock solution was dissolved in 50 mL cell culture media DMEM (1X) 4.5g/L D-Glucose, L-Glutamine supplemented with 1% FCS, 1% pen-strep and 1 mM sodium pyruvate.

3.6.2 Restorative effect of PKC- ζ Inhibition

To investigate the restorative effect of PKC- ζ inhibition, following the 4 h blue LED light exposure at 140.4 W/m^2 on ARPE-19 cells cultured on 8-well ECIS plate, the media of the case study were changed to 100 nM PKC-ζ inhibitor working solution, while the media of the control study were changed to DMEM (1X) 4.5g/L D-Glucose, L-Glutamine supplemented with 1% FCS, 1% pen-strep and 1 mM sodium pyruvate.

3.6.3 Protective effect of PKC- ζ Inhibition

To investigate the protective effect of PKC- ζ inhibition on ARPE-19 cells cultured on 8-well ECIS plate, the media of the case study were changed to 100 nM PKC-ζ inhibitor working solution, while the media of the control study were changed to DMEM (1X) 4.5g/L D-Glucose, L-Glutamine supplemented with 1% FCS, 1% pen-strep and 1 mM sodium pyruvate prior to blue LED light exposure at 140.4 W/m^2.

3.7 Cellular Senescence

3.7.1 Treatment of ARPE-19 cells with TBHP and H_2O_2 to induce senescence

In our study to treat the cells with TBHP and H_2O_2, we have followed the protocol established by Kaczara et al (2010), which document that H_2O_2 concentration in ARPE-19 culture medium exponentially depleted (with the half-life of depletion = 35 min) and reached minimal levels by 2 hour-mark. In our experiments initially, optimisation experiments were conducted to optimize the concentration of TBHP and H_2O_2 that would induce maximum senescence and minimum cell death. Confluent ARPE-19 cells cultured in µ-Slide 8 Well (80826, Ibidi) were treated with either 100 µM tert-butyl hydroperoxide (TBHP) (488139-10ML, Sigma) dissolved in DMEM (1X) 4.5g/L D-Glucose, L-Glutamine supplemented with 1% FCS, 1% pen-strep and 1 mM sodium pyruvate or 750 µM hydrogen peroxide solution at 30 % (H1009-500ML, Sigma) dissolved in DMEM (1X) 4.5g/L D-Glucose, L-Glutamine supplemented with 1% FCS, 1% pen-strep and 1 mM sodium pyruvate. Cells were incubated in an incubator set at 37°C and 5% CO_2 for 2 hours. Then the media were removed and cells were washed with in DMEM (1X) 4.5g/L D-Glucose, L-Glutamine supplemented with 1% FCS, 1% pen-strep and 1 mM sodium pyruvate. Cells were cultured with DMEM (1X) 4.5g/L D-Glucose, L-Glutamine supplemented with 1% FCS, 1% pen-strep and 1 mM sodium pyruvate for further 72 hours in an incubator set at 37°C and 5% CO_2. Then the cells were fixed before treatment with β-galactosidase staining solution.

3.7.2 Treatment of ARPE-19 cells with Blue-Light (470 nm) to induce senescence

In optimisation experiments, ARPE-19 cultured on 8WE1 ECIS arrays were exposed to continuous blue-light (140.4 W/m^2; 470 nm), and statistically significant time points for barrier function break-down and cell coverage decline were observed at 4 and 12.5 hours respectively. Hence in order to simulate cellular features of AMD development (i.e. cellular senescence, barrier function breakdown and mitochondrial dysfunction) in in-vitro before cell coverage declined, 7 hours of blue-light (140.4 W/m^2; 470 nm) was chosen in our study. Confluent ARPE-19 cells cultured in µ-Slide 8 Well (80826, Ibidi) were exposed to 7 hours of 140.4 W/m^2 Blue-Light using an ad hoc LED array circuit with 8 LEDs. Then the cells were fixed before treatment with β-galactosidase working solution.

3.7.3 Preparation of fixative for β-galactosidase staining

Senescence associated β-galactosidase staining of ARPE-19 was based on the protocol used by Dimri et al. (1995). To prepare 10 ml of fixative, a mixture of 1ml of Phosphate-Buffered Saline (10X) pH 7.4, RNase-free (AM9625, Thermo-Fischer), 1.25ml of 16% Formaldehyde (28908, Thermo-Fischer) and 80 µl of 25% glutaraldehyde solution in H_2O (G5882, Sigma) was mixed in the presence of 7.67 ml of Milli-Q water. ARPE-19 cells were fixed using the fixative at room temperature for 10 minutes. The cells were then washed with PBS three times.

3.7.4 Preparation of potassium ferrocyanide solution

To prepare a 50 mM aquous solution, 500 mM potassium ferrocyanide (2.11 g, P3289, Sigma) was dissolved in 100 ml of water. The solution was aliquoted and kept frozen at – 20^0C in the dark.

3.7.5 Preparation of potassium ferricyanide solution

To prepare a 50 mM aquous solution, 500 mM potassium ferricyanide (1.65 g, P3667, Sigma) was dissolved in 100 ml of water. The solution was aliquoted and kept frozen at – 20^0C in the dark.

3.7.6 Preparation of X-gal solution

To prepare 20mg/ml solution, 20 mg of 5-bromo-4-chloro-3-indolyl-beta-D-galacto-pyranoside (X-gal) (R0404, Thermo-Fischer) was dissolved in 1 ml of dimethylformamide (DMF) (20673, Thermo-Fischer).

3.7.7 Preparation of β-galactosidase staining solution

To prepare 100 ml of β-galactosidase staining solution, 400 mM $Na_2HPO_4.7H_2O$ (6.76 g, 431478, Sigma), 200 mM citric acid (1.43 g, 251275, Sigma), 1.5 M NaCl (8.76g, S7653, Sigma) and 20 mM $MgCl_2.6H_2O$ (0.407 g, 255777, Sigma) were mixed in a polypropylene plastic tube.

3.7.8 Preparation of β-galactosidase working solution

To prepare 10 ml of β-galactosidase working solution, 1 ml of β-galactosidase staining solution, 8.75 ml of H_2O, 100 µl of 50mM ferrocyanide solution, 100 µl of 50 mM ferricyanide solution and 50 µl of X-gal solution were mixed together. Fixed ARPE-19 cells were incubated over-night with β-galactosidase working solution at 37 ^{0}C at 0 % CO_2. Then the cells were washed with PBS 3 times before being imaged using a bright-field microscope (Widefield Zeiss Observer). ImageJ software was used to analyse the images of staining experiments.

3.7.9 Image Analysis

The images of β-galactosidase were analysed with ImageJ. The bright field images were split into channels. For β-galactosidase images, both red (C1) and blue (C2) channels were turned into intensity images displayed on a grey colour-map using “LUT” feature from ImageJ, in order to perform mathematical operation and quantitative analysis. First, a noise reduction was applied to the grey images using “Calculator Plus” feature in the next step. Using “Calculator Plus” feature, subtraction operation of “C2 – C1” on grey images were applied to identify the β-galactosidase staining on a dark background. Then thresholding between 255 and 65535 pixels was applied to the resulting images in order to further divide the images in two classes of pixels; foreground

and background. This thresholding was applied with the rationale of reducing & deducting the effect of the background (resulting from empty well) on the images (Fig 19). This thresholding was uniform across all samples and not varied from sample to sample. After thresholding, “Analyze Particles” feature was used to calculate the percentage of the stained area compared to the total area.

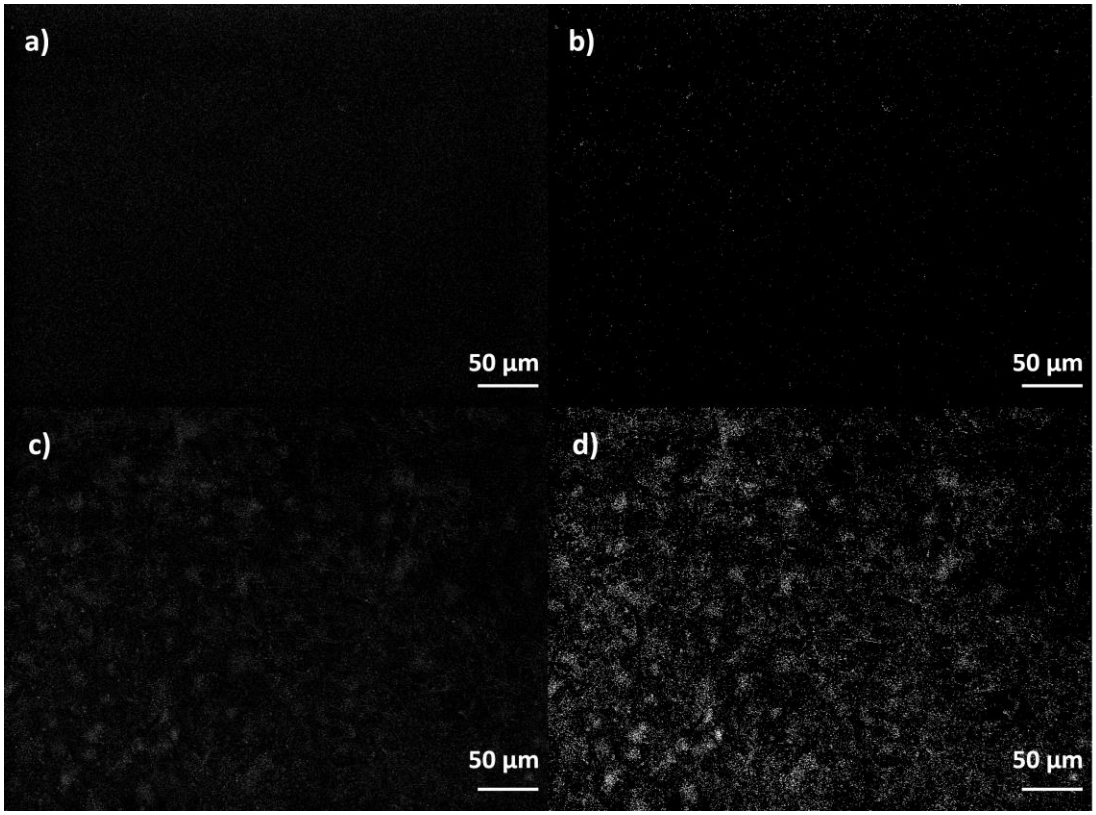

Figure 19 Example of Images pre- and post-thresholding **a)** Pre-thresholding image of background (empty well). **b)** Post-thresholding image of background (empty well) after pixel threshold between 255-65535 was applied. **c)** Pre-thresholding image of β-galactosidase staining with blue-light. **d)** Post-thresholding image of β-galactosidase staining with blue-light after pixel threshold between 255-65535 was applied.

3.8 Detection of Micromotion using ECIS

Fluctuations in resistance measurements at f = 4 kHz in ECIS have experimentally been related to cell micromotion (Lo et al., 1993; Opp et al., 2009; Lovelady et al., 2009; Láng et al., 2017). Chiu et al. (2019) recently established a new ECIS method demonstrating that these micromotions were related to mitochondrial respiration. The resistance fluctuation data were

acquired 24 h after the cells were treated with either blue-light, TBHP or H_2O_2. The variance was calculated following the protocol established by Chiu et al. (2019). The data points were acquired from each electrode at 1 second intervals. Data analysis was performed using the first 1024 data points acquired from each electrode. Each data point in 1024-point data set was first normalized by dividing each one by the average of 1024-point data set. Then, the normalized 1024-points was split into 32 sets of 32 points each, and the variance was calculated and averaged for all the sets (Chiu et al., 2019).

3.9 Mitochondrial Imaging

3.9.1 MitoTracker™ Assay

Twenty four hours after ARPE-19 cells were treated with either 140.4 W/m² blue-light for 7 hours, 100 µM TBHP for 2 hours or 750 µM H_2O_2 for 2 hours, the cells' mitochondria and nuclei were stained using MitoTracker™ Deep Red FM (Invitrogen, M22425) and Hoechst 33342 (Invitrogen). Briefly, this was completed by adding an equal volume of 2X MitoTracker™ Deep Red FM and Hoechst 33342 diluted in Hank's Balanced Salt Solution (HBSS, supplemented with calcium and magnesium) to the ARPE-19 culture media to give final concentrations of 20nM Mitotracker™ and 200nM Hoechst 33342. The cells were then incubated at 37°C for 10 minutes before undergoing three 50% washes with HBSS immediately followed by imaging using an inverted fluorescent microscope (Zeiss Observer).

3.9.2 Image Analysis

The images of MitoTracker™ assay with Hoeschst 33342 were analysed with ImageJ. First Hoeschst 33342 and MitoTracker™ channels were split and images were made binary. Using "Analyze Particles" feature on Hoechst 33342 channel, the number of nuclei were calculated. Then using "Analyze Particles" feature on MitoTracker™ channel with size set between 50 – ∞ µm² and with circularity set between 0.5 – 1.00, the impaired mitochondria were identified and calculated for all conditions. Finally the percentage of the

impaired mitochondria compared to the number of ARPE-19 stained with Hoechst 33342 were calculated.

3.10 A2E as an Age Pigment

3.10.1 Synthesis of A2E and iso-A2E

A2E and iso-A2E mixture was synthesized following the protocol established by Parish et al., (1998). A mixture of all-trans retinal (100 mg, 352 µmol) (1002554894, Sigma) and ethanolamine (9.5 mg, 155 µmol) (398136, Sigma) in ethanol (EtOH) (3.0 ml) (51976 Sigma) was stirred in the presence of acetic acid (9.3 µl, 155 µmol) (A6283, Sigma) at room temperature with a sealed cap in the dark for 2 days. After the mixture was concentrated in vacuo, the residue was purified by silica gel column chromatography. After elution with methanol (MeOH):CH_2Cl_2 (5:95) (34860, Sigma), further elution with MeOH:CH2Cl2:trifluoroacetic acid (TFA) (8:92:0.001) (302031, Sigma), the sample was collected in tubes. Five (5) ml of this sample was taken to a separate tube and left to evaporate in the dark over 2 days. The residue provided 62 mg of mixture of A2E and iso-A2E (104.67 µmol). The mixture was dissolved in DMSO (20688, Thermo-Fischer) to prepare 104.67 mM stock solution. An intermediate dilution of 1 mM was prepared in DMEM (1X) 4.5g/L D-Glucose, L-Glutamine supplemented with 1% FCS, 1% pen-strep and 1 mM sodium pyruvate. Finally, to achieve 100 µM working solution, the intermediate dilution was further dissolved in DMEM (1X) 4.5g/L D-Glucose, L-Glutamine supplemented with 1% FCS, 1% pen-strep and 1 mM sodium pyruvate.

3.10.2 Feeding of A2E and iso-A2E into ARPE-19 cells

ARPE-19 cells were fed with 100 µM and 50 µM A2E and iso-A2E mixture following the protocol by Sparrow et al., (2000) as these amounts were reported to be comparable to A2E levels measured in human primary RPE isolated from healthy donor eyes (34-134 ng/10^5 cells). The cells were incubated for 1 and 2 days with each concentration. Then the mixture was discarded and cells were washed with PBS twice and were kept in DMEM (1X)

4.5g/L D-Glucose, L-Glutamine supplemented with 1% FCS, 1% pen-strep and 1 mM sodium pyruvate.

3.10.3 Detection of internalized A2E

After the incubation with A2E and iso-A2E mixture ARPE-19 cells were fixed with 4 % paraformaldehyde in PBS (J19943K2, Thermo Fisher Scentific). The cells were counterstained using Hoescht (62249, Thermo Fisher Scientific) diluted in modified PBS at 1:10000 ratio, for 10 minutes at room temperature. Then the stain was removed from the wells and the wells were washed with PBS before being imaged using an inverted fluorescent microscope (Widefield Zeiss Observer). A2E containing ARPE-19 cells fixed with paraformaldehyde were imaged at excitation/emission of 488/565 nm. ImageJ software was used to analyze the images of staining experiments. Using ImageJ first Hoescht and A2E channels were split into two intensity channels. Then to measure the pixel intensity for A2E channel, first under “Analyse” menu “Set Measurements” command was applied and “mean grey value”, “standard deviation” and “area” were selected. Then to calculate the pixel intensity, the entire area of the images were selected and for each image the mean pixel intensity was measured through “Measure” command under “Analyse” menu. For each image, the analysed area was the same and consisted of the entire image.

3.11 Imaging of ARPE-19 cells in culture

Prior to imaging Figures 20d and 24c, d, and e, toluidine blue-sodium tetra borate mixture was used to improve image contrast. After the experiments were completed, ARPE-19 cells were fixed with 4 % paraformaldehyde in PBS (J19943K2, Thermo Fisher Scentific) and stained using toluidine blue-sodium tetra borate staining solution which was prepared following the protocol established by Todd et al., (2005) in order to improve image quality. Toluidine blue-sodium tetra borate staining solution was prepared by mixing 0.2 g of toluidine blue (6586-04-5, Sigma) dissolved in 10 ml distilled water (7732-18-5, Sigma) and 0.2 g of sodium tetra-borate (1330-43-4, Sigma) dissolved in 10 ml distilled water (7732-18-5, Sigma) in a 1:1 ratio. After fixed ARPE-19

cells were washed with toluidine blue-sodium tetra borate staining solution for 5 min, cells were washed with PBS 3 times and were imaged using a digital inverted brightfield and phase contrast microscope (6500-FL, EVOS).

3.12 Statistical Analysis

IBM SPSS Statistics was used to perform one-way Analysis of Variance (ANOVA) and Tukey-Kramer test to determine whether the investigated groups were significantly different from each other. A probability value of $P < 0.05$ was set as significant.

4 Effect of Blue-Light on ARPE-19 cells

4.1 Growth of hTERT-RPE1 and ARPE-19 Cells on ECIS

First, to establish which cell line was able to establish a robust epithelial barrier both ARPE-19 and hTERT-RPE1 (5.2 x 10^4 cells/cm^2) were seeded on ECIS electrode plates. From the seeding time-point, the time course of resistance at f = 4 kHz was recorded (Fig. 20a) and following Giaever and Keese's (1991) method the electrical impedance data was modelled to provide the data on barrier function (R_b) over time (Fig. 20b). The barrier function formed by the tight junctions between ARPE-19 cells were observed to be 5 times stronger than those of hTERT-RPE1 (Fig. 20c). Therefore in order to mimic the barrier function of the RPE, ARPE-19 cells were chosen together with ECIS micro-electrode arrays to lay the foundations for an AMD disease model (Fig. 20d).

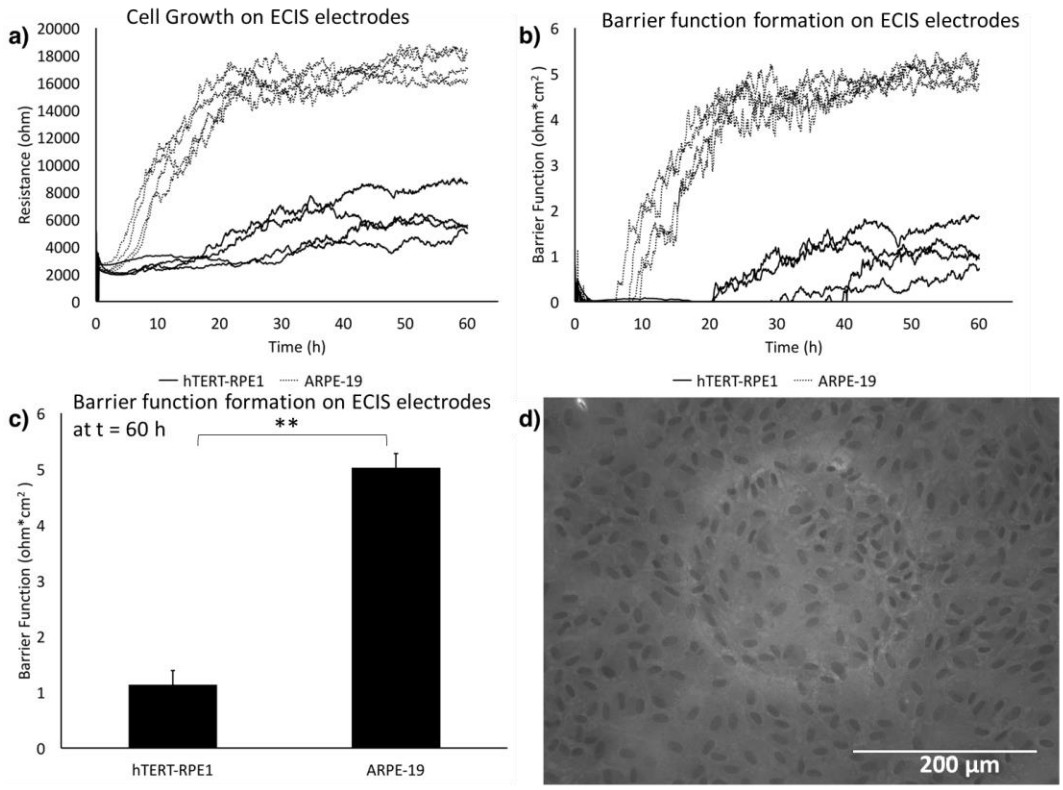

Figure 20 Growth of hTERT-RPE1 and ARPE-19 Cells on ECIS. The time course measurements of the barrier function associated with tight junction formation was 5 times stronger in ARPE-19 com-pared to hTERT-RPE after 60 hours. This made ARPE-19 a better

in-vitro model for replicating in-vivo retinal cell behavior. **a)** Resistance at 4 kHz (n = 4). **b)** Barrier function associated with tight junction formation (n = 4). **c)** Barrier function at t = 60 h (n=4). Bars represent standard error. ** shows P<0.01. **d)** ARPE-19 cells cultured on ECIS micro-electrode array at 100 % confluence forming 5 Ωcm² barrier function. Scale bar represents 200 µm.

4.2 Time-course Measurements of 470 nm Blue-light Exposure on ARPE-19 Cells

Confluent ARPE-19 cultures on a 96 well ECIS micro-electrode array were recorded over the course of continuous blue-light exposure with time zero set at the start of blue light exposure and media change. The media change resulted in a typical transient peak in resistance associated with temperature and dissolved CO_2 variation for all wells, which was also observed at the second media change (t = 50 h) for both wells with cells and wells with media alone.

The raw data resistance recordings at 4 kHz (Fig. 21a) and at 64 kHz (Fig. 21b) were plotted under continuous blue-light exposure. At f = 4 kHz, a marked decrease in resistance in a dose-dependent manner was observed at all exposures, with the highest exposure eventually led to a resistance comparable to the media only control, and was associated to cell coverage decline (Fig. 21a). On the other hand, when the same wells were observed at f = 64 kHz, the time course resistances were strikingly different, with no decrease in resistance before t = 52 h and only the two highest exposures resulted in a decline in resistance (Fig. 21b). These observations were consistent across all the wells (n = 24), and the average values and standard errors were reported in Fig. 21c and Fig. 21d.

The difference in resistance graphs at low frequency and high frequency indicated that blue-light had different effects on paracellular resistance and cell electrode coverage. A drop in resistance occurring only in the lower frequency range could be associated with a decrease in the para-cellular resistance, i.e. a loss of the barrier function. To investigate further, the mathematical model integrated in the ECIS software was used to quantify the barrier function. The mathematical model on barrier function showed that blue light exposure

induced a dose-dependent decrease in barrier function, before cell coverage decline occurred (Fig. 21e). Significant differences ($P < 0.05$) were found from t = 90 h for all groups (Fig. 21f). An early decrease in barrier function was found at time t = 4 h with 118.1 W/m^2, without associated cell coverage decline. On the other hand, a retention in resistance at the high frequency could be associated with cell coverage. To investigate further and quantify the cell coverage, the capacitance at f = 64 kHz was measured. The time course capacitance at f = 64 kHz (Fig. 21g) showed no increase before t = 52 h and only the two highest exposures resulted in a rise in capacitance indicating a decline in cell coverage. Significant differences ($P < 0.05$) were found from t = 90 h for all groups (Fig. 21h).

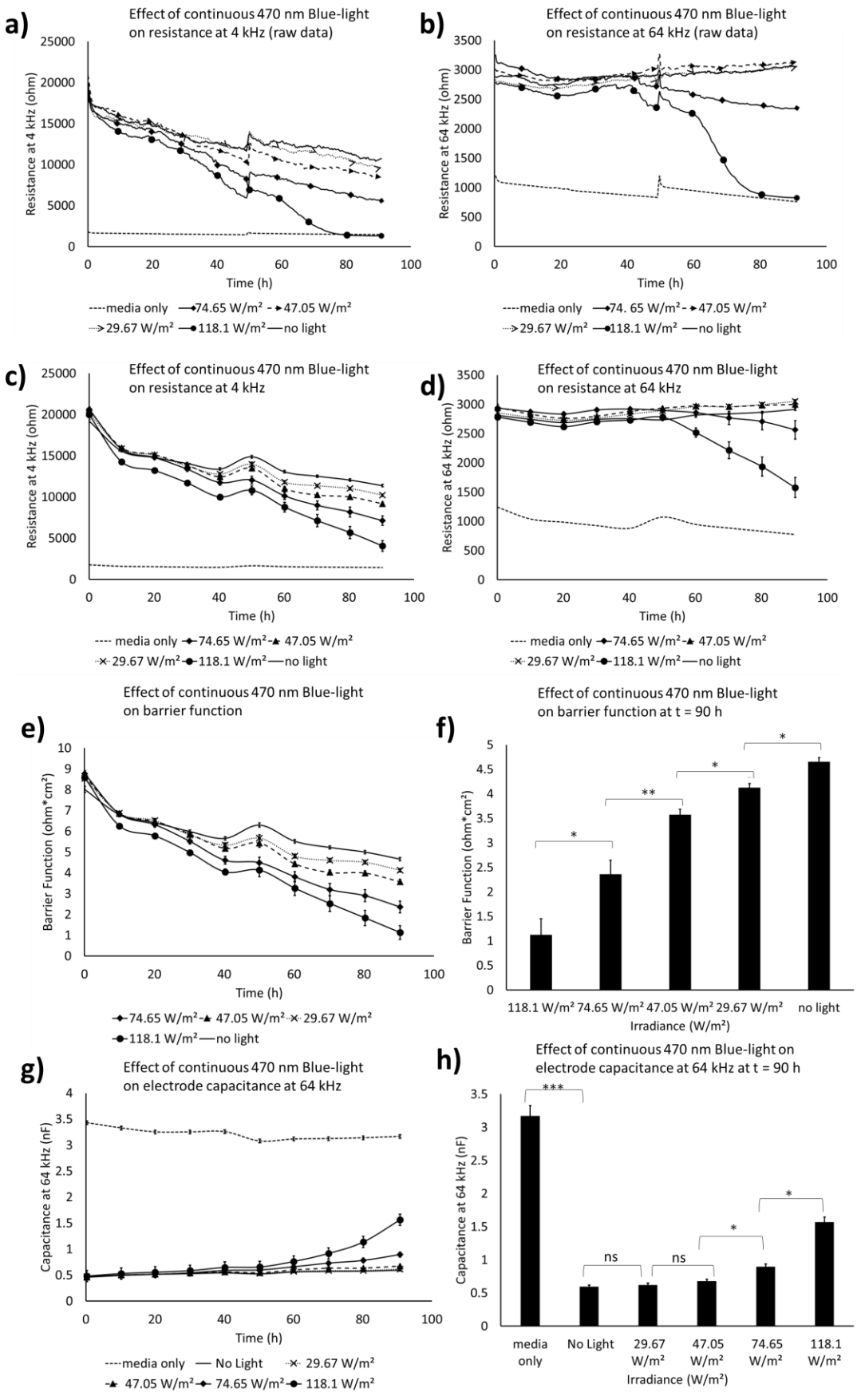
a)
Effect of continuous 470 nm Blue-light on resistance at 4 kHz (raw data)
Resistance at 4 kHz (ohm)
Time (h)
media only
74.65 W/m²
47.05 W/m²
29.67 W/m²
118.1 W/m²
no light
b)
Effect of continuous 470 nm Blue-light on resistance at 64 kHz (raw data)
Resistance at 64 kHz (ohm)
Time (h)
c)
Effect of continuous 470 nm Blue-light on resistance at 4 kHz
d)
Effect of continuous 470 nm Blue-light on resistance at 64 kHz
e)
Effect of continuous 470 nm Blue-light on barrier function
Barrier Function (ohm*cm²)
f)
Effect of continuous 470 nm Blue-light on barrier function at t = 90 h
Irradiance (W/m²)
g)
Effect of continuous 470 nm Blue-light on electrode capacitance at 64 kHz
Capacitance at 64 kHz (nF)
h)
Effect of continuous 470 nm Blue-light on electrode capacitance at 64 kHz at t = 90 h
ns
media only
No Light
29.67 W/m²
47.05 W/m²
74.65 W/m²
118.1 W/m²

Figure 21 Time-course Measurements of 470 nm Blue-light Exposure on ARPE-19 Cells. Confluent ARPE-19 cells were cultured on ECIS microarray wells, and using an ad-hoc LED array together with neutral density filters were simultaneously exposed to continuous blue-light (470 nm) exposure at different irradiances; 118.1 W/m^2, 7565 W/m^2, 47.05 W/m^2, 29.67 W/m^2. Resistance ($\boldsymbol{R}$) data at 4 kHz and 64 kHz were recorded in real-time. Raw data (n =1) for $\boldsymbol{R}$ at 4 kHz (**a**) and raw data (n =1) for $\boldsymbol{R}$ at 64 kHz (**b**) were shown. Using ECIS software mean values for all wells for $\boldsymbol{R}$ at 4 kHz (n =24) (**c**) and for $\boldsymbol{R}$ at 64 kHz (n =24) (**d**) were calculated. Our data showed that continuous blue-light exposure resulted in a decrease in $\boldsymbol{R}$ at 4 kHz in a dose-dependent manner, before any decline in $\boldsymbol{R}$ at 64 kHz. No decline in $\boldsymbol{R}$ at 64 kHz were observed before t = 52 h for highest irradiance. Resistance decline occurring only in low frequency range (4 kHz) could be associated with a decrease in the barrier function ($\boldsymbol{R_b}$) associated with cell-cell tight junction formation. ECIS software possess a built-in feature to model barrier function, which is the inverse measure of cell-cell junction permeability (Giaever and Keese, 1991). Quantifications using the mathematical model integrated in the ECIS software showed a dose-dependent decline in barrier function (**e**). Increase in electrode capacitance $\boldsymbol{C_E}$ at 64 kHz (**g**) (n = 24) showed that cell coverage declined after t =52 h for the highest irradiance. All together these results showed that blue-light induced a dose-dependent decrease in cell-cell tight junction associated barrier function ($\boldsymbol{R_b}$), before cell coverage decline occurred. Statistical analysis performed at t = 90 h for the barrier function (**f**) (n = 24) and electrode capacitance $\boldsymbol{C_E}$ at 64 kHz (**h**) (n = 24) confirmed the significance of our results. Bars show standard error. * shows P<0.05, ** shows P<0.01, *** shows P<0.001, ns shows not significant.

4.3 Mislocalisation of ZO-1 Immunostaining after Blue-light Exposure

As the earliest statistically significant difference in barrier function was observed at time t = 4h, this time point was chosen to perform ZO-1 staining of the ARPE-19, as displayed in Fig. 22. Immunostaining against the tight junction-associated structural protein ZO-1 clearly indicated a progressive mislocalisation of barrier function associated with blue light exposure, therefore validating the previous observations from resistance recordings.

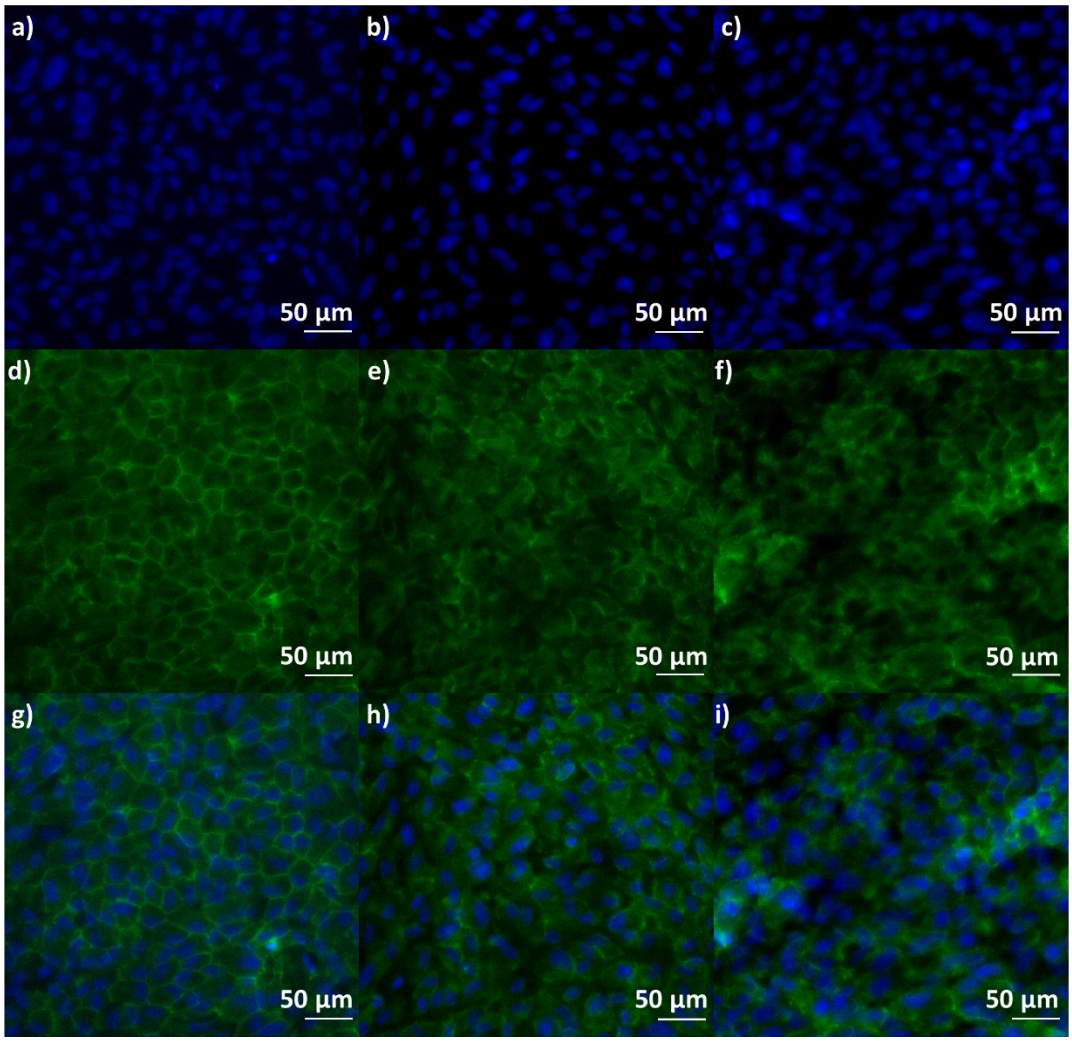

Figure 22 Mislocalisation of ZO-1 Immunostaining after Blue-light Exposure. Immunostaining of the tight-junction associated structural protein, ZO-1, in ARPE-19 showed a progressive mislocalisation of barrier function associated with blue light exposure **a)** DAPI for no-light control (n = 3). **b)** DAPI for irradiance 74.65 W/m² (n = 3). **c)** DAPI for irradiance 118.1 W/m² (n = 3). **d)** ZO-1 staining for no-light control (n = 3). **e)** ZO-1 staining for irradiance 74.65 W/m² after t = 4 h (n = 3). **f)** ZO-1 for irradiance 118.1 W/m² after t = 4 h (n = 3). **g)** Composite image for no-light control (n = 3). **h)** Composite image for irradiance 74.65 W/m² after t = 4 h (n = 3). **i)** Composite image for irradiance 118.1 W/m² after t = 4 h (n = 3).

4.4 Measurement of Oxidative Stress after Blue-light Exposure

The same time point (t = 4h) was investigated for evidence of oxidative stress using the ROS dye carboxy-H2DCFDA. The flow cytometry was set with the DRAQ7 dye in the X axis and the general oxidative stress indicator (carboxy-H2DCFDA) in the Y axis (Fig. 23). This resulted in splitting the figure in 4 quadrants; Carboxy-H2DCFDA (+) / DRAQ7 (-) indicated the population of

oxidative stress positive live cells shown in quadrant 1-1 (Q1-1), Carboxy-H2DCFDA (+) / DRAQ7 (+) indicated the population of oxidative stress positive dead cells shown in quadrant 1-2 (Q1-2), Car-boxy-H2DCFDA (-) / DRAQ7 (-) indicated the population of oxidative stress negative live cells shown in quadrant 1-3 (Q1-3), and Carboxy-H2DCFDA (-) / DRAQ7 (+) indicated the population of oxidative stress negative dead cells shown in quadrant 1-4 (Q1-4). As opposed to ECIS data, cell death likely associated with cell manipulation required for flow cytometry, i.e. cell trypsinization and cell fixation, was also observed. The flow cytometry data showed an increase in oxidative stress in DRAQ7 negative (live) cells, after treatment with TBHP (Fig. 23a) and blue-light (Fig. 23b) compared to untreated control cells (Fig. 23c). The data showed that after blue-light exposure general oxidative stress could be detected at higher levels compared to TBHP treatment and control in DRAQ7 negative cells (Fig. 23d). Hence, lower levels of oxidative stress negative cells were observed amongst DRAQ7 negative cells after blue-light treatment (Fig. 23e).

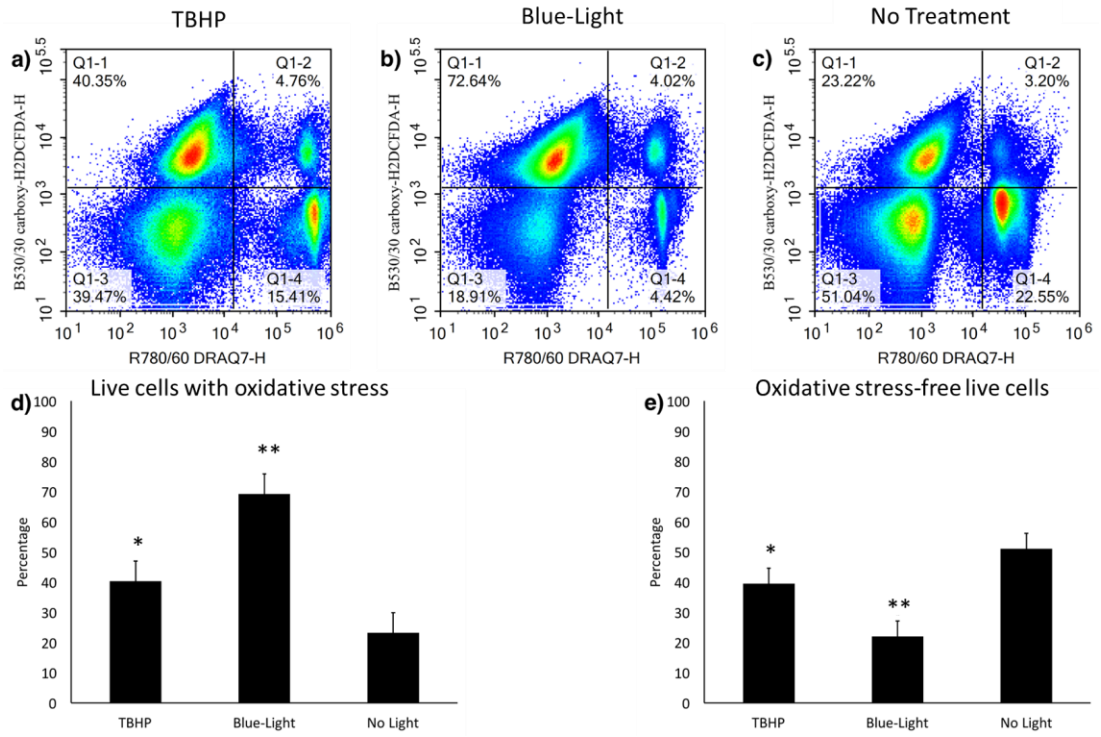

Figure 23 Flow Cytometry Measurement of Oxidative Stress after Blue-light Exposure. Flow cytometry data with DRAQ-7 and carboxy-H2DCFDA showed that TBHP **(a)** and blue-

light exposure **(b)** increased the percentage of Carboxy-H2DCFDA (+) / DRAQ7 (-) ARPE-19 cells shown in Q1-1 compared to no-light control **(c)**. Carboxy-H2DCFDA (+) / DRAQ7 (-) indicated the population of oxidative stress positive live cells (Q1-1). Carboxy-H2DCFDA (-) / DRAQ7 (-) indicated the population of oxidative stress negative live cells (Q1-3). As opposed to ECIS data, cell death likely associated with cell manipulation required for flow cytometry, i.e. cell trypsinization and cell fixation, was also observed in oxidative stress negative (Q1-4) and oxidative stress positive (Q1-2) cells. **a)** ARPE-19 treated with TBHP for 30 min (n = 3). **b)** ARPE-19 exposed to blue-light for 4 h (n = 3). **c)** No light control (n = 3). **d)** Percentage of oxidative stressed live ARPE-19 (Q1-1) (n = 3). **e)** Percentage of healthy live ARPE-19 (Q1-3) (n = 3). Bars show standard error. In each chart * shows P<0.05 compared to no light, ** shows P<0.01 compared to no light.

4.5 Effect of PKC-ζ Inhibition on ARPE-19 Barrier Function After Blue-light Exposure

4.5.1 Restorative Effect of PKC-ζ Inhibition

The time course restorative effect of PKC-ζ pseudo substrate inhibitor which has been shown previously to restore barrier function in diabetic retinopathy (Omri et al., 2013) was investigated by using ECIS. Resistance data at f = 4 kHz along with the model of barrier function showed that PKC-ζ inhibition induced faster restoration of barrier function compared to no treatment after 4 h of blue light (470 nm) damage to the tight junctions (Fig. 24). It was observed that PKC-ζ inhibition restored the barrier function immediately after the media change at time t = 4 h, while the no treatment control restored the barrier function at t = 6.5 h. The images were taken of each well at t = 7h and no visible differences were observed between the cells after the restoration of the barrier function.

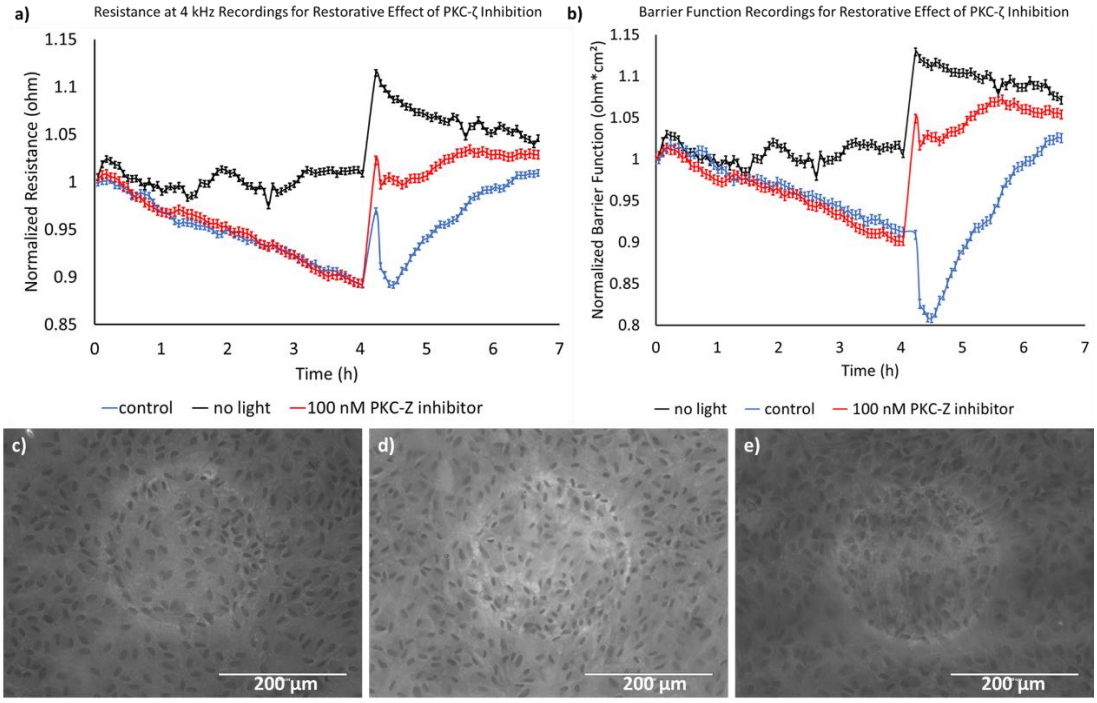

Figure 24 Restorative Effect of PKC-ζ Inhibition. PKC-ζ inhibition restored the barrier function immediately after the media change at time t = 4 h, while no treatment control restored the barrier function at 6.5 h (n = 3). **a)** Normalized resistance at 4 kHz (n = 3). **b)** Normalized barrier function (n = 3). **c)** No light ARPE-19 cells as observed at t = 7 h. **d)** ARPE-19 after 100 nM PKC-ζ inhibitor treatment as observed at t = 7 h. **e)** Control ARPE-19 exposed to blue-light as observed at t = 7 h. Bars show standard error.

4.5.2 Protective Effect of PKC-ζ Inhibition

The time course protective effect of PKC-ζ pseudo substrate inhibitor was also investigated using ECIS. ARPE-19 cells cultured in media containing 100 nM PKC- ζ inhibitor and no inhibitor were exposed to continuous 140.4 W/m^2 blue-light (470 nm) starting from t = 0. Resistance data at f = 4 kHz showed that PKC-ζ inhibition exerted an early protective effect by delaying the decline in para-cellular resistance and also decreased the rate of decline compared to no treatment under continuous blue-light (470 nm) exposure. Furthermore, resistance data at f = 64 kHz showed that PKC-ζ inhibition delayed the decline in cell coverage (Fig 25).

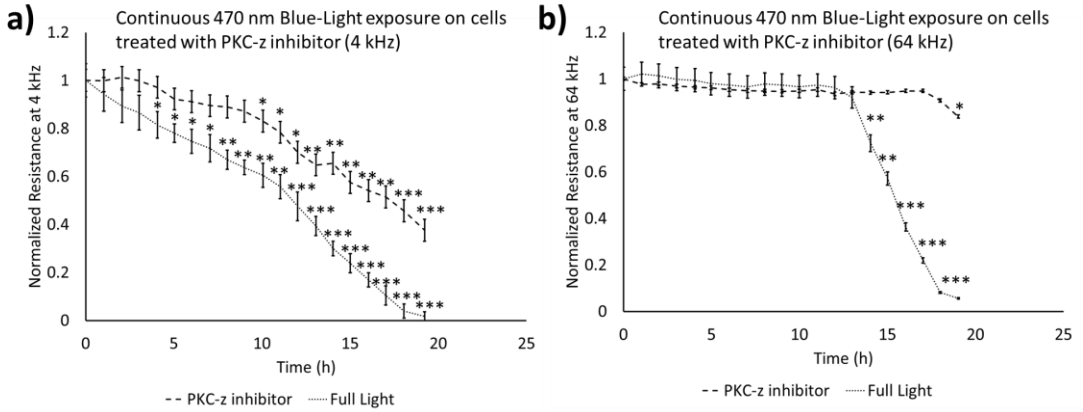

Figure 25 Protective Effect of PKC-ζ Inhibition. PKC-ζ inhibition showed an early protective effect by delaying decline in resistance at f = 4 kHz. It was also observed that PKC-ζ inhibition decreased the rate of decline in resistance at f = 4 kHz compared to no treatment under continuous blue-light (470 nm) exposure. Furthermore, resistance data at f = 64 kHz showed that PKC-ζ inhibition delayed the decline in cell coverage. **a)** Normalized resistance at 4 kHz (n = 3). **b)** Normalized resistance at 64 kHz (n = 3). Bars show standard error. For each time-point statistical significance compared to t = 0 h time-point is shown for each chart. * shows P<0.05 compared to t = 0 h, ** shows P<0.01 compared to t = 0 h, *** shows P<0.001 compared to t = 0 h. Non labelled bars show not statistically significant.

4.6 Effect of Irradiance on the Radiant Exposure Threshold

Then we investigated if the reciprocity is observed in 470 nm photo-damage, in other words if the dose of radiant exposure which is the product of irradiance and the exposure time, sets the threshold damage. To this end, cells were exposed to 470 nm blue-light at different irradiances (E_e = 140.4 W/m^2, 118.1 W/m^2, 74.65 W/m^2, 47.05 W/m^2 and 29.67 W/m^2) and resistance data at 4 kHz and 64 kHz was recorded. For each data point, radiant exposure was determined and resistance data at f = 4 kHz and 64 kHz were plotted against radiant exposure for each irradiance (Fig 26). The data at f = 4 kHz (Fig. 26a) showed that ARPE-19 cells exposed to the same amount of radiant exposure as a result of 118.1 W/m^2, 74.65 W/m^2, 47.05 W/m^2 and 29.67 W/m^2 irradiances responded with the same decline rate. On the other hand, para-cellular resistance decline rate against radiant exposure was significantly increased in ARPE-19 cells exposed to 140.4 W/m^2 irradiance. Therefore, 140.4 W/m^2 blue-light was able to decrease the para-cellular resistance by inducing less radiant exposure compared to lower irradiances of blue-light at

470 nm (Fig 26a). The resistance data at f = 64 kHz showed that while 140.4 W/m^2 irradiance declined the ARPE-19 cell coverage after 0.8 x 10^7 J/m^2 of radiant exposure, 118.1 W/m^2 and 74.65 W/m^2 irradiances were able to decrease the cell coverage after 2.0 x 10^7 J/m^2 of radiant exposure. The cell coverage decline rate against radiant exposure was observed to increase with increased irradiance from 118.1 W/m^2 to 140.4 W/m^2 (Fig 26b).

Taken together these data indicated that reciprocity holds for irradiance values; 118.1 W/m^2, 74.65 W/m^2, 47.05 W/m^2, 29.67 W/m^2 and that same radiant exposure using these irradiance values results statistically similar damage. On the other hand, this reciprocity was not observed using 140.4 W/m^2 irradiance and the damage characterized by para-cellular resistance and cell coverage decline was increased. Hence, this indicated that reciprocity may not hold for high irradiance values. Our data underlined the importance of considering different irradiance values when performing experimental and clinical blue-light studies.

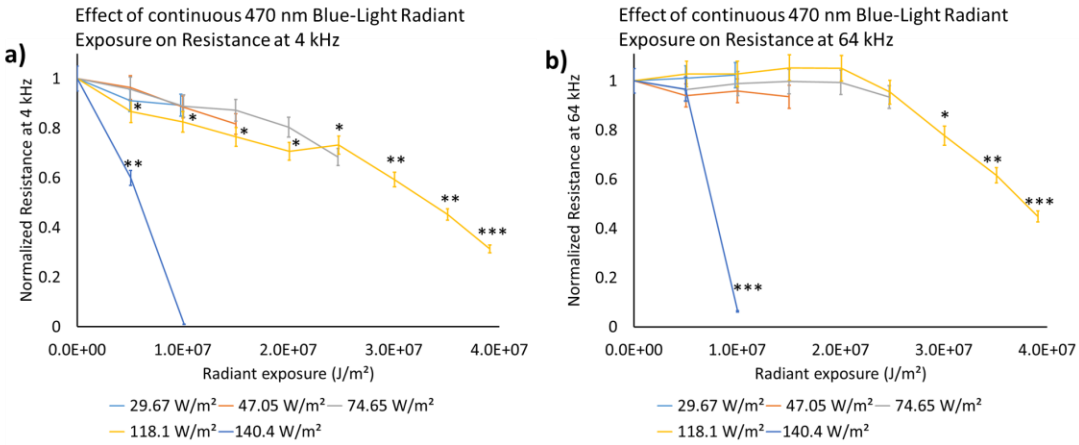

Figure 26 Effect of Irradiance on the Radiant Exposure Threshold. The data at f = 4 kHz showed that ARPE-19 cells exposed to the same amount of radiant exposure as a result of 118.1 W/m^2, 74.65 W/m^2, 47.05 W/m^2 and 29.67 W/m^2 irradiances responded with the same decline rate. On the other hand, para-cellular resistance decline rate against radiant exposure was significantly increased in ARPE-19 cells exposed to 140.4 W/m^2 irradiance. 140.4 W/m^2 blue-light was able to decrease the para-cellular resistance by inducing less radiant exposure compared to lower irradiances of blue-light at 470 nm. Moreover, the resistance data at f = 64 kHz showed that while 140.4 W/m^2 irradiance declined the ARPE-19 cell coverage after 0.8 x 10^7 J/m^2 of radiant exposure, 118.1 W/m^2 and 74.65 W/m^2 irradiances were able to decrease the cell coverage after 2.0 x 10^7 J/m^2 of radiant exposure. The cell coverage decline rate against radiant exposure was observed to increase with increased irradiance from 118.1 W/m^2

to 140.4 W/m^2. **a)** Normalized resistance at 4 kHz against radiant exposure (n = 6). **b)** Normalized resistance at 64 kHz against radiant exposure (n = 6). Bars show standard error. Statistically significant radiant exposure-points for 118.1 W/m^2 and 140.4 W/m^2 groups compared to 0 J/m^2 point are shown in each chart. For each radiant exposure point shown no statistical significance between 118.1 W/m^2, 74.65 W/m^2, 47.05 W/m^2 and 29.67 W/m^2 groups were found. * shows P<0.05 compared to 0 J/m^2, ** shows P<0.01 compared to 0 J/m^2, *** shows P<0.001 compared to 0 J/m^2. Non labelled bars show not statistically significant.

4.7 Time-course Measurements of 420 nm Blue-light Exposure on ARPE-19 Cells

The resistance data recordings at 4 kHz and at 64 kHz were plotted under continuous blue-light (420 nm) exposure. At f = 4 kHz, a marked decrease in resistance in a dose-dependent manner was observed in exposures with 15.8 W/m^2 and 9.97 W/m^2, with the highest irradiance value (15.8 W/m^2) eventually led to a full para-cellular resistance loss, and was associated to cell coverage decline (Fig 27a). On the other hand, when the same wells were observed at f = 64 kHz, the time course resistances were different, with no decrease in resistance before t = 58 h and only the highest exposure resulted in a decline in resistance (Fig 27b). These observations were consistent across all the wells (n = 3). These results indicated that 420 nm blue-light exposure induced a dose-dependent decrease in barrier function, before any cell coverage decline occurred.

The correlation between the para-cellular resistance and radiant exposure as well as the correlation between the cell electrode coverage and radiant exposure were investigated at both irradiances of 420nm blue-light. The para-cellular resistance decline rate against the radiant exposure was significantly increased in the higher irradiance compared to the lower irradiance of blue-light at 420 nm (Fig 27c). Therefore, 15.8 W/m^2 blue-light was able to decrease the para-cellular resistance by inducing less radiant exposure compared to 9.97 W/m^2 of blue-light at 420 nm. On the other hand, the decrease in cell coverage was observed only after the ARPE-19 were exposed to 3.0 x 10^6 J/m^2 of radiant exposure with 15.8 W/m^2 irradiance (Fig 27d). For both irradiance values, the radiant exposure threshold values that caused a

decrease in para-cellular resistance and cell coverage were found to be different from each other.

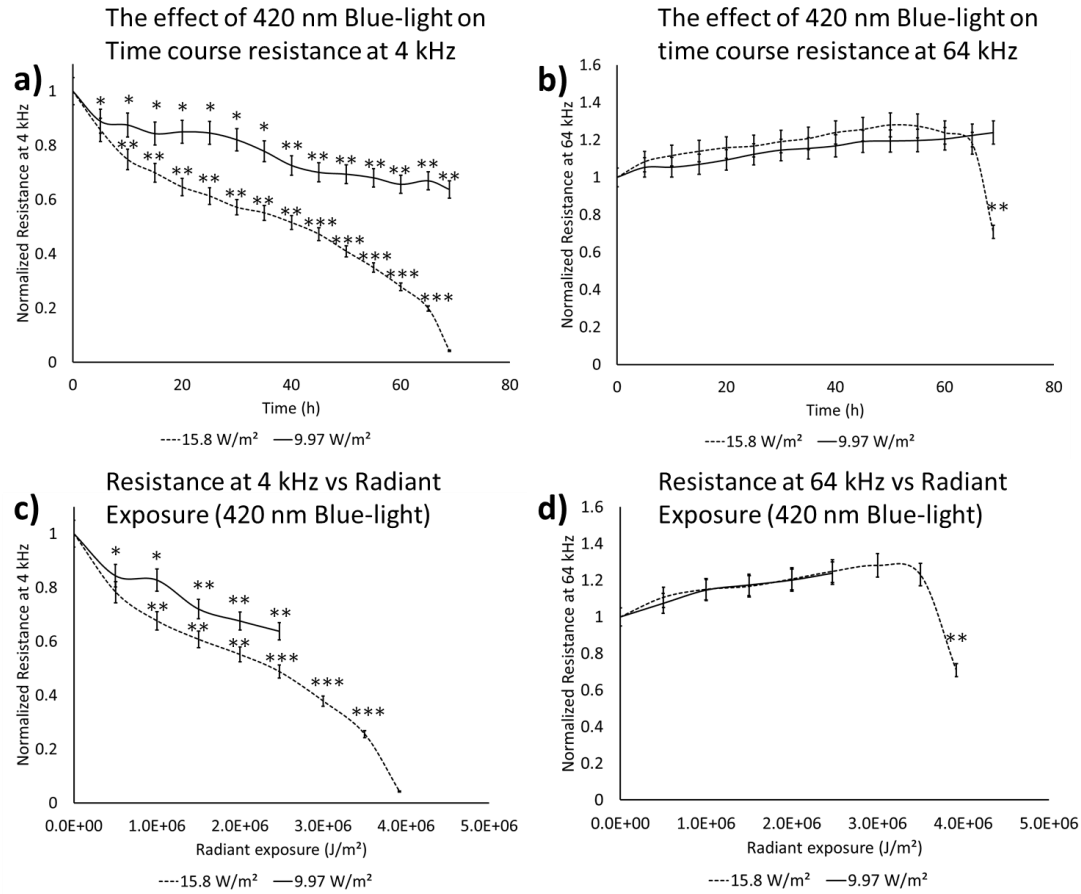

Figure 27 Time-course Measurements of 420 nm Blue-light Exposure on ARPE-19 Cells. Resistance data at f =4 kHz showed a marked decrease in a dose-dependent manner was observed at both exposures, with the highest exposure eventually led to a full para-cellular resistance loss **(a)**, and was associated to cell coverage decline **(b)**. The para-cellular resistance decline rate against the radiant exposure was significantly increased in the higher irradiance compared to the lower irradiance of blue-light at 420 nm under continuous exposure **(c)**. Therefore, 15.8 W/m^2 blue-light was able to decrease the para-cellular resistance by inducing less radiant exposure compared to 9.97 W/m^2 of blue-light at 420 nm under continuous exposure. On the other hand, the decrease in cell coverage was observed only after the ARPE-19 were exposed to 3.0 x 10^6 J/m^2 of radiant exposure with 15.8 W/m^2 irradiance **(d)**. **a)** Normalized resistance at 4 kHz (n = 3). **b)** Normalized resistance at 64 kHz (n = 3). In **a)** and **b)** bars show standard error and for each time-point statistical significance compared to t = 0 h time-point is shown. * shows P<0.05 compared to t = 0 h, ** shows P<0.01 compared to t = 0 h, *** shows P<0.001 compared to t = 0 h. **c)** Normalized resistance at 4 kHz against radiant exposure (n = 3). **d)** Normalized resistance at 64 kHz against radiant exposure (n = 3). In **c)** and **d)** bars show standard error and for each radiant exposure point statistical significance compared to 0 J/m^2 point is shown. . * shows P<0.05 compared to 0 J/m^2 point, ** shows P<0.01 compared to 0 J/m^2 point, *** shows P<0.001 compared to 0 J/m^2 point.

In order to show the effect of blue-light wavelength better on ARPE-19 cells Figs 26 and 27 were combined in Fig 28. Our results showed that both 420 nm and 470 nm blue-light caused decline in paracellular resistance (resistance at 4 kHz) (Fig 28a) before cell coverage decline occurred (Fig 28b). The severity of the blue-light damage increased with shorter wavelength (420 nm) blue-light compared to 470 nm blue-light, even though ~10-fold higher irradiances were used for 470 nm blue-light exposure. Investigation of 0.2 x 10^7 J/m^2 radiant exposure data point, where no cell coverage decline were detected for all groups (Fig 28d), showed that for the same radiant exposure dose administered, the paracellular resistance (4 kHz) damage was increased with shorter wavelength blue-light (Fig 28c).

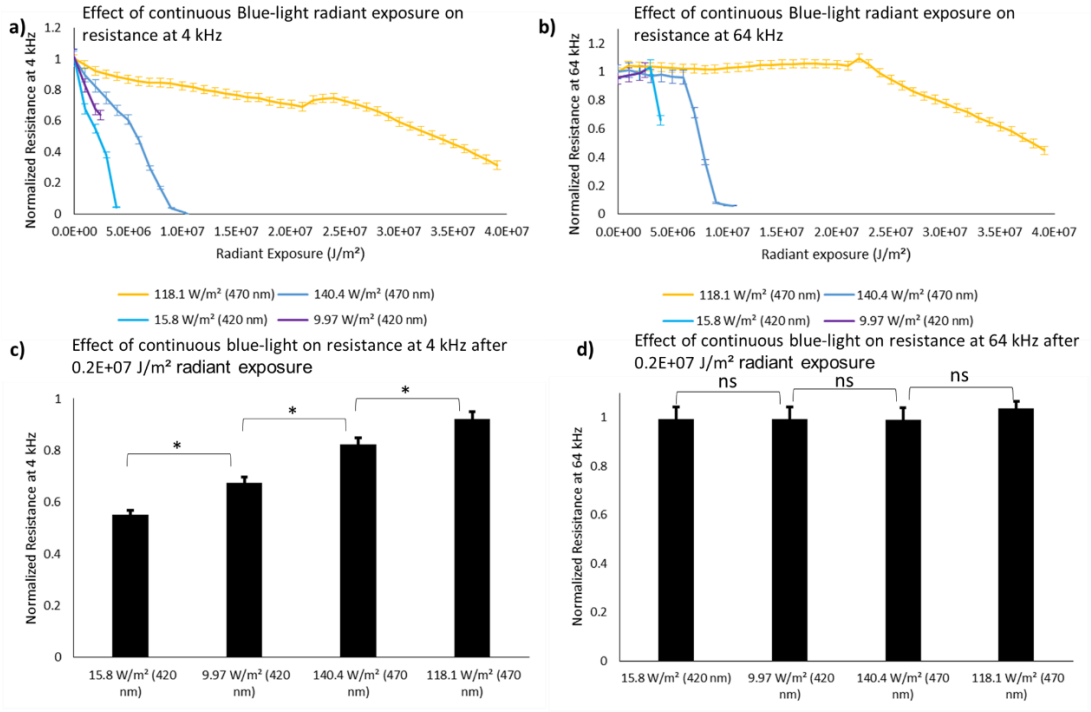

Figure 28 The Effect of blue-light wavelength on damage severity The data for 470 nm and 420 nm continuous blue-light exposure were combined. The decline in resistance at 4 kHz against radiant exposure is shown for 118.1 W/m^2 (470 nm), 140.4 W/m^2 (470 nm), 9.97 W/m^2 (420 nm) and 15.8 W/m^2 (420 nm) groups (a). The decline in resistance at 64 kHz against radiant exposure is shown for 118.1 W/m^2 (470 nm), 140.4 W/m^2 (470 nm), 9.97 W/m^2 (420 nm) and 15.8 W/m^2 (420 nm) groups (b). For statistics of groups investigated in a) and b) please refer to Figs 26 and 27. The data point 0.2 x 10^7 J/m^2 radiant exposure was chosen with the rationale that no cell coverage decline was recorded for all groups at this point (d) and the decline in resistance at 4 kHz for blue-light parameters; 118.1 W/m^2 (470 nm), 140.4 W/m^2 (470 nm), 9.97 W/m^2 (420 nm) and 15.8 W/m^2 (420 nm) were statistically compared (c). These

data shows that at the same radiant exposure dose, shorter wavelength (420 nm) of blue-light caused more decline in resistance at 4 kHz compared to 470 nm blue-light before cell coverage declined, even though the irradiance values used for 470 nm exposure were higher. Moreover, for the same wavelength of light, a faster decline in resistance at 4 kHz was observed with increased irradiance, before cell coverage declined. Bars show standard error. * shows $P<0.05$. ns shows not statistically significant.

4.8 Time-course Measurements of 400 nm Blue-light Exposure on ARPE-19 Cells

The resistance data recordings at 4 kHz and at 64 kHz were plotted under continuous blue-light (400 nm) exposure. At f = 4 kHz a marked decrease in resistance was observed at 17.66 W/m^2 exposure, this eventually led to a full para-cellular resistance loss, and was associated to cell coverage decline (Fig 29a). On the other hand, when the same wells were observed at f = 64 kHz, the time course resistances were different, with no decrease in resistance before t = 8 h (Fig 29b). These observations were consistent across all the wells (n = 3). These results indicated that 400 nm blue-light exposure at 17.66 W/m^2 induced a decrease in barrier function, before any cell coverage decline occurred.

The correlation between the para-cellular resistance and radiant exposure as well as the correlation between the cell electrode coverage and radiant exposure were investigated for 400nm blue-light with 17.66 W/m^2 irradiance. Our results showed that the radiant exposure threshold values that caused a decrease in para-cellular resistance and cell coverage were found to be different from each other (Fig 29c, d).

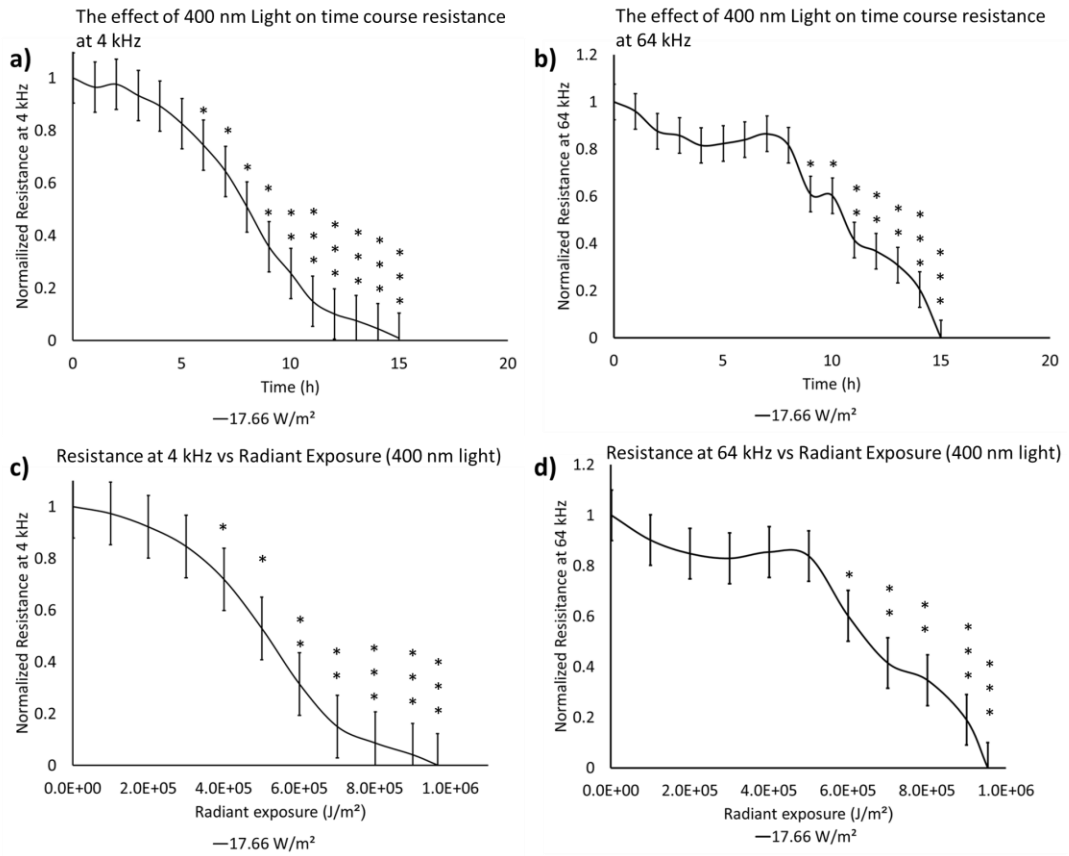

Figure 29 Time-course Measurements of 400 nm Blue-light Exposure on ARPE-19 Cells. At f = 4 kHz a marked decrease in resistance was observed at 17.66 W/m^2 exposure, eventually leading to a full para-cellular resistance loss, and was associated to cell coverage decline **(a)**. On the other hand, at f = 64 kHz, the time course resistances were different, with no decrease in resistance before t = 8 h **(b)**. The radiant exposure threshold values that caused a decrease in para-cellular resistance **(c)** and cell coverage **(d)** were found to be different from each other. **a)** Normalized resistance at 4 kHz (n = 3). **b)** Normalized resistance at 64 kHz (n = 3). **c)** Normalized resistance at 4 kHz against radiant exposure (n = 3). **d)** Normalized resistance at 64 kHz against radiant exposure (n = 3).

4.9 Time-course Measurements of Green Light Exposure on ARPE-19 Cells

The resistance data recordings at 4 kHz and at 64 kHz were plotted under continuous green light exposure. Irradiance levels used with green-light were similar to that of 400 nm blue-light. Our results showed that green light exposure at 18.7 W/m^2 did not cause any decline neither in para-cellular resistance nor in cell coverage (Fig 30).

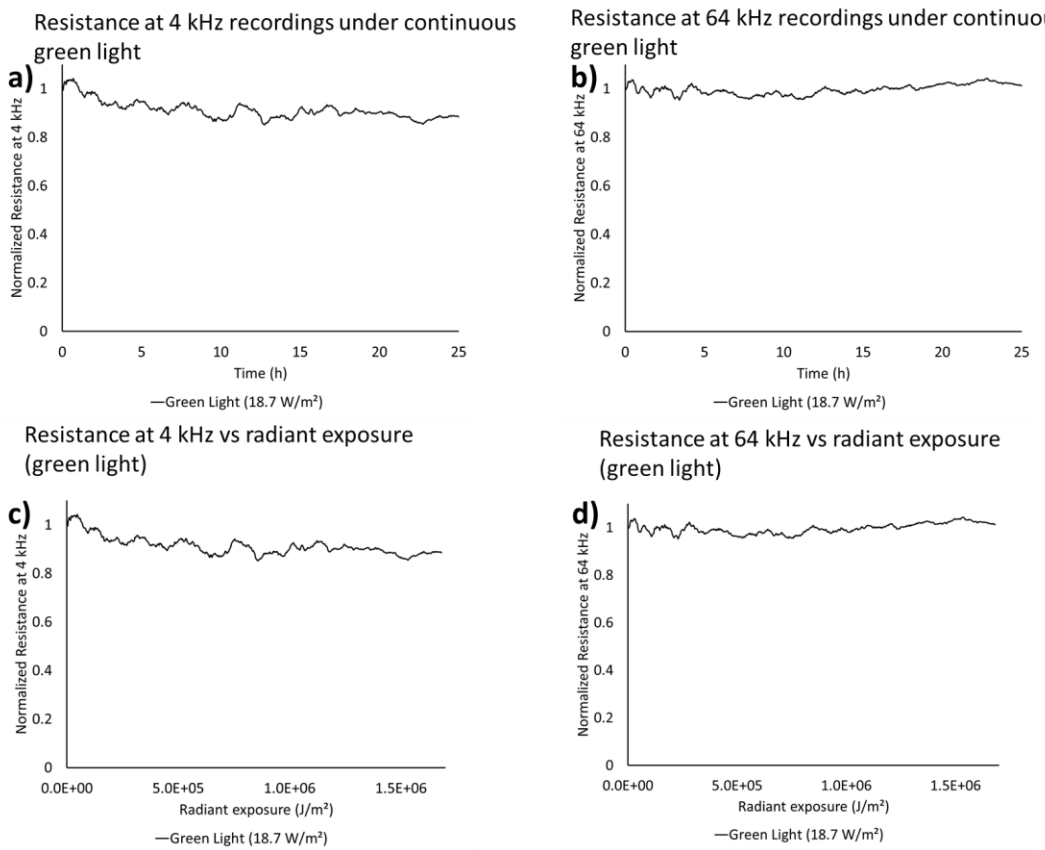

Figure 30 Time-course Measurements of 525 nm Green Light Exposure on ARPE-19 Cells The green light exposure at 18.7 W/m^2, which was similar to irradiance levels used for 400 nm blue-light, did not cause any decline neither in para-cellular resistance nor in cell coverage. **a)** Normalized resistance at 4 kHz (n = 7). **b)** Normalized resistance at 64 kHz (n = 7). **c)** Normalized resistance at 4 kHz against radiant exposure (n = 7). **d)** Normalized resistance at 64 kHz against radiant exposure (n = 7).

5 ARPE-19 exposed to blue light (470 nm) recapitulates cellular features associated with Age-related Macular Degeneration

5.1 Premature Senescence

Seventy two hours after the ARPE-19 cells were treated with either 750 µM H_2O_2 for 2 hours, 100 µM TBHP for 2 hours or 140.4 W/m^2 blue-light exposure for 7 hours, cells were fixed and stained for senescence-associated β-galactosidase (Fig 31). Our results documented, without any associated cell coverage decline, a 190-fold increase (9.5 % stained area) in senescence associated staining after blue-light compared to no treatment control (0.05 % stained area). It was observed that TBHP and H_2O_2 treatments induced respectively 50-fold (2.5 % stained area) and 5.5-fold (0.275 % stained area) increase in senescence associated staining. Statistical significance ($P < 0.05$) were found between all groups.

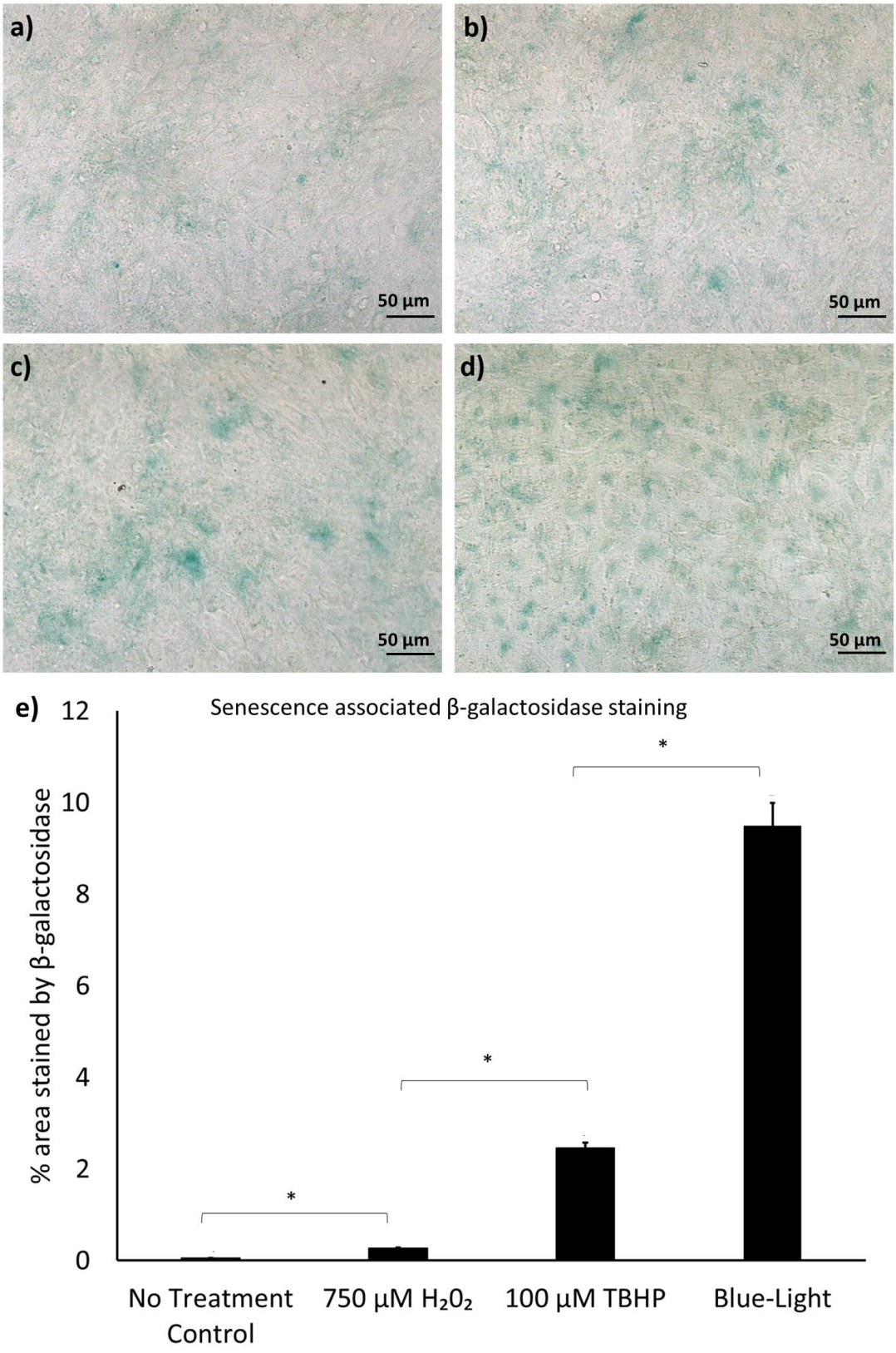
a)
50 µm
b)
50 µm
c)
50 µm
d)
50 µm
e)
Senescence associated β-galactosidase staining
% area stained by β-galactosidase
0
2
4
6
8
10
12
*
*
*
No Treatment Control
750 µM H_2O_2
100 µM TBHP
Blue-Light

Figure 31 Senescence-associated β-galactosidase immunostaining & its quantification. **a)** No light control (n = 3). **b)** ARPE-19 cells were treated with 750 µM H_2O_2 for 2 hours (n =3). **c)** ARPE-19 cells were treated with 100 µM TBHP for 2 hours (n = 3). **d)** ARPE-19 cells were treated with 140.4 W/m² for 7 hours (n = 3). **e)** Using ImageJ the percentage of the stained area compared to the total area was calculated. Blue-light, TBHP and H_2O_2 treatments induced respectively 190-fold, 50-fold and 5.5-fold increase in senescence associated staining. Bars show standard error. * shows P<0.05.

5.2 Retinal Pigment Epithelium Barrier Function Breakdown

ARPE-19 cells cultured on a 8 well ECIS micro-electrode array were treated with either 100 µM TBHP for 2 hours, 750 µM H_2O_2 for 2 hours or 140.4 W/m^2 blue-light exposure for 7 hours and analysed over 80 h period, with time zero set at the beginning of the treatment (Fig 32). The media change at t= 2h for TBHP and H_2O_2 resulted in a typical peak in resistance associated with temperature and dissolved CO_2 variation for all wells. A similar peak was observed at t = 7 h at the end of blue-light treatment, as a result of opening of the incubator to remove the ad hoc LED array circuit. As we wanted to mimic the loss of outer blood retina barrier in AMD with blue-light, the media was not changed after the 7 hours of blue-light exposure.

The difference in resistance graphs at low frequency (Fig 32a) and high frequency (Fig 32b) indicated that TBHP, H_2O_2 and blue-light had different effects on barrier function (Fig 32c) and cell electrode coverage (Fig 32d). Simultaneous decline of the barrier function and cell coverage by 20 % was observed on the cells treated with TBHP, starting from t = 0 h. The media change at t = 2 h restored both the barrier function and cell coverage of TBHP treated ARPE-19, in 16 hours. On the contrary, the barrier function of H_2O_2 treated ARPE-19 declined from t = 3 h until t = 15.5 h, followed by a stationary phase of 10 hours, before it began to recover from t = 25.5 h and was fully restored in 20 hours. While, significant decline in cell coverage was not observed after H_2O_2 treatment. On the other hand, blue-light exposure for 7 hours declined the barrier function by 15 % without any decline in cell coverage. As the media was not changed after blue-light exposure no recovery on the barrier function was observed.

Taken together these data indicated that 7h of blue-light and maximum usable/safe dose of TBHP and H_2O_2 have different effects on ARPE-19 cells, as characterized by barrier function breakdown before cell coverage decline occurred. This further indicated that oxidative stress mechanisms and predominant damage sites as a result of blue-light, TBHP and H_2O_2 treatments may be different from each other, moreover each treatment may give rise to different types of reactive oxygen species.

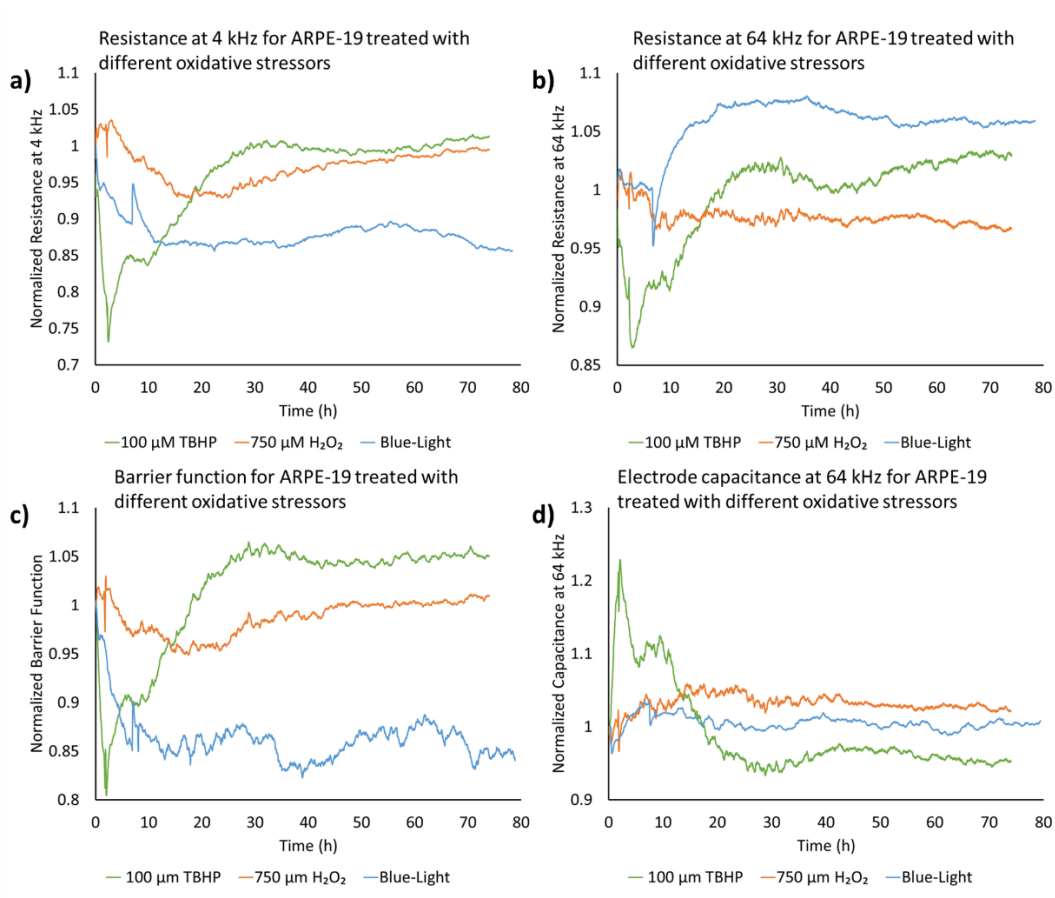

Figure 32 Retinal Pigment Epithelium Barrier Function Breakdown as a result of blue-light, TBHP and H_2O_2 treatments. ARPE-19 cells cultured on a 8 well ECIS micro-electrode array were treated with either 100 µM TBHP for 2 hours, 750 µM H_2O_2 for 2 hours or 140.4 W/m² blue-light exposure for 7 hours and analysed over 80 h period, with time zero set at the beginning of the treatment. Resistance data at f = 4 kHz **(a)** and f = 64 kHz **(b)** were recorded. The difference in resistance graphs at low frequency and high frequency indicated that TBHP, H_2O_2 and blue-light had different effects on barrier function **(c)** and cell electrode coverage **(d)**. TBHP treatment resulted in simultaneous decline of the barrier function and cell coverage starting from t = 0 h. The media change at t = 2 h restored both the barrier function and cell coverage of TBHP treated ARPE-19, in 16 hours. The barrier function of H_2O_2 treated ARPE-19 declined from t = 3 h until t = 15.5 h, followed by a stationary phase of 10 hours, before it

began to recover from t = 25.5 h and was fully restored in 20 hours. While, significant decline in cell coverage was not observed after H_2O_2 treatment. On the other hand, blue-light exposure for 7 hours declined the barrier function by 15 % without any decline in cell coverage. As the media was not changed after blue-light exposure no recovery on the barrier function was observed.

5.3 Mitochondrial Dysfunction

Twenty-four hours after each treatment, cellular micromotion was calculated to evaluate the change in mitochondrial respiration of the cells (Fig 33). Our results suggested that blue-light exposure declined cell micromotion related to mitochondrial respiration by 52 %. It was also observed that treatment with TBHP and H_2O_2 decreased the cellular micromotion by respectively 36 % and 13.5 %. Our results showed that differences found between all groups are statistically significant ($P < 0.05$).

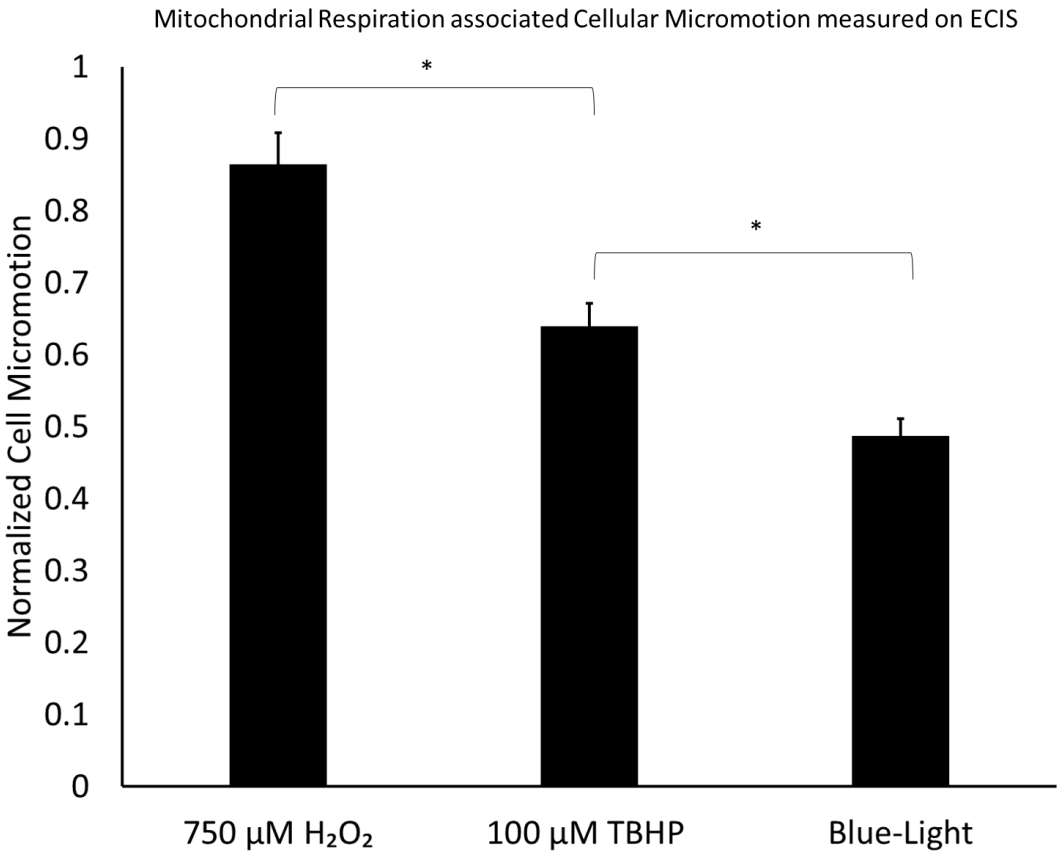

Figure 33 Quantification of Cellular Micromotion using ECIS. 24h after each treatment, cellular micromotion was calculated to evaluate the change in mitochondrial respiration of the cells. Treatments with blue-light (n = 3), TBHP (n = 3) and H_2O_2 (n = 3) decreased the cellular micromotion by respectively 52 %, 36 % and 13.5 %. Bars show standard error. * shows $P<0.05$.

In order to confirm this mitochondrial damage, twenty four hours after the ARPE-19 cells were treated with either 750 µM H_2O_2 for 2 hours, 100 µM TBHP for 2 hours or 140.4 W/m² blue-light exposure for 7 hours, MitoTracker™ assay was used to visualize and quantify the number of impaired mitochondria (Fig 34). Mitotracker™ assay validated the previous observations from resistance recordings. It was observed that treatment with blue-light, TBHP and H_2O_2 increased the number of impaired mitochondria by respectively 18.7-fold, 7.8-fold and 6.5-fold (Fig 35). Statistical significance ($P < 0.05$) was found between all groups.

Taken together, our results showed that blue-light induced increased senescence associated staining, mitochondrial dysfunction and barrier function breakdown before any cell coverage decline occurred. Therefore, this information can be leveraged into designing blue-light induced in-vitro AMD models that demonstrate the barrier function break-down between “aged” dysfunctional RPE during AMD development process before cell death occurs, using ECIS. Our results also showed that 7 h of blue-light induced greater senescence associated staining, mitochondrial dysfunction and barrier function breakdown compared to maximum usable/safe dose of TBHP and H_2O_2 without inducing any cell coverage decline.

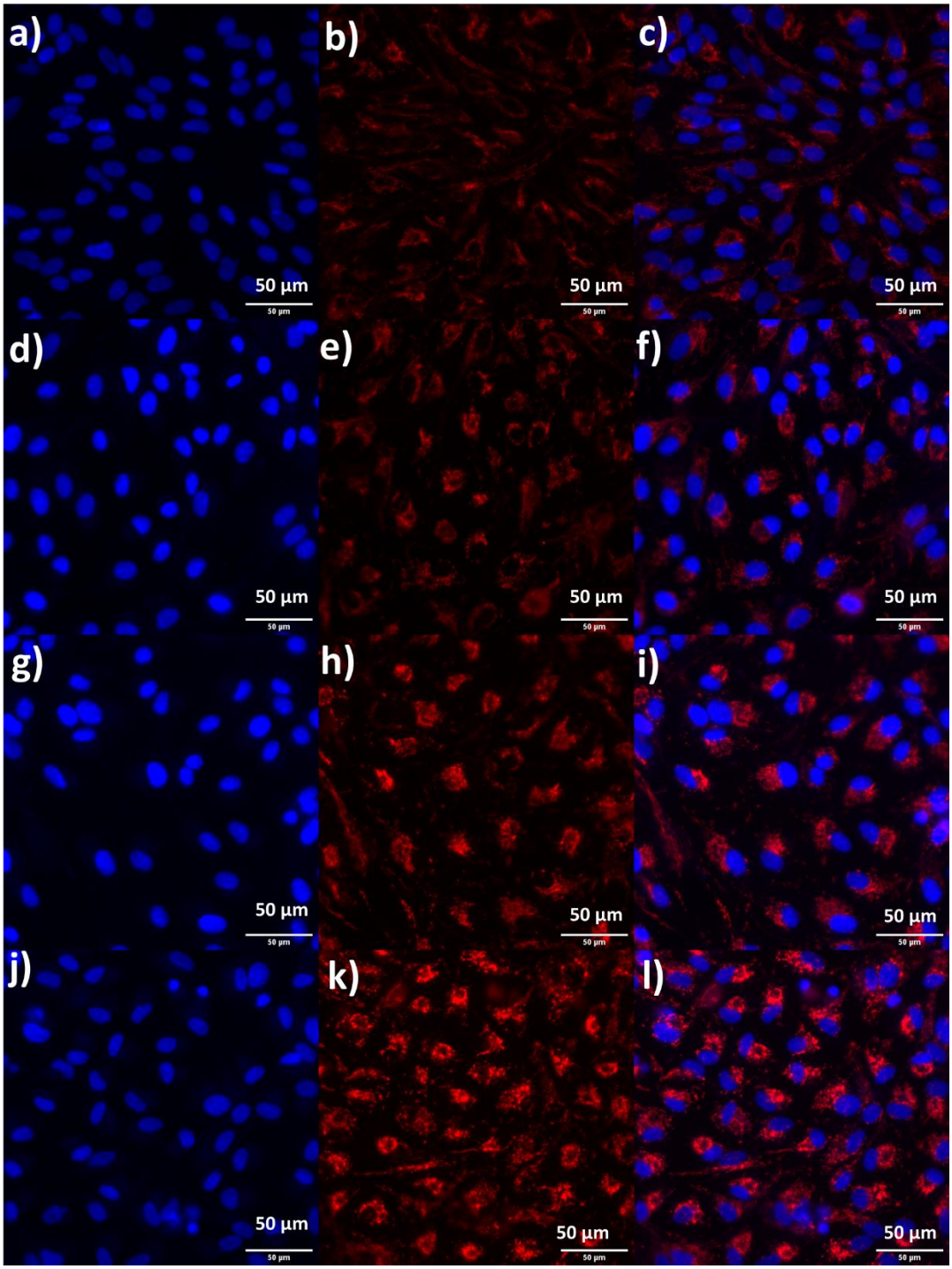

Figure 34 MitoTracker™ immunostaining. **a)** DAPI for no light control. **b)** MitoTracker™ for no light control. **c)** Composite image for no light control. **d)** DAPI for 750 µM H_2O_2 treatment for 2 hours. **e)** MitoTracker™ for 750 µM H_2O_2 treatment for 2 hours. **f)** Composite image for 750 µM H_2O_2 treatment for 2 hours. **g)** DAPI for 100 µM TBHP treatment for 2 hours. **h)** MitoTracker™ for 100 µM TBHP treatment for 2 hours. **i)** Composite image for 100 µM TBHP treatment for 2 hours. **j)** DAPI for 140.4 W/m² blue-light exposure for 7 hours. **k)** MitoTracker™ for 140.4 W/m² blue-light exposure for 7 hours. **l)** Composite image for 140.4 W/m² blue-light exposure for 7 hours.

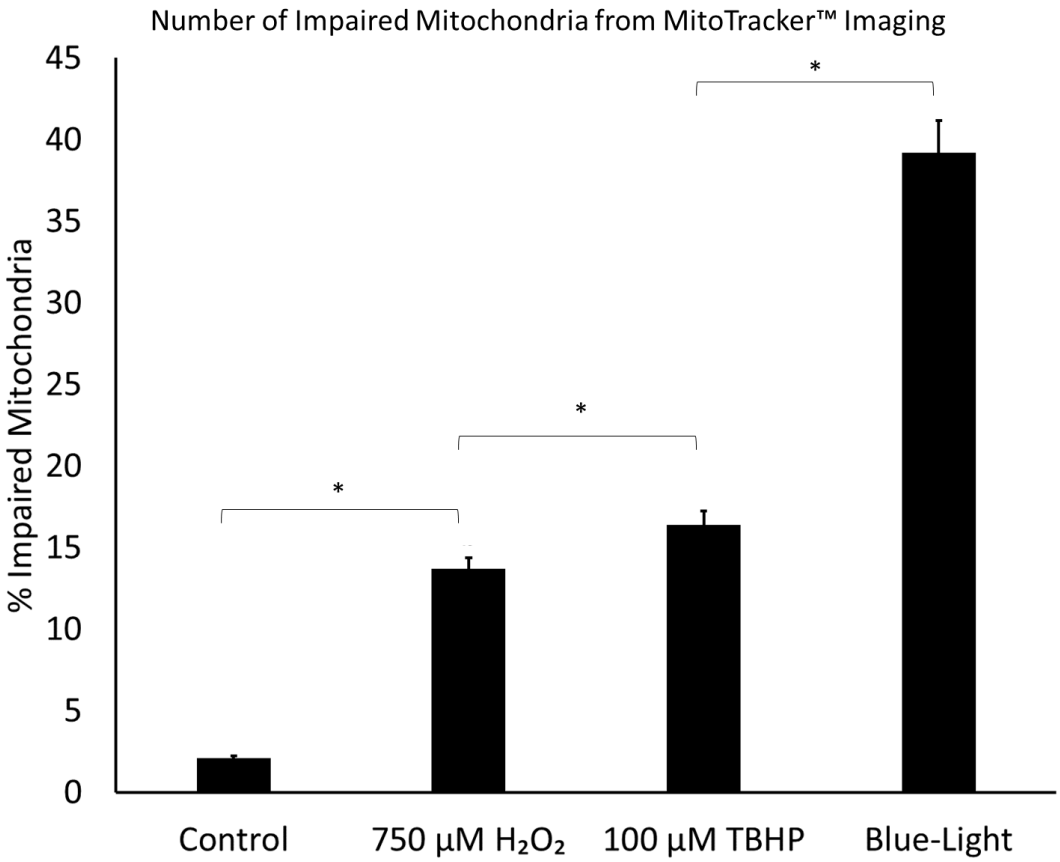

Figure 35 Quantification of impaired mitochondria using MitoTracker™ imaging. Using ImageJ the percentage of the impaired mitochondria to the total number of ARPE-19 cells present was calculated. The percentage of impaired mitochondria found in control (n = 3), 750 µM H_2O_2 treatment for 2 hours (n = 3), 100 µM TBHP treatment for 2 hour (n = 3) and 140.4 W/m² blue-light exposure for 7 hours (n = 3) were respectively 2.1 %, 13.7 %, 16.4 % and 39.2 %. Bars show standard error. * shows P<0.05.

5.4 Continuous vs Daily Blue-Light Induced AMD Models

Blue-light induced in-vitro AMD models can be modulated using different exposure methods; continuous and daily/intermittent, to investigate the effect of different blue-light stress conditions on cellular response. In our models, ARPE-19 cells were exposed to continuous blue-light, 4 h of blue-light for 1 day (daily (i)), 4 h of blue-light for 2 days (daily (ii)) and 4 h of blue-light for 3 days (daily (iii)) (Fig 36). The data on f = 4 kHz and f = 64 kHz acquired from

these models were compared. The daily exposures were performed between 0 - 4 h, 24 - 28 h and 48 – 52 h.

The resistance data on daily exposure at f = 4 kHz (Fig 36a) showed that after 4 h of blue-light exposure, the barrier function declined to 85 % at the end of the first day (t = 24 h). A significant decline in the barrier function was observed at t = 28 h between the cells exposed to blue-light for a second day (shown in Daily (ii) and Daily (iii)), and the cells exposed to blue-light only for the first day (Daily (i)). Furthermore, a significant barrier function decline, coinciding with the beginning of third daily blue-light exposure at t= 48 h, was observed between cells daily exposed for two days (Daily (ii)) and cells daily exposed for three days (Daily (iii)). Taken together, our data on daily blue-light exposure showed three statistically significant stages of blue-light damage on barrier function. As the first statistically significant point (º) occurred after 4 hours of exposure, up to 4 hours of exposure showed the first stage. Between 4 hours of exposure up to the next statistically significant point (ºº) occurring after 8 hours of total exposure time, showed the second stage. Finally the third stage started with the next significance point (ººº) when the total exposure time exceeded 8 hours.

Comparison of resistance data on continuous and daily exposure at f = 4 kHz showed that 8 hours of continuous exposure induced the same level of barrier function decline as 4 hours of daily exposure for 2 days induced. However no statistically significant difference was observed between the barrier function decline as a result of 12 hours of continuous exposure and the barrier function decline when the total exposure time exceeded 8 hours with daily exposure on third day. This observation might be due to the emergence of post exposure oxidative stress after 8 hours, where excess intracellular ROS continue to exert damage on cell-cell junctions post exposure, which may be related to depletion of enzymatic antioxidant mechanisms, impairment of protein & lipid synthesis from endoplasmic reticulum complex as well as inhibition of glycolysis

(Hockberger et al., 1999; Fagone and Jackowski, 2009; Roehlecke et al., 2009; Jaadane et al., 2017).

Furthermore, our resistance data at f = 64 kHz (Fig 36b) showed that while 4 hours of daily exposure for 3 days did not induce any decline in cell coverage, continuous exposure over 12 hours induced cell coverage decline. Therefore, while 12 hour mark presented a threshold for cell coverage decline induced by 140.4 W/m^2 continuous blue light (470 nm) exposure, the same threshold was not present for daily exposure. This observed effect may indicate that ARPE-19 cells generated different cellular stress responses due to continuous and daily/intermittent blue-light exposure that affected cell coverage.

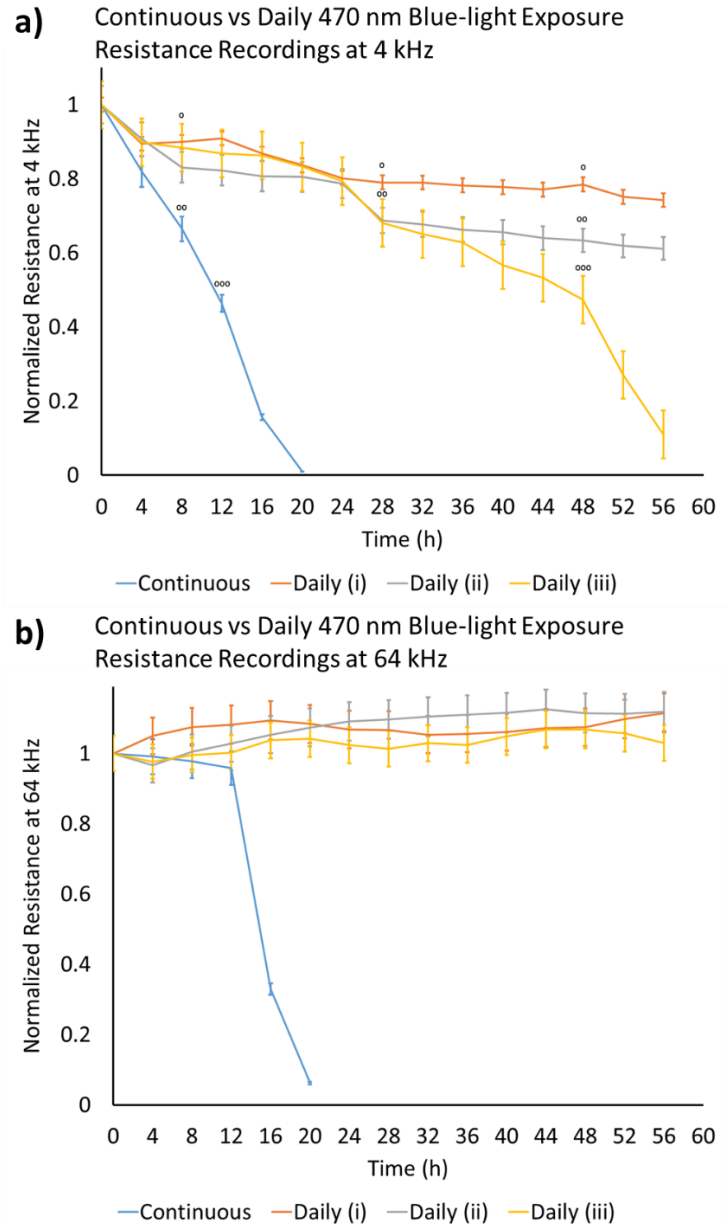

Figure 36 Continuous vs Daily Blue-Light Induced AMD Models. ARPE-19 cells were exposed to continuous blue-light, 4 h of blue-light for 1 day (daily (i)), 4 h of blue-light for 2 days (daily (ii)) and 4 h of blue-light for 3 days (daily (iii)). The data on f = 4 kHz **(a)** and f = 64 kHz **(b)** acquired from these models were compared. The daily exposures were performed between 0 - 4 h, 24 - 28 h and 48 – 52 h. The data on daily blue-light exposure showed three statistically significant stages of blue-light damage on barrier function. As the first statistically significant point occurred after 4 hours of exposure, up to 4 hours of exposure showed the first stage. Between 4 hours of exposure up to the next statistically significant point occurring after 8 hours of total exposure time, showed the second stage. Finally third stage started with the next significance point when the total exposure time exceeded 8 hours. Comparison of resistance data on continuous and daily exposure at f = 4 kHz showed the emergent effect of post exposure oxidative stress on the barrier function. Comparison of resistance data on continuous and daily exposure at f = 64 kHz showed that while 12 hour mark presented a threshold for cell coverage decline induced by 140.4 W/m² continuous blue light (470 nm)

exposure, the same threshold was not present for daily exposure, which may indicate different cellular stress responses due to continuous and daily exposure, that affected cell coverage.

5.5 Internalization of A2E

In order to model the lipofuscin accumulation occurring in vivo with age, ARPE-19 cells were fed with a component of lipofuscin; a mixture of A2E:iso-A2E, which is widely used in in-vitro studies for being easy to chemically synthesise (Boulton, 2014). Auto-fluorescence at excitation/emission of 488/565 nm was used to investigate the internalization of A2E with fluorescence microscope after confluent ARPE-19 cells were incubated with 50 μM or 100 μM of A2E:iso-A2E mixture for 1 and 2 days for each concentration, washed with PBS twice and kept in cell culture media. Exponentially growing ARPE-19 and confluent ARPE-19 cells were used as controls (Fig 37). The mean pixel intensity for green channel images were calculated using ImageJ (Fig 37 a,c,e,g,I,k). Our results showed that the green auto-fluorescence observed on ARPE-19 cells increased after the cells were incubated with A2E:iso-A2E mixture. On the other hand, no statistical significance was observed on mean pixel intensity of green channels between cells incubated with 50 μM and 100 μM of A2E:iso-A2E mixture. No difference in auto-fluorescence was observed between 2-day incubation and 1-day incubation (Fig 38).

These results demonstrated that ARPE-19 cells internalized A2E:iso-A2E mixture in less than 24 hours

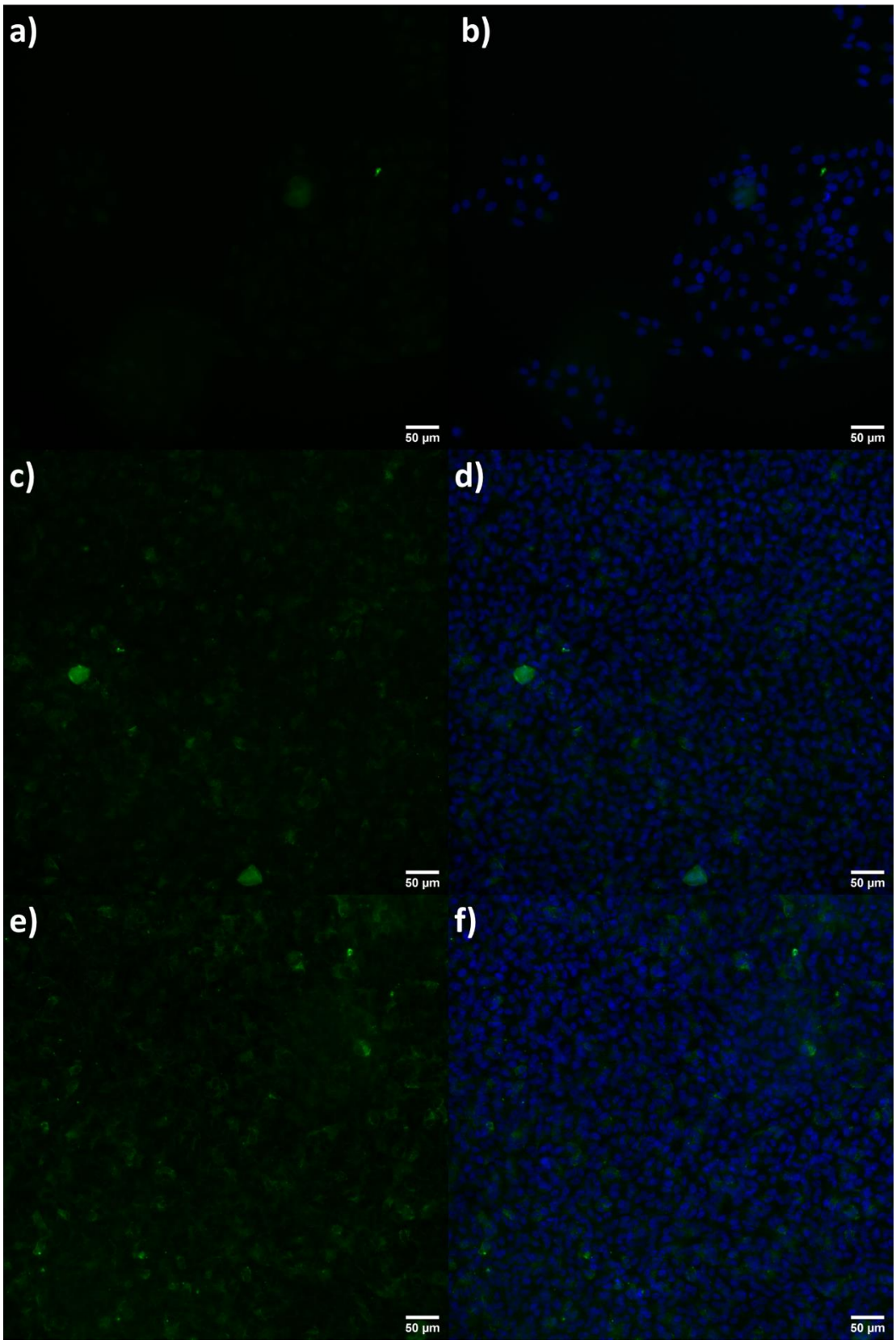
a)
50 µm
b)
50 µm
c)
50 µm
d)
50 µm
e)
50 µm
f)
50 µm

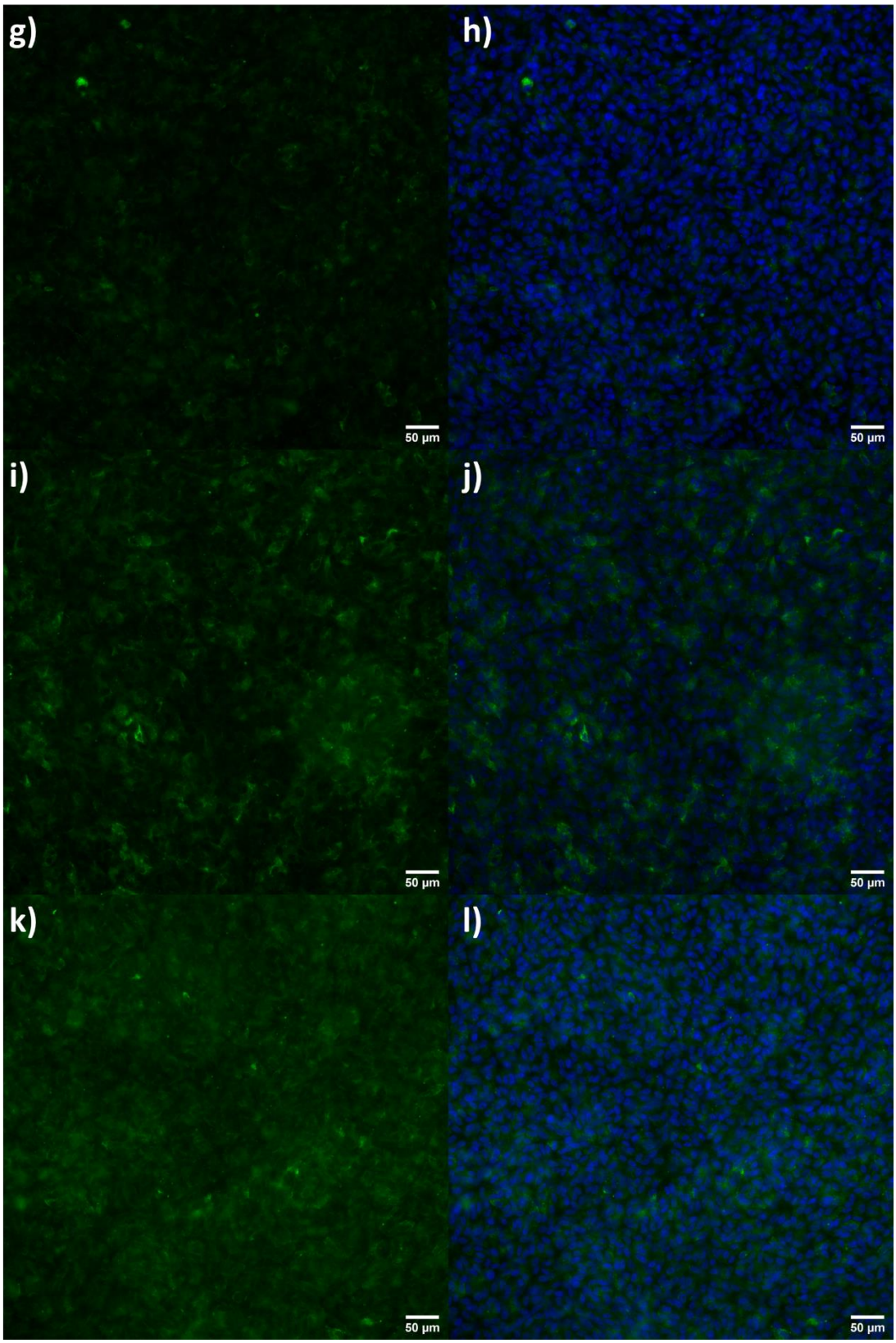
g)
50 µm
h)
50 µm
i)
50 µm
j)
50 µm
k)
50 µm
l)
50 µm

Figure 37 Detection of internalized autofluorescent A2E granules. a) Green channel for exponentially growing ARPE-19 (n =3). **b)** Composite image for exponentially growing ARPE-19 (n = 3). **c)** Green channel for confluent ARPE-19 (n = 3). **d)** Composite image for confluent ARPE-19 (n = 3). **e)** Green channel for ARPE-19 cells incubated with 50 μM of A2E:iso-A2E mixture for 1 day (n = 3). **f)** Composite image for ARPE-19 cells incubated with 50 μM of A2E:iso-A2E mixture for 1 day (n = 3). **g)** Green channel for ARPE-19 cells incubated with 50 μM of A2E:iso-A2E mixture for 2 days (n = 3). **h)** Composite image for ARPE-19 cells incubated with 50 μM of A2E:iso-A2E mixture for 2 days (n = 3). **i)** Green channel for ARPE-19 cells incubated with 100 μM of A2E:iso-A2E mixture for 1 day (n = 3). **j)** Composite image for ARPE-19 cells incubated with 100 μM of A2E:iso-A2E mixture for 1 day (n = 3). **k)** Green channel for ARPE-19 cells incubated with 100 μM of A2E:iso-A2E mixture for 2 days (n = 3). **l)** Composite for ARPE-19 cells incubated with 100 μM of A2E:iso-A2E mixture for 2 days (n = 3).

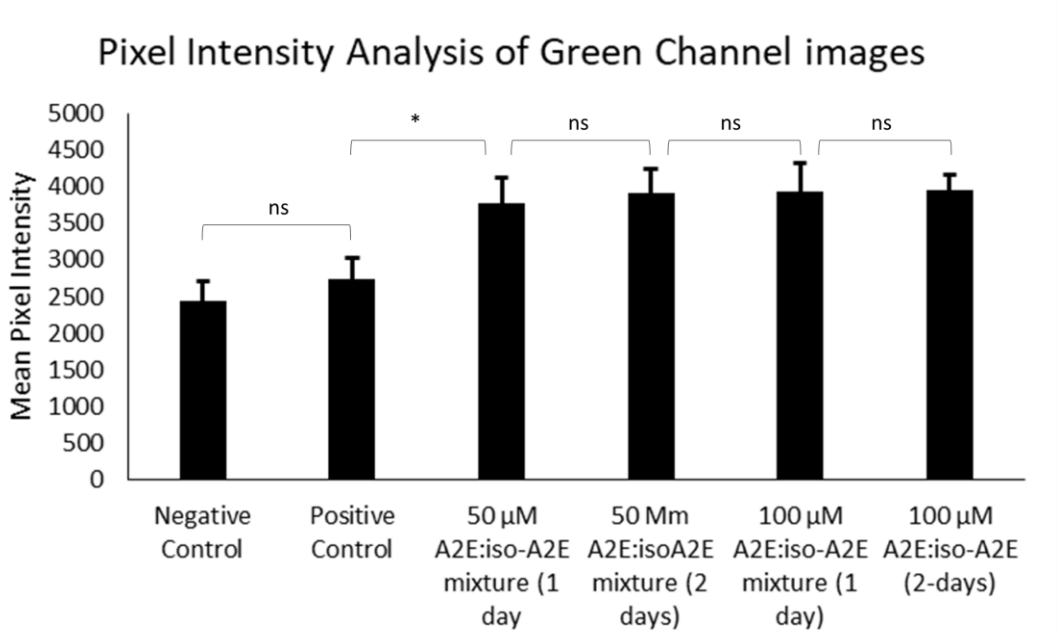

Figure 38 Mean Pixel Intensity Analysis of Green channel images for A2E internalization Using ImageJ, mean pixel intensity of green channel images for exponsentially growing ARPE-19 (negative control), confluent ARPE-19 (positive control) and ARPE-19 incubated with 50 μM or 100 μM of A2E:iso-A2E mixture for 1 and 2 days were calculated. ImageJ analysis showed no statistical significance between green channel mean pixel intenisty of exponentially growing and confluent ARPE-19 cells. ImageJ analysis showed that mean pixel intensity of green channel increased as a result of A2E:iso-A2E incubation. However no statistical differences were found between the mean pixel intensities of ARPE-19 incubated with 50 μM or 100 μM of A2E:iso-A2E mixture for 1 and 2 days. Bars show standard error. * shows $P<0.05$.

5.6 Time-course Measurements of 470 nm Blue-light Exposure on A2E loaded ARPE-19 cells

ARPE-19 cells incubated with 100 μM of A2E:iso-A2E mixture for 1 day and unfed ARPE-19 cells, both cultured on a 8 well ECIS micro-electrode array were exposed to continuous blue-light (470 nm) at 140.4 W/m^2, and the

resistance data recording at 4 kHz and at 64 kHz were plotted (Fig 39). Our results showed no significant difference in para-cellular resistance and cell coverage decline between ARPE-19 cells fed with 100 µM of A2E:iso-A2E mixture and unfed ARPE-19 cells.

This result indicated that A2E, mimicking the age pigment lipofuscin, is not a photosensitizer at 470nm.

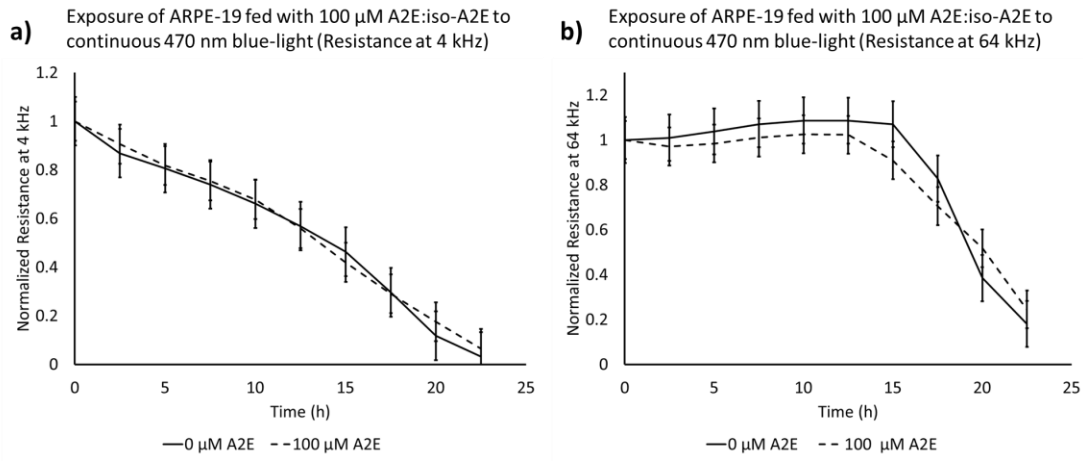

Figure 39 Time-course Measurements of 470 nm Blue-light Exposure on A2E loaded ARPE-19 cells. No significant difference in para-cellular resistance and cell coverage decline was observed between ARPE-19 cells fed with 100 µM of A2E:iso-A2E mixture and unfed ARPE-19 cells. **a)** Normalized resistance at 4 kHz (n = 3). **b)** Normalized resistance at 64 kHz (n = 3).

6 Discussion

To the best of our knowledge, the effect of blue-light on the barrier function of human cells has not been studied previously. Our study quantitatively characterized the effect of blue-light on the outer-BRB, with regard to AMD studies and demonstrated a blue-light induced in-vitro model that recapitulates cellular features associated with AMD; premature senescence, barrier function breakdown and mitochondrial dysfunction in RPE cells, using real-time quantitative ECIS measurements as a novel approach.

6.1 Advantage of ECIS over Biochemical Assays

While biochemical assays are widely used for detecting, quantifying and studying various behaviours, they usually consist of complex steps requiring addition of multiple reagents at scheduled time-points. They are limited to the time points investigated and can miss changes that are happening over time. Furthermore some of these assays are end point invasive protocols that require fixed cells for further investigation (Hildebrandt et al., 2010; Kim et al., 2011; Jun et al., 2013; Lee et al., 2013). On the other hand, electrical cell-substrate impedance sensing (ECIS) is a label free, non-invasive technique that enables real-time, high-throughput quantitative measurements on live cells. Therefore, it is particularly useful in disease modelling, cytotoxicity and wound healing studies, and drug/compound testing assays (Ciambrone et al., 2004; Gamal et al., 2015).

Photo-biological and photochemical studies to date implicated that reciprocity between irradiance and time of exposure, which states that the effect of a light induced reaction is directly proportional to the retinal exposure dose, may only be valid for certain irradiance and time of exposure combinations. Thus, in experimental and clinical studies it is important to include different combinations of irradiance and exposure duration (Karu, 1989; Potapenko et al., 1991; Van Breughel and Bar, 1992; Gilchrest et al., 1999; Schindl et al., 2001; Morgan et al., 2009). However, previous phototoxicity studies are often

limited to few fixed time-points when performing quantitative assays (Seko et al., 2001; Jaadane et al., 2017). In our study we used ECIS microelectrode arrays to quantitatively investigate the effect of blue-light on RPE cells in a high-throughput, real-time manner. In experiments done by Jaadane et al., (2017) on rat RPE immunofluorescence and biochemical analysis of RPE were performed once the rat eyes were enucleated and dissected after different rats were exposed to continuous light using single irradiance for different exposure times; 4.75, 6, 12, 18 and 24 hours. In our study the real-time aspect of ECIS was used to determine the exact time point where the significant decline in barrier function first appeared between case and controls. For 118.1 W/m^2 this significant decline was observed at t = 4 h. Hence it provided us valuable insight on when to perform ZO-1 staining as well as PKC-ζ inhibition. Previous blue-light studies on RPE performed by Seko et al., (2001) achieved different irradiance values by increasing the power output of the light source on separate experiments. In our study, using an ad hoc LED array illumination system together with a set of neutral density filters and a 3D printed filter holder on ECIS multi-well arrays, allowed us to study multiple irradiances simultaneously and explore time of exposure irradiance relationship on a single ECIS multi-well array.

6.2 Choice of Cell Line

In this study, ARPE-19 and hTERT-RPE1 cells were investigated for their capacity to form tight junctions to mimic in-vivo RPE. While ARPE-19 established a confluent monolayer with 16000 Ω para-cellular resistance after 20 hours, hTERT-RPE1 established a confluent monolayer with 5000 Ω para-cellular resistance after 40 hours. In the light of the results obtained from the growth curves of hTERT-RPE1 and ARPE-19 cells, ARPE-19 was chosen to be further analysed on ECIS microelectrode arrays to lay the foundations for an AMD disease model, due to its superior barrier function formation capacity.

In addition, the decision to choose the ARPE-19 cell line was also motivated by the fact that as opposed to hTERT-RPE1, ARPE-19 cells express RPE

specific markers; retinal pigment epithelium-specific 65 kDa protein (RPE-65) and cellular retinaldehyde-binding protein (CRALBP) that are involved in 11-cis retinal regeneration in visual cycle. Furthermore, ARPE-19 exhibit a tendency for senescence, confirming that they are not transformed (Dunn et al., 1996).

In a previous study by Gamal et al., (2015) using ECIS, hiPSC-derived RPE were shown to establish a pigmented monolayer with 6000 Ω para-cellular resistance after 25-day maturation period. In a study by Gong et al., (2020) where hiPSC-derived RPE from AMD patients were compared with age-matched controls, documented that hiPSC-derived from AMD patients exhibited reduced metabolism, mitochondrial respiration and matrix interactions which affected cell attachment as well as induced the expression of complement genes. In a more recent study by Maruotti et al. (2020) hiPSC-derived RPE exposed to long term (1-2 weeks) blue-light (430 nm) induced oxidative stress, antioxidant response, complement activation and inflammatory response and eventually led to progressive cell death. Therefore in the future our current study should be performed using hiPSC derived RPE cells in a pigmented RPE model.

6.3 Effect of Blue-Light on Cell-Cell Tight Junctions

The results in this study document the time course that blue LED light (470 nm) exposure decreases human RPE barrier function in vitro in a dose dependent manner, before any cell coverage decline occurs. This study is the first to show in-vitro evidence that the blue-light induced breakdown of barrier function on human RPE cells is mediated by PKC- ζ over-activation and oxidative stress. Furthermore, this study demonstrated both protective and recovery effect of PKC- ζ inhibition on human RPE barrier function. In their in vivo studies on albino rats (Wistar rats) Jaadane et al., (2017) demonstrated that white LED light, which have a strong emission peak at 470 nm, disrupts outer-BRB via induced activation of PKC- ζ by oxidative stress and pro-inflammatory cytokine response (Jaadane et al., 2015b). In this study, Jaadane

et al., (2017) observed that the outer-BRB of albino rats is completely lost with signs of cell death as indicated by the translocation of PKC- ζ staining from the plasma membrane to the cell nucleus (Crisanti et al., 2006; Jaadane et al., 2017). Moreover, Jaadane et al., (2017) demonstrated that the use of PKC- ζ inhibitor restored the outer-BRB on albino rats. Another study by the same group had previously demonstrated that the blue component of white LED is the cause of this retinal injury on albino rats (Jaadane et al., 2015a). Therefore, our in-vitro results obtained on human RPE cells are in line with previous in-vivo studies on albino rats.

Previous studies on blue light showed that the retinal damage induced is oxygen-dependent and not related to local increase in temperature (Crockett and Lawwill, 1984; Ruffolo Jr. et al., 1984; Jaffe et al., 1988; Rózanowska,1995; Rozanowska, 2012) and depends on irradiance, radiation wavelength and time of exposure (Ham et al., 1980; Wu et al., 2006; Behar-Cohen et al., 2011; Jaadane et al., 2015a).

Increase in oxidative stress with prolonged blue-light exposure is well documented (Godley et al., 2005; Jaadane et al., 2015a; Alaimo et al., 2019). In our research group a recent study by Gamal et al., (2017) demonstrated using ECIS that acetaminophen which exerts oxidative stress via cytochrome metabolism, followed by glutathione and ATP depletion, and mitochondrial dysfunction (Cubero et al., 2016), induced breakdown of tight junctions in human hepatic cells (HepaRG) through disruption of tight junction associated ZO-1 protein. In our current study, we followed a similar experimental protocol and demonstrated that blue-light induced a breakdown of barrier function through disruption of ZO-1 at the ARPE-19 tight junctions. At the tight junctions, PKC-ζ phosphorylates occludin on specific threonine residues, and co-localizes with ZO-1, to link ZO-1 with occludin (Stuart and Nigam, 1995; González-Mariscal et al., 2008; Jain et al., 2011). Moreover as part of the protein scaffold complex Par6/Par3/PKC-ζ it regulates the polarity of the tight junctions (Jain et al., 2011). It has been reported by Gopalakrishna and Jaken,

(2000) that the two domains of PKC-ζ; amino- (N-terminal) and carboxyl- (C-terminal) domains respond differently to two types of agents; oxidants and anti-oxidants. While ROS such as peroxide stimulate PKC-ζ activation by binding to amino domain, anti-oxidants such as vitamin E bind with carboxyl domain to inhibit PKC- ζ. Consequently, we observed that para-cellular resistance declined under continuous blue-light as the wavelength and irradiance remained unchanged. Our results suggested that blue light (470 nm) induced oxidative stress and damaged para-cellular junctions in ARPE-19. We investigated the time course protective and recovery effect of PKC- ζ pseudo substrate inhibitor, which reversibly binds to PKC-ζ regulatory domain (Gopalakrishna and Jaken, 2000), on the tight junctions. Our results showed that PKC- ζ inhibition showed an early protective and recovery effect against blue-light induced barrier function decline. This suggests that PKC- ζ over-activation plays a role in blue-light induced barrier function breakdown of tight junctions in ARPE-19.

It was first documented by Ham et al. (1976) in in-vivo experiments on rhesus monkey that the action spectrum for photochemical effects in the retina (as characterized by funduscopic photographs 24 hours post-exposure) increased exponentially as wavelength was decreased towards 400 nm as irradiance and duration exposure remained unchanged. Later Różanowska et al. (1995) showed that the rate of oxygen uptake exponentially increases with decreasing wavelength of light in the range of 578nm to 290nm in both pigmented and non-pigmented RPE cells, and is at minimal levels in the green spectral range (Rózanowska et al., 1995). Moreover, the same study showed that the photodependent rate of O_2 uptake and formation of ROS in in-vitro human RPE are linearly correlated. In line with these studies by Ham et al. (1976) and Różanowska et al. (1995), in our study on ARPE-19 it was observed that the rate at which paracellular resistance declined with radiant exposure increased as the wavelength of light decreased. This indicates an increased ROS mechanism for human RPE with decreasing wavelength. Furthermore, in line

with Różanowska et al. (1995), in our study no decline in paracellular resistance was observed with green light exposure on ARPE-19.

It was first documented by Ham et al. (1976) in in-vivo experiments on rhesus monkey that photochemical damage radiant exposure threshold may be lowered due to increased irradiance levels. While in this current research, similar level of damage on paracellular resistance was observed when ARPE-19 were exposed to the same radiant exposure with 118.1 W/m^2, 74.65 W/m^2, 47.05 W/m^2 and 29.67 W/m^2 at 470 nm, the rate at which paracellular resistance declined with radiant exposure was significantly higher in the case of 140.4 W/m^2. Likewise, at 420 nm, increased irradiance from 9.97 W/m^2 to 15.8 W/m^2 resulted in a higher rate at which paracellular resistance declined with radiant exposure. This may suggest a significant increase in the mechanism of ROS generation in ARPE-19 over certain irradiance levels and/or difference in damage response by ARPE-19. As explained by Ham et al. (1980) this may be due to **a)** two-photon absorption, where a molecule simultaneously absorbs two photons to reach excited state, **b)** frequency doubling, where upon interaction with a molecule two photons with same frequency combine their energy to give rise to a new photon with doubled energy. Moreover, Seko et al., (2001) demonstrated in rat RPE cells that while blue light (440 ±10 nm) at 20 W/m^2 for 60 h resulted in apoptosis, same wavelength blue-light at 40 W/m^2 for 36 h resulted in necrosis. In addition Seko et al., (2001) showed that both apoptosis and necrosis were caused by reactive oxygen species (ROS). Therefore, difference in paracellular resistance decline rate against radiant exposure observed in ARPE-19 between 140.4 W/m^2 and 118.1 W/m^2 (and below) may indicate different cell death processes, both caused by ROS. While short exposures with high irradiances may cause necrosis, long exposures with lower irradiances may result in apoptosis. However, further studies need to be performed with specific assays against apoptosis and necrosis, moreover future blue-light studies on RPE should investigate different irradiances for each wavelength.

It is important to note that due to human RPE uptaking more O_2 with decreased wavelength (increasing the ROS formation) and one single photosensitizer being able to give rise to numerous free radicals in the presence of O_2, it is difficult to quantitatively compare different blue light irradiances at different wavelengths; as wavelength and irradiance represent different experimental variables.

6.4 Effect of Blue-Light on Mitochondria

Previous studies on the effect of blue-light identify mitochondria as the target and initiator of blue light damage to the retina (King et al., 2004; Godley et al., 2005; Jarrett et al., 2008; Alaimo et al., 2019; Tao et al., 2019). King et al., (2004) showed in ARPE-19 that ROS derived from mitochondrial electron transport chain mediate blue-light (425 ± 25 nm; $10 \cdot 10^3$ W/m^2; 7 min) induced RPE death. Furthermore, Godley et al., (2005) demonstrated in primary human RPE that blue-light (400 - 500 nm; 28 W/m^2; 6 h) induced chromatin breaks in the mtDNA and ROS production in the mitochondria. More recently, Alaimo et al., (2019) showed that blue LED light (445 ± 18 nm; 44.3 W/m^2; 1h) impaired mitochondrial dynamics through ROS production. In line with the previous studies, this study demonstrated that blue light (470 ± 10 nm; 140.4 W/m^2; 7 h) exposure induced mitochondrial dysfunction on ARPE-19 (Fig 33, 34 and 35). Two major mitochondrial chromophores have been identified as targets for blue light damage in previous studies. These are porphyrins (eg. cytochromes) and flavins (eg. FAD and FMN) which absorb throughout the blue-light spectrum with absorption peaks respectively at 420-440 nm and 450-520 nm (Hockberger et al., 1999; Tao et al., 2019). This suggests that while blue-light in the 400 - 500 nm range can be damaging to both chromophores, predominant damage occurring at 470 nm may be due to dysfunction of flavins such as FAD and FMN, and predominant damage occurring at 420 nm may be due to dysfunction of porphyrins such as cytochromes.

6.5 Effect of Blue-Light on Senescence

Induction of senescence through disturbing gene transcription, DNA replication and shortening telomeres due to excessive ROS production is well documented (Colavitti and Finkel, 2005; Passos et al., 2007; Lu and Finkel, 2008; Moiseeva et al., 2009; Imai et al., 2014; Van Deursen, 2014; Ziegler et al., 2015). Moreover, previously Kernt et al., (2012) demonstrated that filtering blue light from the visible spectra reduced light-induced oxidative stress and senescence in primary human RPE cells to the control levels where primary human RPE cells were unexposed. In our study, we showed that high irradiance (140.4 W/m^2) blue-light (470 nm) can be modulated by using continuous exposure for certain duration (7 hours) to induce cellular senescence on ARPE-19 cells cultured on ECIS micro-electrode arrays without any associated cell death. With this method, we were able to simultaneously recapitulate cellular features of AMD; premature senescence, barrier function breakdown and mitochondrial dysfunction on ARPE-19 cells without any cell coverage decline. Hence our blue-light induced in vitro model can be used to simultaneously study cellular features of RPE which occur during AMD disease development process before AMD progresses into its advanced stage.

6.6 Comparison of Blue-Light Induced AMD model against TBHP- and H_2O_2-induced AMD models

Current in-vitro models of AMD mostly use tetr-butyl hydroperoxide (TBHP) and hydrogen peroxide (H_2O_2) assays to study the effect of oxidative stress following various protocols. Before comparing blue-light induced model to TBHP- and H_2O_2- induced models, trial and error experiments were performed by Dr. Vlastimil Srsen to optimize the concentration of TBHP and H_2O_2 that would induce maximum senescence and minimum cell death on ARPE-19. Empirical results showed that for quiescent ARPE-19 cultured in media supplemented with 1% of FBS, appropriate dose of TBHP treatment is 100µM whereas 150 µM could be safely used for exponentially growing ARPE-19. In

case of H_2O_2, the dose 750 µM is safe to treat confluent quiescent ARPE-19 cultured in 1 % of FBS whereas the exponentially growing cells should be treated with 375 µM.

Previous studies have implicated different mechanisms of damage in epithelial cells as a result of blue-light, TBHP and H_2O_2. The studies on the effect of blue-light identified mitochondria as the target and initiator of ROS production in the retina (King et al., 2004; Godley et al., 2005; Jarrett et al., 2008; Alaimo et al., 2019; Tao et al., 2019). Godley et al., (2005) showed that ROS produced in the mitochondria as a result of blue-light exposure are superoxide anion (O_2^-), hydroxyl radical (•OH) and singlet oxygen ($^1O_2$). These ROS interact with NADH dehydrogenase, cytochrome c oxidase and ATP synthase found in mitochondrial inner membrane. NADH dehydrogenase, cytochrome c oxidase and ATP synthase are part of mitochondrial respiratory chain complex which catalyse phosphorylation of ADP to ATP. Therefore blue-light induced oxidative damage to the mitochondrial respiratory chain complex impairs mitochondrial energy production (Guo et al., 2013). Furthermore, interaction of reactive hydroxyl radical (•OH) with deoxyribose in the mtDNA can induce loss of DNA base similar to single strand breaks (Imlay and Stuart Linn, 1988; Farber, 1994) . On the other hand, Spector et al., (2002) showed that H_2O_2 reacts directly on DNA causing single strand breaks. Ma and Kleiman (2004) documented that DNA damage due to ROS involves formation of hydroxyl radicals (•OH). Moreover, Ma et al., (2002) demonstrated that H_2O_2 stimulated high polyADP-ribosyl polymerase (PARP) activation by 6-fold, causing a decline in nicotinamide adenine dinucleotide (NAD) and adenosine tri-phosphate (ATP) levels. On another note, Spector et al., (2002) showed that TBHP primarily reacts through membrane disruption. Ma and Kleiman (2004) demonstrated that the cytotoxic mechanism of TBHP involves formation of superoxide anions (O_2^-) but may not involve hydroxyl radicals (•OH). Hence, TBHP treatment primarily damage cellular and mitochondrial membranes via generation of superoxide anions (O_2^-). Furthermore, in the studies performed

by Ma et al., (2002) contrarily to H_2O_2, TBHP only increased PARP activity by 30 % and no decrease in NAD was observed, consequently ATP decline was much slower with TBHP.

In line with these previous studies, this research demonstrated the difference in response on ARPE-19 cells after blue-light, TBHP and H_2O_2 exposure. Blue-light decreased the paracellular resistance before cell coverage declined. TBHP resulted in an immediate decline in paracellular resistance as well as cell coverage and the media change after TBHP treatment induced recovery of both the paracellular resistance and cell coverage. This suggested that TBHP induced oxidative stress damage to ARPE-19 may be reversible through media change at t = 2 h mark. On the other hand, paracellular resistance decline due to H_2O_2 started 1 hour after the media change, which indicated that the damage was not immediate. Furthermore, slower paracellular resistance recovery rate after H_2O_2 treatment may indicate decreased ATP levels, resulting from decline in PARP activity, thus impairing cellular recovery after oxidative stress.

Overall, blue-light induced AMD in-vitro models presented potential advantages over current models that use TBHP and H_2O_2. Our research showed that blue-light induced loss of barrier function, mitochondrial damage and senescence in ARPE-19 cells before cell death occurred. Therefore it is a valuable tool to mimic in-vivo AMD development process. Furthermore, blue-light dose could be easily controlled in space and modulated in time as opposed to TBHP and H_2O_2 concentrations. Therefore, blue-light allowed in-situ experiments as opposed to TBHP and H_2O_2 treatments which usually require media change at the end of the treatment. As a result of media change the cells might benefit from a boost of antioxidants, therefore the real effect of TBHP and H_2O_2 could be masked. On the other hand, in-situ blue-light exposure allowed accurate study of cell repair in in-vitro AMD models. Furthermore, in addition to continuous exposure, daily/intermittent exposure was also studied with blue-light induced models. The comparison of

continuous and daily/intermittent exposure on blue-light induced models allowed study of emergent effect of post-exposure oxidative stress. For example, our study indicated that ARPE-19 cells may have generated different cellular stress responses due to continuous and daily/intermittent blue-light exposure which affected cell death. This difference between continuous and daily/intermittent exposure might be due to overwhelmed antioxidant systems as well as inability for RPE cells to build adequate stress response under continuous blue-light exposure to prevent cell death. While as a result of daily/intermittent blue-light exposure, RPE may have time to generate stress responses to prevent or delay cell death. Roehlecke et al., (2009) showed that non-lethal blue-light (405 nm) exposure on ARPE-19 cells increased ROS levels and expression of stress related proteins; heme oxygenase-1, osteopontin, heat shock protein-27; manganese superoxide dismutase and cathepsin D as well as inducing conformational changes in mitochondria, enhanced advanced glycation end-products (AGEs) and a delay in cell cycle, which may have implications for AMD pathogenesis. Blue-light is an exogenous risk factor in AMD (Cruickshanks et al., 1993; Klein et al.,1998), therefore blue-light induced models are important for investigation of the underlying mechanism and discovery of potential AMD treatments.

6.7 Pigmentation in blue-light induced AMD model: Considerations and Limitations

Although there have been various attempts to re-pigment RPE cell lines in-vitro, an ideal RPE cell culture that contains all of melanosomes and lipofuscin has not yet been produced (Boulton, 2014). Melanosomes in the RPE act as an absorber of light and minimize light scatter and refractions, due to their melanin content (Rozanowska, 2012). However, it is important to note that melanosomes undergo significant age-related changes through a combination of photochemical modification and lysosomal degradation which alters their spectral characteristics and increases their photoreactivity, hence increasing their potential for phototoxic damage to RPE (Boulton et al., 1990; Rózanowski et al., 2008; Boulton, 2014). The total number of pure melanin granules in RPE

melanosomes decline with age. This decline correlates with an increase in melanolipofuscin granules (Boulton and Dayhaw-barker, 2001). By repigmenting confluent ARPE-19 with melanosomes isolated from either bovine (as a model for young melanosomes) and ex-vivo old human RPE cells, Rózanowski et al., (2008) demonstrated that cell death significantly increased in ARPE-19 fed with melanosomes from old donors compared to ARPE-19 fed with bovine melanosomes after blue-light exposure (390-550nm; 28 W/m^2; up to 96 h). Therefore, in the light of these studies, it may be valuable to compare the effect of blue-light on ARPE-19 fed with melanosomes from old and young human donors.

In addition, with age, cumulative oxidative stress, causes acidification of lysosome/phagosome, as well as oxidation of their lipid and protein content (Boulton and Dayhaw-barker, 2001) resulting in increased lipofuscin granules in in-vivo RPE. Lipofuscin shows broad structureless absorption spectra between 300 - 550 nm with the absorption declining with increasing wavelength (Avalle et al., 2005). Rózanowska et al. (1995) showed that just as pigmented and non-pigmented RPE cells uptake oxygen when irradiated with narrow-band light (290-578 nm) in aerobic conditions, lipofuscin granules also uptake oxygen in this narrow-band light range. Moreover, similarly to RPE cells, the oxygen uptake of lipofuscin granules increases exponentially with decreasing wavelength of light in the range of 578nm to 290nm (Rózanowska et al., 1995). In addition, the photoreactivity of lipofuscin granules increases with age (Rózanowska et al., 2004). Photo-excitation of lipofuscin granules with blue-light leads to generation of singlet oxygen, superoxide, hydrogen peroxide, lipid hydro-peroxides and melondialdehyde, as they contain abundance of polyunsaturated lipids (Boulton et al., 1993). The action spectrum for singlet oxygen production by lipofuscin is between 300 – 450 nm with a peak at 380 nm (Avalle et al., 2005). Previously Davies et al., (2001) demonstrated that lipid peroxidation, protein oxidation, loss of lysosomal integrity and membrane blebbing culminating in cell death increased in primary human RPE cultures fed with isolated lipofuscin granules from human eyes

compared to unfed primary human RPE after short wavelength visible light exposure (390 - 550nm; 48h). All in all, previous studies have demonstrated that presence of lipofuscin enhanced the blue-light induced damage to RPE. Therefore for the future the blue-light induced AMD model introduced in this research could be fed with isolated lipofuscin to better replicate aged in-vivo RPE and study paracellular resistance decline, mitochondrial damage and senescence in the presence of lipofuscin.

In order to model the lipofuscin accumulation occurring in vivo with age, in our research ARPE-19 cells were fed with a component of lipofuscin; a mixture of A2E:iso-A2E, which is widely used in in-vitro studies for being easy to chemically synthesize (Boulton, 2014). We demonstrated the proof of principle that blue-light induced AMD model could be enhanced with pigment granules. This was shown by feeding chemically synthesized 100 µM A2E into RPE cultures. However, no statistical difference was observed between ARPE-19 fed with 100 µM A2E and unfed ARPE-19 after 470nm blue-light exposure. The absorbance spectra of A2E is between 300 – 550 nm and displays a major peak at 435 nm and a lesser peak at 335 nm (Parish et al., 1998). However, the action spectra for ROS production by A2E is associated to be most efficient between 415-455 nm with a peak at 430 nm, as previous studies demonstrated by using blue light irradiances normalized with respect to the natural, direct sunlight reaching the retina on primary porcine RPE cells (Arnault et al., 2013; Marie et al., 2018). The study by Marie et al., (2018) used 10 nm-wide light bands and estimated that ROS production rate of A2E in primary porcine RPE at 470 nm was 0.25 of its maximum. In our research LED irradiances at 470nm were over 3-times lower than the blue-light irradiances used by Marie et al. (2018) at 470 nm. Hence, our results indicate that A2E may not be highly photoreactive with 470 nm blue-light at LED irradiance levels used in our research. However importantly, taken together our results suggested that 470 nm blue-light at irradiances used in our research (E_e = 140.4 W/m^2, 118.1 W/m^2, 74.65 W/m^2, 47.05 W/m^2 and 29.67 W/m^2) can be damaging to the human RPE cells irrespective of chemically synthesised and fed A2E

presence. In addition, further photochemical studies are needed to be performed using A2E fed human RPE cells under different irradiances for each wavelength to study A2E photo-reactivity in detail.

It is important to note that the action spectra associated with A2E is different from ground state action spectra of lipofuscin (Avalle et al., 2005). Furthermore, it was demonstrated that the role of A2E in lipofuscin phototoxicity and photoreactivity is only minor (Cantrell et al., 2001; Davies et al., 2001; Lamb et al., 2001; Pawlak et al., 2002; Pawlak et al., 2003). While A2E is used for its convenience in lipofuscin and AMD studies, its relevance to lipofuscin cytotoxicity is still open to question, furthermore there is no evidence that A2E can be released once complexed into lipofuscin (Boulton, 2013). Therefore, to represent in-vivo RPE better blue-light induced in-vitro AMD model could be improved by feeding lipofuscin granules instead of A2E. Wassell et al. (1998) showed that cultured human RPE accumulated auto-fluorescent granules regardless of an exogenous substrate when cultured in basal medium for as long as 1 year. In addition when fed with rod outer segments daily for 56 days, the accumulation of these auto-fluorescent granules increased. This indicates involvement of autophagy as well as phagocytosis in the formation of lipofuscin-like granules. Although these auto-fluorescent granules showed some spectral similarities with RPE lipofuscin, they differed in solubility and chromatographic motility from RPE lipofuscin. This suggests that additional properties of RPE cells or of the materials they phagocytose are needed to generate auto-fluorescent granules with lipofuscin-characteristics (Wassell et al., 1998). Therefore, currently lipofuscin accumulation in cultured RPE that reflect the in-vivo case is only reached by feeding cultured RPE cells with intact lipofuscin granules isolated from ex vivo RPE cells as demonstrated by Davies et al., (2001). After resuspension and washing, lipofuscin granules are suspended in culture medium and fed to confluent RPE at about 300 granules per cell for 24 hours to allow the phagocytosis of the granules where they end up in lysosome of the RPE similar to in-vivo case (Davies et al., 2001; Boulton, 2014).

In order to dissect the melanin and lipofuscin independent mechanism of blue-light damage, pigmentation and lipofuscin content were not included in the overall study of in-vitro model in this research.

6.8 Blue-light induced ARPE-19 damage in relation to in-vivo blue-light funduscopic studies

As the RPE cells were directly cultured under blue-light in this study, the irradiances reported in this research correspond to the irradiance reaching the retina at the back of the eye. To translate the back of the eye irradiances into the corresponding front of the eye irradiances coming from a light source, the eye/light source model developed by Le Grand (1972) can be used. According to this eye/light source model, retinal irradiance $(E_{e,retina})$ can be estimated as:

$$E_{e,retina}(\lambda) = 0.07 E_{e,source}(\lambda)\tau(\lambda) \qquad \textit{Eq.14}$$

where $E_{e,retina}(\lambda)$ is the retinal irradiance, $E_{e,source}(\lambda)$ is the irradiance of the light source and $\tau(\lambda)$ is the transmittance of the ocular media in the eye (Arnault et al., 2013). Hence, the back of the eye irradiances investigated in this study can be translated respectively into the front of the eye lighting source irradiances seen in Table 1. As a comparison, Scientific Committee on Emerging and Newly-Identified Health Risks (SCENIHR) (2007) calculated that the irradiance at the retina when a person looks at snow or white sand on a clear sunny day is between 30-60 W/m^2. Moreover, retinal irradiances from operating microscope, ophthalmoscope and slit lamp which all use blue LED technology (470 nm) are reported to reach up to respectively 9700 W/m^2, 1300 W/m^2 and 3500 W/m^2 (Kirkness, 1986; Rozanowska et al., 2009). On the other hand, blue autofluorescence imaging mode of Spectralis HRA+OCT which is widely used for RPE and lipofuscin imaging in clinical practice, was estimated to exhibit retinal irradiance of 1.9 W/m^2 at 488 ± 2 nm (Teussink et al., 2017). In our study, we used LED irradiances ranging from 29.67 – 140.4 W/m^2 at 470 nm on ARPE-19 cells and documented breakdown of barrier function

before cell death. Blue-light irradiance generated by Spectralis HRA+OCT is ~15–fold lower than irradiance values we used in our experiments and ~10^3-fold lower than other ophthalmological instruments. Moreover, in our study on ARPE-19 it was observed that the rate of barrier function decline against radiant exposure was faster when exposed to shorter wavelength blue-light. Therefore, Spectralis HRA+OCT using 1.9 W/m^2 at 488 ± 2 nm may be safer compared to other devices used in clinical practice. However, it is important to note that as opposed to ARPE-19 cells, diseased RPE may be susceptible to blue-light toxicity at lower levels in blue autofluorescence imaging (Borrelli et al., 2019), especially if exposures are repeated (Figure 36) as part of monitoring process.

Table 1 Retinal (Back of the eye) irradiances translated into real-life source (front of the eye) irradiances

λ = 470 nm	
τ(470) = 0.7	
Retinal (back of the eye) Irradiance (W/m²)	Real-life Source (front of the eye) Irradiance (W/m²)
29.67	605.5
47.05	960.2
75.65	1523.5
118.1	2410.2
140.4	2865.3

λ = 420 nm	
τ(420) = 0.45	
Retinal (back of the eye) Irradiance (W/m²)	Real-life Source (front of the eye) Irradiance (W/m²)
9.97	316.5
15.8	501.6

λ = 400 nm	
τ(400) = 0.08	
Retinal (back of the eye) Irradiance (W/m²)	Real-life Source (front of the eye) Irradiance (W/m²)
17.66	3153.6

λ = 525 nm	
τ(525) = 0.8	
Retinal (back of the eye) Irradiance (W/m²)	Real-life (front of the eye) Irradiance (W/m²)
18.7	333.9

Studies in vivo need to consider both RPE and photoreceptor damage by blue-light. Previously, in-vivo studies showed that different sites of retinal injury occurred depending on irradiation conditions (eg. prior adaptation of the light), wavelength, irradiance and exposure length. Rats have been the most widely used animals for in vivo photobiological studies (Rozanowska et al., 2009). At retinal irradiances lower than 10 W/m^2, a damage exclusive to rat retinas was observed on photoreceptor rods after exposures more than 1.5 hours by Noell et al. (1966) and Williams and Howell (1983). The rats spent at least 24 hours

prior to exposure in the dark and the damage was classified using an electroretinogram and later histology, as any structural alteration or changes in measured function from which recovery was partial or slow, if any, hence it ranged from cell death to structural and/or functional changes that impair physiological performance of the cells (Noell et al., 1966; Noell, 1980). The action spectrum of this damage was documented between 434 - 590 nm with a peak at 500 nm, and closely matched with the absorption spectra of rhodopsin which is between 400-600 nm with a peak at 500 nm (Noell et al., 1966; Noell, 1980; Williams and Howell, 1983; Rozanowska et al., 2009). It is important to note that rods are very sensitive to light and can be triggered by a single photon. Hence at very low irradiances vision is based only on rods. On the other hand cones are less sensitive and require higher irradiances (larger amounts of photons) to produce a visual signal (Hecht et al., 1942; Baylor et al., 1979; Ingram et al., 2016). In addition, as opposed to primate retina, approximately 75 % of the rat retina consists mostly but not exclusively of rod cells (Noell et al., 1980). On the other hand, using funduscopy and histology in their in-vivo studies on rats Gorgels and Van Norren (1995) showed that at higher irradiance (>10 W/m^2) where rhodopsin was completely bleached, the efficiency of the light damage, characterized by a change (swelling/different morphological appearance) just visible in fundus increased between 320 -500 nm with decreasing wavelength. Interestingly, while light between 440-500 nm mainly damaged RPE, blue-light below 440 nm and UV also damaged photoreceptors as well as RPE. Importantly, it was observed that the action spectrum of damage below 440 nm matched the absorption spectra of bleached rhodopsin (Figure 40) (Gorgels and Van Norren, 1995; Rozanowska et al., 2009). It was observed that in experimental conditions in studies by Noell et al. (1966) and Williams and Howell (1983), rhodopsin bleached by 15-90 %, whereas in experimental conditions in studies by Gorgels and Van Norren (1995) rhodopsin was fully bleached. Hence a hypothesis first speculated by Kremers and Van Norren (1988) and later shared by Van Norren and Gorgels (2011) states that at low irradiances the

damage is mediated by rhodopsin, being the most sensitive chromophore, while at high irradiances rhodopsin is bleached away and other less sensitive chromophores mediate the damage, however more experiments are needed in the subject.

On the other hand, in-vivo studies on monkeys documented that retinal damage occurred with blue-light before 4 hours, at or above 100 W/m^2 retinal irradiance (Ham et al., 1976; Ham et al., 1982; Lund et al., 2006), which is similar to irradiances used in our study. In studies by Ham et al. (1976) and Ham et al. (1982) the light damage was characterized by production of a ophthalmoscopically visible lesion immediately after the exposure and histological studies were performed using unstained phase contrast light micrograph. It was observed that rhodopsin was completely bleached and similar to in-vivo experiments on rats the efficiency of the light damage increased between 320-500nm with decreasing wavelength (Figure 40). Again similarly to rats, while light between 440-500 nm mainly damaged RPE, blue-light below 440 nm and UV also damaged photoreceptors as well as RPE (Ham et al., 1982; Gorgels and Van Norren, 1995; Rozanowska et al., 2009; Hunter et al., 2012). The action spectrum of this damage on photoreceptors occurring below 440 nm correlated with the absorption spectra of S-cone opsins which has a peak at 420 nm (Sperling, 1980) as well as bleached rhodopsin (Van Norren and Gorgels, 2011). Moreover, experiments performed on monkeys also showed that the light damage on RPE was oxygen-dependent as elevated O_2 levels in blood increased photosensitivity, lowered the threshold and increased the extent of damage at a certain radiant exposure (Ruffolo Jr. et al., 1984; Jaffe et al., 1988; Rozanowska et al., 2009).

It is important to note that different irradiance values were used in these previous studies on different species due to different characteristics of the eyes. However, in all species it was observed that less radiant exposure was needed to exert photobiological damage on RPE as the wavelength of light decreased (Van Norren and Gorgels, 2011; Hunter et al., 2012).

a)

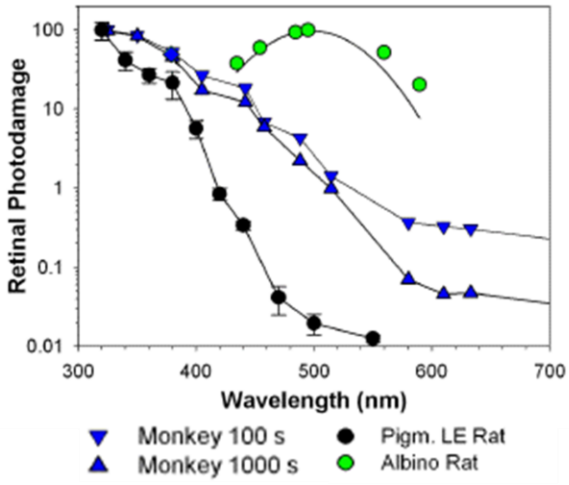

Monkey (100 s)		Monkey (1000 s)		Pigm. LE Rat			Albino Rat (6 h)	
Wavelength (nm)	Retinal Irradiance (W/m²)	Wavelength (nm)	Retinal Irradiance (W/m²)	Wavelength (nm)	Retinal Irradiance (W/m²)	Duration (min)	Wavelength (nm)	Retinal Irradiance (W/m²)
325	500	325	51	320	1.3	22-70	434	9.2
350	5400	350	55	340	6.6	15-25	452	8.8
380	8100	380	93	360	9.6	15-24	480	8.3
405	1500	405	230	380	17.6	8-23	486	8.2
442	2000	442	300	400	63	8-19	560	7.1
458	5200	458	600	420	83	60-70	590	6.7
488	7700	488	1500	440	226	50-60		
515	22000	515	3200	470	460	134-285		
580	76000	580	40000	500	980	125-330		
610	81000	610	58000	550	960	260-300		
633	84000	633	54000	600	1820	300		

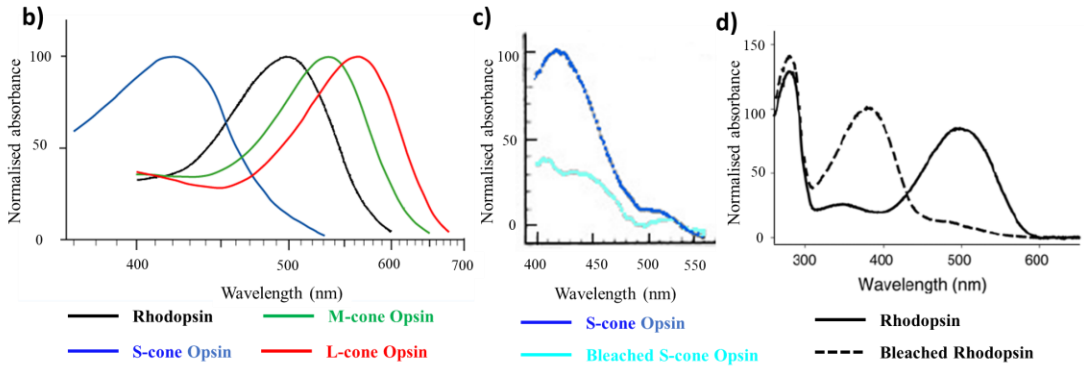

Figure 40 In-vivo blue-light funduscopic studies from the literature. a) Action spectra of retinal photo-damage in the rat and rhesus monkey shown in logarithmic scale based on Ham et al. (1976); Ham et al. (1982) Williams and Howell (1983); Gorgels and Van Norren (1995). ***b)*** Absorption spectrum of photoreceptor opsins in humans, rhesus monkey. ***c)*** Absorption spectrum of unbleached and bleached S-cone (blue-cone) opsin in humans and rhesus monkey. ***d)*** Absorption spectrum of unbleached and bleached rhodopsin in humans, rhesus monkey and rats. [Modified from Bowmaker and Dartnall (1980); National Research Council (US) Committee on Vision, (1990); Rozanowska et al. (2009); Jastrzebska B., (2015)].

In the light of these animal studies Scientific Committee on Emerging and Newly-Identified Health Risks (SCENIHR) (2007) defined two classes of photodamage to retina. Class I is mainly located in photoreceptor and has an action spectrum that is identical to the absorption spectrum of pigments found in photoreceptors. This damage can be mainly attributed to impairments in opsin pigment regeneration cycle. On the other hand, Class II damage is confined to RPE and the occurrence is oxygen dependent. This photo-oxidative damage is cumulative and depends on the anti-oxidant status and oxidative stress in the retina. The action spectrum of this damage appears to increase with declining wavelengths in the blue-light spectra.

In this current in-vitro study, as only human RPE cells were exposed to blue-light, only Class II retinal damage was investigated. However in the future the proposed in-vitro model could be enhanced by co-culturing ARPE-19 with photoreceptor cells which contain rhodopsin to investigate both Class I and II photodamage on retina.

7 Conclusion and Perspectives

7.1 Summary

This research aimed to understand better the effect of blue-light (470 nm) on RPE cells and to leverage this understanding to develop a blue-light induced in-vitro disease model that recapitulates cellular features of AMD.

Our results document that blue LED light exposure decreases tight junction associated with barrier function on human RPE in vitro in a dose dependent and time-course manner, before any cell death occurs. This study is the first to show that blue-light induced break-down of barrier function on human RPE cells is mediated by oxidative stress through PKC-ζ over-activation (Ozkaya et al., 2019). In addition, we showed that blue light induced barrier function decline on human RPE is irradiance-, radiation wavelength- and time of exposure- dependent, in contrast to green-light (525 nm).

In the second part of the research, by leveraging this understanding, we demonstrated that ARPE-19 cells exposed to blue-light recapitulates cellular features associated with AMD; senescence, mitochondrial dysfunction and loss of barrier function, before cell coverage declined. Comparison and quantification of blue-light induced changes against current widely used oxidative stress inducers; TBHP and H_2O_2 showed statistically different response from APRE-19 cells. On this basis we established a new blue-light induced in-vitro model that recapitulates some of the cellular features of AMD. This model showed greater cellular senescence induction, barrier function breakdown and mitochondrial damage before cell coverage decline even when compared to models using optimal doses (maximum induced oxidative stress with only few cell death) of TBHP and H_2O_2. Therefore blue-light induced in-vitro model should allow better understanding of these cellular features as they better reflect the in-vivo AMD development process, before RPE cell death. Blue-light induced model also demonstrated potential advantages such as easier modulability, spatial resolution and in-situ experiments. In addition, our

study investigated in-vitro AMD model induced by daily/intermittent blue-light exposure that takes into account the emergent effect of post-exposure oxidative stress. The comparison between the daily/intermittent exposure models and continuous exposure model allowed quantification of stage effect of blue-light damage on barrier function. Finally, by feeding chemically synthesized A2E, a component of age pigment lipofuscin, into ARPE-19 it was also demonstrated that the blue-light induced AMD model could be enhanced with pigment granules. However no statistical difference was observed between A2E-fed and unfed ARPE-19 after 470 nm blue-light exposure.

7.2 Perspectives

This work, investigated and quantified the time course effect of blue-light on human RPE cells in a label free manner using a novel ad-hoc LED illumination system combined with ECIS technology. This revealed that blue light decreased tight junction associated barrier function on human RPE before loss of cell coverage. This damage induced by blue-light on tight junctions was mediated by oxidative stress through PKC-ζ over-activation. We have identified PKC-ζ activity as a potential target in the early events taking place in blue-light induced barrier function breakdown. In addition, more studies with different concentrations of PKC-ζ inhibitor can be performed. In both wet and dry AMD the outer blood-retina barrier (outer BRB) formed by the tight junctions between RPE cells are altered or lost (Sarks et al., 1988; Killingsworth et al., 1990; Johnson et al., 2005; Curcio and Johnson, 2013). Therefore new therapies that prevent targeting of PKC-ζ could be investigated in AMD studies.

Blue-light induced model by using 96-well ECIS plates showed potential for development of high throughput AMD drug screening assays. This experimental design can allow multiple drug testing in a label free manner, can provide insight on the optimal time-points to perform different drugs and monitor & quantify the wound healing in real-time. In addition more studies with different light parameters; irradiance, wavelength as well as conditions;

continuous, daily/intermittent exposure can be performed to examine difference in cellular response. Moreover, studies exploring the underlying cell death mechanism due to different blue-light conditions are needed.

The model proposed in this study can be improved using hiPSC derived RPE. In a previous study developed in our group by Gamal et al., (2015), it has been shown that hiPSC derived RPE grown on ECIS plates exhibited a pigmented monolayer with 6000 Ω para-cellular resistance after 25-day maturation period. Improving our blue-light induced model using hiPSC from both healthy donors and AMD-patients can allow comparative study of blue-light induced barrier function decline, senescence and mitochondrial dysfunction to those seen in AMD. In addition blue-light induced hiPSC derived RPE from heathy donors and hiPSC derived RPE from AMD patients can be compared for oxidative stress, antioxidant response, complement activation and inflammatory response.

In order to better mimic in vivo micro-environment of outer blood retina barrier and its physiological interactions as well as improve cell morphology, mechanical properties and differentiation, three dimensional (3D) organ-on-a-chip model could be used. Using Microfluidic Transflow Chip (Be-Transflow, BEOnChip), RPE cells could be co-cultured on top of human umbilical vein endothelial cells (HUVEC), which could then be used to mimic the choroidal vasculature network. Blue-light can be used to induce barrier function breakdown, mitochondrial dysfunction and senescence in these 3D models. In addition, VEGF concentration gradient may be used to explore the possibility of generating choroidal neovascularization to model wet-AMD.

7.3 Conclusions

In-vitro exposure of blue-light on human RPE cells using an ad-hoc blue LED illumination system combined with ECIS allowed us to document in real-time tight junction associated barrier function breakdown before cell death. This study is first to show on human RPE cells that this blue-light induced barrier

function breakdown is mediated by oxidative stress through PKC- ζ over-activation. Therefore, this research has given us insights for designing new high throughput screening assays to test efficiency of novel therapies such as PKC-ζ inhibition. We modelled simultaneously in an in-vitro model induced by only blue-light cellular features associated with AMD; premature senescence, barrier function breakdown and mitochondrial damage, before cell death occurred, therefore showed proof of principle for a new model for AMD based on blue-light damage.

8 References

Abdulhag, U.N., Soiferman, D., Schueler-Furman, O., Miller, C., Shaag, A., Elpeleg, O., Edvardson, S., Saada, A., 2015. Mitochondrial complex IV deficiency, caused by mutated COX6B1, is associated with encephalomyopathy, hydrocephalus and cardiomyopathy. Eur. J. Hum. Genet. 23, 159–164. https://doi.org/10.1038/ejhg.2014.85

Ablonczy, Z., Dahrouj, M., Tang, P.H., Liu, Y., Sambamurti, K., Marmorstein, A.D., Crosson, C.E., 2011. Human retinal pigment epithelium cells as functional models for the RPE in vivo. Investig. Ophthalmol. Vis. Sci. 52, 8614–8620. https://doi.org/10.1167/iovs.11-8021

Adijanto, J., Philp, N.J., 2014. Cultured primary human fetal retinal pigment epithelium (hfRPE) as a model for evaluating RPE metabolism. Exp. Eye Res. 126, 77–84. https://doi.org/10.1016/j.exer.2014.01.015

Adler, A. S., Sinha, S., Kawahara, T. L., Zhang, J. Y., Segal, E., & Chang, H. Y., 2007. Motif module map reveals enforcement of aging by continual NF-kappaB activity. Genes & development, 21(24), 3244–3257. https://doi.org/10.1101/gad.1588507

Age-Related Eye Disease Study Research Group. 2001. A randomized, placebo-controlled, clinical trial of high-dose supplementation with vitamins C and E, beta carotene, and zinc for age-related macular degeneration and vision loss: AREDS report no 8. Arch Ophthalmol 2001; 119: 1417–36.

Ahmado A., Carr A-J., Vugler A.A., Semo M., Gias C., Lawrence J.M., Chen L.L., Chen F.K., Turowski P., da Cruz L., Coffey P.J., 2011 Induction of Differentiation by Pyruvate and DMEM in the Human Retinal Pigment Epithelium Cell Line ARPE-19. Invest. Ophthalmol. Vis. Sci. 2011;52(10):7148-7159. doi: https://doi.org/10.1167/iovs.10-6374.

Alaimo, A., Liñares, G.G., Bujjamer, J.M., Gorojod, R.M., Alcon, S.P., Martínez, J.H., Baldessari, A., Grecco, H.E., Kotler, M.L., 2019. Toxicity of blue led light and A2E is associated to mitochondrial dynamics impairment in ARPE-19 cells: implications for age-related macular degeneration. Arch. Toxicol. 93, 1401–1415. https://doi.org/10.1007/s00204-019-02409-6

Ambati, J., Atkinson, J. & Gelfand, B., 2013. Immunology of age-related macular degeneration. Nat Rev Immunol 13, 438–451 (2013). https://doi.org/10.1038/nri3459

Arnault, E., Barrau, C., Nanteau, C., Gondouin, P., Bigot, K., Viénot, F., Gutman, E., Fontaine, V., Villette, T., Cohen-Tannoudji, D., Sahel, J.A., Picaud, S., 2013. Phototoxic Action Spectrum on a Retinal Pigment Epithelium Model of Age-Related Macular Degeneration Exposed to Sunlight Normalized Conditions. PLoS One. https://doi.org/10.1371/journal.pone.0071398

Avalle, L.B., Dillon, J., Tari, S., Gaillard, E.R., 2005. A New Approach to Measuring the Action Spectrum for Singlet Oxygen Production by Human Retinal Lipofuscin. Photochem. Photobiol. 81, 1347. https://doi.org/10.1562/2005-05-17-rn-531

Aveleira, C.A., Lin, C.M., Abcouwer, S.F., Ambrósio, A.F., Antonetti, D.A., 2010. TNF-α signals through PKCζ/NF-κB to alter the tight junction complex and increase retinal endothelial cell permeability. Diabetes 59, 2872–2882. https://doi.org/10.2337/db09-1606

Bavik, C., Henry, S.H., Zhang, Y., Mitts, K., McGinn, T., Budzynski, E., Pashko, A., Lieu, K.L., Zhong, S., Blumberg, B., Kuksa, V., Orme, M., Scott, I., Fawzi, A., Kubota, R., 2015. Visual cycle modulation as an approach toward preservation of retinal integrity. PLoS One 10, 1–16. https://doi.org/10.1371/journal.pone.0124940

Baylor, D.A., Lamb, T.D., Yau, K.W., 1979. Responses of retinal rods to single photons. The Journal of Physiology. 288: 613–634. doi:10.1113/jphysiol.1979.sp012716 (inactive 2020-01-22). PMC 1281447. PMID 112243

Beatty, S., Koh, H.H., Phil, M., Henson, D., Boulton, M., 2000. The role of oxidative stress in the pathogenesis of age-related macular degeneration. Surv. Ophthalmol. 45, 115–134. https://doi.org/10.1016/S0039-6257(00)00140-5

Behar-Cohen, F., Martinsons, C., Viénot, F., Zissis, G., Barlier-Salsi, A., Cesarini, J.P., Enouf, O., Garcia, M., Picaud, S., Attia, D., 2011. Light-emitting diodes (LED) for domestic lighting: Any risks for the eye? Prog. Retin. Eye Res. 30, 239–257. https://doi.org/10.1016/j.preteyeres.2011.04.002

Bi W.M., Sun K., 2014. Light-induced retinal damageand potential benefits and side effects of blue light-filtering intraocular lens Recent Adv. Opthalmology., 34 (3) (2014), pp. 289-293

Birben, E., Sahiner, U.M., Sackesen, C., Erzurum, S., Kalayci, O., 2012. Oxidative stress and antioxidant defense. World Allergy Organ. J. 5, 9–19. https://doi.org/10.1097/WOX.0b013e3182439613

Black J., Lowckwood H., Mayburg S., 1963. Recombination Radiation in GaAs. Journal of Applied Physics 34, 178; https://doi.org/10.1063/1.1729062

Blasiak, J., Piechota, M., Pawlowska, E., Szatkowska, M., Sikora, E., Kaarniranta, K., 2017. Cellular senescence in age-related macular degeneration: Can autophagy and DNA damage response play a role? Oxid. Med. Cell. Longev. 2017. https://doi.org/10.1155/2017/5293258

Bloch S.B., Larsen M., Munch I.C. 2012. Incidence of Legal Blindness From Age-Related Macular Degeneration in Denmark: Year 2000 to 2010,

American Journal of Ophthalmology, Volume 153, Issue 2, 2012, Pages 209-213.e2, ISSN 0002-9394, https://doi.org/10.1016/j.ajo.2011.10.016.

Boettner E.A., 1967. Spectral transmission of the eye. Ann Arbor: The university of Michigan. 46 p.

Borrelli E., Nittala M.G., Abdelfattah N.S., Lei J., Hariri A.H., Shi Y., Fan W., Cozzi M., Sarao V., Lanzetta P., Staurenghi G., Sadda S.V.R., 2019. Comparison of short-wavelength blue-light autofluorescence and conventional blue-light autofluorescence in geographic atrophy British Journal of Ophthalmology 2019;103:610-616.

Boulton, M., Dayhaw-barker, P., 2001. The role of the retinal pigment epithelium: topographical variation and ageing changes. Eye (London, England), 15(Pt 3), 384–389. https://doi.org/10.1038/eye.2001.141.

Boulton, M., Docchio, F., Dayhaw-Barker, P., Ramponi, R., Cubeddu, R., 1990. Age-related changes in the morphology, absorption and fluorescence of melanosomes and lipofuscin granules of the retinal pigment epithelium. Vision Res. 30, 1291–1303. https://doi.org/10.1016/0042-6989(90)90003-4

Boulton, M., Dontsov, A., Jarvis-Evans, J., Ostrovsky, M., Svistunenko, D., 1993. Lipofuscin is a photoinducible free radical generator. J. Photochem. Photobiol. B Biol. 19, 201–204. https://doi.org/10.1016/1011-1344(93)87085-2

Boulton, M., Marshall, J., Mellerio, J., 1984. Retinitis pigmentosa: a quantitative study of the apical membrane of normal and dystrophic human retinal pigment epithelial cells in tissue culture in relation to phagocytosis. Graefe's Arch. Clin. Exp. Ophthalmol. 221, 214–229. https://doi.org/10.1007/BF02134143

Boulton, M., McKechnie, N.M., Breda, J., Bayly, M., Marshall, J., 1989. The

formation of autofluorescent granules in cultured human RPE. Investig. Ophthalmol. Vis. Sci.

Boulton, M.E., 2014. Studying melanin and lipofuscin in RPE cell culture models. Exp. Eye Res. https://doi.org/10.1016/j.exer.2014.01.016

Boulton, M.E., 2013. Ageing of the Retina and Retinal Pigment Epithelium, Age-Related Macular Degeneration. https://doi.org/10.1007/978-3-642-22107-1_3

Bowmaker J.K. and Dartnall H.J.A., 1980. Visual pigments of rods and cones in a human retina. J. Physiol. 298: pp501-511 (1980).

Brantley, M.A., Sternberg, P., 2012. Mechanisms of Oxidative Stress in Retinal Injury, Fifth Edit. ed, Retina Fifth Edition. Elsevier Inc. https://doi.org/10.1016/B978-1-4557-0737-9.00022-9

Brizzee K.R., Ordy J.M., 1981. Cellular features, regional accumulation and prospects of modification of age pigments in mammals. In: Sohal R.S., eds, Age Pigments. Amsterdam: Elsevier/North Holland Biomedical Press, 101-154.

Brown, D.M., Kaiser, P.K., Michels, M., Soubrane, G., Heier, J.S., Kim, R.Y., Sy, J.P., Schneider, S. & the ANCHOR Study Group. 2006. Ranibizumab versus Verteporfin for Neovascular Age-Related Macular Degeneration. N Engl J Med 2006; 355:1432-1444 DOI: 10.1056/NEJMoa062655

Bunsen R., Roscoe H.E. 1855. Photochemische Untersuchungen, Poggendorff´s Annalen 1855: 96: 373-394, 1857: 100: 43-88 and 481-516, 1857: 101: 235-263, 1859: 108: 193-273.

Caldwell M.M., Camp L.B., Warner C.W., Flint S.D., 1986. Action Spectra and Their Key Role in Assessing Biological Consequences of Solar UV-B Radiation Change. In: Worrest R.C., Caldwell M.M. (eds) Stratospheric Ozone Reduction, Solar Ultraviolet Radiation and Plant Life. NATO ASI

Series (Series G: Ecological Sciences), vol 8. Springer, Berlin, Heidelberg

Campochiaro, P.A., Hackett, S.F., 1993. Corneal Endothelial Cell Matrix Promotes Expression of Differentiated Features of Retinal Pigmented Epithelial Cells: Implication of Laminin and Basic Fibroblast Growth Factor as Active Components. Exp. Eye Res. https://doi.org/10.1006/exer.1993.1158

Cantrell, A., McGarvey, D.J., Roberts, J., Sarna, T., Truscott, T.G., 2001. Photochemical studies of A2-E. J. Photochem. Photobiol. B Biol. 64, 162–165. https://doi.org/10.1016/S1011-1344(01)00224-X

Chahory, S., Keller, N., Martin, E., Omri, B., Crisanti, P., Torriglia, A., 2010. Light induced retinal degeneration activates a caspase-independent pathway involving cathepsin D. Neurochem. Int. 57, 278–287. https://doi.org/10.1016/j.neuint.2010.06.006

Chahory, S., Padron, L., Courtois, Y., & Torriglia, A., 2004. The LEI/L-DNase II pathway is activated in light-induced retinal degeneration in rats. Neuroscience letters, 367(2), 205–209. https://doi.org/10.1016/j.neulet.2004.06.004

Chakravarthy, U., Wong, T.Y., Fletcher, A., Piault, E., Evans, C., Zlateva, G., Buggage, R., Pleil, A., Mitchell, P., 2010. Clinical risk factors for age-related macular degeneration: A systematic review and meta-analysis. BMC Ophthalmol. 10, 31. https://doi.org/10.1186/1471-2415-10-31

Chiu, S.-P., Lee, Y.-W., Wu, L.-Y., Tung, T.-H., Gomez, S., Lo, C.-M., Wang, J.-Y., 2019. Application of ECIS to Assess FCCP-Induced Changes of MSC Micromotion and Wound Healing Migration. Sensors 19, 3210. https://doi.org/10.3390/s19143210

Ciambrone, G.J., Liu, V.F., Lin, D.C., McGuinness, R.P., Leung, G.K., Pitchford, S., 2004. Cellular dielectric spectroscopy: A powerful new

approach to label-free cellular analysis. J. Biomol. Screen. 9, 467–480. https://doi.org/10.1177/1087057104267788

Colavitti, R., Finkel, T., 2005. Reactive oxygen species as mediators of cellular senescence. IUBMB Life 57, 277–281. https://doi.org/10.1080/15216540500091890

Cosentino-Gomes, D., Rocco-Machado, N., Meyer-Fernandes, J.R., 2012. Cell signaling through protein kinase C oxidation and activation. Int. J. Mol. Sci. 13, 10697–10721. https://doi.org/10.3390/ijms130910697

Crabb, J.W., Miyagi, M., Gu, X., Shadrach, K., West, K.A., Sakaguchi, H., Kamei, M., Hasan, A., Yan, L., Rayborn, M.E., Salomon, R.G., Hollyfield, J.G., 2002. Drusen proteome analysis: An approach to the etiology of age-related macular degeneration. Proc. Natl. Acad. Sci. U. S. A. 99, 14682–14687. https://doi.org/10.1073/pnas.222551899

Crisanti, P., Laplace, O., Lecain, E., Jonet, L., Jeanny, J.C., Omri, B., 2006. The role of PKCζ in NMDA-induced retinal ganglion cell death: Prevention by aspirin. Apoptosis 11, 983–991. https://doi.org/10.1007/s10495-006-6750-2

Cristofalo, V. and Pignolo, R. 1995. Chapter 4: Cell culture as a model. In Handbook of Physiology Sect 11: Aging (ed. Masoro E. J.), pp. 53-82. American Physiological Society: New York.

Crockett R.S., Lawwill T., 1984. Oxygen dependence of damage by 435 nm light in cultured retinal epithelium Curr. Eye Res., 3 (1) (1984), pp. 209-222, 10.3109/02713688408997202

Cruickshanks, K.J., Klein, R., Klein, B.E.K., 1993. Sunlight and agerelated macular degeneration—the Beaver Dam Eye Study. Arch. Ophthalmol. 111, 514–518.

Cubero, F.J., Zoubek, M.E., Hu, W., Peng, J., Zhao, G., Nevzorova, Y.A., Al

Masaoudi, M., Bechmann, L.P., Boekschoten, M. V., Muller, M., Preisinger, C., Gassler, N., Canbay, A.E., Luedde, T., Davis, R.J., Liedtke, C., Trautwein, C., 2016. Combined Activities of JNK1 and JNK2 in Hepatocytes Protect Against Toxic Liver Injury. Gastroenterology 150, 968–981. https://doi.org/10.1053/j.gastro.2015.12.019

Cugati S., Mitchell P., Rochtchina E., Tan A.G., Smith W., Wang J.J., 2006 Cataract surgery and the 10-year incidence of age-related maculopathy: the Blue Mountains Eye Study. Ophthalmology 2006;113: 2020–25.

Cunha-Vaz, J., 2009. The Blood–Retinal Barrier in Retinal Disease. Eur. Ophthalmic Rev. 03, 105. https://doi.org/10.17925/eor.2009.03.02.105

Cunha-Vaz, J., Bernardes, R., & Lobo, C., 2011. Blood-retinal barrier. European journal of ophthalmology, 21 Suppl 6, S3–S9. https://doi.org/10.5301/EJO.2010.6049

Curcio, C.A., Johnson, M., 2013. Retina - Curcio2013.pdf. Anat. Rec. A. Discov. Mol. Cell. Evol. Biol. 284, 544–549. https://doi.org/10.1002/ar.a.20192

Curcio, C.A., Messinger, J.D., Sloan, K.R., McGwin, G., Medeiros, N.E., Spaide, R.F., 2013. Subretinal drusenoid deposits in non-neovascular age-related macular degeneration: morphology, prevalence, topography, and biogenesis model. Retina 33, 1–24. https://doi.org/10.1097/IAE.0b013e31827e25e0.Subretinal

Darzins, P., Mitchell, P., Heller, R.F., 1997. Sun exposure and agerelated macular degeneration—an Australian case-control study. Ophthalmology 104, 770–776.

Davalli, P., Mitic, T., Caporali, A., Lauriola, A., D'Arca, D., 2016. ROS, Cell Senescence, and Novel Molecular Mechanisms in Aging and Age-Related Diseases. Oxid. Med. Cell. Longev. 2016.

https://doi.org/10.1155/2016/3565127

Davidson, P.C., Sternberg, P., 1993. Potential retinal phototoxicity. Am. J. Ophthalmol. 116, 497–501.

Davidson, P.C., Sternberg, P., Jones, D.P., Reed, R.L., 1994. Synthesis and transport of glutathione by cultured human retinal pigment epithelial cells. Investig. Ophthalmol. Vis. Sci. 35, 2843–2849.

Davies, S., Elliott, M.H., Floor, E., Truscott, T.G., Zareba, M., Sarna, T., Shamsi, F.A., Boulton, M.E., 2001. Photocytotoxicity of lipofuscin in human retinal pigment epithelial cells. Free Radic. Biol. Med. 31, 256–265. https://doi.org/10.1016/S0891-5849(01)00582-2

Dixon J.A., Oliver S.C.N, Olson J.L. & Mandava N. 2009. VEGF Trap-Eye for the treatment of neovascular age-related macular degeneration, Expert Opinion on Investigational Drugs, 18:10, 1573-1580, DOI: 10.1517/13543780903201684

Docchio, F., Boulton, M., Cubeddu, R., Ramponi, R. and Barker, P.D., 1991. Age-related Changes in the fluorescence of melanin and lipofuscin granules of the retinal pigment epithelium: A time-resolved fluorescence spectroscopy study. Photochemistry and Photobiology, 54: 247-253. doi:10.1111/j.1751-1097.1991.tb02013.x

Downie L.E., Wormald R., Evans J., Virgili G., Keller P.R., Lawrenson J.G., Li T., 2019. Analysis of a Systematic Review About Blue Light-Filtering Intraocular Lenses for Retinal Protection: Under-standing the Limitations of the Evidence. JAMA Ophthalmol. 21. doi: 10.1001/jamaophthalmol.2019.0019

Dunn K.C., Aotaki-Keen A.E., Putkey F.R. and Hjelmeland L.M., 1996. ARPE-19, A human retinal pigment epithelial cell line with differentiated properties. Exp. Eye Res. 62: 155-170. doi: 10.1006/exer.1996.0020

Dunn K.C., Mormorstein A.D., Bonilha V.L., Rodriguez-Boulan E., Giodano F., Hjelmeland L.M., 1998. Use of the ARPE-19 Cell Line as a Model of RPE Polarity: Basolateral Secretion of FGF5. Invest Ophthalmol Vis Sci. 1998; 39:2744-2749

Earnshaw, S.R., Moride, Y., Rochon, S., 2007. Cost-effectiveness of pegaptanib compared to photodynamic therapy with verteporfin and to standard care in the treatment of subfoveal wet age-related macular degeneration in Canada. Clin. Ther. 29, 2096–2106. https://doi.org/10.1016/j.clinthera.2007.09.001

Einstein, V.A., 1905. Uber einen die Erzeugung und Verwandlung des Lichts betre enden heuristischen Gesichtspunkt. Ann. Phys.

Eldred G.E., 1987. Questioning the nature of fluoreophores in age pigments. In: Totaro E.A., GleesP., Pisanti F.A., eds, Advances in Age Pigments Research. Oxford: Pergamon Press, 23-26.

Erik, S., Nilsson, G., Sundelin, S.P., Wihlmark, U., Brunk, U.T., 2003. Aging of cultured retinal pigment epithelial cells: oxidative reactions, lipofuscin formation and blue light damage, Documenta Ophthalmologica.

Esterbauer, H., 1996. Estimation of peroxidative damage. A critical review. Pathol. Biol. 44, 25–28.

Evans J., Wormald R. 1996. Is the incidence of registrable age-related macular degeneration increasing?. Br J Ophthalmol. 1996;80(1):9-14. doi:10.1136/bjo.80.1.9

Fagone, P., Jackowski, S., 2009. Membrane phospholipid synthesis and endoplasmic reticulum function. J. Lipid Res. 50, 311–316. https://doi.org/10.1194/jlr.R800049-JLR200

Farber, J.L., 1994. Mechanisms of cell injury by activated oxygen species. Environ. Health Perspect. 102, 17–24. https://doi.org/10.2307/3432207

Feher, J., Kovacs, I., Artico, M., Cavallotti, C., Papale, A., Balacco Gabrieli, C., 2006. Mitochondrial alterations of retinal pigment epithelium in age-related macular degeneration. Neurobiol. Aging 27, 983–993. https://doi.org/10.1016/j.neurobiolaging.2005.05.012

Firestone, R.A., Pisano, J.M., Bonney, R.J., 1979. Lysosomotropic Agents. 1. Synthesis and Cytotoxic Action of Lysosomotropic Detergents. J. Med. Chem. 22, 1130–1133. https://doi.org/10.1021/jm00195a026

Flood, M.T., Gouras, P., Kjeldbye, H., 1980. Growth characteristics and ultrastructure of RPE in vitro 1309–1320.

Franceschi, C., Bonafe, M., Valensin, S., Olivieri, F., De Luca, M., Ottaviani, E., De Benedictis, G., 2006. Inflamm-aging: An Evolutionary Perspective on Immunosenescence. Ann. N. Y. Acad. Sci. 908, 244–254. https://doi.org/10.1111/j.1749-6632.2000.tb06651.x

Freeney-Burns L., Katz M.L., 1992. Retinal Pigment Epithelium. In: Tasman W., Jaeger E., eds, Duane's Foundations of Clinical Ophthalmology. Lippincott: Philedelphia, 1-20.

Freund, A., Orjalo, A. V., Desprez, P.Y., Campisi, J., 2010. Inflammatory networks during cellular senescence: causes and consequences. Trends Mol. Med. 16, 238–246. https://doi.org/10.1016/j.molmed.2010.03.003

Fritsche, L.G., Loenhardt, T., Janssen, A., Fisher, S.A., Rivera, A., Keilhauer, C.N., Weber, B.H.F., 2008. Age-related macular degeneration is associated with an unstable ARMS2 (LOC387715) mRNA. Nat. Genet. 40, 892–896. https://doi.org/10.1038/ng.170

Gamal, W., Borooah, S., Smith, S., Underwood, I., Srsen, V., Chandran, S., Bagnaninchi, P.O., Dhillon, B., 2015. Real-time quantitative monitoring of hiPSC-based model of macular degeneration on Electric Cell-substrate Impedance Sensing microelectrodes. Biosens. Bioelectron.

https://doi.org/10.1016/j.bios.2015.04.079

Gamal, W., Treskes, P., Samuel, K., Sullivan, G.J., Siller, R., Srsen, V., Morgan, K., Bryans, A., Kozlowska, A., Koulovasilopoulos, A., Underwood, I., Smith, S., Del-Pozo, J., Moss, S., Thompson, A.I., Henderson, N.C., Hayes, P.C., Plevris, J.N., Bagnaninchi, P.O., Nelson, L.J., 2017. Low-dose acetaminophen induces early disruption of cell-cell tight junctions in human hepatic cells and mouse liver. Sci. Rep. 7, 1–16. https://doi.org/10.1038/srep37541

Gamal, W., Wu, H., Underwood, I., Jia, J., Smith, S., & Bagnaninchi, P. 2018. Impedance-based cellular assays for regenerative medicine. *Philosophical Transactions of the Royal Society B: Biological Sciences*, *373*(1750). https://doi.org/10.1098/rstb.2017.0226

Gavrilov, L.A., Gavrilova, N.S., 2002. Evolutionary theories of aging and longevity. ScientificWorldJournal. 2, 339–356. https://doi.org/10.1100/tsw.2002.96

Giaever, I., Keese, C.R., 1991. Micromotion of mammalian cells measured electrically. Proc. Natl. Acad. Sci. U. S. A. 88, 7896–7900. https://doi.org/10.1073/pnas.88.17.7896

Gilchrest BA, Eller MS, Geller AC, Yaar M, 1999. The pathogenesis of melanoma induced by ultraviolet radiation. N Engl J Med 1999: 340: 1341-1348.

Glotin, A.L., Debacq-Chainiaux, F., Brossas, J.Y., Faussat, A.M., Tréton, J., Zubielewicz, A., Toussaint, O., Mascarelli, F., 2008. Prematurely senescent ARPE-19 cells display features of age-related macular degeneration. Free Radic. Biol. Med. 44, 1348–1361. https://doi.org/10.1016/j.freeradbiomed.2007.12.023

Godley, B.F., Shamsi, F. a, Liang, F.-Q., Jarrett, S.G., Davies, S., Boulton, M.,

2005. Blue Light Induces Mitochondrial DNA Damage and Free Radical Production in Epithelial Cells. J. Biol. Chem. 280, 21061–21066. https://doi.org/10.1074/jbc.M502194200

Godley B.F., Xu H., Havey A., Zhong X., Lin H., Boulton M.E., 2008. Mitochondrial DNA Repair Capacity Decreases With Progression of Age-Related Macular Degeneration. Invest. Ophthalmol. Vis. Sci. 2008;49(13):4548.

Gold, B., Merriam, J.E., Zernant, J., Hancox, L.S., Taiber, A.J., Cramer, K., Neel, J., Bergeron, J., Barile, G.R., Theodore, R., Clinical, G., Group, S., Hageman, G.S., Dean, M., Allikmets, R., 2010. NIH Public Access 38, 458–462. https://doi.org/10.1038/ng1750.Variation

Gong, J., Cai, H., Noggle, S., Paull, D., Rizzolo, L.J., Del Priore, L. V., Fields, M.A., 2020. Stem cell-derived retinal pigment epithelium from patients with age-related macular degeneration exhibit reduced metabolism and matrix interactions. Stem Cells Transl. Med. 9, 364–376. https://doi.org/10.1002/sctm.19-0321

González-Mariscal, L., Tapia, R., Chamorro, D., 2008. Crosstalk of tight junction components with signaling pathways. Biochim. Biophys. Acta - Biomembr. 1778, 729–756. https://doi.org/10.1016/j.bbamem.2007.08.018

Gopalakrishna, R., Jaken, S., 2000. Protein kinase C signaling and oxidative stress. Free Radic. Biol. Med. 28, 1349–1361. https://doi.org/10.1016/S0891-5849(00)00221-5

Gorgels T.G., Van Norren D., 1995. Ultraviolet and green light cause different types of damage in rat retina. Invest Ophthalmol Vis Sci. 1995;36(5):851-863.

Gorton H.L., 2010. "Biological Action Spectra". Photobiological Sciences

Online. American Society for Photobiology. Retrieved 2020-01-18

Gragoudas, E. S., Adamis, A. P., Cunningham, E. T., Jr, Feinsod, M., Guyer, D. R., & VEGF Inhibition Study in Ocular Neovascularization Clinical Trial Group. 2004. Pegaptanib for neovascular age-related macular degeneration. The New England journal of medicine, 351(27), 2805–2816. https://doi.org/10.1056/NEJMoa042760

Green, W.R. and Enger, C., 1993. Age-related macular degeneration histopathologic studies: the 1992 Lorenz E. Zimmerman Lecture. Ophthalmology , 100 , 1519 –1535.

Greenham, N.C., Friend, R.H. and Bradley, D.D.C., 1994. Angular Dependence of the Emission from a Conjugated Polymer Light-Emitting Diode: Implications for efficiency calculations. Adv. Mater., 6: 491-494. doi:10.1002/adma.19940060612

Guha, S., Baltazar, G.C., Coffey, E.E., Tu, L.A., Lim, J.C., Beckel, J.M., Patel, S., Eysteinsson, T., Lu, W., O'Brien-Jenkins, A., Laties, A.M., Mitchell, C.H., 2013. Lysosomal alkalinization, lipid oxidation, and reduced phagosome clearance triggered by activation of the P2X7 receptor. FASEB J. 27, 4500–4509. https://doi.org/10.1096/fj.13-236166

Guo, C., Sun, L., Chen, X., & Zhang, D., 2013. Oxidative stress, mitochondrial damage and neurodegenerative diseases. Neural regeneration research, 8(21), 2003–2014. https://doi.org/10.3969/j.issn.1673-5374.2013.21.009

Hageman, G.S., Luthert, P.J., Victor Chong, N.H., Johnson, L. V., Anderson, D.H., Mullins, R.F., 2001. An integrated hypothesis that considers drusen as biomarkers of immune-mediated processes at the RPE-Bruch's membrane interface in aging and age-related macular degeneration. Prog. Retin. Eye Res. 20, 705–732. https://doi.org/10.1016/S1350-9462(01)00010-6

Haines, J.L., Hauser, M.A., Schmidt, S., Scott, W.K., Olson, L.M., Gallins, P., Spencer, K.L., Shu, Y.K., Noureddine, M., Gilbert, J.R., Schnetz-Boutaud, N., Agarwal, A., Postel, E.A., Pericak-Vance, M.A., 2005. Complement factor H variant increases the risk of age-related macular degeneration. Science (80-.). 308, 419–421. https://doi.org/10.1126/science.1110359

Ham W.T,, Mueller H.A., Ruffolo J.J., Guerry D., Guerry R.K., 1982. Action spectrum for retinal injury from near-ultraviolet radiation in the aphakic monkey. Am J Ophthalmol 1982;93:299-306.

Ham, W. T., Jr, Mueller, H. A., & Sliney, D. H., 1976. Retinal sensitivity to damage from short wavelength light. Nature, 260(5547), 153–155. https://doi.org/10.1038/260153a0

Ham, W.T., Ruffolo, J.J., Mueller, H.A., 1980. The nature of retinal radiation damage: dependence on wavelength, power level and exposure time; the quantitative dimensions of intense light damage as obtained from animal studies, Section II. Appl. Res. 20, 1005–1111. https://doi.org/10.1016/0166-218X(94)90028-0

Hecht, S., Shlar, S., Pirenne, M.H., 1942. Energy, Quanta, and Vision. Journal of General Physiology. 25 (6): 819–840. doi:10.1085/jgp.25.6.819. PMC 2142545. PMID 19873316

Henrique, D., Schweisguth, F., 2003. Cell polarity: The ups and downs of the Par6/aPKC complex. Curr. Opin. Genet. Dev. 13, 341–350. https://doi.org/10.1016/S0959-437X(03)00077-7

Hildebrandt, C., Büth, H., Cho, S., Impidjati, Thielecke, H., 2010. Detection of the osteogenic differentiation of mesenchymal stem cells in 2D and 3D cultures by electrochemical impedance spectroscopy. J. Biotechnol. 148, 83–90. https://doi.org/10.1016/j.jbiotec.2010.01.007

Hoare, M., Narita, M., 2013. Transmitting senescence to the cell

neighbourhood. Nat. Cell Biol. 15, 887–889. https://doi.org/10.1038/ncb2811

Hockberger, P.E., Skimina, T.A., Centonze, V.E., Lavin, C., Chu, S., Dadras, S., Reddy, J.K., White, J.G., 1999. Activation of flavin-containing oxidases underlies light-induced production of H2O2 in mammalian cells. Proc. Natl. Acad. Sci. U. S. A. 96, 6255–6260. https://doi.org/10.1073/pnas.96.11.6255

Holz F.G., Pauleikhoff D., Spaide R.F., Bird A.C., 2012. Age-Related Macular Degeneration 2nd Edition. ISBN 978-3-642-22107-1 doi: 10.1007/978-3-642-22107-1

Hornof, M., Toropainen, E., Urtti, A., 2005. Cell culture models of the ocular barriers. Eur. J. Pharm. Biopharm. 60, 207–225. https://doi.org/10.1016/j.ejpb.2005.01.009

Hunter, J. J., Morgan, J. I., Merigan, W. H., Sliney, D. H., Sparrow, J. R., & Williams, D. R., 2012. The susceptibility of the retina to photochemical damage from visible light. Progress in retinal and eye research, 31(1), 28–42. https://doi.org/10.1016/j.preteyeres.2011.11.001

Hyman, L.G., Lilienfeld, A.M., Ferris, F.L., Fine, S.L., 1983. Senile macular degeneration: a case-control study. Am. J. Epidemiol. 118, 213–227.

Imai, Y., Takahashi, A., Hanyu, A., Hori, S., Sato, S., Naka, K., Hirao, A., Ohtani, N., Hara, E., 2014. Crosstalk between the Rb Pathway and AKT Signaling Forms a Quiescence-Senescence Switch. Cell Rep. 7, 194–207. https://doi.org/10.1016/j.celrep.2014.03.006

Imlay, J.A., Stuart Linn, 1988. Linked references are available on JSTOR for this article : DNA Damage and Oxygen Radical Toxicity 240, 1302–1309.

Ingram, N.T., Sampath, A.P. and Fain, G.L., 2016. Why are rods more sensitive than cones?. J Physiol, 594: 5415-5426. doi:10.1113/JP272556

Jaadane, I., Boulenguez, P., Chahory, S., Carré, S., Savoldelli, M., Jonet, L., Behar-Cohen, F., Martinsons, C., Torriglia, A., 2015a. Retinal damage induced by commercial light emitting diodes (LEDs). Free Radic. Biol. Med. 84, 373–384. https://doi.org/10.1016/j.freeradbiomed.2015.03.034

Jaadane, I., Chahory, S., Leprêtre, C., Omri, B., Jonet, L., Behar-Cohen, F., Crisanti, P., Torriglia, A., 2015b. The activation of the atypical PKC zeta in light-induced retinal degeneration and its involvement in L-DNase II control. J. Cell. Mol. Med. 19, 1646–1655. https://doi.org/10.1111/jcmm.12539

Jaadane, I., Villalpando Rodriguez, G.E., Boulenguez, P., Chahory, S., Carré, S., Savoldelli, M., Jonet, L., Behar-Cohen, F., Martinsons, C., Torriglia, A., 2017. Effects of white light-emitting diode (LED) exposure on retinal pigment epithelium in vivo. J. Cell. Mol. Med. https://doi.org/10.1111/jcmm.13255

Jaffe, G. J., Irvine, A. R., Wood, I. S., Severinghaus, J. W., Pino, G. R., & Haugen, C., 1988. Retinal phototoxicity from the operating microscope. The role of inspired oxygen. Ophthalmology, 95(8), 1130–1141. https://doi.org/10.1016/s0161-6420(88)33065-4

Jain, S., Suzuki, T., Seth, A., Samak, G., & Rao, R., 2011. Protein kinase Cζ phosphorylates occludin and promotes assembly of epithelial tight junctions. The Biochemical journal, 437(2), 289–299. https://doi.org/10.1042/BJ20110587

Jarrett, S.G., Boulton, M.E., 2012. Consequences of oxidative stress in age-related macular degeneration. Mol. Aspects Med. 33, 399–417. https://doi.org/10.1016/j.mam.2012.03.009

Jarrett, S.G., Lewin, A.S., Boulton, M.E., 2010. The importance of Mitochondria in age-related and inherited eye disorders. Ophthalmic Res. 44, 179–190. https://doi.org/10.1159/000316480

Jarrett, S.G., Lin, H., Godley, B.F., Boulton, M.E., 2008. Mitochondrial DNA damage and its potential role in retinal degeneration. Prog. Retin. Eye Res. 27, 596–607. https://doi.org/10.1016/j.preteyeres.2008.09.001

Jastrzebska B., 2015. Oligomeric State of Rhodopsin Within Rhodopsin–Transducin Complex Probed with Succinylated Concanavalin A. In: Jastrzebska B. (eds) Rhodopsin. Methods in Molecular Biology, vol 1271. Humana Press, New York, NY

Johnson, P.T., Brown, M.N., Pulliam, B.C., Anderson, D.H., Johnson, L. V., 2005. Synaptic pathology, altered gene expression, and degeneration in photoreceptors impacted by drusen. Investig. Ophthalmol. Vis. Sci. 46, 4788–4795. https://doi.org/10.1167/iovs.05-0767

Jomova, K., Vondrakova, D., Lawson, M., Valko, M., 2010. Metals, oxidative stress and neurodegenerative disorders. Mol. Cell. Biochem. 345, 91–104. https://doi.org/10.1007/s11010-010-0563-x

Jorgensen, I., Rayamajhi, M., Miao, E.A., 2017. Programmed cell death as a defence against infection. Nat. Rev. Immunol. 17, 151–164. https://doi.org/10.1038/nri.2016.147

Jun, H.S., Dao, L.T.M., Pyun, J.C., Cho, S., 2013. Effect of cell senescence on the impedance measurement of adipose tissue-derived stem cells. Enzyme Microb. Technol. 53, 302–306. https://doi.org/10.1016/j.enzmictec.2013.07.001

Jung T., Höhn A., Grune T., 2010. Lipofuscin: Detection and Quantification by Microscopic Techniques. In: Armstrong D. (eds) Advanced Protocols in Oxidative Stress II. Methods in Molecular Biology (Methods and Protocols), vol 594. Humana Press, Totowa, NJ

Kaczara, P., Sarna, T., Burke, J.M., 2010. Dynamics of H2O2 availability to ARPE-19 cultures in models of oxidative stress. Free Radic. Biol. Med.

48, 1064–1070. https://doi.org/10.1016/j.freeradbiomed.2010.01.022

Kaemmerer, E., Schutt, F., Krohne, T.U., Holz, F.G., Kopitz, J., 2007. Effects of lipid peroxidation-related protein modifications on RPE lysosomal functions and POS phagocytosis. Investig. Ophthalmol. Vis. Sci. https://doi.org/10.1167/iovs.06-0549

Karu T. 1989. Photobiology of low-power laser effects. Health physics, 56(5), 691–704. https://doi.org/10.1097/00004032-198905000-00015

Kazilek C.J., Cooper K., 2010. Rods and Cones. ASU - Ask A Biologist. Retrieved from https://askabiologist.asu.edu/rods-and-cones

Keese C.R. and Giaever I., 1994. A biosensor that monitors cell morphology with electrical fields, in IEEE Engineering in Medicine and Biology Magazine, vol. 13, no. 3, pp. 402-408.

Kernt, M., Walch, A., Neubauer, A.S., Hirneiss, C., Haritoglou Md, C., Ulbig, M.W., Kampik, A., 2012. Filtering blue light reduces light-induced oxidative stress, senescence and accumulation of extracellular matrix proteins in human retinal pigment epithelium cells. Clin. Exp. Ophthalmol. 40. https://doi.org/10.1111/j.1442-9071.2011.02620.x

Killingsworth, M.C., Sarks, J.P., Sarks, S.H., 1990. Macrophages related to bruch’s membrane in age-related macular degeneration. Eye 4, 613–621. https://doi.org/10.1038/eye.1990.86

Kim, J.Y., Park, H.E., Kim, D., Koh, H.S., Cho, S., Sung, J.S., 2011. Real-time monitoring of neural differentiation of human mesenchymal stem cells by electric cell-substrate impedance sensing. J. Biomed. Biotechnol. 2011. https://doi.org/10.1155/2011/485173

King, A., Gottliebt, E., Brooks, D.G., Murphy, M.P., Dunaief, J.L., Kirby, F.M., 2004. Mitochondria-derived Reactive Oxygen Species Mediate Blue Light-induced Death of Retinal Pigment Epithelial Cellsq. Photochem.

Photobiol. 79.

Kirchhoff, G., 1847. Ueber die Auflösung der Gleichungen, auf welche man bei der Untersuchung der linearen Vertheilung galvanischer Ströme geführt wird. Ann. Phys., 148: 497-508. doi:10.1002/andp.18471481202

Kirkness C.M., 1986. Do ophthalmic instruments pose a hazard of light-induced damage to the eye? In: Cronly-Dillon J, Rosen ES, Marshall J (eds), Hazards of Light; Myths & Realities; Eye and Skin. Oxford: Pergamon Press; 1986:179-186.

Klein, R., Cruickshanks, K. J., Nash, S. D., Krantz, E. M., Nieto, F. J., Huang, G. H., Pankow, J. S., & Klein, B. E., 2010. The prevalence of age-related macular degeneration and associated risk factors. Archives of ophthalmology (Chicago, Ill. : 1960), 128(6), 750–758. https://doi.org/10.1001/archophthalmol.2010.92

Klein, R., Klein, B.E.K., Jensen, S.C., Cruickshanks, K.J., 1998. The relationshipof ocular factors to the incidence and progression of age-related maculopathy. Arch. Ophthalmol. 116, 506–513.

Kremers J.J., Van Norren D., 1988. Two classes of photochemical damage of the retina. Laser and Light in Ophthalmology. 1988;2 41-52-41-52.

Kriete, A., & Mayo, K. L., 2009. Atypical pathways of NF-kappaB activation and aging. Experimental gerontology, 44(4), 250–255. https://doi.org/10.1016/j.exger.2008.12.005

Kriete, A., Mayo, K. L., Yalamanchili, N., Beggs, W., Bender, P., Kari, C., & Rodeck, U., 2008. Cell autonomous expression of inflammatory genes in biologically aged fibroblasts associated with elevated NF-kappaB activity. Immunity & ageing : I & A, 5, 5. https://doi.org/10.1186/1742-4933-5-5

Kuilman, T., & Peeper, D. S., 2009. Senescence-messaging secretome: SMS-ing cellular stress. Nature reviews. Cancer, 9(2), 81–94.

https://doi.org/10.1038/nrc2560

Lamb L.E., Ye T., Haralampus-Grynaviski N., Williams T.R., Pawlak A, Sarna T. and Simon J.D., 2001. The primary photophysicalproperties of A2E in solution. J. Phys. Chem. B 105, 11507–11512.

Láng, O., Kőhidai, L., Wegener, J., 2017. Label-free profiling of cell dynamics: A sequence of impedance-based assays to estimate tumor cell invasiveness in vitro. Exp. Cell Res. 359, 243–250. https://doi.org/10.1016/j.yexcr.2017.07.023

Leão, R., Apolónio, J.D., Lee, D., Figueiredo, A., Tabori, U., Castelo-Branco, P., 2018. Mechanisms of human telomerase reverse transcriptase (hTERT) regulation: Clinical impacts in cancer. J. Biomed. Sci. 25, 1–12. https://doi.org/10.1186/s12929-018-0422-8

Lee, R., Jung, I., Park, M., Ha, H., Yoo, K.H., 2013. Real-time monitoring of adipocyte differentiation using a capacitance sensor array. Lab Chip 13, 3410–3416. https://doi.org/10.1039/c3lc50453k

Le Grand, Y., 1972. Optique Physiologique, Vol 2, Lumie're et Couleurs. Masson & CIE, pp. 490.

Lei, L., Tzekov, R., McDowell, J.H., Smith, W.C., Tang, S., Kaushal, S., 2013. Formation of lipofuscin-like material in the RPE Cell by different components of rod outer segments. Exp. Eye Res. https://doi.org/10.1016/j.exer.2013.04.006

Liang, F.Q., Godley, B.F., 2003. Oxidative stress-induced mitochondrial DNA damage in human retinal pigment epithelial cells: A possible mechanism for RPE aging and age-related macular degeneration. Exp. Eye Res. 76, 397–403. https://doi.org/10.1016/S0014-4835(03)00023-X

Lim, L.S., Mitchell, P., Seddon, J.M., Holz, F.G., Wong, T.Y., 2012. Age-related macular degeneration. Lancet 379, 1728–1738.

https://doi.org/10.1016/S0140-6736(12)60282-7

Lin, C. mao, Titchenell, P.M., Keil, J.M., Garcia-Ocaña, A., Bolinger, M.T., Abcouwer, S.F., Antonetti, D.A., 2018. Inhibition of Atypical Protein Kinase C Reduces Inflammation-Induced Retinal Vascular Permeability. Am. J. Pathol. 188, 2392–2405. https://doi.org/10.1016/j.ajpath.2018.06.020

Liu, T., Zhang, L., Joo, D., & Sun, S. C., 2017. NF-κB signaling in inflammation. Signal transduction and targeted therapy, 2, 17023–. https://doi.org/10.1038/sigtrans.2017.23

Lo, B., Parham, L., 2009. Ethical issues in stem cell research. Endocr. Rev. 30, 204–213. https://doi.org/10.1210/er.2008-0031

Lo, C.M., Keese, C.R., Giaever, I., 1993. Monitoring motion of confluent cells in tissue culture. Exp. Cell Res. https://doi.org/10.1006/excr.1993.1014

Lovelady, D.C., Friedman, J., Patel, S., Rabson, D.A., Lo, C.M., 2009. Detecting effects of low levels of cytochalasin B in 3T3 fibroblast cultures by analysis of electrical noise obtained from cellular micromotion. Biosens. Bioelectron. 24, 2250–2254. https://doi.org/10.1016/j.bios.2008.09.033

Lu, T., Finkel, T., 2008. Free radicals and senescence. Exp. Cell Res. 314, 1918–1922. https://doi.org/10.1016/j.yexcr.2008.01.011

Lund, D. J., Stuck, B. E., & Edsall, P., 2006. Retinal injury thresholds for blue wavelength lasers. Health physics, 90(5), 477–484. https://doi.org/10.1097/01.HP.0000190115.83416.cb

Ma W., Kleiman N.J., 2004. Tertiary Butyl Hydroperoxide (tbhp) Conditioned Human Retinal Pigment Epithelial (rpe) Cells Resist Oxidative Stress Induced Cell Death And Dna Damage . Invest. Ophthalmol. Vis. Sci. 2004;45(13):747. doi: https://doi.org/.

Ma W., Sun F., Kleiman N.J., Spector A., 2002. The Effect of H2O2 and Tertiary Butyl Hydroperoxide on an Immortal Lens Epithelial Cell Line, Alpha TN4-1 . Invest. Ophthalmol. Vis. Sci. 2002;43(13):2372. doi: https://doi.org/.

Margrain, T. H., Boulton, M., Marshall, J., & Sliney, D. H., 2004. Do blue light filters confer protection against age-related macular degeneration?. Progress in retinal and eye research, 23(5), 523–531. https://doi.org/10.1016/j.preteyeres.2004.05.001

Marie, M., Bigot, K., Angebault, C., Barrau, C., Gondouin, P., Pagan, D., Fouquet, S., Villette, T., Sahel, J.A., Lenaers, G., Picaud, S., 2018. Light action spectrum on oxidative stress and mitochondrial damage in A2E-loaded retinal pigment epithelium cells. Cell Death Dis. https://doi.org/10.1038/s41419-018-0331-5

Marmorstein, A. D., Marmorstein, L. Y., Sakaguchi, H., & Hollyfield, J. G., 2002. Spectral profiling of autofluorescence associated with lipofuscin, Bruch's Membrane, and sub-RPE deposits in normal and AMD eyes. Investigative ophthalmology & visual science, 43(7), 2435–2441.

Martelli, A.M., Evangelisti, C., Nyakern, M., Manzoli, F.A., 2006. Nuclear protein kinase C. Biochim. Biophys. Acta - Mol. Cell Biol. Lipids 1761, 542–551. https://doi.org/10.1016/j.bbalip.2006.02.009

Martin D.F., Maguire M.G., Fine S.L., Ying G., Jaffe G.J., Grunwald J.E., Toth C., Redford M., Ferris F.L. 2012. Ranibizumab and Bevacizumab for Treatment of Neovascular Age-related Macular Degeneration: Two-Year Results, Ophthalmology, Volume 119, Issue 7, 2012, Pages 1388-1398, ISSN 0161-6420,https://doi.org/10.1016/j.ophtha.2012.03.053.

Maruotti J., Tartary A., Biggs R., Katti S., Lauder S., Onteniente B., 2020. Development of a high-throughput assay for dry AMD based on chronic exposure of hiPSC-RPE to A2E and blue light.. Invest. Ophthalmol. Vis.

Sci. 2020;61(7):4151.

Michels, M., Lewis, H., Abrams, G. W., Han, D. P., Mieler, W. F., & Neitz, J., 1992. Macular phototoxicity caused by fiberoptic endoillumination during pars plana vitrectomy. American journal of ophthalmology, 114(3), 287–296. https://doi.org/10.1016/s0002-9394(14)71792-1

Michels, M., Sternberg, P., 1990. Operating microscope-induced retinal phototoxicity–pathophysiology, clinical manifestations and prevention. Surv. Ophthalmol. 34, 237–252.

Mirshahi, A., Hoehn, R., Lorenz, K., Kramann, C., Baatz, H., 2012. Anti-tumor necrosis factor alpha for retinal diseases: Current knowledge and future concepts. J. Ophthalmic Vis. Res. 7, 39–44.

Mitchell, P., Smith, W., Wang, J.J., 1998. Iris color, skin sun sensitivity, and age-related maculopathy: The Blue Mountains Eye Study. Ophthalmology 105, 1359–1363. https://doi.org/10.1016/S0161-6420(98)98013-7

Modenese A, Gobba F. 2019. Macular degeneration and occupational risk factors: a systematic re-view. Int Arch Occup Environ Health. 92 (1): 1-11. doi: 10.1007/s00420-018-1355-y.

Mohammed-Ali, Z., Cruz, G. L., & Dickhout, J. G., 2015. Crosstalk between the unfolded protein response and NF-κB-mediated inflammation in the progression of chronic kidney disease. Journal of immunology research, 2015, 428508. https://doi.org/10.1155/2015/428508

Moiseeva, O., Bourdeau, V., Roux, A., Deschenes-Simard, X., Ferbeyre, G., 2009. Mitochondrial Dysfunction Contributes to Oncogene-Induced Senescence. Mol. Cell. Biol. 29, 4495–4507. https://doi.org/10.1128/mcb.01868-08

Morgan, J. I., Hunter, J. J., Merigan, W. H., & Williams, D. R. 2009. The reduction of retinal autofluorescence caused by light exposure.

Investigative ophthalmology & visual science, 50(12), 6015–6022. https://doi.org/10.1167/iovs.09-3643

Murakami, T., Felinski, E.A., Antonetti, D.A., 2009. Occludin phosphorylation and ubiquitination regulate tight junction trafficking and vascular endothelial growth factor-induced permeability. J. Biol. Chem. 284, 21036–21046. https://doi.org/10.1074/jbc.M109.016766

Murakami, T., Frey, T., Lin, C., Antonetti, D.A., 2012. Protein kinase Cβ phosphorylates occludin regulating tight junction trafficking in vascular endothelial growth factor - Induced permeability in vivo. Diabetes 61, 1573–1583. https://doi.org/10.2337/db11-1367

Nair, U., Bartsch, H., Nair, J., 2007. Lipid peroxidation-induced DNA damage in cancer-prone inflammatory diseases: A review of published adduct types and levels in humans. Free Radic. Biol. Med. 43, 1109–1120. https://doi.org/10.1016/j.freeradbiomed.2007.07.012

Nasir, N., Al Ahmad, M., 2020. Cells Electrical Characterization: Dielectric Properties, Mixture, and Modeling Theories. J. Eng. (United Kingdom) 2020. https://doi.org/10.1155/2020/9475490

National Research Council (US) Committee on Vision., 1990. Advances in Photoreception: Proceedings of a Symposium on Frontiers of Visual Science. Washington (DC): National Academies Press (US); 1990. Cone Visual Pigments in Monkeys and Humans. Available from: https://www.ncbi.nlm.nih.gov/books/NBK235548/

Noell W. K., 1980. Possible mechanisms of photoreceptor damage by light in mammalian eyes. Vision research, 20(12), 1163–1171. https://doi.org/10.1016/0042-6989(80)90055-3

Noell, W. K., Walker, V. S., Kang, B. S., & Berman, S. 1966. Retinal damage by light in rats. Investigative ophthalmology, 5(5), 450–473.

Nordgaard C.L., Karunadharma P.P., Feng X., Olsen T.W., Ferrington D.A., 2008. Mitochondrial proteomics of the retinal pigment epithelium at progressive stages of age-related macular degeneration. Invest Ophthalmol Vis Sci. 2008;49(7):2848–2855. doi:10.1167/iovs.07-1352

Ohm G.S., 1827. Die galvanische Kette, mathematisch bearbeitet. Berlin: T. H. Riemann.

Oka, C., Tsujimoto, R., Kajikawa, M., Koshiba-Takeuchi, K., Ina, J., Yano, M., Tsuchiya, A., Ueta, Y., Soma, A., Kanda, H., Matsumoto, M., Kawaichi, M., 2004. HtrA1 serine protease inhibits signaling mediated by Tgfβ family proteins. Development 131, 1041–1053. https://doi.org/10.1242/dev.00999

Omri, S., Behar-Cohen, F., Rothschild, P.R., Gélizé, E., Jonet, L., Jeanny, J.C., Omri, B., Crisanti, P., 2013. PKCζ mediates breakdown of outer blood-retinal barriers in diabetic retinopathy. PLoS One. https://doi.org/10.1371/journal.pone.0081600

Omri, S., Omri, B., Savoldelli, M., Jonet, L., Thillaye-Goldenberg, B., Thuret, G., Gain, P., Jeanny, J. C., Crisanti, P., & Behar-Cohen, F., 2010. The outer limiting membrane (OLM) revisited: clinical implications. Clinical ophthalmology (Auckland, N.Z.), 4, 183–195. https://doi.org/10.2147/opth.s5901

Opp, D., Wafula, B., Lim, J., Huang, E., Lo, J.C., Lo, C.M., 2009. Use of electric cell-substrate impedance sensing to assess in vitro cytotoxicity. Biosens. Bioelectron. 24, 2625–2629. https://doi.org/10.1016/j.bios.2009.01.015

Ozkaya, E. K., Anderson, G., Dhillon, B., & Bagnaninchi, P., 2019. Blue-light induced breakdown of barrier function on human retinal epithelial cells is mediated by PKC-ζ over-activation and oxidative stress. Experimental Eye Research, 189, 107817. https://doi.org/10.1016/j.exer.2019.107817

Pais, A., 1979. Einstein and the quantum theory. Rev. Mod. Phys. 51, 863–914. https://doi.org/10.1103/RevModPhys.51.863

Palczewski, K., 2006. G Protein–Coupled Receptor Rhodopsin. Ann. Rev. Biochem. https://doi.org/10.1016/j.biotechadv.2011.08.021.Secreted

Parish, C.A., Hashimoto, M., Nakanishi, K., Dillon, J., Sparrow, J., 1998. Isolation and one-step preparation of A2E and iso-A2E, fluorophores from human retinal pigment epithelium. Proc. Natl. Acad. Sci. https://doi.org/10.1115/ES2007-36129

Passos, J.F., Nelson, G., Wang, C., Richter, T., Simillion, C., Proctor, C.J., Miwa, S., Olijslagers, S., Hallinan, J., Wipat, A., Saretzki, G., Rudolph, K.L., Kirkwood, T.B.L., Von Zglinicki, T., 2010. Feedback between p21 and reactive oxygen production is necessary for cell senescence. Mol. Syst. Biol. 6, 1–14. https://doi.org/10.1038/msb.2010.5

Passos, J.F., Saretzki, G., Ahmed, S., Nelson, G., Richter, T., Peters, H., Wappler, I., Birket, M.J., Harold, G., Schaeuble, K., Birch-Machin, M.A., Kirkwood, T.B.L., Von Zglinicki, T., 2007. Mitochondrial dysfunction accounts for the stochastic heterogeneity in telomere-dependent senescence. PLoS Biol. 5, 1138–1151. https://doi.org/10.1371/journal.pbio.0050110

Patel, N., Adewoyin, T., Chong, N. V., 2008. Age-related macular degeneration: A perspective on genetic studies. Eye 22, 768–776. https://doi.org/10.1038/sj.eye.6702844

Pawlak, A., Różanowska, M., Zareba, M., Lamb, L.E., Simon, J.D., Sarna, T., 2002. Action spectra for the photoconsumption of oxygen by human ocular lipofuscin and lipofuscin extracts. Arch. Biochem. Biophys. 403, 59–62. https://doi.org/10.1016/s0003-9861(02)00260-6

Pawlak, A., Wrona, M., Rózanowska, M., Zareba, M., Lamb, L.E., Roberts,

J.E., Simon, J.D., Sarna, T., 2003. Comparison of the Aerobic Photoreactivity of A2E with its Precursor Retinal¶. Photochem. Photobiol. 77, 253. https://doi.org/10.1562/0031-8655(2003)077<0253:cotapo>2.0.co;2

Pennesi M.E., Neuringer M., Courtney R.J., 2012. Animal models of age related macular degeneration. Mol Aspects Med. 2012;33(4):487-509. doi:10.1016/j.mam.2012.06.003

Pennington, M. R., & Van de Walle, G. R. (2017). Electric Cell-Substrate Impedance Sensing To Monitor Viral Growth and Study Cellular Responses to Infection with Alphaherpesviruses in Real Time. mSphere, 2(2), e00039-17. https://doi.org/10.1128/mSphere.00039-17

Popoola WO. 2016. Impact of VLC on Light Emission Quality of White LEDs. Journal of Light-wave Technology. 34 (10) 2526 – 2532. doi: 10.1109/JLT.2016.2542110

Potapenko AY, Agamalieva MA, Nagiev AI, Lysenko EP, Bezdetnaya LN, Sukhorukov VL, 1991. Photochemolysis sensitzed by psoralen: reciprocity law is not fulfilled. Photochem Photobiol 1991: 54: 375-379.

Progelhof, R.C. and Throne, J.L., 1974. Predicting radiant energy transmission through polymer sheets. Polym Eng Sci, 14: 760-763. doi:10.1002/pen.760141104

Rak, D.J., Hardy, K.M., Jaffe, G.J., McKay, B.S., 2006. Ca++-switch induction of RPE differentiation. Exp. Eye Res. https://doi.org/10.1016/j.exer.2005.09.002

Rao, R.K., Basuroy, S., Rao, V.U., Karnaky, K.J., Gupta, A., 2002. Tyrosine phosphorylation and dissociation of occludin-ZO-1 and E-cadherin-β-catenin complexes from the cytoskeleton by oxidative stress. Biochem. J. 368, 471–481. https://doi.org/10.1042/BJ20011804

Reynolds, R., Rosner, B., Seddon, J.M., 2010. Serum lipid biomarkers and hepatic lipase gene associations with age-related macular degeneration. Ophthalmology 117, 1989–1995. https://doi.org/10.1016/j.ophtha.2010.07.009

Rickers E., Walter K.J., and Johnson T.E., 2008. Characterization of neutral density filters for use in near infrared lasers, Proc. SPIE 6854, Optical Interactions with Tissue and Cells XIX, 68541H (20 February 2008); https://doi-org.ezproxy.is.ed.ac.uk/10.1117/12.768248

Robilliard, L. D., Kho, D. T., Johnson, R. H., Anchan, A., O'Carroll, S. J., & Graham, E. S. 2018. The Importance of Multifrequency Impedance Sensing of Endothelial Barrier Formation Using ECIS Technology for the Generation of a Strong and Durable Paracellular Barrier. Biosensors, 8(3), 64. https://doi.org/10.3390/bios8030064

Roehlecke, C., Schaller, A., Knels, L., & Funk, R. H., 2009. The influence of sublethal blue light exposure on human RPE cells. Molecular vision, 15, 1929–1938

Romano A.D., Serviddio G., de Matthaeis A., Bellanti F., Vendemiale G. 2010. Oxidative stress and aging. J Nephrol. 23(Suppl 15): S29–36. [PubMed: 20872368]

Rosenfeld, P.J., Brown, D.M., Heier, J.S., Boyer, D.S., Kaiser, P.K., Chung, C.Y., Kim, R.Y. & the MARINA Study Group. 2006. Ranibizumab for Neovascular Age-Related Macular Degeneration. N Engl J Med 2006; 355:1419-1431 DOI: 10.1056/NEJMoa054481

Rovillain, E., Mansfield, L., Caetano, C., Alvarez-Fernandez, M., Caballero, O. L., Medema, R. H., Hummerich, H., & Jat, P. S., 2011. Activation of nuclear factor-kappa B signalling promotes cellular senescence. Oncogene, 30(20), 2356–2366. https://doi.org/10.1038/onc.2010.611

Rozanowska, M.B., 2012. Light-induced damage to the retina: Current understanding of the mechanisms and unresolved questions: A symposium-in-print, in: Photochemistry and Photobiology. https://doi.org/10.1111/j.1751-1097.2012.01240.x

Rózanowska M., Jarvis-Evans J., Korytowski W., Boulton M.E., Burke J.M., Sarna T., 1995. Blue light-induced reactivity of retinal age pigment. In vitro generation of oxygen-reactive species. J Biol Chem. 1995;270(32):18825-18830. doi:10.1074/jbc.270.32.18825

Rózanowska, M., Pawlak, A., Rózanowski, B., Skumatz, C., Zaręba, M., Boulton, M.E., Burke, J.M., Sarna, T., Simon, J.D., 2004. Age-related changes in the photoreactivity of retinal lipofuscin granules: Role of chloroform-insoluble components. Investig. Ophthalmol. Vis. Sci. 45, 1052–1060. https://doi.org/10.1167/iovs.03-0277

Rozanowska, M., Różanowski, B. and Boulton, M., 2009. Photobiology of the retina: light-induced damage to the retina. In: Smith, K. C. ed. Photobiological Sciences Online, American Society for Photobiology, Available at http://www.photobiology.info/Rozanowska.html

Rozanowska, M., Sarna, T., 2005. Invited Review Light-induced Damage to the Retina: Role of Rhodopsin Chromophore Revisited. Photochem. Photobiol. 81, 1305–1. https://doi.org/10.1562/2004-11-13-1R3-371

Rózanowski, B., Cuenco, J., Davies, S., Shamsi, F.A., Ząd̨ło, A., Dayhaw-Barker, P., Rózanowska, M., Sarna, T., Boulton, M.E., 2008. The phototoxicity of aged human retinal melanosomes. Photochem. Photobiol. 84, 650–657. https://doi.org/10.1111/j.1751-1097.2007.00259.x

Rubbo H., Batthyany C., & Radi R., 2000. Nitric Oxide: Oxygen Radical Interactions in Atherosclerosis. Biological Research, 33(2), 167-175. https://dx.doi.org/10.4067/S0716-97602000000200017

Ruffolo J., Jr., Ham W., Jr., Mueller H., Millen J. 1984. Photochemical lesions in the primate retina under conditions of elevated blood oxygen. Invest Ophthalmol Vis Sci 1984;25:893-898.

Salminen, A., Huuskonen, J., Ojala, J., Kauppinen, A., Kaarniranta, K., & Suuronen, T., 2008. Activation of innate immunity system during aging: NF-kB signaling is the molecular culprit of inflamm-aging. Ageing research reviews, 7(2), 83–105. https://doi.org/10.1016/j.arr.2007.09.002

Sandberg M.A., Tolentino M.J., Miller S., Berson E.L., Gaudio A.R., 1993. Hyperopia and neovascularization in age-related macular degeneration. Ophthalmology 1993; 100: 1009–13.

Sarks, J.P., Sarks, S.H., Killingsworth, M.C., 1994. Evolution of soft drusen in age-related macular degeneration. Eye 8, 269–283. https://doi.org/10.1038/eye.1994.57

Sarks, J.P., Sarks, S.H., Killingsworth, M.C., 1988. Evolution of geographic atrophy of the retinal pigment epithelium. Eye 2, 552–577. https://doi.org/10.1038/eye.1988.106

Schindl, A., Rosado-Schlosser, B., & Trautinger, F. 2001. Die Reziprozitätsregel in der Photobiologie. Eine Ubersicht [Reciprocity regulation in photobiology. An overview]. Der Hautarzt; Zeitschrift fur Dermatologie, Venerologie, und verwandte Gebiete, 52(9), 779–785. https://doi.org/10.1007/s001050170065

Schmitz-Valckenberg, S., Jorzik, J., Unnebrink, K., Holz, F.G., 2002. Analysis of digital scanning laser ophthalmoscopy fundus autofluoroscence images of geographic atrophy in advanced age-related macular degeneration. Graefe's Arch. Clin. Exp. Ophthalmol. 240, 73–78. https://doi.org/10.1007/s00417-001-0413-3

Schwan, H.P., 1957. Electrical properties of tissue and cell suspensions.,

Advances in biological and medical physics. ACADEMIC PRESS INC. https://doi.org/10.1016/b978-1-4832-3111-2.50008-0

Scientific Committee on Emerging and Newly-Identified Health Risks, 2007. The appropriateness of the risk assessment methodology in accordance with the Technical Guidance Documents for new and existing substances for assessing the risks of nanomaterials, Environment. https://doi.org/10.2772/8624

Seddon, J.M., 2001. Age-related macular degeneration. In Ryan, S.J. (ed.), Retina (3rd edn), Mosby, St Louis, MO, pp. 1039 –1050.

Seddon, J.M., Cote, J., Davis, N., Rosner, B., Ho, A.C., 2003. Progression of age-related macular degeneration. Evidence-Based Eye Care 4, 202–203. https://doi.org/10.1097/00132578-200310000-00010

Seddon, J.M., Willett, W.C., Speizer, F.E., Hankinson, S.E., 1996. A prospective study of cigarette smoking and age-related macular degeneration in women. J. Am. Med. Assoc. 276, 1141–1146. https://doi.org/10.1001/jama.276.14.1141

Seehafer S.S., Pearce D.A., 2006. You say lipofuscin, we say ceroid: defining autofluore¬scent storage material. Neurobiol Aging 27:576–588

Seko, Y., Pang, J., Tokoro, T., Ichinose, S., Mochizuki, M., 2001. Blue light-induced apoptosis in cultured retinal pigment epithelium cells of the rat. Graefe's Arch. Clin. Exp. Ophthalmol. 239, 47–52. https://doi.org/10.1007/s004170000220

Sikora, E., Arendt, T., Bennett, M., Narita, M., 2011. Impact of cellular senescence signature on ageing research. Ageing Res. Rev. 10, 146–152. https://doi.org/10.1016/j.arr.2010.10.002

Sliney, D.H., 2005. Exposure Geometry and Spectral Environment Determine Photobiological Effects on the Human Eye Symposium-in-Print Exposure

Geometry and Spectral Environment Determine Photobiological Effects on the Human Eye. Source Photochem. Photobiol. Photochem. Photobiol. 81, 483–489. https://doi.org/10.1562/2005-02-14-RA-439.1

Smith, W., Assink, J., Klein, R., Mitchell, P., Klaver, C.C.W., Klein, B.E.K., Hofman, A., Jensen, S., Wang, J.J., De Jong, P.T.V.M., 2001. Risk factors for age-related macular degeneration: Pooled findings from three continents. Ophthalmology 108, 697–704. https://doi.org/10.1016/S0161-6420(00)00580-7

Smith-thomas L., Richardson P., Thody A.J., Graham A., Palmer I., Flemming L., Parsons M.A., Rennie I.G. & Macneil S., 1996. Human ocular melanocytes and retinal pigment epithelial cells differ in their melanogenic properties in vivo and in vitro, Current Eye Research, 15:11, 1079-1091, DOI: 10.3109/02713689608995139

Snow, K.K., Seddon, J.M., 1999. Age-related macular degeneration and cardiovascular disease share common antecedents? Ophthalmic Epidemiol. 6, 125–143. https://doi.org/10.1076/opep.6.2.125.1558

Sohal R. S., 1984. Assay of lipofuscin/ceroid pigment in vivo during aging. Methods in enzymology, 105, 484–487. https://doi.org/10.1016/s0076-6879(84)05067-9

Sparrow, J.R., Nakanishi, K., Parish, C.A., 2000. The lipofuscin fluorophore A2E mediates blue light-induced damage to retinal pigmented epithelial cells. Investig. Ophthalmol. Vis. Sci. 41, 1981–1989.

Sparrow, J.R., Parish, C.A., Hashimoto, M., Nakanishi, K., 1999. A2E, a Lipofuscin Fluorophore, in Human Retinal Pigmented Epithelial Cells in Culture. Invest. Ophthalmol. Vis. Sci. 1999;40(12):2988-2995.

Spector, A., Ma, W., Sun, F., Li, D., Kleiman, N.J., 2002. The effect of H2O2 and tertiary butyl hydroperoxide upon a murine immortal lens epithelial

cell line, αTN4-1. Exp. Eye Res. 75, 573–582. https://doi.org/10.1006/exer.2002.2045

Sperling H.G., 1980. Prolonged intense spectral light effects on Rhesus retina. In The Effects of Constant Light in Visula Processes. (Edited by Williams T.P. and Baker B.N.) pp. 195-214. Plenum Press. New York.

Srinivasan, S., Avadhani, N.G., 2012. Cytochrome c oxidase dysfunction in oxidative stress. Free Radic. Biol. Med. 53, 1252–1263. https://doi.org/10.1016/j.freeradbiomed.2012.07.021

Streeten B.W., 1961. The sudanophilic granules of the human retinal pigment epithelium. Arch Ophthalmol 66: 391-398.

Stuart, R. 0, Nigam, S.K., 1995. Regulated assembly of tight junctions by protein kinase C, Cell Biology.

Szulcek, R., Bogaard, H.J., van Nieuw Amerongen, G.P., 2014. Electric cell-substrate impedance sensing for the quantification of endothelial proliferation, barrier function, and motility. J. Vis. Exp. 1–12. https://doi.org/10.3791/51300

Tao, J.X., Zhou, W.C., Zhu, X.G., 2019. Mitochondria as Potential Targets and Initiators of the Blue Light Hazard to the Retina. Oxid. Med. Cell. Longev. 2019, 6435364. https://doi.org/10.1155/2019/6435364

Taylor, H.R., West, S., Munoz, B., Rosenthal, F.S., Bressler, S.B., et al., 1992. The long-term effects of visible-light on the eye. Arch. Ophthalmol. 110, 99–104.

Teussink, M. M., Lambertus, S., de Mul, F. F., Rozanowska, M. B., Hoyng, C. B., Klevering, B. J., & Theelen, T., 2017. Lipofuscin-associated photo-oxidative stress during fundus autofluorescence imaging. PloS one, 12(2), e0172635. https://doi.org/10.1371/journal.pone.0172635

Thampi, P., Rao, H.V., Mitter, S.K., Cai, J., Mao, H., Li, H., Seo, S., Qi, X., Lewin, A.S., Romano, C., Boulton, M.E., 2012. The 5HT 1a receptor agonist 8-OH DPAT induces protection from lipofuscin accumulation and oxidative stress in the retinal pigment epithelium. PLoS One 7, 1–11. https://doi.org/10.1371/journal.pone.0034468

Todd, M.M., Lee, J.W., Marks, V.J., 2005. Rapid toluidine blue stain for Mohs' micrographic surgery. Dermatologic Surg. 31, 244–245. https://doi.org/10.1097/00042728-200502000-00024

Tomi M., Hosoya K., 2008. Molecular Mechanisms of the Inner Blood-Retinal Barrier Transporters. In: Tombran-Tink J., Barnstable C.J. (eds) Ocular Transporters In Ophthalmic Diseases And Drug Delivery. Ophthalmology Research. Humana Press

Van Breugel H.H.F., Bär P.R.D., 1992. Power density and exposure time of He-Ne laser irradiation are more important than total energy dose in photo-biomodulation of human fibroblasts in vitro. Lasers Surg Med 1992: 12: 528-537

Van Deursen, J.M., 2014. The role of senescent cells in ageing. Nature 509, 439–446. https://doi.org/10.1038/nature13193

Van Norren, D., & Gorgels, T. G., 2011. The action spectrum of photochemical damage to the retina: a review of monochromatic threshold data. Photochemistry and photobiology, 87(4), 747–753. https://doi.org/10.1111/j.1751-1097.2011.00921.x

Vives-Bauza, C., Anand, M., Shirazi, A.K., Magrane, J., Gao, J., Vollmer-Snarr, H.R., Manfredi, G., Finnemann, S.C., 2008. The age lipid A2E and mitochondrial dysfunction synergistically impair phagocytosis by retinal pigment epithelial cells. J. Biol. Chem. 283, 24770–24780. https://doi.org/10.1074/jbc.M800706200

Wang, A.L., Lukas, T.J., Yuan, M., Du, N., Tso, M.O., Neufeld, A.H., 2009. Autophagy and exomoses in the aged retinal pigment epithelium: Possible relevance to drusen formation and age-related macular degeneration. PLoS One 4. https://doi.org/10.1371/journal.pone.0004160

Wang, A.L., Lukas, T.J., Yuan, M., Neufeld, A.H., 2008. Increased mitochondrial DNA damage and down-regulation of DNA repair enzymes in aged rodent retinal pigment epithelium and choroid. Mol. Vis. 14, 644–651.

Wang, W., Mani, A. M., & Wu, Z. H., 2017. DNA damage-induced nuclear factor-kappa B activation and its roles in cancer progression. Journal of cancer metastasis and treatment, 3, 45–59. https://doi.org/10.20517/2394-4722.2017.03

Wang, G., Silva, J., Krishnamurthy, K., Tran, E., Condie, B.G., Bieberich, E., 2005. Direct binding to ceramide activates protein kinase Cζ before the formation of a pro-apoptotic complex with PAR-4 in differentiating stem cells. J. Biol. Chem. 280, 26415–26424. https://doi.org/10.1074/jbc.M501492200

Wassell, J., Ellis, S., Burke, J., & Boulton, M., 1998. Fluorescence properties of autofluorescent granules generated by cultured human RPE cells. Investigative ophthalmology & visual science, 39(8), 1487–1492.

Weaver J.C. and Schoenbach K. H., 2003. Biodielectrics, in IEEE Transactions on Dielectrics and Electrical Insulation, vol. 10, no. 5, pp. 715-716.

Wegener, J., Keese, C.R. & Giaever, I., 2000. Electric cell-substrate impedance sensing (ECIS) as a noninvasive means to monitor the kinetics of cell spreading to artificial surfaces. Experimental cell research, 259(1), pp.158–66.

West, S. K., Rosenthal, F. S., Bressler, N. M., Bressler, S. B., Munoz, B., Fine,

S. L., & Taylor, H. R., 1989. Exposure to sunlight and other risk factors for age-related macular degeneration. Archives of ophthalmology (Chicago, Ill. : 1960), 107(6), 875–879. https://doi.org/10.1001/archopht.1989.01070010897038

Wickens, A.P., 2001. Ageing and the free radical theory. Respir. Physiol. 128, 379–391. https://doi.org/10.1016/S0034-5687(01)00313-9

Williams T.P., Howell W.L., 1983. Action spectrum of retinal light-damage in albino rats. Invest Ophthalmol Vis Sci 1983;24:285-287.

Wu, J., Seregard, S., Algvere, P. V., 2006. Photochemical Damage of the Retina. Surv. Ophthalmol. 51, 461–481. https://doi.org/10.1016/j.survophthal.2006.06.009

Yam, F.K., Hassan, Z., 2005. Innovative advances in LED technology. Microelectronics J. 36, 129–137. https://doi.org/10.1016/j.mejo.2004.11.008

Young, R.W., 1988. Solar radiation and age-related macular degeneration. Surv. Ophthalmol. 32, 252–269.

Zhang, X.-M., Lu, M.-Y., Zhang, Y., Chen, L.-J. and Wang, Z.L., 2009. Fabrication of a High-Brightness Blue-Light-Emitting Diode Using a ZnO-Nanowire Array Grown on p-GaN Thin Film. Adv. Mater., 21: 2767-2770. doi:10.1002/adma.200802686

Zhao, W., Feng, H., Sun, W., Liu, K., Lu, J.J., Chen, X., 2017. Tert-butyl hydroperoxide (t-BHP) induced apoptosis and necroptosis in endothelial cells: Roles of NOX4 and mitochondrion. Redox Biol. 11, 524–534. https://doi.org/10.1016/j.redox.2016.12.036

Ziegler, D. V., Wiley, C.D., Velarde, M.C., 2015. Mitochondrial effectors of cellular senescence: Beyond the free radical theory of aging. Aging Cell 14, 1–7. https://doi.org/10.1111/acel.12287

Appendix

Experimental Eye Research 189 (2019) 107817

Contents lists available at ScienceDirect

Experimental Eye Research

journal homepage: www.elsevier.com/locate/yexer

Blue-light induced breakdown of barrier function on human retinal epithelial cells is mediated by PKC-ζ over-activation and oxidative stress

Ege Kaan Ozkaya[a], Graham Anderson[a], Baljean Dhillon[b], Pierre-Olivier Bagnaninchi[a,*]

[a] MRC Centre for Regenerative Medicine, The University of Edinburgh, EH16 4UU, United Kingdom
[b] Centre for Clinical Brain Sciences, The University of Edinburgh, EH16 4SB, United Kingdom

ARTICLE INFO

Keywords:
Blue-light
Barrier function
Impedance sensing
ARPE-19
Macular degeneration
Disease model
Oxidative stress
Protein kinase C- ζ

ABSTRACT

We aimed to study the time course decrease of human retinal pigment epithelium (RPE) barrier function when exposed to blue light. To this end, we cultured ARPE-19 cells on Electrical Cell-substrate Impedance Sensing (ECIS) multi-well arrays. Using an ad hoc light emitting diode (LED) array illumination system together with a set of neutral density filters and a 3-dimensional (3D) printed filter holder, cells were exposed to a gradient of irradiances of blue-light with a measured peak at 468 nm. The electrical resistance between 4 kHz and 64 kHz was recorded during the exposure. Blue light exposure induced a dose-dependent decrease in the resistances at 4 kHz, however the time course resistance at 64 kHz did not show any decrease before t = 52 h. Quantification of the barrier function using mathematical model integrated in the ECIS software showed that blue-light exposure induced a dose-dependent decrease in the barrier function associated with tight junction formation ($P < 0.05$). This was confirmed by the immunostaining of the tight-junction associated structural protein, Zonula occludens-1 (ZO-1). The detection of reactive oxygen species by carboxy-H2DCFDA confirmed that the blue light induced dose-dependent decrease in the barrier function is mediated by oxidative stress. On a separate experiment, blue-light exposed ARPE-19 cells were treated with 100 nM Protein Kinase C zeta (PKC-ζ) pseudo substrate inhibitor to identify underlying pathway for blue-light induced damage on the barrier function. The treatment with 100 nM PKC-ζ pseudo substrate inhibitor induced faster recovery of the barrier function compared to no treatment. Altogether our results document that blue LED light exposure decreased RPE barrier function in-vitro in a dose-dependent manner, before any cell death occurred. This damage induced by blue-light on tight junctions is mediated by oxidative stress through PKC-ζ activation. The quantification of the healing effect observed by inhibition of PKC-ζ might lead to development of high throughput wound healing assays through ECIS in the future.

1. Introduction

Most of the electronic devices today use light emitting diode (LED) technology, which emit strong blue-light (470 nm) to improve screen brightness and clarity. Blue-light is able to penetrate through the lens to the retina and can lead to irreversible photochemical retinal damage (Rózanowska et al., 1995; Bi and Sun, 2014) through production of reactive oxygen species (ROS) (Crockett and Lawwill, 1984; Rózanowska et al., 1995).

The retina is susceptible to photochemical injuries as it is one of the highest oxygen consuming tissues in the body. It is abundant in poly-unsaturated fatty acids and contains high levels of photo-sensitizers while frequently being exposed to visible light. This micro-environment of retina along with its high energy demand promote generation of reactive oxygen species (ROS). The retina is protected from the negative effects of ROS by means of antioxidants and efficient repair mechanisms that capture ROS. However with age, the repair mechanisms and the antioxidant capacity of the retina become weakened creating an imbalance between ROS and the protective mechanisms of retina. This imbalance favoring ROS results in oxidative stress to the retina (Jarrett and Boulton, 2012). Oxidative stress is an underlying factor in many age-related neurodegenerative diseases including neovascular Age-related Macular Degeneration (AMD) (Beatty et al., 2000; Jarrett et al., 2010; Jomova et al., 2010; Romano et al., 2010), which is the most common cause of blindness in the developed world (Johnson et al., 2005).

The blood-retinal barrier (BRB) plays a fundamental role in the retinal microenvironment by regulating the selective nutrient-waste

* Corresponding author.
E-mail addresses: egekaanozkaya@gmail.com (E.K. Ozkaya), s1139761@ed.ac.uk (G. Anderson), Baljean.Dhillon@ed.ac.uk (B. Dhillon), Pierre.Bagnaninchi@ed.ac.uk (P.-O. Bagnaninchi).

https://doi.org/10.1016/j.exer.2019.107817
Received 24 February 2019; Received in revised form 16 July 2019; Accepted 25 September 2019
Available online 26 September 2019
0014-4835/

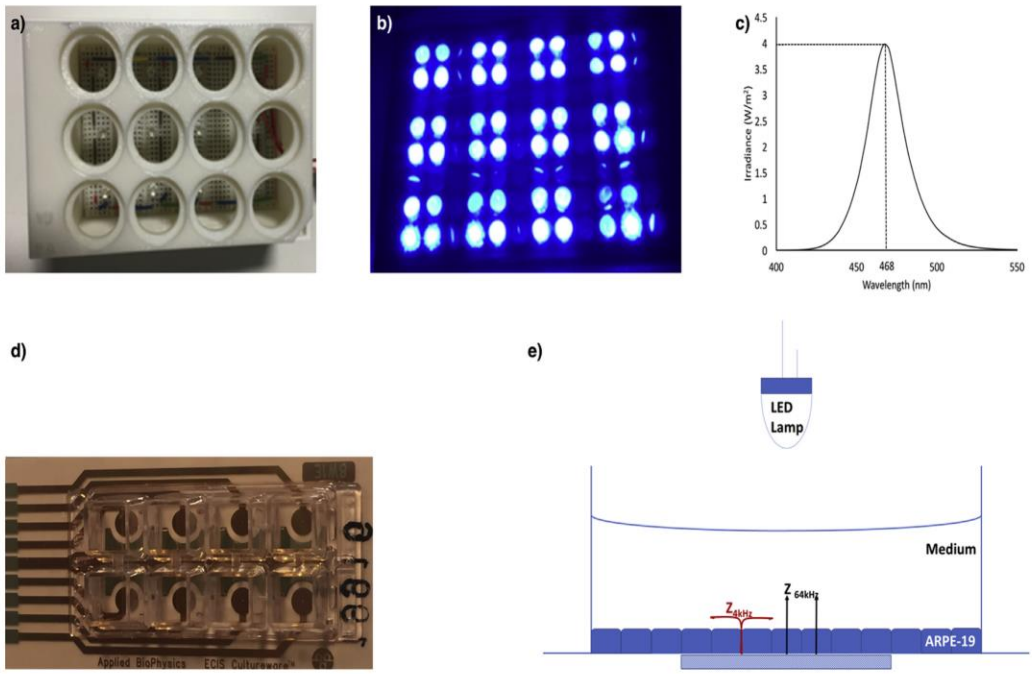

Fig. 1. An ad hoc LED array circuit with 12 LEDs (Cree 5 mm Blue, 470 nm) and four 100 Ω resistances were connected on a breadboard. By using this ad hoc LED array illumination system together with a set of neutral density filters and a 3D printed filter holder, ECIS multi-well arrays with a single 250 μm diameter micro-electrode in each well, were exposed to a gradient of irradiances (118.1 W/m^2, 74.65 W/m^2, 47.05 W/m^2 and 29.67 W/m^2) of blue-light with a peak at 468 nm. The resistances at 4 kHz and 64 kHz, and capacitance at 64 kHz were plotted during the exposure. (a) Ad hoc LED array illumination system with 3D printed filter holder. (b) Blue light exposure on 96 well ECIS plate. (c) Irradiance peak of 470 nm blue LED as measured by using a spectroradiometer (SR9910, Irradian Limited, UK). (d) 8W1E, an example of an ECIS multi-well array with single 250 μm diameter micro-electrodes which allowed resistance and capacitance to be measured in a time-course manner every 180 s at 11 frequencies (e) Diagram of our experimental set-up designed by combining an ad hoc LED array illumination system with ECIS multi-well arrays.

exchange between the blood and the retina, contributing to the homeostasis of the photoreceptors (Ambati et al., 2013). The integrity of BRB is important in order to maintain normal visual function. The BRB consists of two components: inner BRB and outer BRB. The tight junctions (zonulae occludentes) between retinal endothelial cells establish the barrier function at the inner BRB, while the barrier function at the outer BRB is established by the tight junctions between retinal pigment epithelium (RPE) cells (Cunha-Vaz, 2012). In neovascular AMD, abnormal leaky choroidal vessels break through the retina and Bruch's membrane, disrupting the outer blood-retina barrier (BRB) (Ambati et al., 2013).

Multiple protein complexes play an important role in the integrity of BRB tight junctions. The trans-membrane protein complex at the tight junctions is formed by occludin, claudin, junctional adhesion molecule and tricellulin. The scaffold protein Zonulae occludentes-1 (ZO-1) is responsible for cross-linking and adhering these proteins together by interacting with their intra-cellular C-terminal domain (Jain et al., 2011). The protein scaffold complex Par6/Par3/PKC-ζ has a critical role regulating the polarity of the tight junctions (Henrique and Schweisguth, 2003). Protein Kinase C zeta (PKC-ζ) from this protein complex also phosphorylates occludin to promote tight junction assembly (Jain et al., 2011).

The activation of PKC isoforms by ROS is well established and was reviewed (Cosentino-Gomes et al., 2012). In the context of the retina, experiments performed in rats showed that oxidative stress triggeres the translocation of PKC-ζ to the nucleus (Jaadane et al., 2017). In their in-vivo study on rats, Omri et al. (2013) demonstrated that hyperglycemia induced over-activation of PKC-ζ is associated with outer BRB breakdown and photoreceptor degeneration in diabetic retinopathy and inhibition of PKC-ζ restores the outer barrier structure and reduces photoreceptor cell death. Both diabetic retinopathy and neovascular AMD share the main features of the breakdown of BRB along with retinal edema (Cunha-Vaz, 2012). Therefore, for AMD studies, it is important to study the effect of oxidative stress on the outer BRB and its association with PKC-ζ pathway.

To this end, in this study we aimed to evaluate in ARPE-19 cells, the time course effect of blue light emitting diodes (LEDs) on the barrier function of tight junctions and the potential recovery effect of PKC-ζ inhibition after blue light induced breakdown of barrier function.

2. Materials and methods

Unless otherwise stated all experiments were carried out within a sterile laminar flow hood after the establishment of a barrier function, which was evaluated by Electrical Cell-Substrate Impedance Sensing (ECIS).

2.1. Cell seeding & culturing of hTERT-RPE1 and ARPE-19 cell lines

All cell cultures were incubated at 37 °C and 5% CO_2. hTERT-RPE1 cells (ATCC CRL-4000) and ARPE-19 cells (ATCC CRL-2302) were cultured on T75 flasks (5.2 x 10^4 cell/cm^2) and passaged using modified Phosphate Buffer Saline (PBS) without magnesium chloride and calcium chloride (D8537, Sigma) and Trypsin-EDTA, 0.25% (25200-072, Life Tech.) and seeded as a monolayer. These cultures were maintained in Dulbecco's Modified Eagle Medium (DMEM) (1X) 4.5 g/L D-Glucose, L-Glutamine (41965-039, Life Tech.) supplemented with 10% Fetal Calf Serum (FCS) (10270106, Life Tech.), 1% penicillin streptomycin (pen-strep) (15140-122, Invitrogen) and 1 mM sodium pyruvate (S8636, Sigma) until they reached confluence. When the cells were 100%

confluent, the media were changed to DMEM (1X) 4.5 g/L D-Glucose, L-Glutamine supplemented with 1% FCS, 1% pen-strep and 1 mM sodium pyruvate and the cells were kept in culture for 3 weeks to allow for the establishment of the barrier function.

2.2. Light source

All the light exposures were performed in the dark, in an incubator set at 37 °C and 5% CO_2 to control the background lighting.

Cells cultured on 96-well ECIS plates, were exposed using an ad hoc LED array circuit with 12 LEDs (Cree 5 mm Blue, 470 nm) and four 100 Ω resistances connected on a breadboard (Fig. 1a). The forward current, luminous intensity and LED angle of each lamp were respectively 30 mA, 23500 mcd and 15°. The resulting irradiance as characterized by using a spectroradiometer (SR9910, Irradian Limited, UK), was 127 W/m^2. The blue-light irradiance reaching the cells through the media was measured to be 118.1 W/m^2. Using neutral density filters, the ARPE-19 cells cultured in 96-well ECIS plate were exposed to 118.1 W/m^2, 74.65 W/m^2, 47.05 W/m^2 and 29.67 W/m^2 of blue-light with a peak at 468 nm (Fig. 1c) for various durations with this ad hoc LED array illumination system.

Cells cultured on 8-well ECIS plates, were exposed using an ad hoc LED array circuit with 8 LEDs (Cree 5 mm Blue, 470 nm) and two 150 Ω resistances connected on a breadboard. The resulting irradiance as characterized by using a spectroradiometer, was 151 W/m^2. The blue-light irradiance reaching the cells through the media was measured to be 140.4 W/m^2.

2.3. Electrical cell-substrate impedance sensing

RPE cells were cultured on ECIS multi-well electrode arrays (8W1E and 96W1E) (5.2 x 10^4 cell/cm^2), in a 8 or 96 well format with a single 250 μm diameter micro-electrode in each well (Fig. 1d). The resistance was measured in a time-course manner every 180 s for 8W1E and every 15 min for 96W1E at 11 frequencies as in our previous study (Gamal et al., 2015). For the sake of clarity, only the resistances at 4 kHz and 64 kHz were plotted in this study (Fig. 1e), however the full spectroscopic information was used to model the barrier function. For each well, a model was used to quantify the changes in the barrier function associated with tight junction formation using ECIS software.

The capacitance was measured in a time-course manner every 15 min for 96W1E at 11 frequencies. Capacitance at 64 kHz was plotted to analyze the time course changes in the cell coverage.

2.4. Zonula occludens-1 (ZO-1) staining

ARPE-19 cells cultured in 12 well plates (5.2 x 10^4 cell/cm^2) were exposed to 118.1 W/m^2 and 74.65 W/m^2 blue-light with a peak at 468 nm for 4 h with an ad hoc LED illumination system. Immediately after the exposure, media were discarded and cells were washed with modified PBS twice. Cells were fixed in 4% formaldehyde (9713.9010, VWR Chemicals) for 15 min at room temperature. Formaldehyde was washed off with modified PBS twice. The plates were blocked using Super-Block® solution (37515, Thermo Fisher Scientific) for 15 min at room temperature. The cells were then incubated over-night at 4 °C within an antibody solution consisting of rabbit anti-ZO-1 (1 mg/ml; ab216880, Abcam) diluted in Super-Block® at 1:1000 ratio. The ZO-1 antibody was washed off with modified PBS five times. The cells were then incubated, in the dark, for 1 h at room temperature with AlexaFluor 488-conjugated anti-rabbit immunoglobulin G (IgG) (2 mg/ml; A11034, Invitrogen) diluted in Super-Block® solution at 1:100 ratio. Finally, cells were counterstained using 4′,6-diamidino-2-phenylindole (DAPI) (1 mg/ml; 62248, Thermo Fisher Scientific) diluted in modified PBS at 1:1000 ratio, for 1 min before being imaged using an inverted fluorescent microscope (Widefield Zeiss Observer). ImageJ software was used to analyze the images of staining experiments.

2.5. Protein kinase C zeta (PKC- ζ) inhibition

To inhibit selectively PKC-ζ, myristoylated PKC-ζ pseudo substrate inhibitor (539624-500UG, Calbiochem) was used. To prepare a 500 μM stock solution, 500 μg of the inhibitor was dissolved in 500 μL of water. Then, to prepare 100 nM PKC-ζ inhibitor working solution, 10 μL of the stock solution was dissolved in 50 mL cell culture media DMEM (1X) 4.5 g/L D-Glucose, L-Glutamine supplemented with 1% FCS, 1% pen-strep and 1 mM sodium pyruvate. Following the 4 h blue LED light exposure at 140.4 W/m^2 on ARPE-19 cells cultured on 8-well ECIS plate, the media of the case study were changed to 100 nM PKC-ζ inhibitor working solution, while the media of the control study were changed to DMEM (1X) 4.5 g/L D-Glucose, L-Glutamine supplemented with 1% FCS, 1% pen-strep and 1 mM sodium pyruvate.

2.6. Reactive oxygen species (ROS) detection

ROS was detected/quantified using the Image-iT LIVE Green Reactive Oxygen Species Detection Kit (I36007, Invitrogen, Thermo Fisher Scientific) containing 275 μg carboxy-H_2DCFDA to detect general reactive oxygen species. A stock solution of 10 mM was prepared by adding 50 μL of dimethylsulfoxide (DMSO) (20688, Thermo Fisher Scientific) to a vial containing 275 μg carboxy-H_2DCFDA. Then an intermediate dilution of 2 μM of carboxy-H_2DCFDA was made by dissolving 10 μL of this stock solution in 50 mL of cell culture media. Equal volume of 2 μM of carboxy-H_2DCFDA solution and cell culture media were mixed to give the final concentration of 1 μM carboxy-H_2DCFDA working solution. As the positive control, 50 μL 7.78 M 70% tert-butyl hydroperoxide (TBHP) in water was provided as a part of the Image-iT LIVE Green Reactive Oxygen Species Detection Kit. First, an intermediate dilution of 50 mM was prepared and then it was diluted in the cell culture media to prepare 200 μM TBHP working solution. After the ARPE-19 cells were exposed to 118.1 W/m^2 blue-light for 4 h or incubated with 200 μM TBHP working solution for 30 min, the cell culture media were discarded and the cells were incubated with 1 μM carboxy-H_2DCFDA working solution for 30 min at 37 °C. The Flow Cytometry analysis was performed with a NovoCyte flow cytometer (ACEA Biosciences, San Diego, USA samples). Cell viability was assessed via Deep Red Anthraquinone 7 (DRAQ7) (ab109202, Abcam) exclusion. The R780/60 channel was set for DRAQ7 and the B530/30 channel was set for carboxy-H_2DCFDA.

2.7. Statistical analysis

IBM SPSS Statistics was used to perform one-way Analysis of Variance (ANOVA) and Tukey-Kramer test to determine whether the investigated groups were significantly different from each other. A probability value of $P < 0.05$ was set as significant.

3. Results

3.1. Growth of hTERT-RPE1 and ARPE-19 cells on ECIS

First, to establish which cell line was able to establish a robust epithelial barrier both ARPE-19 and hTERT-RPE1 (5.2 x 10^4 cells/cm^2) were seeded on ECIS electrode plates. The resistance time course at f = 4 kHz from the seeding time point was recorded (Fig. 2a) and the electrical impedance data was modeled following Giaever and Keese (1991) method to provide the data on barrier function (Rb) over time (Fig. 2b). The barrier function formed by the tight junctions between ARPE-19 cells were observed to be 5 times stronger than those of hTERT-RPE1 (Fig. 2c). Therefore in order to mimic in vivo RPE cells better, ARPE-19 was chosen to be further analyzed on ECIS microelectrode arrays to lay the foundations for an AMD disease model (Fig. 2d).

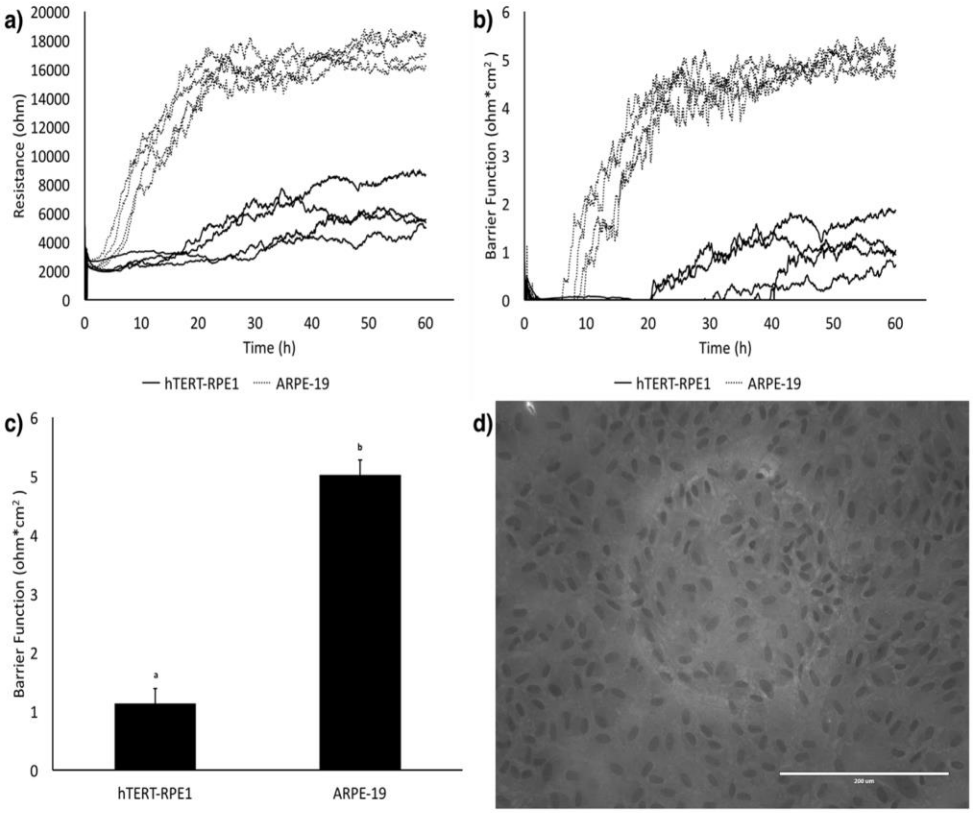

Fig. 2. The time course measurements of the barrier function associated with tight junction formation was 5 times stronger in ARPE-19 compared to hTERT-RPE after 60 h. This made ARPE-19 a better in-vitro model for replicating in-vivo retinal cell behavior. (a) Resistance at 4 kHz (n = 4). (b) Barrier function associated with tight junction formation (n = 4). (c) Barrier function at t = 60 h (n = 4). (d) ARPE-19 cells cultured on ECIS micro-electrode array at 100% confluence forming 5 Ωcm^2 barrier function. Scale bar represents 200 μm.

3.2. Time-course measurements of blue-light exposure on ARPE-19 cells

ARPE-19 cells cultured on a 96 well ECIS micro-electrode array were analyzed over the course of continuous blue-light exposure with time zero set at the start of blue light exposure and media change. The media change resulted in a typical transient peak in resistance associated with temperature and dissolved CO_2 variation for all wells, which was also observed at the second media change (t = 50 h).

The raw data resistance recordings at 4 kHz (Fig. 3a) and at 64 kHz (Fig. 3b) were plotted under continuous blue light exposure. At f = 4 kHz, a marked decrease in resistance in a dose-dependent manner was observed at all exposures, with the highest exposure eventually led to a resistance comparable to the media only control, and was associated to cell death (Fig. 3a). On the other hand, when the same wells were observed at f = 64 kHz, the time course resistances were strikingly different, with no decrease in resistance before t = 52 h and only the two highest exposures resulted in a decline in resistance (Fig. 3b). These observations were consistent across all the wells (n = 24), and the average values and standard errors were reported in Fig. 3c and d.

The difference in resistance graphs at low frequency and high frequency indicated that blue-light had different effects on paracellular resistance and cell electrode coverage. A drop in resistance occurring only in the lower frequency range could be associated with a decrease in the paracellular resistance, i.e. a loss of the barrier function. To investigate further, the mathematical model integrated in the ECIS software was used to quantify the barrier function. The mathematical model on barrier function showed that blue light exposure induced a dose-dependent decrease in barrier function, before cell death occurred (Fig. 3e). Significant differences ($P < 0.05$) were found from t = 90 h for all groups (Fig. 3f). An early decrease in barrier function was found at time t = 4 h with 118.1 W/m^2, without associated cell death. On the other hand, a retention in resistance at the high frequency could be associated with cell coverage. To investigate further and quantify the cell coverage, the capacitance at f = 64 kHz was measured. The time course capacitance at f = 64 kHz (Fig. 3g) showed no increase before t = 52 h and only the two highest exposures resulted in a rise in capacitance indicating a decline in cell coverage. Significant differences ($P < 0.05$) were found from t = 90 h for all groups (Fig. 3h).

3.3. Loss of ZO-1 immunostaining after blue-light exposure

As the earliest statistically significant difference in barrier function was observed at time t = 4 h, this time point was chosen to perform ZO-1 staining of the ARPE-19, as displayed in Fig. 4. Immunostaining against the tight junction-associated structural protein ZO-1 clearly indicated a progressive loss of barrier function associated with blue light exposure, therefore validating the previous observations from resistance recordings.

3.4. Measurement of oxidative stress after blue-light exposure

The same time point (t = 4 h) was investigated for evidence of oxidative stress using the ROS dye carboxy-H2DCFDA. The flow cytometry was set with the DRAQ7 dye in the X axis and the general oxidative stress indicator (carboxy-H2DCFDA) in the Y axis (Fig. 5). This resulted in splitting the figure in 4 quadrants; Carboxy-H2DCFDA

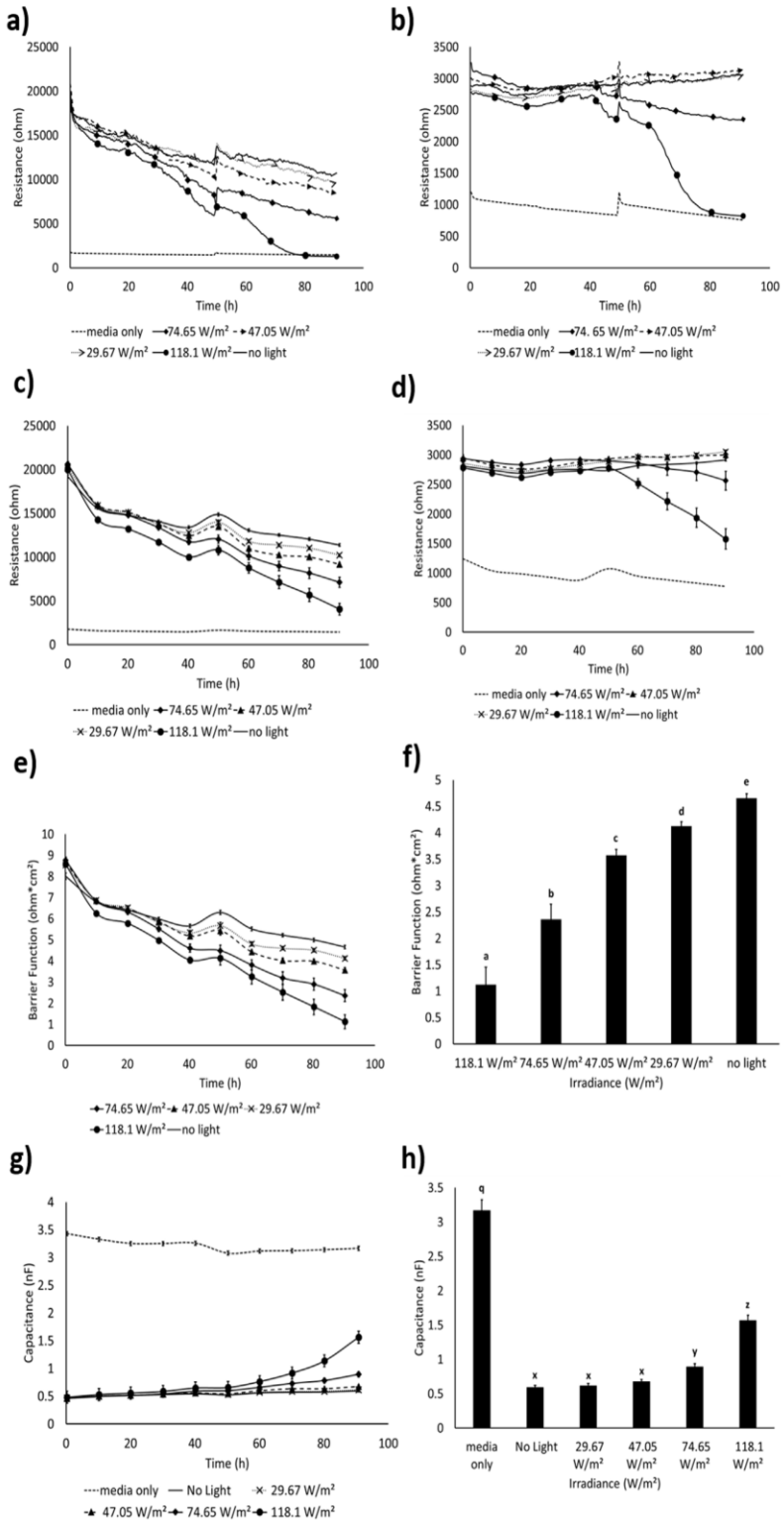

Fig. 3. Continuous blue light exposure caused a decrease in resistance at 4 kHz in a dose dependent manner. However, when the same $_{wells}$ were observed at 64 kHz the time course resistance was strikingly different, with no decrease in resistance before t = 52 h. A drop-in resistance occurring only in the lower frequency range could be associated with a decrease in the barrier function associated with tight junction formation. Quantifications using the mathematical model integrated in the ECIS software showed that blue light induces a dose dependent decrease in the barrier function, before cell death occurred. Statistical analysis performed at t = 90 h confirmed the significance of our results ($P < 0.05$). (a) Resistance at 4 kHz (source data). (b) Resistance at 64 kHz (source data). (c) Resistance at 4 kHz (n = 24). (d) Resistance at 64 kHz (n = 24). (e) Barrier function associated with tight junction formation (n = 24). (f) Barrier function at t = 90 h (n = 24). (g) Capacitance at 64 kHz associated with cell coverage (n = 24). (h) Capacitance at 64 kHz at t = 90 h (n = 24).

(+)/DRAQ7 (-) indicated the population of oxidative stress positive live cells shown in quadrant 1-1 (Q1-1), Carboxy-H2DCFDA (+)/DRAQ7 (+) indicated the population of oxidative stress positive dead cells shown in quadrant 1–2 (Q1-2), Carboxy-H2DCFDA (-)/DRAQ7 (-) indicated the population of oxidative stress negative live cells shown in quadrant 1–3 (Q1-3), and Carboxy-H2DCFDA (−)/DRAQ7 (+) indicated the population of oxidative stress negative dead cells shown in quadrant 1–4 (Q1-4). As opposed to ECIS data, cell death likely

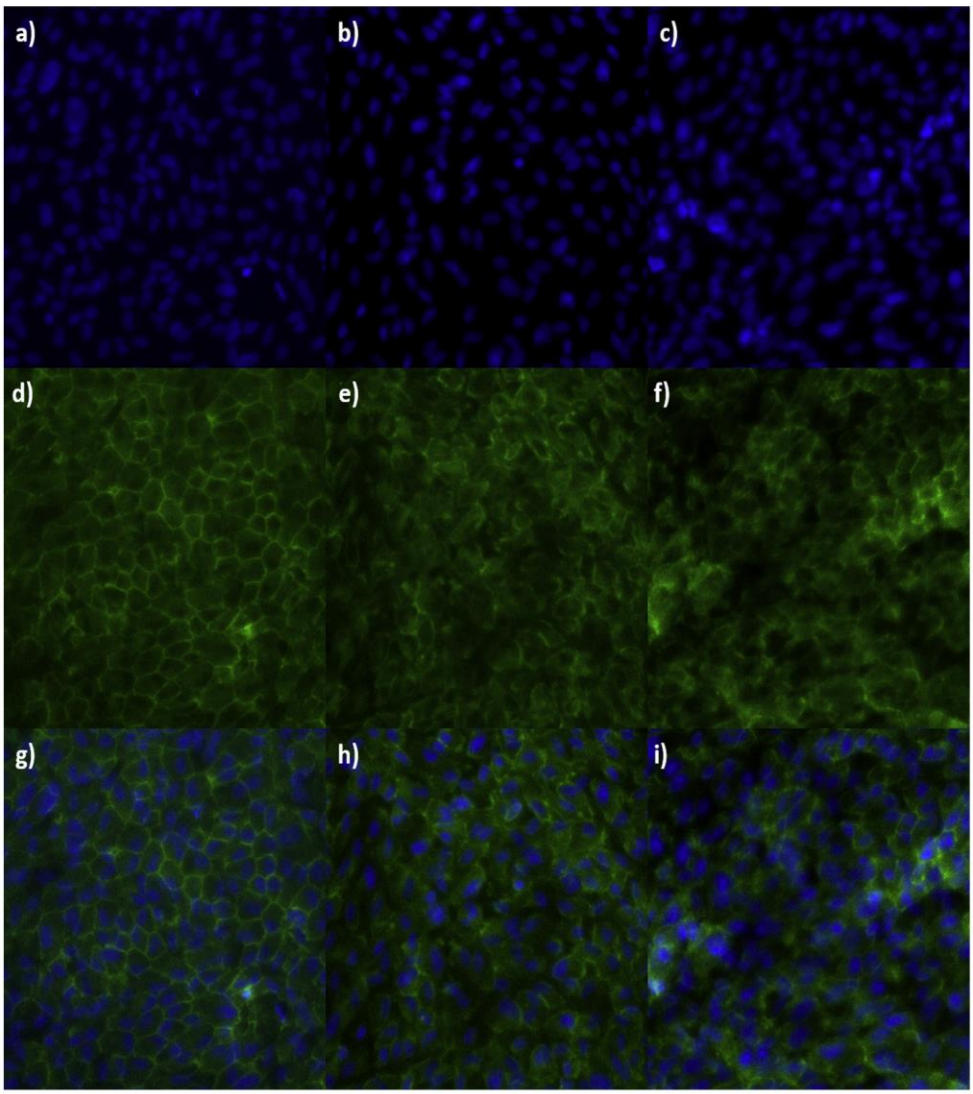

Fig. 4. Immunostaining of the tight-junction associated structural protein, ZO-1, in ARPE-19 showed a progressive loss of barrier function associated with blue light exposure (a) DAPI for no-light control (n = 3). (b) DAPI for irradiance 74.65 W/m^2 (n = 3). (c) DAPI for irradiance 118.1 W/m^2 (n = 3). (d) ZO-1 staining for no-light control (n = 3). (e) ZO-1 staining for irradiance 74.65 W/m^2 after t = 4 h (n = 3). (f) ZO-1 for irradiance 118.1 W/m^2 after t = 4 h (n = 3). (g) Composite image for no-light control (n = 3). (h) Composite image for irradiance 74.65 W/m^2 after t = 4 h (n = 3). (i) Composite image for irradiance 118.1 W/m^2 after t = 4 h (n = 3). (For interpretation of the references to colour in this figure legend, the reader is referred to the Web version of this article.)

associated with cell manipulation required for flow cytometry, i.e. cell trypsinization and cell fixation, was also observed. The flow cytometry data showed an increase in oxidative stress in DRAQ7 negative (live) cells, after treatment with TBHP (Fig. 5a) and blue-light (Fig. 5b) compared to untreated control cells (Fig. 5c). The data showed that after blue-light exposure general oxidative stress could be detected at higher levels compared to TBHP treatment and control in DRAQ7 negative cells (Fig. 5d). Hence, lower levels of oxidative stress negative cells were observed amongst DRAQ7 negative cells after blue-light treatment (Fig. 5e).

3.5. Effect of PKC-ζ inhibition on ARPE-19 barrier function after blue-light exposure

Finally, the time course healing effect of PKC-ζ pseudo substrate inhibitor which has been shown previously to restore barrier function in diabetic retinopathy (Omri et al., 2013) was investigated by using ECIS. Resistance data at f = 4 kHz along with the model of barrier function showed that PKC-ζ inhibition induced faster restoration of barrier function compared to no treatment after 2022 kJ/m^2 of blue light damage to the tight junctions (Fig. 6). It was observed that PKC-ζ inhibition restored the barrier function immediately after the media change at time t = 4 h, while the no treatment control restored the barrier function after 2.5 h.

Taken together, these results indicate that blue light exposure induces a dose-dependent decrease of the human cell line, ARPE-19, barrier function mediated by oxidative stress through the PKC-ζ pathway.

4. Discussion

Previously, the effect of blue-light on the barrier function of human cells has not been studied. This study characterized the effect of blue-light on the outer BRB, with regard to AMD studies. As a novel

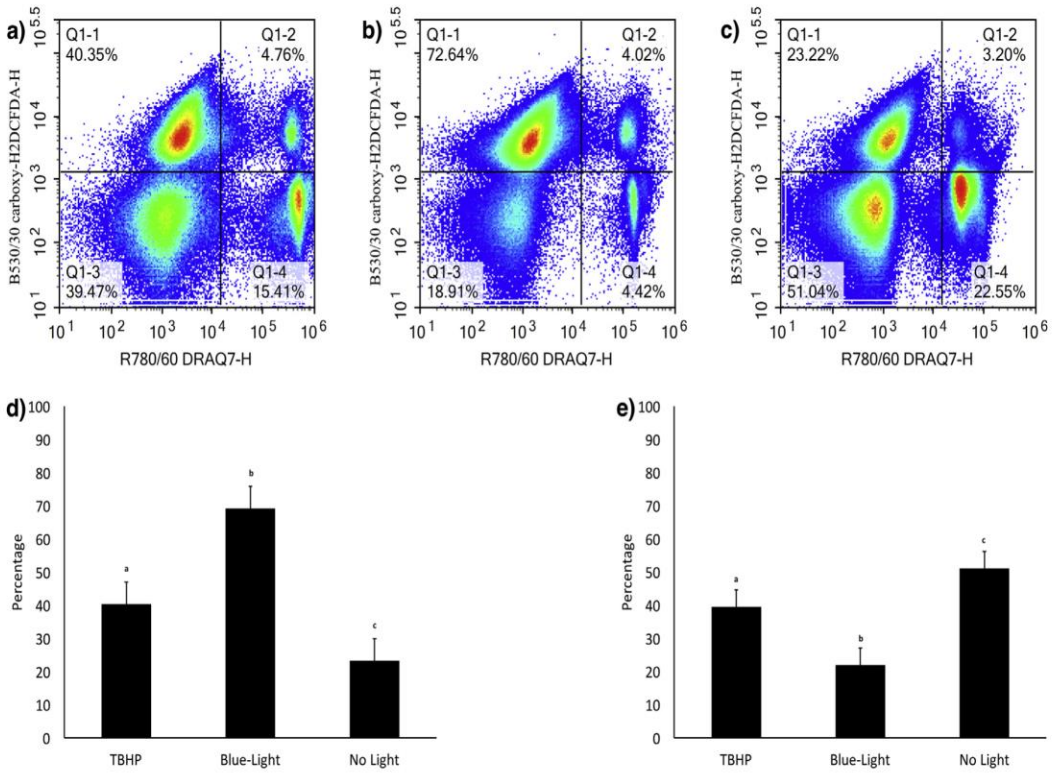

Fig. 5. Flow cytometry data with DRAQ-7 and carboxy-H2DCFDA showed that TBHP (a) and blue-light exposure (b) increased the percentage of Carboxy-H2DCFDA (+)/DRAQ7 (-) ARPE-19 cells shown in Q1-1 compared to no-light control (c). Carboxy-H2DCFDA (+)/DRAQ7 (-) indicated the population of oxidative stress positive live cells (Q1-1). Carboxy-H2DCFDA (-)/DRAQ7 (-) indicated the population of oxidative stress negative live cells (Q1-3). As opposed to ECIS data, cell death likely associated with cell manipulation required for flow cytometry, i.e. cell trypsinization and cell fixation, was also observed in oxidative stress negative (Q1-4) and oxidative stress positive (Q1-2) cells. (a) ARPE-19 treated with TBHP for 30 min (n = 3). (b) ARPE-19 exposed to blue-light for 4 h (n = 3). (c) No light control (n = 3). (d) Percentage of oxidative stressed live ARPE-19 (Q1-1) (n = 3). (e) Percentage of healthy live ARPE-19 (Q1-3) (n = 3). (For interpretation of the references to colour in this figure legend, the reader is referred to the Web version of this article.)

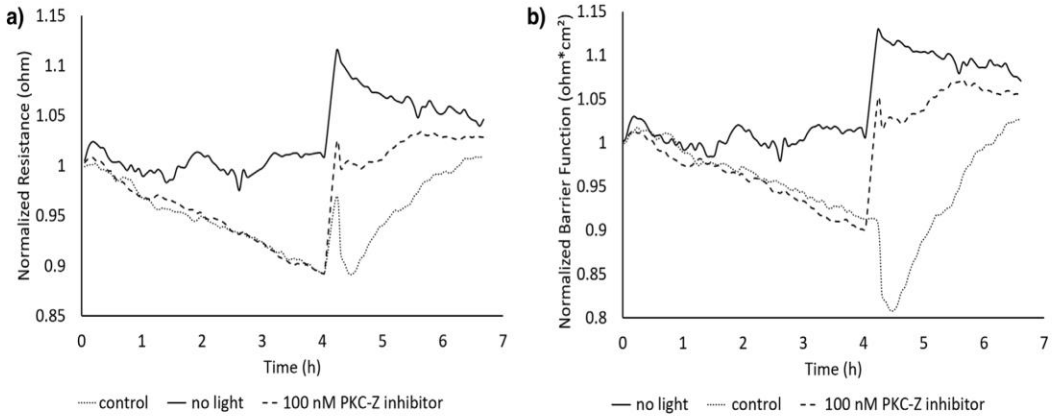

Fig. 6. PKC-ζ inhibition restored the barrier function immediately after the media change at time t = 4 h, while no treatment control restored the barrier function after 2.5 h. (a) Normalized resistance at 4 kHz (n = 3). (b) Normalized barrier function (n = 3).

approach, this study used ECIS model to quantify the effect of blue-light in real-time on in-vitro studies of AMD.

In order to mimic in-vivo RPE barrier function, ARPE-19 and hTERT-RPE1 cells were investigated for their capacity to form tight junctions on ECIS plates. ARPE-19 was chosen due to their superior barrier function formation capacity. In addition, our decision to choose the ARPE-19 cell line was also motivated by the fact that these cells express RPE specific markers; retinal pigment epithelium-specific 65 kDa protein (RPE-65) and cellular retinaldehyde-binding protein (CRALBP) that are involved in 11-cis retinal regeneration in visual cycle. ARPE-19 are also capable of forming monolayer tight-junctions in-vitro after 4 weeks with a maximum of 50–100 Ωcm^2 (Dunn et al., 1996).

Although there have been various attempts to re-pigment these RPE cell lines in-vitro, an ideal RPE cell culture that contains all of melanin, lipofuscin has not yet been produced (Boulton, 2014). However, RPE

cells can be loaded with *N*-Retinylidene-*N*-Retinylethanolamine (A2E) a major retinoid component of lipofuscin, and a well established age-related photo-sensitizer with absorption peaks at 335 nm and 435 nm. When the A2E concentration in the lysosome exceeds a critical level, the lysosomal membrane gets disrupted, causing leakage and cell death. Previous studies by Sparrow et al. (2000) and Marie et al. (2018), highlighted that blue-light damage to cells was considerably enhanced in the presence of A2E due to the generation of high levels of intracellular ROS. In this study, we wanted to dissect the melanin and lipofuscin independent mechanism of blue-light damage, therefore pigmentation and lipofuscin content were not included in our in vitro model. Consequently, the irradiance reported here might not be translated directly to an in vivo case. However, the demonstration of a dose-response relationship clearly reinforced the causality of the loss of barrier function with blue light exposure, and the model was useful to investigate the underlying mechanisms associated with a decrease in paracellular resistance.

We used the eye/light source model developed by Le Grand (1972) to translate the back of the eye irradiances that the ARPE-19 cells were exposed to in this study into the corresponding front of the eye irradiances coming from a light source. The back of the eye irradiances investigated in with our model; 29.67 W/m^2, 47.05 W/m^2, 74.65 W/m^2, 118.1 W/m^2, 140.4 W/m^2 translated respectively into the front of the eye lighting source irradiances; 605.5 W/m^2, 960.2 W/m^2, 1523.5 W/m^2, 2410.2 W/m^2, 2865.3 W/m^2. International Commission on Non-Ionizing Radiation Protection, 2013 evaluated 110 kJ/m^2 as the blue light toxic dose from ocular instruments that could induce macroscopically observable retinal lesions. This toxic energy dose evaluated by ICNIRP corresponded to 38 s of exposure with the highest irradiance in our setup. However previous study by Jaadane et al. (2017) has suggested that the dose recommended by ICNIRP might not be adapted to LED because LED light could cause oxidative damage and photoreceptor loss without inducing any microscopically observable alterations at fundus examination.

The use of blue LEDs is generally associated with electronic devices to improve screen brightness and clarity (Yam and Hassan, 2004). In addition, there is an increase in the use of low energy white LEDs as source of general lightning, which have a strong emission peak at 470 nm, in the blue region of the spectra. Due to its high energy and being able to reach the retina, blue-light is an identified risk factor for AMD (Sparrow et al., 2002). Godley et al. (2005) demonstrated in RPE cells that blue-light exposure generated ROS; singlet oxygen, superoxide anion and hydroxyl radical via both mitochondria and lipofuscin. Previously Rózanowska et al. (1995) showed that blue-light induced ROS caused lipid peroxidation in RPE. Moreover, by comparing blue-light damage to RPE cells in aerobic and anaerobic conditions, Crockett and Lawwill (1984) showed that blue-light induced oxygen dependent damage and observed a positive correlation between oxygen concentration and blue-light damage to RPE. Together these studies show that blue-light damage is primarily mediated via photooxidative stress.

Our results suggested that blue-light (470 nm) induced oxidative stress and damaged paracellular junctions. These results are in line with previous studies by Jaadane et al. (2015) and Omri et al. (2013). Jaadane et al. (2015) demonstrated that oxidative stress produced by LED exposure upregulated the unfolded protein response genes, lead to endoplasmic reticulum stress activation and induced pro-inflammatory cytokine response. Pro-inflammatory cytokines activate PKC-ζ (Jaadane et al., 2015; Omri et al., 2013). PKC-ζ is identified as a key player in the regulation of tight junctions. PKC-ζ phosphorylates occludin to promote the assembly of tight junctions (Jain et al., 2011) and as a part of the protein scaffold complex Par6/Par3/PKC-ζ, it regulates the polarity of the tight junctions (Henrique and Schweisguth, 2003). PKC-ζ localizes in the tight junction protein complexes of RPE and in photoreceptor inner segments (Omri et al., 2013). Upon induced activation, PKC-ζ delocalizes from the plasma membrane to the cell nucleus. The delocalization of PKC-ζ to the nucleus leads to outer-BRB breakdown (Jaadane et al., 2015) and is a sign of cell death (Crisanti et al., 2006; Jaadane et al., 2017). Therefore, we investigated the time course healing effect of PKC-ζ pseudo substrate inhibitor on the tight junctions. Our results showed that PKC-ζ inhibition induced faster restoration of the barrier function compared to no treatment after 2022 kJ/m^2 of blue light damage to the tight junctions. This suggests that PKC-ζ over-activation plays a role in blue light induced barrier function breakdown of tight junctions in ARPE-19.

In their recent study, Gamal et al. (2017) demonstrated by using ECIS that acetaminophen induced breakdown of tight junctions in human hepatic cells (HepaRG) through disruption of tight junction associated ZO-1 protein. In our current study, we followed a similar experimental protocol and demonstrated that blue-light induced breakdown of barrier function through disruption of ZO-1 at the ARPE-19 tight junctions. In the future additional barrier markers could be considered (eg. occludin). Although, it was demonstrated by Chen et al. (2002) that the decrease in transepithelial electrical resistance increased the translocation of ZO-1 from tight junctions while translocation of ZO-2, dephosphorylation or translocation of occludin were not induced in T84 colonocyte cells following *Clostridium difficile* Toxin A exposure.

Previous blue-light studies on ARPE-19 have reported that 35 kW/m^2 single spot blue light for 60 s (2100 kJ/m^2) at 480 nm caused oxidative stress induced cell death (Sparrow et al., 2002). In their in-vivo studies on rats, Jaadane et al. (2017) demonstrated that white LED light disrupts the outer BRB after 6 h of exposure corresponding to 52.3 kJ/m^2 of energy at the back of the eye, by inducing oxidative stress. The same study suggests after 18 h of exposure amounting to 157 kJ/m^2 of energy at the back of the eye, the outer BRB is completely lost with signs of cell death as indicated by the translocation of PKC-ζ staining from the plasma membrane to the cell nucleus (Crisanti et al., 2006; Jaadane et al., 2017). In their in-vivo studies on rabbits, Putting et al. (1992), used vitreous fluorophotometry to quantitatively evaluate the changes in BRB permeability induced by blue light. These studies demonstrated that blue light induces blood-retinal barrier dysfunction in rabbits. In their studies, the threshold energy for blue-light induced increase in BRB permeability translated into 500 kJ/m^2 (140 W/m^2 for 1 h) at the back of the eye and the translated threshold energy at the back of the eye for funduscopically visible lesions was between 2300 and 4300 kJ/m^2. As the blood fluorescein levels decrease with time the efficiency of vitreous fluorophotometry is critically dependent on the time after injection that vitreous fluorophotometry readings were taken (Prager et al., 1981).

In our previous study, we developed a tissue on a chip approach by combining ECIS with reproducible electrical wound healing assays of human induced pluripotent stem cell (hiPSC) based model of AMD (Gamal et al., 2015). The developed disease model on a chip enabled real-time, quantitative and reproducible patient-specific RPE cell repair studies. In our present study, we improved on our disease model on a chip, by developing blue-light induced wound healing assay that could model the BRB damage in neovascular AMD. Our findings suggest that blue light decreased the barrier function before loss of cell coverage. We have observed the presence of different energy thresholds for the decline of the barrier function and the cell coverage for ARPE-19 in vitro. The threshold energy that caused a significant decline in the BRB is quantified to be 1701 kJ/m^2 at the back of the eye. The decline of the barrier function due to different irradiances after 90 h is found to be energy dose dependent ($P < 0.05$).

The impact of blue-light on the susceptible macula has clinically significant implications in age-related macular degeneration (AMD) pathogenesis and progression. The shortcomings and inconsistencies inherent in epidemiological studies to date have not allowed clinical researchers to make evidence-based recommendations on how best to prevent or reduce progression in AMD with respect to blue-light protection. Nevertheless, in clinical practice patients are advised to wear blue/UV blocking glasses and blue-blocking intraocular lenses are used

in cataract surgery. Little is known about the long-term photobiological impact of intermittent and sustained ambient exposure on the target tissue relevant to AMD, the retinal pigment epithelium. In order to better understand the mechanisms and derive evidence to inform clinical practice, relevant in vitro studies are required to define the risk and mitigate long term consequences especially with increased use in blue-emitting screens and the likely increase in light as a means of wireless communication. The clinical context of conclusions arising from this and other studies should also consider the role blue-light plays in entraining circadian rhythms mediated through photoreceptive ganglion cells of the retina. Therefore, blue-light exposure levels in terms of power and duration needs better defined to allow a logical approach to the risk/benefit both for individuals at risk of AMD and those already affected, stratified by genotype-phenotype (Modenese and Gobba, 2019; Downie et al., 2019; Popoola, 2016).

5. Conclusion

Our results document the time course that blue LED light exposure decreases retinal pigment epithelium barrier function in vitro in a dose-dependent manner, before any cell death occurs. This study is the first to show that blue light induced break-down of barrier function on human retinal pigment epithelial cells is mediated by PKC-ζ over-activation and oxidative stress. The damage of the barrier function associated with tight junction formation between RPE cells disrupts the outer blood retina barrier and is one of the symptoms of neovascular AMD (Cunha-Vaz et al., 2011; Ambati et al., 2013). Therefore, it is important to further investigate the link between blue-light exposure and the PKC-ζ pathway in AMD. Finally, our results suggest that PKC-ζ over-activation could potentially be inhibited by drugs to protect against the outer-BRB breakdown in AMD.

Acknowledgements

The authors thank Fiona Rossi and the flow cytometry facility at the MRC Centre for Regenerative Medicine for their help. The authors also thank the imaging facility at the MRC Centre for Regenerative Medicine for their support.

References

Ambati, J., Atkinsons, J.P., Gelfand, B.D., 2013. Immunology of age-related macular degeneration. Nat. Rev. Immunol. 13 (6), 438–451. https://doi.org/10.1038/nri3459.

Beatty, S., Koh, H., Phil, M., Henson, D., Boulton, M., 2000. The role of oxidative stress in the pathogenesis of age-related macular degeneration. Surv. Ophthalmol. 45 (2), 115–134 [PubMed: 11033038].

Bi, W.M., Sun, K., 2014. Light-induced retinal damageand potential benefitsand side effects of blue light-filtering intraocular lens. Recent Adv. Opthalmology. 34 (3), 289–293.

Boulton, M.E., 2014. Studying melanin and lipofuscin in RPE cell culture models. Exp. Eye Res. 126, 61–67. https://doi.org/10.1016/j.exer.2014.01.016.

Chen, M.L., Pothoulakis, C., LaMont, J.T., 2002. Protein kinase C signaling regulates ZO-1 translocation and increased paracellular flux of T84 colonocytes exposed to *Clostridium difficile* Toxin A. J. Biol. Chem. 277 (6), 4247–4254. https://doi.org/10.1074/jbc.M109254200.

Cosentino-Gomes, D., Rocco-Machado, N., Meyer-Fernandes, J.R., 2012. Cell signaling through protein kinase C oxidation and activation. Int. J. Mol. Sci. 13, 10697–10721. https://doi.org/10.3390/ijms130910697.

Crisanti, P., Laplace, O., Lecain, E., Jonet, L., Jeanny, J.C., Omri, B., 2006. The Role of PKCzeta in NMDA-induced retinal ganglion cell death: prevention by asprin. Apoptosis 11, 983–991. https://doi.org/10.1007/s10495-006-6750-2.

Crockett, R.S., Lawwill, T., 1984. Oxygen dependence of damage by 435 nm light in cultured retinal epithelium. Curr. Eye Res. 3 (1), 209–222. https://doi.org/10.3109/02713688408997202.

Cunha-Vaz, J., 2012. Blood-retinal barrier and its relevance in retinal disease. Med. Retina. 1, 6–10. https://doi.org/10.1159/000336698.

Cunha-Vaz, J., Bernardes, R., Lobo, C., 2011. Blood-retinal barrier. Eur. J. Opthalmology. 21 (6), 3–9. https://doi.org/10.5301/EJO.2010.6049.

Downie, L.E., Wormald, R., Evans, J., Virgili, G., Keller, P.R., Lawrenson, J.G., Li, T., 2019. Analysis of a systematic review about blue light-filtering intraocular lenses for retinal protection: understanding the limitations of the evidence. JAMA Ophthalmol 21. https://doi.org/10.1001/jamaophthalmol.2019.0019.

Dunn, K.C., Aotaki-Keen, A.E., Putkey, F.R., Hjelmeland, L.M., 1996. ARPE-19, A human retinal pigment epithelial cell line with differentiated properties. Exp. Eye Res. 62, 155–170. https://doi.org/10.1006/exer.1996.0020.

Gamal, W., Borooah, S., Smith, S., Underwood, I., Srsen, V., Chandran, S., Bagnaninchi, P.O., Dhillon, B., 2015. Real-time quantitative monitoring of hiPSC-based model of macular degeneration on Electric Cell-substrate Impedance Sensing microelectrodes. Biosens. Bioelectron. 71, 445–455. https://doi.org/10.1016/j.bios.2015.04.079.

Gamal, W., Treskes, P., Samuel, K., Sullivan, G.J., Siller, R., Srsen, V., Morgan, K., Bryans, A., Kozlowska, A., Koulovasilopoulos, A., Underwood, I., Smith, S., del-Pozo, J., Moss, S., Thompson, A.I., Henderson, N.C., Hayes, P.C., Plevris, J.N., Bagnaninchi, P.O., Nelson, L.J., 2017. Low-dose acetaminophen induces early disruption of cell-cell tight junctions in human hepatic cells and mouse liver. Sci. Rep. 7https://doi.org/10.1038/srep37541. 37541.

Giaever, I., Keese, C.R., 1991. Micromotion of mammalian cells measured electrically. Proc. Natl. Acad. Sci. 88, 7896–7900. https://doi.org/10.1073/pnas.88.17.7896.

Godley, B.F., Shamsi, F.A., Liang, F.Q., Jarrett, S.G., Davies, S., Boulton, M., 2005. Blue light induces mitochon-drial DNA damage and free radical production in epithelial cells. J. Biol. Chem. 280, 21061–21066 10.1074jbc.M502194200.

Henrique, D., Schweisguth, F., 2003. Cell polarity: the ups and downs of the Par6/aPKC complex. Curr. Opin. Genet. Dev. 13 (4), 341–350. https://doi.org/10.1016/S0959-437X(03)00077-7.

International Commission on Non-Ionizing Radiation Protection, 2013. ICNIRP Guidelines on limits of exposure to incoherent visible and infrared radiation. Health Phys. 105, 74–96. https://doi.org/10.1097/HP.0b013e318289a611.

Jaadane, I., Chahory, S., Leprêtre, C., Omri, B., Jonet, L., Behar-Cohen, F., Crisanti, P., Torriglia, A., 2015. The activation of the atypical PKC zeta in light-induced retinal degeneration and its involvement in L-DNase II control. J. Cell Mol. Med. 19 (7), 1646–1655. https://doi.org/10.1111/jcmm.12539.

Jaadane, I., Rodziguez, G.E.V., Boulenguez, P., Chahory, S., Carre, S., Savodelli, M., Jonet, L., Behar-Cohen, F., Martinsons, C., Torriglia, A., 2017. Effects of white light-emmiting diode (LED) exposure on retinal pigment epithelium in-vivo. J. Cell Mol. Med. 21 (12), 3453–3466. https://doi.org/10.1111/jcmm.12539.

Jain, S., Suzuki, T., Seth, A., Samak, G., Rao, R., 2011. Protein kinase C zeta phosphorylates occludin and promotes assembly of epithelial tight junctions. Biochem J. England. 437 (2), 289–299. https://doi.org/10.1042/BJ20110587.

Jarrett, S.G., Boulton, M.E., 2012. Consequences of oxidative stress and macular degeneration. 2013. NIH Public Access 33 (4), 399–417. https://doi.org/10.1016/j.mam.2012.03.009.

Jarrett, S.G., Lewin, A.S., Boulton, M.E., 2010. The importance of mitochondria in age-related and inherited eye disorders. Ophthalmic Res. 44 (3), 179–190 [PubMed: 20829642].

Johnson, P.T., Brown, M.N., Pulliam, B.C., Anderson, D.H., Johnson, L.V., 2005. Synaptic Pathology, altered gene expression, and degeneration in photoreceptors impacted by drusen. Investig. Ophthalmol. Vis. Sci. 46, 4788–4795. https://doi.org/10.1167/iovs.05-0767.

Jomova, K., Vondrakova, D., Lawson, M., Valko, M., 2010. Metals, oxidative stress and neurodegenerative disorders. Mol. Cell. Biochem. 345 (1–2), 91–104 [PubMed: 20730621].

Le Grand, Y., 1972. Optique Physiologique, Vol 2, Lumie're et Couleurs. Masson & CIE, pp. 490.

Marie, M., Bigot, K., Angebault, C., Barrau, C., Gondouin, P., Pagan, D., Fouquet, S., Villette, T., Sahel, J., Lenaers, G., Picaud, S., 2018. Light action spectrum on oxidative stress and mitochondrial damage in A2E-loaded retinal pigment epithelium cells Cell Death and Disease. 9 (3), 287. https://doi.org/10.1038/s41419-018-0331-5.

Modenese, A., Gobba, F., 2019. Macular degeneration and occupational risk factors: a systematic review. Int. Arch. Occup. Environ. Health 92 (1), 1–11. https://doi.org/10.1007/s00420-018-1355-y.

Omri, S., Behar-Cohen, F., Rothschild, P.-R., Gelize, E., Jonet, L., Jeanny, J.C., Omri, B., Crisanti, P., 2013. PKCζ mediates breakdown of outer blood-retinal barriers in diabetic retinopathy. PLoS One 8 (11), e81600. https://doi.org/10.1371/journal.pone.0081600.

Popoola, W.O., 2016. Impact of VLC on light emission quality of white LEDs. J. Light. Technol. 34 (10), 2526–2532. https://doi.org/10.1109/JLT.2016.2542110.

Prager, T.C., Wilson, D.J., Avery, G.D., Merritt, J.H., Garcia, C.A., Hopen, G., Anderson, R.E., 1981. Vitreous fluorophotometry: identification of sources of variability. Invest. Opthalmol. Vis. Sci. 21, 854–864.

Putting, B.J., Zweypfenning, R.C.V.J., Vrensen, G.F.J.M., Oosterhuis, J.A., van Best, J.A., 1992. Blood-retinal barrier dysfunction at the pigment epithelium induced by blue light. Investig. Ophthalmol. Vis. Sci. 33, 3385–3393.

Romano, A.D., Serviddio, G., de Matthaeis, A., Bellanti, F., Vendemiale, G., 2010. Oxidative stress and aging. J. Nephrol. 23 (Suppl. 15), S29–S36 [PubMed: 20872368].

Rózanowska, M., Jarvis-Evans, J., Korytowski, W., Boulton, M.E., Burke, J.M., Sarna, T., 1995. Blue light-induced reactivity of retinal age pigment in vitro generation of oxygen-reactive species. J. Biol. Chem. 270, 18825–18830. https://doi.org/10.1074/jbc.270.32.18825.

Sparrow, J.R., Nakanishi, K., Parish, C.A., 2000. The lipofuscin fluorophore A2E mediates blue light-induced damage to retinal pigmented epithelial cells. Investig. Ophthalmol. Vis. Sci. 41, 1981–1989.

Sparrow, J.R., Zhou, J., Ben-Shabat, S., Vollmer, H., Itagaki, Y., Nakanishi, K., 2002. Involvement of oxidative mechanisms in blue-light-Induced damage to A2e-laden RPE. Investig. Ophthalmol. Vis. Sci. 43 (4), 1222–1227.

Yam, F.K., Hassan, Z., 2004. Innovative advances in LED technology. Microelectron. J. 36 (2), 129–137. https://doi.org/10.1016/j.mejo.2004.11.008.